UNIVERSITAT POLITÈCNICA DE CATALUNYA BARCELONATECH

Analysis and control of multi–area HVDC interconnected power systems by using virtual inertia

Elyas Rakhshani

ADVERTIMENT La consulta d'aquesta tesi queda condicionada a l'acceptació de les següents condicions d'ús: La difusió d'aquesta tesi per mitjà del repositori institucional UPCommons (http://upcommons.upc.edu/tesis) i el repositori cooperatiu TDX (http://www.tdx.cat/) ha estat autoritzada pels titulars dels drets de propietat intel·lectual **únicament per a usos privats** emmarcats en activitats d'investigació i docència. No s'autoritza la seva reproducció amb finalitats de lucre ni la seva difusió i posada a disposició des d'un lloc aliè al servei UPCommons o TDX.No s'autoritza la presentació del seu contingut en una finestra o marc aliè a UPCommons (*framing*). Aquesta reserva de drets afecta tant al resum de presentació de la tesi com als seus continguts. En la utilització o cita de parts de la tesi és obligat indicar el nom de la persona autora.

ADVERTENCIA La consulta de esta tesis queda condicionada a la aceptación de las siguientes condiciones de uso: La difusión de esta tesis por medio del repositorio institucional UPCommons (http://upcommons.upc.edu/tesis) y el repositorio cooperativo TDR (http://www.tdx.cat/?locale-attribute=es) ha sido autorizada por los titulares de los derechos de propiedad intelectual **únicamente para usos privados enmarcados** en actividades de investigación y docencia. No se autoriza su reproducción con finalidades de lucro ni su difusión y puesta a disposición desde un sitio ajeno al servicio UPCommons No se autoriza la presentación de su contenido en una ventana o marco ajeno a UPCommons (*framing)*. Esta reserva de derechos afecta tanto al resumen de presentación de la tesis como a sus contenidos. En la utilización o cita de partes de la tesis es obligado indicar el nombre de la persona autora.

WARNING On having consulted this thesis you're accepting the following use conditions: Spreading this thesis by the institutional repository UPCommons (http://upcommons.upc.edu/tesis) and the cooperative repository TDX (http://www.tdx.cat/?locale-attribute=en) has been authorized by the titular of the intellectual property rights **only for private uses** placed in investigation and teaching activities. Reproduction with lucrative aims is not authorized neither its spreading nor availability from a site foreign to the UPCommons service. Introducing its content in a window or frame foreign to the UPCommons service is not authorized (framing). These rights affect to the presentation summary of the thesis as well as to its contents. In the using or citation of parts of the thesis it's obliged to indicate the name of the author.

UNIVERSITAT POLITÈCNICA
DE CATALUNYA
BARCELONATECH

PhD Thesis

Analysis and Control of Multi–area HVDC Interconnected Power Systems by using Virtual Inertia

Elyas Rakhshani

Barcelona, September 2016

Analysis and Control of Multi–area HVDC Interconnected Power Systems by using Virtual Inertia

Elyas Rakhshani

Dissertation submitted to the Doctorate Office of the Universitat Politècnica de Catalunya in partial fulfillment of the requirements for the degree of Doctor of Philosophy by the

UNIVERSITAT POLITÈCNICA DE CATALUNYA

Electrical Engineering Department
Research Center on
Renewable Electrical Energy Systems

Barcelona, September 2016

Analysis and Control of Multi–area HVDC Interconnected Power Systems by using Virtual Inertia

Copyright © Elyas Rakhshani, 2016
Printed by the UPC
Barcelona, September 2016

Research Projects: ENE 2011-29041-C02-01,
ENE 2013-48428-C2-2-R,
ENE 2014-60228-R.

UNIVERSITAT POLITÈCNICA DE CATALUNYA (UPC)
Electrical Engineering Department (DEE)
Research Center on
Renewable Electrical Energy Systems (SEER)

Rambla Sant Nebridi s/n, GAIA Research Building, UPC Campus,
08222-Terrassa, Barcelona, Spain.
Web: http://seer.upc.edu
http://www.upc.edu

To my beloved Parents,

ACKNOWLEDGEMENTS

I like to thank God to give me the opportunity of more learning and try to be a better person in my life. These recent years of my life, during my Ph.D., was one of the most rewarding and also challenging years that I truly had a chance for meeting and understanding the people from several countries. It enriched my life with sharing a vast variety of traditions with several cultural backgrounds.

First of all, I would like to express my deepest gratitude to my supervisor **Professor Pedro Rodriguez** for his guidance, patience and his great support throughout my doctoral studies. For me it was a golden opportunity to work with him. He let me to increase my experience/knowledge in new fields which will help me in the future. Without his help, this thesis would not have been possible. He was always available to discuss my research with providing priceless comments and inspiring ideas which were/will be always advantageous in my works. As an international student, I never felt lonely due to his brilliant guidance during this period.

I also want to express my thanks to **Professor Remus Teodorescu** and his group at institute of energy technology in Aalborg, Denmark for their support in part of my research during my stay in Aalborg. Thanks for sharing with me their knowledge and time.

Especial thanks to **Professor Antonio Gómez Expósito**, and **Dr. Juan Manuel Mauricio** at electrical engineering department of University of Seville for their valuable academic advices in part of my studies.

I also like to say thank you to the great people at Renewable Electrical Energy Systems (SEER) research center at the Technical University of Catalonia, UPC for all of their kind support during my Ph.D., especially for **Dr. Alvaro Luna**, **Dr. Jose Ignacio Candela**, **Dr. Joan Rocabert**, **Dr. Raúl Santiago Muñoz**, **Dr. Juan Ramon Hermoso** and **Lidia Herrera**.

Many thanks to all the people in Abengoa Research for supporting me during my Ph.D., especially **Professor Manuel Doblaré**, **Dr. Hasan Mehrjerdi**, **Dr. Jimmy Faria**, **Dr. Mria Pilar**, **Dulce Mellado** and **Pedro Martin Sanchez**.

Many thanks to my friends in Barcelona during my first years of stay that make a very good and memorable time for me: Kumars, Reza, Ramin, Hamid Reza, Mehdi, Costantino and Catalin. Also especial thanks to all of my friends and colleagues in Abengoa Research during my stay in south of Spain, especially Mohamed, Pau, Toni, Dani and Cosmin.

I also offer my truthful thanks to my previous supervisor, **Prof. Javad Sadeh**, who has also given me valuable academic advices and decisive guidance.

And last, but not least, I also like to present my eternal gratitude and love to my parents, my brothers and my lovely sister for their everlasting love and continuous support. Without their supports none of my achievements would have been possible.

Elyas Rakhshani
September 2016, Spain

Abstract

Virtual inertia is recognized as an inevitable part of the future modern power systems. The recent trend of research in different part of modern power systems is oriented in different methods for emulating virtual inertia and many research projects have been studied this issue. This dissertation is focused on modeling, analyzing and applying the virtual inertia concept to frequency control and Automatic Generation Control (AGC) in high-level control of AC/DC interconnected power systems. Since the virtual inertia is provided by advanced control concepts of power electronics based components, the HVDC links are the main focus of this dissertation for emulating virtual inertia.

During load and resource variation in multi-area interconnected system, AGC plays a key role and it is recognized as a very important mechanism that can facilitate various tasks, such as frequency restoration, tie-line power flow control between authority areas and economic dispatch of generation units. The tasks of frequency control and the tie line power exchanges will be established by proper operation of the AGC. The AGC concept is known as a high-level control in power transmission. This high-level control generates the set-points for all the local components, like generation units or power converter stations, which are under control by their local controllers.

AGC in multi-area interconnected power systems is experiencing several adaptions due to increasing penetration of power converter based components in the grid. In this dissertation, two different methods for emulating virtual inertia are proposed and introduced in AGC modeling and control for HVDC/AC interconnected systems.

The first method is based on the Derivative Control technique. In this dissertation, the derivative control technique is used for high-level application of inertia emulation. This method of inertia emulation is developed for a two-area AGC system which is connected by parallel AC/DC transmission lines. Based on the proposed technique, the dynamic effect of emulated inertia for frequency and active power control of interconnected systems is evaluated. The effects of frequency measurement delay and Phase Locked Loop (PLL) are also considered by introducing a second-order function. Simulations results, which are obtained using Matlab software show and demonstrate how virtual inertia emulation effectively improves the performance of the power system. Detailed eigenvalue and sensitivity analyses have been also performed to support the positive effects of the proposed method.

Since the first method is based on derivation for grid frequency, the measurement of frequency is very important and application of different techniques for frequency measurements like PLL will bring some limitations for this method. Therefore, as an ultimate solution, a second method for virtual inertia emulation is introduced in this dissertation. The second method is based on the Virtual Synchronous Power (VSP) concept. The concept of VSP to emulate the dynamic effects of virtual inertia by HVDC links for high-level control applications is introduced and reflected in the multi-area AGC model. By using this proposed combination in the AGC model, the dynamic performance of the system shows a significant improvement. The active power loop control on VSP based HVDC link has a second-order characteristic which makes a simultaneous enabling of damping and inertia emulations into the system. Trajectory sensitivities and eigenvalue analyses are used to study the effects of VSP on the system stability. The effectiveness of proposed concept on dynamic improvements is tested through Matlab simulation of a multi-area test system.

Finally, it became clear that virtual inertia will add an additional degree of freedom to the system dynamics which makes a considerable improvement in first overshoot responses in addition to damping characteristics of HVDC links. Comparing the results of these two different methods of inertia emulation shows that the VSP technique has better performance with several advantages for emulating the inertia. In the VSP technique, PLL and frequency estimation are not required. Also considering the fact that simultaneous damping and inertia could be emulated, a powerful method based on VSP for improving the system dynamics during the contingencies is proposed.

FIGURES

TABLES

Acronyms

AGC	Automatic Generation control
AVR	Automatic Voltage Control
ACM	Active Control and Management
APF	Area Participation Factor
DG	Distributed Generation
DPS	Distributed Power System
DISCO	Distribution Company
ESS	Energy Storage System
GA	Genetic Algorithm
GENCO	Generation Company
HVDC	High Voltage Direct Current
ISE	Integral of Squared Error
ISO	Independent System Operator
LFC	Load Frequency Control
MMC	Multi Modular Converter
POD	Power Oscillation Damping
PSO	Particle Swarm Optimization
PLL	Phase Locked Loop
RES	Renewable Energy Resource
ROCOF	Rate of Change of Frequency

SMES	Supper Magnetic Energy Storage
SPC	Synchronous Power Controller
SQP	Sequential Quadratic Programming
TRANSCO	Transmission Companies
VIU	Vertically Integrated Utility
VSG	Virtual Synchronous Generator
VSC	Voltage Source Converter
VSP	Virtual Synchronous Power

CONTENTS

CHAPTER
1.

Introduction

Power systems are experiencing a fast revolution considering power market and deregulations and high penetration of power electronic based components like renewable power sources (distributed generation, Wind, PV with energy storage technologies). These changes make power systems very complex with more uncertainties. Generally renewable resource of energy will have some stochastic nature that eventually could have different effects on power grid. Managing new modern power systems in a deregulated scheme with high penetrate renewable resources is difficult and the matter of inertia from stability point of view is very important [1.1]-[1.8]. In order to cope with new challenges in modern power systems more detailed research in this filed is necessary.

This dissertation is part of research projects at the ABENGOA Company, Abengoa Research department, in collaboration with SEER research center at UPC University. The title of the thesis is "Analysis and Control of Multi-area HVDC Interconnected Power Systems by using virtual inertia". Since several topics have been covered during this project, the main focus of this dissertation is related to modeling, analyzing and application of virtual inertia concept in frequency stability and AGC issue in high level control of AC/DC interconnected power systems. The AGC concept is known as high level control at the transmission systems. This high level control will generate the set-points for all the local components, like generation units or power converter station, which are under control by their local controllers [1.9]-[1.11].

Since the virtual inertia is provided by advanced control concepts for power electronic based components [1.12]-[1.14], the HVDC links are the main focus of this dissertation for emulating the inertia. Global oscillation is caused by interaction among large groups of generators, which are spread out throughout a large geographical area. This type of oscillations has widespread impact and can lead to partial or full blackout. Application of HVDC links in parallel with AC links is one of the ways which can improve the negative impacts of this kind of oscillations [1.15]-[1.17].

Modern power system control and analysis with high penetration of PV resources and with DC interconnections are increasingly under consideration. For providing a better performance during operation and also to increase the stability of the system, different installations with new technologies are necessary, e.g., advanced components of power electronics, HVDC links and Flexible AC Transmission Systems (FACTS) equipment in the power system. The main application area for HVDC is the interconnection between systems which cannot be interconnected by AC link because of different operating frequencies or different frequency controls. By means of global RE integration and competitive markets, it would be necessary to equip the network with several DC interconnections at high voltage level between the areas. Therefore, in addition to more stability in the whole system by applying DC interconnections, there is a better possibility to transfer more power for any kind of long distance link. Providing additional inertia by means of power electronic components (like HVDC station) is another advantage that could provide different ancillary services like providing the damping and virtual inertia for frequency control improvements. The main goal, objectives and contributions in this thesis are as follows:

1.1 Goals and Objectives

As stated, the matter of inertia and analyzing the impact of virtual inertia in multi area power system is very important. Therefore, the main goal of this thesis is the improvement of dynamic response and overall performance of Multi Area Power Systems (MAPS) using Virtual Synchronous Power (VSP) concept, considering HVDC links of interconnected systems. The main focus is related to frequency control stability analysis of multi area interconnected systems. Based on this explanation, here are the main objectives of this thesis:

1- To present a novel approach for inertia emulation through the VSP based HVDC transmission systems. This control strategy proposes a new method for power converter control in HVDC link. Let them behaving as a synchronous

generator with the ability of emulating synchronous inertia during the transients in HVDC stations without the drawbacks of conventional generators. This new application of VSP in power system transmission provide more flexibility to the power system. It will increase the mitigation of power system oscillation by emulating inertia and sufficient damping to the system through HVDC interconnections.

2- To propose a new approach of frequency stability analysis in multi area AGC system considering the derivative term of grid frequency for emulating inertia in the interconnected AC/DC systems.

3- To propose a new approach of frequency stability analysis in multi area AGC system adding the VSP concept in HVDC links of interconnected systems.

The proposed models should provide a systematic modeling and control technique of a large scale interconnected power system and specifically should be devoted to frequency support and power oscillation damping (POD) by means of parallel AC/DC transmission line and Energy Storage Systems (ESS) technologies in AGC systems of power industry.

4- To propose a model which is very useful for pre-evaluation of dynamic effects of converter stations of HVDC link in higher level control design for power systems applications.

5- To preform dynamic analyses for multi area AGC model with eigenvalue and sensitivity analyses considering virtual inertia effects on the overall system performance.

1.2 Contributions of the Thesis

The contributions of the research work reported in this thesis can be grouped into the following issues:

- Proposing new approach on emulating the virtual inertia for AGC analysis in multi area power systems. This virtual inertia will bring more flexibility to the transmission system for damping the inter-area oscillation and emulating the inertia.

- Improving the frequency stability and control of generation in multi-area interconnected power systems by adding the virtual inertia concept. This virtual inertia is contributing during transients caused by load variations.

- Proposing a new application of virtual inertia emulation based on derivative control for AGC analyses of interconnected power systems. Proper modeling for higher level control applications with proper coordination between DC link and AGC is provided.
- Incorporating the effects of frequency measurements and PLL dynamics on AGC analyses of interconnected power systems. The effects of PLL is introduced for the system with virtual inertia based on derivative control technique.
- Proposing a new application of VSP technique for higher level application in AGC power system. This method can be used to provide possible inertia in to the modern scenario of power industry for frequency supports and POD tasks. By means of proposed technique based on VSP control, better dynamic performance compared to other methods of inertia emulation like derivative control is obtained. The proposed control of VSP is a power electronics based synchronous generator which is naturally synchronized with the electrical grid by balancing the exchange of power with AC grid. Therefore, it does not require any external synchronization system, such as a PLL, to work. Therefore all the limitations and dependencies to PLL and frequency measurements will be avoided.
- In this study by means of proposed models, it is possible to have a clear image about the system conditions and required energy or power references considering the control issue of AC/DC interconnected system. Proposed model could be extended to any type of multi area system with different complexity.

1.3 Thesis Organization

The thesis will continue by a complete state of the art on conventional power system control and its modifications to the modern power systems in C**hapter 2**. In this Chapter the importance of power electronic based components in the future of power industry is explained. It will continued by reviewing the main control functions in power system considering the main ancillary services that could be offered in modern scenario of power system. Brief review about HVDC application and its control structure is also presented by the end of this Chapter.

In **Chapter 3**, a brief presentation about two-terminal HVDC links and its control functions are presented. Different modeling for power system applications is also presented. The main focus is related to averaged model of voltage source converters and

simplifications. The small signal model of HVDC link which used in this thesis is the last part of this Chapter.

The main focus of **Chapter 4** is to present the fundamental of frequency control in power grid and is explaining the dynamic model of multi-area AGC system. The conventional AC model and the modified model considering HVDC link based on supplementary power modulation control (SPMC) is presented. Mathematical equations for multi-area interconnected AGC system are presented and a general simulation for two-area system is the last part of this Chapter.

In this thesis two different methods for emulating virtual inertia is proposed and introduced in AGC modeling and control for HVDC/AC interconnected systems. The first method is based on derivative control and the second methods is based on virtual synchronous power concept. In addition to incorporating the coordinated model of DC link in AGC model, these methods of emulating virtual inertia are the main contribution of this thesis. Both methods are presented and analyzed in Chapters 5 and 6, respectively.

Therefore, in **Chapter 5**, the derivative control technique is proposed for higher level application of inertia emulation. This method of inertia emulation is developed for two-area AGC systems which is connected by parallel AC/DC transmission lines. Based on the proposed technique, the dynamic effect of inertia emulated by storage devices for controlling the frequency and active power variations are evaluated. The effects of frequency measurement delay and PLL effects are also considered by introducing a second-order function. Simulations results using the Matlab software, shows and demonstrate how virtual inertia emulation can effectively improve the performance of the power system. A detailed eigenvalue and sensitivity analyses have been also performed to support the positive effects of proposed method.

In **Chapter 6**, the second method for virtual inertia emulation is introduced. The second method is based on VSP concept. The concept of VSP to simulate the dynamic effects of inertia emulations by HVDC links for higher level control applications is introduced and reflected in the multi-area AGC model. With using this proposed combination in AGC model, the dynamic performance of the system shows a significant improvement. Trajectory sensitivities and eigenvalue analyses are used to analyze the effects of VSP on the system stability. The effectiveness of proposed concept on dynamic improvements is tested through Matlab simulation of multi-area test system.

Finally, it became clear that virtual inertia will add additional degree of freedom to the system dynamics which makes a considerable improvement in first overshoot responses

in addition to damping characteristics of HVDC links. Comparing the results of these two different methods of inertia emulation shows that the VSP technique has better performance with several advantages for emulating the inertia. In the VSP technique, PLL and frequency estimation are not required.

Finally, the dissertation is summarized in C**hapter 7**. In this Chapter the main conclusions considering the possible future works are presented.

1.4 Publications

Patent:

- Jorge Martinez Garcia, Pedro Rodriguez Cortes, **Elyas Rakhshani**; "*Virtual Power Controller and Method for Multi-terminal HVDC Interconnected Network*," European Patent, 2016.

Book chapter:

- **E. Rakhshani**, P. Rodriguez, "*Active Power and Frequency Control Considering Large-Scale RES*", in Large Scale Renewable Power Generation, Springer, pp. 233-271, 2014.

Journals (2011-2016):

- **E. Rakhshani**, D. Remon, A.M. Cantarellas, J.M. Garcia and P. Rodriguez, "Virtual Synchronous Power Strategy for Multiple HVDC Interconnections of Multi-Area AGC Systems", *IEEE Transactions on Power Systems*, 2016, DOI: 10.1109/TPWRS.2016.2592971.

- **E. Rakhshani**, D. Remon, A. Mir Cantarellas, and P. Rodriguez, "Analysis of Derivative Control Based Virtual Inertia in Multi-Area HVDC Interconnected AGC Power Systems", *IET Generation Transmission & Distribution*, vol. 10, no. 6, pp. 1458-1469, 2016.

- **E. Rakhshani**, D. Remon, A.M. Cantarellas, J.M. Garcia and P. Rodriguez, "Modeling and Sensitivity Analyses of VSP based Virtual Inertia Controller in

HVDC links of Interconnected Power Systems", *Electric Power Systems Research*, Elsevier, vol. 141, pp. 246–263, 2016.

- **E. Rakhshani**, D. Remon, and P. Rodriguez, "Effects of PLL and Frequency Measurements on LFC problem in Multi-Area HVDC Interconnected Systems", *International Journal of Electrical Power and Energy Systems*, Elsevier, vol. 81, pp. 140-152, 2016.

- **E. Rakhshani**, "Intelligent linear quadratic optimal output feedback regulator for a deregulated automatic generation control system", *Electric power Component & systems*, Vol. 40, No. 5, pp. 513-533, 2012.

Conference (2011-2016):

- **E. Rakhshani**, D. Remon, A.M. Cantarellas, P. Rodriguez, "Frequency control of HVDC Interconnected systems considering derivative based inertia emulation", *IEEE PES General Meeting*, Boston, 2016.

- **E. Rakhshani**, D. Remon, A.M. Cantarellas, H. Mehrjerdi, P. Rodriguez, "Derivative based Inertia Emulation of Interconnected Systems Considering Phase-Locked Loop Dynamics," *IEEE PES General Meeting*, Boston, 2016.

- **E. Rakhshani**, D. Remon, A.M. Cantarellas, K. Rouzbehi, P. Rodriguez, "Integration of renewable generation for frequency support of HVDC/AC interconnected systems under power market scenario", *IEEE PES General Meeting Conference & Exposition*, pp. 1-5, 2014.

- D. Remon, A.M. Cantarellas, **E. Rakhshani**, I. Candela, P. Rodriguez, "An active power synchronization control loop for grid-connected converters", *IEEE PES General Meeting Conference & Exposition*, 2014.

- **E. Rakhshani**, A.M. Cantarellas, D. Remon, P. Rodriguez, I. Candela, "Modeling and control of multi modular converters using optimal LQR controller with integral action", *IEEE Energy Conversion Congress and Exposition* (ECCE), pp. 3965-3970, 2013.

- **E. Rakhshani**, A.M. Cantarellas, D. Remon, A. Luna, P. Rodriguez, "PSO-based LQR controller for multi modular converters", *IEEE ECCE Asia Downunder (ECCE Asia)*, pp. 1023-1027, 2013.
- **E. Rakhshani**, A.M. Cantarellas, P. Rodriguez, R. Teodorescu, "Comparative Study on Power Transmission Modeling in Large Scale AGC Power System", *International Conference on Renewable Energy and Power Quality* (ICREPQ), Bilbao, Spain, 2013.
- **E. Rakhshani**, A. Luna, J. Sadeh, P. Rodriguez, "PSO Based Optimal Output Feedback Controller for Two-Area LFC System", *20th Mediterranean Conference on Control and Automation*, (MED), Barcelona, Spain, 2012.
- **E. Rakhshani**, A. Luna, K. Rouzbehi, P. Rodriguez, "Application of Imperialist Competitive Algorithm to Design a New Optimal Controller for Two-Area Deregulated LFC System", *IEEE Industrial Electronics Conference, IECON*, Canada, 2012.
- **E. Rakhshani**, A. Luna, K. Rouzbehi, P. Rodriguez, "Effect of VSC-HVDC on Load Frequency Control in Multi-Area Power System", *IEEE Energy Conversion Congress & Exposition*, (ECCE), USA, 2012

CHAPTER 2.

State of the Art

Energy is a very important issue in all around the world while energy demands increased incessantly in the last decade. Beside of problems associated to energy production from coal, the new trend in the world are to increase the share of renewable energy sources in the production of electrical energy. In parallel, the concept of deregulation and competition in energy have forced scientists and engineers to think deeper about the challenges related to the paradigm change in large scale power system [2.1]-[2.2].

2.1 Introduction

2.1.1 Deregulation

In the deregulated scenario of power industry, the vertical structure is replaced by a fully deregulated power system with many independent producers. Therefore, in many countries, Vertically Integrated Utilities (VIU) are not exist anymore. In the competitive scenario of power industry, Transmission Companies or (TRANSCOs), Distributed Companies or (DISCOs) and Generation Companies or (GENCOs) are the main players which are working under supervision of Independent System Operator (ISO) [2.3]-[2.5]. In the deregulated power system, competition is the main goal of energy privatization. In this way, access to the transmission system and the possibility of presenting ancillary services are two relevant issues in this environment, where there can exist a lot of power producers (like DGs) and DC interconnections (like VSC-HVDC). In this kind of environment, DC interconnections are very important to act as corridors to transfer power based on possible scenarios.

2.1.2 Growth of renewable energy

According to Figure 2.1, energy consumption in the industrial sector will be rapidly increased in the next decades but, in parallel, new policies will be set around renewable energies. So by this increment, it is obvious that traditional sources of energy have to be replaced by renewable source of energy while, at the same time, necessary infrastructures and new technologies should be implemented until 2030 [2.6].

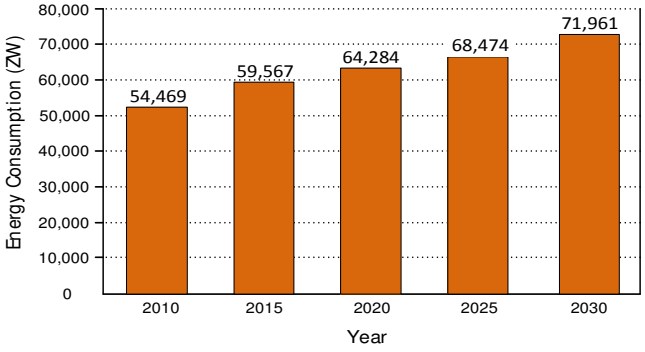

Figure 2.1. Consumption of industrial sectors in the world in the period of 2006–2030 [2.6].

For example, solar power is a type of energy with great future potential. Based on European Photovoltaic Industry Association (EPIA) and International Energy Agency (IEA) reports, the world cumulative PV capacity, for example, reach at least to 178 GW, which was sufficient enough to supply at least 1 percent of global demand of electricity. While for 2015, the global deployment of about 55 GW is expected and the installed capacity should be double or triple around 500 GW from now until 2020.

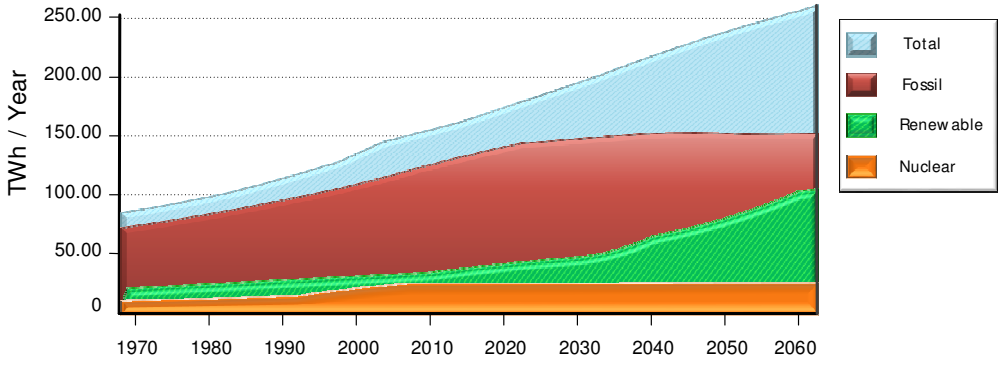

Figure 2.2. Global energy consumption [2.7].

As shown in Figure 2.2, the electricity based renewable will be faced with a remarkable increase by 2030 [2.7]-[2.9] while, at the same time, we can see a significant growth of global energy consumption [2.7]-[2.8]. This suggest that renewable type of energy can play a very important role in the future modern power system. However, in order to enable distributed generation as a major source of energy in the near future, it is very important to make an intensive effort for developing such advanced technologies.

2.1.3 Growth of DC interconnections

Nowadays, we are facing with growth and extension of AC systems and as a result with more complexity and stability problems. As it was explained in previous Sections, increasing level of distributed generations and deregulated energy markets get in conflict with increasing rate issues with increasing rates of energy consuming, making necessary to apply more advanced technologies. One of the way for increasing the overall stability and reliability in large-scale power system, is to interconnecting the neighboring areas. These interconnections could be performed by HVDC links especially in the case connections between asynchronous areas or in case of very large distance connection between a source of energy and demand centers. In addition, the actions of HVDC links, as a secure and safe corridors for fast transferring the power, will be very important in the liberalized scenario of power markets. All of these new challenges could be faced up with advanced technologies of HVDC transmissions.

One of the main advantages of DC links is related to direct and fast power flows between two areas without overloading of existing AC system.

Furthermore, in addition to higher reliability, the HVDC links can act as a useful firewall during cascaded disturbances. Therefore, it can prevents overall blackouts. It should be noted that, in some applications, the HVDC or hybrid interconnections, consisting of HVAC and HVDC links, turned into the preferred solution. The HVDC link between Sweden and island of Gotland is known as a first commercial application of DC link in 1954 [2.10]. After that, a huge increase for HVDC application can be observed all around the world. As shown in Figure 2.3, HVDC become a reliable technology and more than 120 GW HVDC transmission capacities have been installed worldwide up to now. There will be a huge increasing in HVDC applications in future power systems and researching in this area is very important.

As shown in Figure 2.4, energy capacities vary from one part of the world to other, making transportation of this energy to load centers, especially based on open market, a very interesting issue. For example, in north of Africa there are a huge area with an

outstanding capability for solar energy and applying DC links from north of Africa to south of Europe is one of the main important applications in this field.

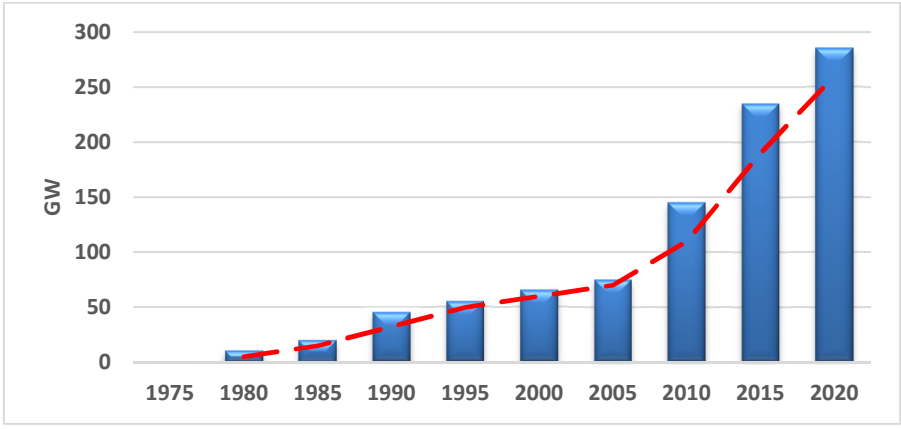

Figure 2.3. Worldwide DC transmission capacity.

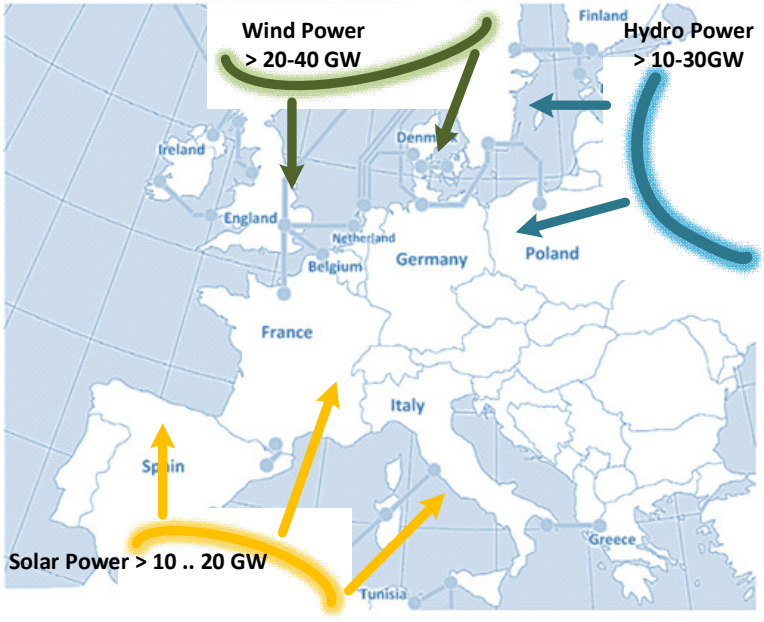

Figure 2.4. Energy accessibilities and HVDC applications for transferring.

Based on this brief introduction, what is clear is that future power systems are a very challenging issue with high penetration of DGs, DC transmission and high complexity.

Scientists and engineers have concentrated their research efforts to change such challenging electrical scenario. Advancements in technologies, such as the use of modern power processing systems, energy storage and control techniques in high-power applications, as well as high penetrations of renewable source of energies and liberalization of power markets, have led to a reformulation of the conventional power systems, moving to a more flexible scheme, which is broadly known as modern power systems. Modern distributed power systems are still going through their first steps nowadays. So far, the most significant advancement is related to the generation side. DGs are proposed by some new generation approaches considering the fact that generated electricity should be as close as the load centers. However, many other fields still remain in a very initial state. It is the case of the HVDC Supergrids, which are planned to act as energy corridors between different countries and to integrate far distance renewables. Even though HVDC is reached to the level that is ready for different application with capability of long distance transmissions for large amounts of power, the typical projects including multi-terminal HVDC connections are not yet an the most optimum industrial reality. Energy storage systems is another technology which is expected to become essential in future power systems. EES will allow improving the performance of the system by optimizing energy flows, attenuating power disturbances, and minimizing negative effects associated to the intermittent behavior of RES. It should be noted that the EES systems have attracted lots of attentions in the recent years and more large scale application are predictable by the future.

It should be noted that, the capability of generating and processing power in modern power system must be supported with a significant level of computational capacity considering the whole structure of the system. The control patterns which is currently in use for conventional systems cannot be extended to a modern scenario, which makes necessary to look for new solutions.

2.2 Modern Power System

Conventional power systems is changed and developed into a rapid steps of deregulation. Integration of power electronic based components, distributed applications of energy storage and different concerns regarding climate change and high penetration of renewable energy resources like PV in the power system are the main factors of interests in modern power system studies [2.11].

2.2.1 Conventional power system

In conventional power system, the utilities are typically managed by government. In other words, traditional power system was a kind of vertical structure which maintains a large amount of physical components, considering all the generation units and transmission systems. The utility has the control of all the generators and based on real time power flow a new set-point to all the units will be allocated for different situation. That is clear that this type of unchallenged situation is not fair and considering a huge increment in the amount of distributed generation and independent power producers, a new restructure and kind of deregulation was necessary for power system [2.3].

2.2.2 Conventional energy sources

Generally, the main source of energy in conventional generation are related to the base power generation (fossil fuel or coal based generations or nuclear power plants) and fast ramping generation (like hydro power or gas turbines). Figure 2.5 shows one the most common scenarios in conventional generation which is based on coal fired power.

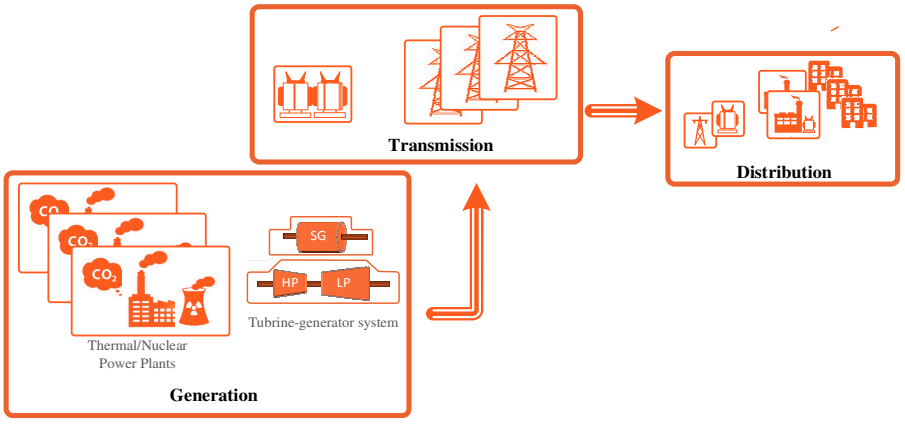

Figure 2.5. One example of conventional power generation.

The generated power in this type of units will be transmitted to load centers with high voltage transmission line or sometimes with under-ground cables.

In such generation system, coal will be prepared and passed to a boiler. Usually a boiler will be a complex system consisting of many sequences for abstraction of energy from the fuel. [2.11].

2.2.3 Power system deregulation and its requirements

As it was explained, GENCOs, DISCOs and TRANSCOs considering ISO are the main players of competitive scenarios of power market [2.3]-[2.5]. The main goal of restructured power system is competition. Therefore, the main issue in such scenario is the possibilities of open access to the transmission system and the possibility of providing different ancillary services.

It is very important to involve the ISO in a way that a fair transmission system be provided for all the players of the market. In this way, it would be possible that each GENCO have the possibility of making individualized contract for each specific DISCO in the market. Ancillary services should be also involved as well as competitiveness of the system to provide a high quality electricity to the consumers. It should be note that, in modern power system, ancillary service could be kind of complementary task in terms of a grid operation with high penetration of renewable sources. It can reduce the level of uncertainty which will be produced by renewables [2.12].

2.2.4 Ancillary services

Ancillary services are known as individual parts of electric services that required to provide sufficient support to energy supply, delivery of high quality power in reliable manner and acceptable operation for the transmission system. Some of the main parts of the ancillary services are related to operation of reserve capacities, regulation of reactive power, voltage regulation and active power or frequency regulation [2.3].

2.2.4.1 Active power balance and frequency control

Figure 2.6 shows a general scheme of typical frequency control regulation at different control levels. Usually frequency regulations will consists three different control level with different time responses. Based on the UCTE standard, three control levels are named as primary (droop) control, secondary (supplementary) control and tertiary

control level. Usually, all of these three different control action are presented during operation of large-scale interconnected power systems [2.13]-[2.14].

Primary (droop) control. This local automatic control will adjust the active power generated by each generator units to naturally maintain the balance between consumption and generation [2.13]-[2.16]. At this control level, the generation units which are located in one area with the same frequency will be involved. This control will be performed based on the inertia of each unit and their natural responses of the governors.

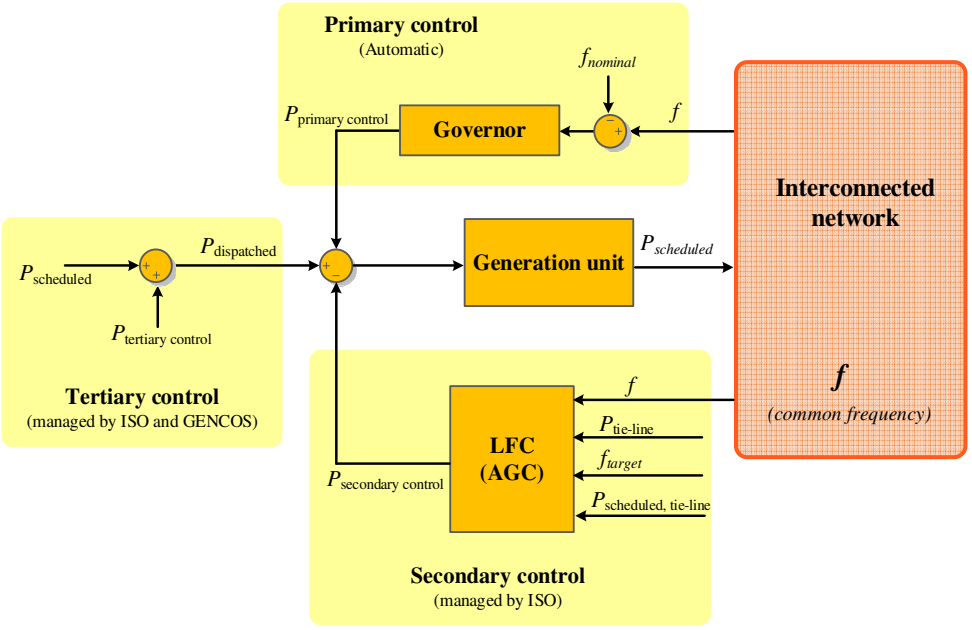

Figure 2.6. General structure of frequency control based on UCTE regulation.

Secondary (supplementary) control. This control action is higher level control trying to minimize the steady state error of active power or frequency control deviations. This control level will deliver sufficient reserve powers to control the frequency and tie-line power in their scheduled values.

Tertiary level of control. This level of regulation is mainly related to manual tuning of dispatched units and unit commitment to act as back-up for secondary control and taking care of optimal operation of generation units and managing severe contingencies of transmission systems.

2.2.4.2 Spinning reserves

In fact, for performing a suitable frequency regulation it is necessary to maintain some amount of power as a reserved capacity. This reserved power can be used for performing the required balance between generation and consumption during the time. In Figure 2.7 different type of reserve capacity which will be used in real practices are presented. These reserves are related to different contingencies with different time frames [2.14]. Usually in literatures, the spinning reserve is known as an unused capacity that could be activated based on the decision of ISO. This reserve could be provided with different devices which have to be synchronized to the grid. They should be able to contribute on changing the active power [2.14].

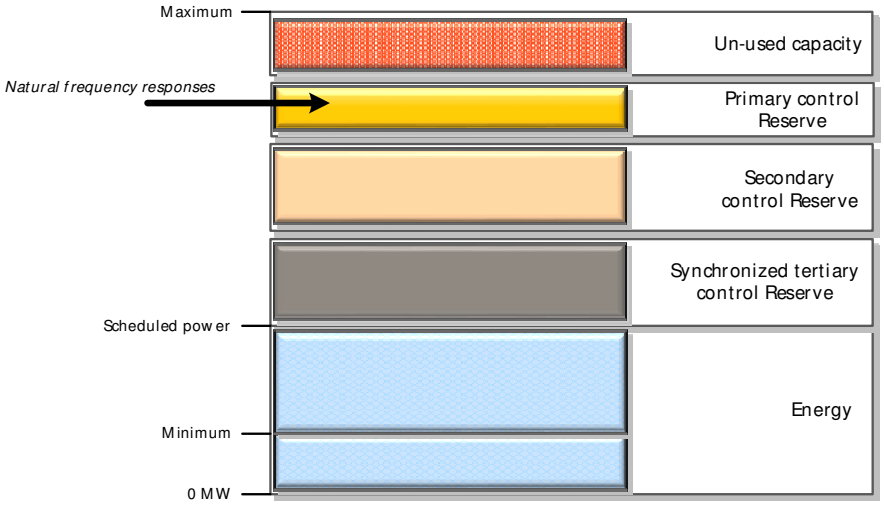

Figure 2.7. Participated of reserved unit for different levels of frequency regulation [2.14].

2.2.4.3 Reactive/voltage control services

Normally the controllable generators can control the voltage level at the terminal node with modifying (injecting or absorbing) reactive power. For example, in case of lower value for terminal voltage the amount of reactive power will be increased [2.14]-[2.16]. Different control levels are presented in Figure 2.8. The first control level for terminal voltage regulation in one synchronous generator. This control will be performed by the excitation system. In the hierarchical structure of voltage regulation, the set-points of lower levels will be provided by higher level controls. Usually, the AVR (Automatic Voltage Regulator) in the control loops of synchronous generators is known as lowest

level. The second level is known as coordinated Secondary Voltage Regulator (SVC) and the last level will be Tertiary Voltage Control (TVC) which is the highest level.

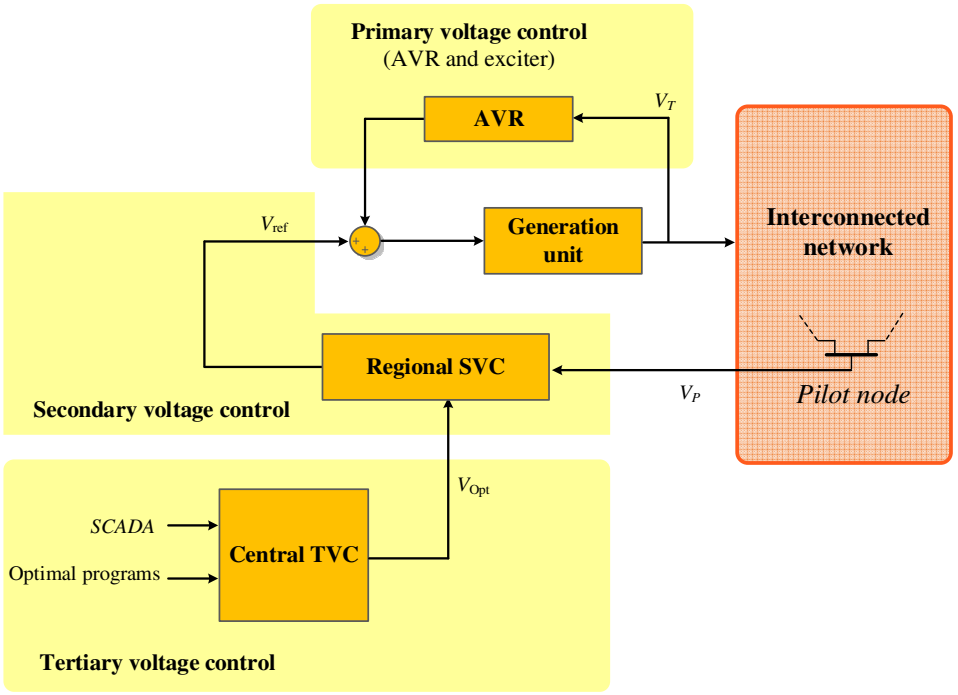

Figure 2.8. Levels of voltage control.

Primary voltage control. As it was mentioned, this control level is mainly related to local controller. Local controllers are AVR for synchronous generator or Load Tap Changer (LTC) for some transformers. They can provide a very fast control actions in case of any load variation. Their main responsibility is to keep the voltage bus at its desired values. There are also different type of controllable devices for this purpose. Static voltage compensators is one of this devices that can also participate in this primary control action [2.15].

Secondary voltage control. This control level is a kind of centralized automatic regulation that can coordinate all the local controllers in their regional voltage zone. This coordination will be performed by changing the local set-points by injecting or absorbing reactive powers. In many different countries, some sort of experience for this secondary control is reported [2.17]-[2.18]. Usually, for this control level, a pilot bus will be defined. This bus will be used to manage the reactive power resources for

providing a suitable voltage profile. This pilot bus voltage will represent the voltage which is related to its neighborhood.

Tertiary voltage control. This control level will be used for more coordination and better optimization. In this level, different type of optimal power flow programs can be used which will bring more regulation. Usually the time constant of this control level is in the range of 15 minute to hours [2.19]-[2.20].

2.2.4.4 Ancillary services and technologies

For supporting the operation of the power grid, ancillary services will be required. Some of the well-known ancillary services are frequency regulation, load flow control, voltage and reactive power regulation and some security responsibilities which are handled by operator of the systems.

However, as soon as the grid becomes more and more complex, new installations and technologies are needed to provide such functionalities to the system. For example HVDC and FACTS equipments are very important tools in this area [2.21]-[2.22]. In case of HVDC technologies, its main application is for interconnecting the areas with different frequencies. Considering the global integration of renewable energies and exigencies from competitive markets, make necessary to equip the network with several DC interconnections at high voltage level between its areas. For this reason, it is necessary to perform more investigation in VSC-HVDC links as a bi-directional interface between areas based on applying the last technologies in power electronics. Back to Back topology is one of this type of DC interconnections which usually linked for long distance transmission overhead lines or by submarine cable. It mainly used for large amount of power. A much more frequent use of these type of HVDC links can be predicted in near future which will accomplish the requirements in the restructured power system [2.22]-[2.24].

Also, storage technologies depending on their characteristics may aid the integration of renewable sources and they could assist the operation/control of a power system especially in case of ancillary services [2.10]. The main technologies include: pumped hydro [2.24], compressed air storage [2.25], batteries [2.26], super capacitors and super magnetic energy storage (SMES) [2.27].

2.2.5 Importance of distributed power systems

Advances in power processing and control systems and liberalization of electrical markets have led to a deregulation in electrical power grids. It moves the system from centralized approaches the some more flexible generation schemes, which usually known as distributed power systems (DPS).

Currently, electricity is mostly generated by large centralized facilities, mainly supported by fossil fuels, nuclear, or hydro. The electricity generated by these plants is radically transmitted long distances, since they are usually built away from consumption centers [2.28]-[2.29].

The generation scheme used in DPS, known as DG, proposes a new electric power systems approach, being electricity generated near where it is used, mainly using RES. Some of the main factors behind the growth of DG are about environmental issues (since DG limits the greenhouse gas emission), efficient use of energy and competitive issues [2.28]. Usually distributed generation can be divided on three different types. This classification is mainly related to the manner of their connection to the power grid. For example they can be connected directly to the grid (like gas turbine generators, GTG) or connecting by power electronic components like PV. They can be mixing of these connection approaches like wind turbine generation (WTG) [2.30]. Recent advancements in power processing issue of power converter components will bring more capabilities in terms of control of a DG. It can bring more possibilities to participate in power grid by providing more ancillary services. In some application, the drawbacks of conventional generators control can be improved [2.29].

2.2.5.1 Scientific and technological efforts

In order to have DPS in reality, several challenging issues need to be taken in to account for more study and research in both academia and industry. For example, the growing use of distributed power units based on RES will be switched to a highly stochastic situation that could have a considerable impact on the instantaneous power variations [2.31]-[2.33]. Furthermore, optimized large scale integration of DG will be led to a scenario with higher implementation of energy resources. This issue can cause the power grid to work very close to their limits of stability [2.34]. The large-scale integration of RES will contribute to the expansion of DC networks to interconnect more and more areas by using HVDC links. The matter of control and coordination will be extremely challenging and important issue in large scale power grid application.

2.2.5.2 Advanced control concepts in DPS

As it was explained, the increase of renewable based generation like wind and solar, with their highly stochastic behavior, can affect the operation and stability of power system. Accordingly, the DPS should be provided by newer and completely advanced control approaches with some abilities in coordination of multiple power sources operation in real time application. This real time coordination will let the system to operate with high penetration of RES. Adding the issue of market and competitiveness of the overall system will bring more and more complex scenario in terms of control and operation which will be challenging issue. So it is necessary to make an serious research effort in this field to apply advanced optimal control method [2.34] and new concepts, like active networks and smart grid [2.35]-[2.36], to enable an efficient and more reliable control and operation for modern power grid.

In conventional power network, usually the control problems were traditionally solved at the planning stage and the nature of the system is passive (means the direction of power is from generation to consumption [2.37]. However, modern power systems, with high penetration of RES, are extremely stochastic, which eventually results in a strong impact on the instantaneous power balance [2.36]. Many DGs can act as an active element especially considering the act of energy storage elements. Therefore, in such scenario, active control and management (ACM) of DGs will be extremely important especially in terms of stability and performance improvements of the grid [2.38].

One of the main challenges of ACM application is in term of control, especially considering the large scale multi area interconnected power systems. By increasing the number of large-scale power electronic based generations like PV, wave and wind, proposing new advanced control and also suitable grid synchronization are very important. By means of new advanced control concepts, there will be a possibility of interacting DGs in power grids with more functionalities like ancillary services and more positive effects on dynamics. In this way, it would be predictable that storage systems can play a key role for solving many of drawbacks of high scale integration of DGs to the grid. There is a great possibility to expand the EES application in different parts of the system, like generation level [2.39] and distribution levels [2.40]-[2.42]. For example in the generation level, conventionally, power converters works in a constant power manner which is not appropriated for the stability of the grid, especially in the abnormal conditions. Application of EES presents solutions to the control of power converters to behave like a synchronous generators. In such concept, a short-term storage system will be combined by renewable resources [2.41]. Also in order to

increase the designer capabilities and degrees of freedom for achieving a better controller, different type of intelligent control method may be used. As an example, recent researches explore some heuristic methods, like genetic algorithm [2.42], particle swarm optimization [2.43], or imperialist competitive algorithm, to find the most optimal solution for the plant under control [2.44].

2.2.5.3 DC interconnection in Modern Power Systems

Electricity was originally dispersed by using direct current (DC) and with the existence of some small local networks in the late of 19th century. But, during that moments, lack of technology and losses in the conductors, made the DC approach ineffective for transporting high amount of power for a very long distances. Therefore, Alternating current (AC) presented a better performance with much acceptable efficiency. Because by using transformers, it can be shifted to high-voltage levels with much less losses. But these days, considering significant improvement in power electronic technologies, it became possible again to use high-voltage DC (HVDC) transmission systems with a very effective manner. HVDC systems overcome the main drawbacks of HVAC transmission especially for a very long distance applications. As it was explained, there will be a significant increase on HVDC application in the future and considerable part of the future grid will be operated with several DC links [2.45].

Also, at the low-voltage level, many of the generation units used in DG will work with DC voltage in its primary conversion stage, like photovoltaic, electrochemical batteries or fuel cells. As results, it looks more logic the growing interest on using low-voltage distribution DC networks (LVDC) for avoiding unnecessary power transformations. Moreover, LVDC distributed power systems are very suitable scenarios to accept electrical distributed energy storage systems, e.g., batteries in electrical vehicles or residential generation facilities, uninterruptible power systems (UPS), or thermal storage, which allows supporting the AC distribution networks by providing ancillary services [2.46]-[2.47].

Therefore, research activities should be focused on control and stability issues considering mixed AC/DC systems with multi-terminal DPS considering their interactions with neighboring AC areas in multi areas interconnected scheme.

2.2.5.4 Regulation of ancillary services with DPS

Ancillary services, such as frequency control, regulating and management of reserved capacities, reactive power control and voltage or power flow management can be provided in a distributed manner by using DGs [2.49]-[2.52], that can allows improving

the controllability of the multiple buses of the system. The need for much better advanced control of DGs is very important. This issue became clearer when several generators are connected to a weak grid and many power quality problem can be observed. Therefore, it is necessary to analyse in detail the ancillary services provided by DG to improve performance and reliability of DPS. It is also important to investigate different mechanisms to regulate the grid services market at the distribution systems level [2.53].

It is necessary to note that, in case of frequency control, lack of inertia is known as one of the most important issue that bring serious instability problems in a system with high penetration of DGs. It is predictable that any method for adding sufficient virtual inertia to the DGs, can significantly improve the dynamic and robustness of the system [2.54]-[2.55]. Therefore, the main research and technological effort to be made in the field of DPS should be focused on analyzing modern configurations of power systems. These methods should propose new design solutions and control techniques which is addressed to optimization of their rating and to guarantee their stability. Power flow analysis, modal analysis, transient and steady-state stability studies, unit commitment issue and considering economic load dispatch analysis are some of the techniques that will be extensively applied to analyse DPS consisting of both conventional power plants and DG units equipped with modern power processors based on power electronics, which offer a high controllability degree. Moreover, other cutting edge technical solutions, such a FACTS, power conditioners, energy storage, HVDC networks, intelligent measuring systems, and communication networks will be also considered in this analysis.

2.3 Advanced DC Interconnection

The need for transmitting power over long distances with lower losses and higher stability has been always the main challenge for transmission technologies. This issue is more critical considering the facts like AC power deregulation, competitive markets with high penetration of power electronic based components in modern power systems. Recent developments of renewable energy integration and super-grid interconnections in modern power systems, attracts a lot of attentions to HVDC transmission which is known as a proven tool for dealing with new challenges of future power system. The capability of DC systems to transmit higher power over longer distances, the possibility of interconnecting asynchronous networks, and their high efficiency, has maintained the interest of both industry and academia.

According to previous Sections, complex and highly stochastic power systems will experience more problems than simple ones regarding their operation and stability. For example, active power losses, reactive power losses, optimal active power transmission, frequency control issues, interconnection, lack of inertia in weak areas and finally black out prevention. As shown in Table 2.1, the HVDC system which is based on voltage source converter (VSC) technologies are a very good solution for these issues because of its advantages in fast and decoupled active/reactive power control [2.56].

Table 2.1. Comparison of transmission with different technologies [2.57].

Low Voltage Line	**HVAC**	**LCC-HVDC**	**VSC-HVDC**
Max Voltage Level	750 kV	800 kV	640 kV
Substation volume	Small	Big	Medium
Cable installation	Complex	Simple	Simple
Installation Cost - Substation - Cables	 - Low - High	 - High - Low	 - Highest - Low
Need for Compensation	Yes	Yes	No
Losses - Substation - Cables	 0.3% High	 0.8% Low	 1.6 to 1.8% Low
P control	No	Yes	Yes
Q control	No	No	Yes
Grid interconnections	Synchronous	Any	Any
Power flow reversal	Fast	Slow	Fast

In Table 2.1, a general comparison between HVDC and HVAC lines is presented. It should be noted that in HVDC systems there is not any limit regarding transmitted distance. The VSC technology could be a better technology in the future. Some of the main reasons are: the ability of VSC in fast and independent control of both active and reactive power and changing the direction of power transmission in VSC could be done without problem (while in classical HVDC system, is can be done by DC voltage reversal). Also in VSC technology, compared to classic HVDC, the risk of communication failure is reduced a lot (VSC is a self-commutated switched). Better possibility for black start with VSC is another advantage of this technology compared to classical one.

Nowadays, developments in power electronics have made possible to use high voltage DC (HVDC) lines in an effective manner, which makes possible to question original reasons justifying the extended use of AC networks. DC links have a very fast control on power flow, which implies stability improvements. Moreover, power flow direction can be changed very quickly (bi-directional) and HVDC can carry more power for a given size of conductor. VSC technology allows controlling active and reactive power independently without any need for extra compensating equipment (like STATCOM or SVC).

2.3.1 HVDC configurations

As shown in Figure 2.9, there are four main configurations in HVDC power transmission systems such as monopolar, bipolar, back-two-back and multi terminal HVDC transmissions. As shown in this figure, for monopole configuration, two converters could be separated using a single pole line. This configuration is usually applied for cable transmission with submarine connections [2.56]-[2.59]. In the bipolar configuration, two conductors (one positive and other negative) are used. Connections between each end converter are grounded and as a result, the two poles may be used independently. This type is so common configuration in modern system.

In other topology (back-to-back), two stations are located in a common site and the length of line distance will be kept as short as possible [2.60]. This type of HVDC system is used for interconnecting two AC systems with different frequencies (asynchronous interconnection) [2.61].

The multi-terminal HVDC transmission system consists of several (more than two) converter substations, some of them working as inverters and the others as rectifiers [2.62]. It is expected that in a near future, when protection of meshed DC networks and

long distance multi-terminal transmission become economically effective, this topology will replace the conventional point-to-point topology which is currently used in HVDC transmission systems. Moreover, based on the allocation of the power conversion substations, normally two type arrangements are used, i.e, series and parallel multi-terminal HVDC systems which are explained in the following sub-Sections.

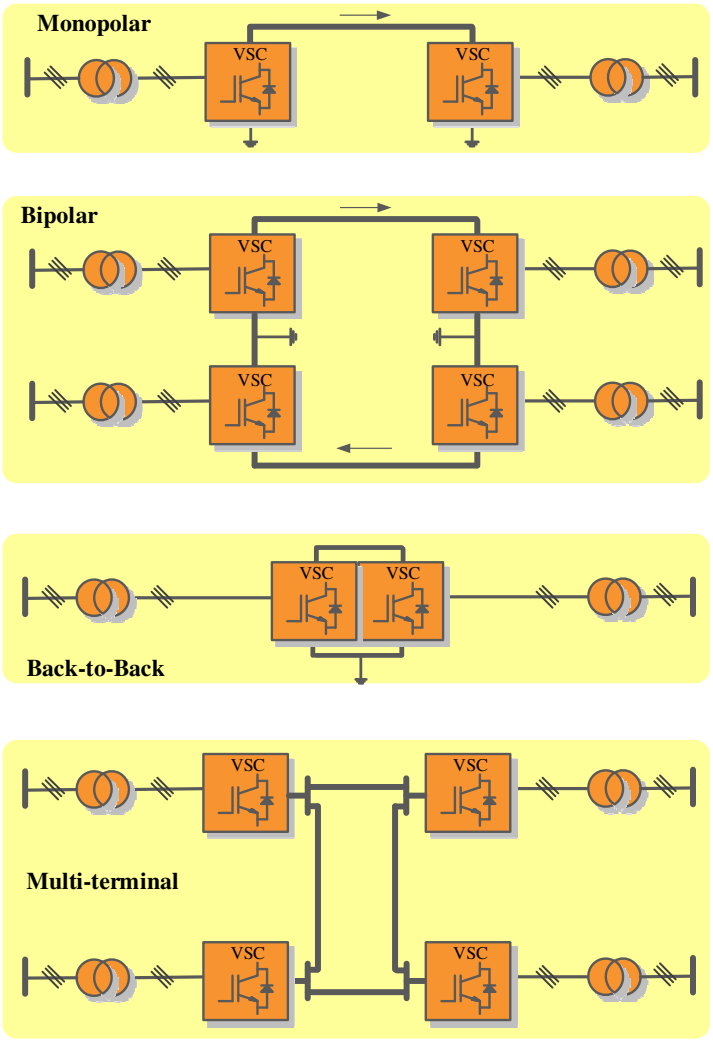

Figure 2.9. General configurations of HVDC systems.

2.3.2 Classic HVDC

A classic HVDC system operating in conventional bipolar mode and consists of AC filters, shunt capacitor banks or other reactive compensators, converters, transformers, DC reactors, DC filters and DC lines or cables.

For controlling these conventional topology, one of the power converters controls the DC voltage and the other controls the active power transported through the DC-link.

Line-commutated current source converters (LCC HVDC) based in silicon controlled rectifiers (SCR) is one of the conventional techniques used in classical DC transmission of power. The HVDC schemes based on the LCC technology absorb reactive power from the connected grid due to the fact that the commutation of the valves is driven by the connected power grid. The reactive power mentioned has to be compensated by using switched capacitor banks on the AC side. In addition to this, filtering is necessary both on the AC and on the DC sides in order to fulfil the corresponding requirements. In LCC HVDC connections, the power flow can be bidirectional and, depending on power flow direction, the polarity of the DC voltages must be changed [2.56].

2.3.3 VSC HVDC

HVDC connections based on voltage source conversion (VSC HVDC) present many advantages respect to the ones based on the LCC HVDC technology. The power converters used in VSC HVDC systems are controlled by using the pulse width modulation (PWM) technique, making possible a bi-directional control of active power flow without changing DC polarity. Moreover, the VSC allows full reactive power control, without any extra compensating equipment [2.56]. These power converters can operate in capacitive and inductive mode, with positive or negative active power flow. The VSC-HVDC can be used for voltage control to compensate the needs of the connected network within the converter rating.

There are two main control loops in this type of power transmission systems. One of the loops is devoted to active power and/or DC voltage control, while the other one is in charge of reactive power and/or AC voltage control. The rectifier parts usually are responsible for controlling the AC active power flow whereas the inverter parts are in charge of controlling the DC voltage level. Each converter is also responsible for controlling reactive power or AC voltage.

Recent developments in modular multilevel converters (MMC) have revolutionized the VSC technology. This converter type, which was proposed by R. Marquardt [2.63], consists of several units, referred to as sub-modules, connected in series as shown in Figure 2.10.

2.3.3.1 *Multi Modular HVDC Systems*

Voltage source converters (VSC) are very important in future DC transmission systems. Their topologies and modulation schemes have a significant effect on the performances of VSC-HVDC. Currently, the main VSC-HVDC projects are based on two-level or three-level topologies, with high blocking voltage switches and a switching frequency much higher than fundamental frequency, which brings demanding filtering requirements and significant power losses.

To solve these limitation a new VSC topology, shown in Figure 2.10, based on modular multilevel converter (MMC), which is very suitable for HVDC and FACTS applications, has been proposed in recent studies [2.62]-[2.64].

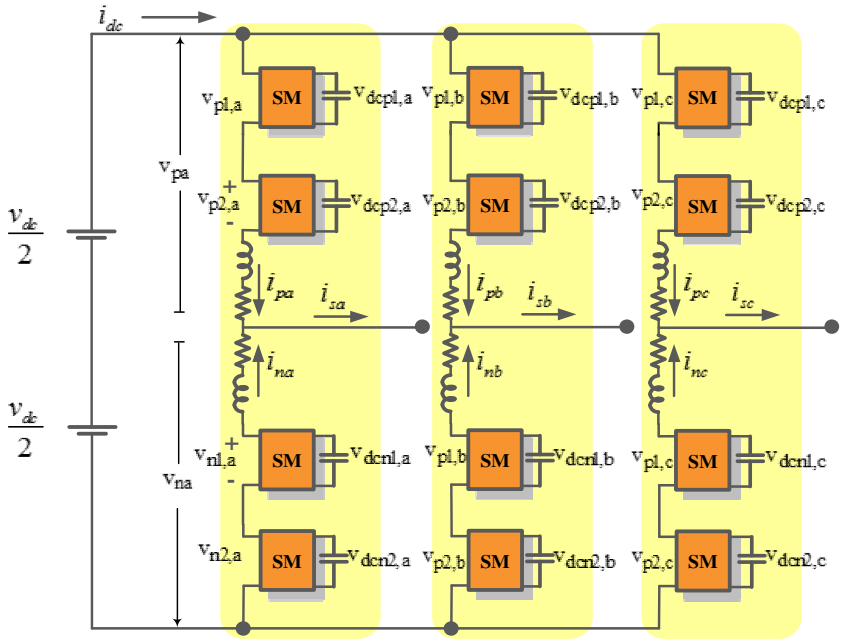

Figure 2.10. Average model of MMC.

Among various types of multi-level topologies of converter, the multi modular converters have received a lot of attractions. The main application of these MMC will be

on medium and high power level of application mainly for HVDC systems [2.64]. By means of several modules at each arm of the modular topologies is possible to have an excellent output AC waveform without special requirements regarding grid filtering [2.65]-[2.66]. Moreover, considering its unique topologies, a highly modular design is achievable. Therefore, the overall topology will bring brilliant scalability. The complete design could be implemented for a very high range of voltage and power with a great flexibility with much lower range of switching frequency and therefore with much lower losses in the system. Due to its modular construction, this topology is optimal for medium and high voltage application like HVDC transmission [2.65].

The basic operation of MMC is described in [2.65]. By comparing the structure of conventional VSC technologies [2.67]-[2.68] with the one for the MMCs, various advantages can be found, such as a higher voltage application with modular structure and more reliability. Also, harmonics compensation is another interesting feature of MMC to improve the quality of voltage [2.66]. However, in spite of these advantages, control of the MMC is a very critical and challenging issue.

The main technical challenges in control of an MMC are related to modelling and balancing the sub-module capacitor voltages to their nominal values and minimizing the circulating currents. Recently, several papers discussed the modelling and control of MMC in various ways [2.69]-[2.74]. For solving the limitation of high computation time of MMC during the simulation cases with very high level converters, a simplified dynamic model based on the Kirchhoff's Law is presented in [2.69]. In [2.70]-[2.72] different issues regarding voltage balancing and suppression of voltage oscillations in the capacitors of MMC are discussed and presented. Application of model predictive control is also reported by [2.73]. In this reference, another way for eliminating the circulating currents and voltage balancing is presented.

It should be note that in the real applications of MMC, with high voltage levels, the system will consists of a large number of sub-modules, which make its control a very challenging issue. Considering the number of sub-modules, especially for real applications of MMC, the number of states that should be under control dramatically will increase. Therefore, application of conventional control theory for such complex multi input multi output system will not be an easy task. Application of advanced modern control could be one of the main solutions for this issue. In this sense, linear quadratic regulators (LQR) could be a good candidate for this purpose [2.75]-[2.76].

2.3.4 Control of HVDC Systems

In conventional VSC based HVDC transmission, one converter will control the DC link and the other converter station will take care of active power control. It has the ability of controlling the power transmission in both direction. In terms of control of HVDC system, there are several methods for controlling the HVDC as discussed before. Many research papers are using damping and transient improvement for controllable components based on modulation control for damping the oscillation modes [2.77]-[2.80]. Some works are focused on developing a system with parallel AC line and HVDC link for dynamic improvement. A modal analysis considering the deviations of grid frequency or the difference angle between the connected nodes is presented [2.81]-[2.82]. Identification based modelling is another control approach for analysing the system which is presented in [2.83]-[2.86] and application of single controllable components to the HVDC system (like static var compensator or Thyristor-controlled series capacitor link), have been proposed to improve the performance of the system, as discussed in [2.87]-[2.89].

Linearized based model and advanced control approach were proposed in [2.90]-[2.92] for HVDC links, while some proposals are based on nonlinear exact-feedback linearization [2.93]-[2.94]. In this method, by means of nonlinear feedback, the system is transformed to a linear one, making possible to apply well-known linear control. This approach is based on MIMO linearization and could be applied to small-signal and also transient stability analysis for the whole system. But in order to have better understanding for choosing the best control approach, it is necessary to make a review on the main control concepts in HVDC. The main control structure of HVDC system will be explained by the next Chapter.

2.3.5 Multi-Terminal Interconnected HVDC Systems

The most common HVDC systems have two converters. But as an extension, a Multi Terminal HVDC (MT-HVDC) system can be used in some application with more than two long distance geographic zones which have to be connected [2.95]. Such a system with several converters gives rise to more challenges, as well as more flexibility in term of control and dynamic stability improvement. Based on different topologies and applications, the main control challenges in MT-HVDC systems are in the regulation of DC voltage and the coordination with neighbour AC areas.

Multi-terminal systems have more than two terminals for interconnections and the main topologies for MT-HVDC system are series or parallel. In series systems, the DC

current is set by one terminal and it is a common magnitude for other terminals. In series MT-HVDC systems, overloading cannot exceed 20% of total rating in major terminal of MTDC system. On the other hand, the parallel arrangement is more practical than series and voltage is common for all paralleled terminals. In case of parallel system the ratings cannot be less than 20% of total rating in major MTDC system [2.95]-[2.98].

As shown in Figure 2.11, parallel topologies are classified in two radial or mesh multi terminal HVDC systems. It should be noted that, one of the main limitation of radial system is that if one segment became disconnected, the rest of the terminals will be disturbed. But in case of mesh systems, if one segment interrupted, the rest of the system will remain functional without any problem for power flow transmission [2.98].

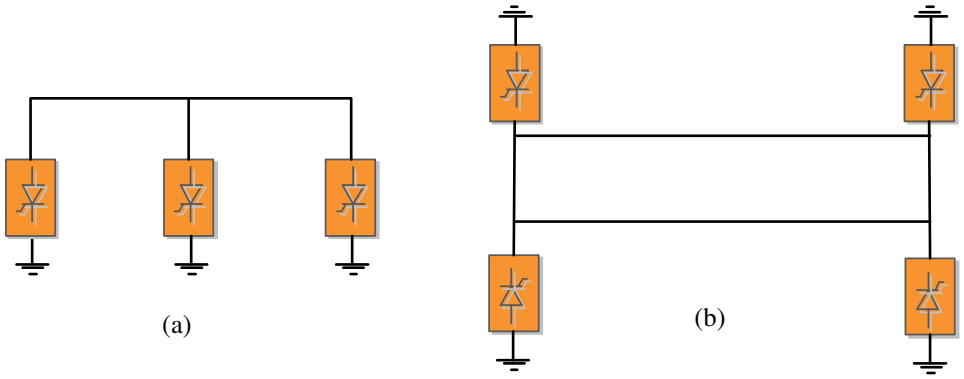

Figure 2.11. Parallel shape of MTHVDC system: (a) radial, (b) mesh.

Controlling of multi terminal HVDC system is a complex task and limited research has considered the possibility of full control in several HVDC links in connection with AC system. A new way of coordinated control of several DC links with improving the inter-area oscillating modes was proposed in [2.95] and [2.99]. There is a lack of complete research in this area, especially in multi area complex systems and more study in this field will be quite merited.

CHAPTER 3.

Review on HVDC Modeling and Control for Power Systems Applications

In power electronic applications, the highest power ratings are those associated with the power conversion stages of HVDC power transmission lines. Transmission systems based on HVDCs have shown to be a good solution for large scale bulk power transfer over long distances. In large scale modern power system analysis, DGs and power electronic components, as in the case of HVDC, are increasing, and it is necessary to have reliable models in order to improve the design and application studies. In this Chapter, a general background on HVDC modelling and control for high level control application in interconnected power systems is briefly presented and some models for different applications are reviewed. Finally, a proper small signal model, useful for AGC application, is also explained.

3.1 Two-Terminal HVDC

Today, there are two main technologies for HVDC system. One of them is based on voltage source converter (VSC) technology and the other type is related to thyristor based classical technologies. Currently, it is well-known that VSC based systems has different advantages in comparison with the classical system [3.1]-[3.2]. For instance, as it was mentioned, the VSC system provides a fast and independent control for both active and reactive powers. In addition, the power transfer in VSC based systems are bidirectional. By using this technology, interconnections between two weak AC systems is also possible.

The typical configuration and control structure of DC transmission with two-terminals is presented in Figure 3.1. The core of this system are two VSC stations. Usually, one of this stations can act as a rectifier and the second station will act as an inverter. Generally, the rectifier station will control the DC link and the inverter station can contribute in controlling of active power transmission. Power flow in this system has the ability of transferring in both direction (Bi-directional). There are several methods for controlling the current in the HVDC links. In this field several research works have been presented based on the use of PI controllers in the dq synchronous frame, as well as some other which are based on the implementation of proportional resonant (PR) controllers working in the $\alpha\beta$ frame [3.3].

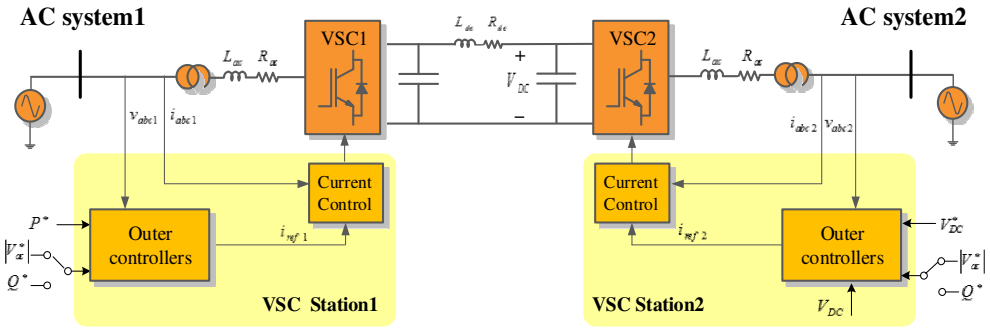

Figure 3.1. General structure of the VSC based HVDC control system.

The main control blocks in DC transmission are depicted in Figure 31, where the inner loops and outer control loops are shown. The inner loop of control or current loop control of HVDC is a fast dynamic control system which is responsible of controlling the AC current injection by means of acting on the PWM of the power converter. The current reference for the inner controller are provided by the outer control loop. As it was introduced in the previous paragraph different control methodologies can be used for implementing the inner controller [3.3].

One the other hand, the outer control loops is responsible for generating the current reference to be provided to the inner loop. The active current component of the reference is obtained from the DC voltage, active power and frequency controllers, being thus a combination of these three in order to comply with the needs of the frequency control, the power delivery and the controllability of the device itself. Likewise, the reference value for the reactive current to be delivered can be derived from AC voltage controller and reactive power controller.

3.2 Averaged modeling and control structure of HVDC system

As shown in Figure 3.2, the average model of power converters is based on a controllable sources in both side. In the AC sides, a controllable voltage source and for the DC side, a controllable type of a current source could be used for modeling purpose. This could be a general model of a normal grid feeding converter. Usually, a proportional integral ,PI, control can be used for controlling the DC voltage or energy state of DC link and for controlling the injected current a proportional resonant, PR controller, could be used for generating the proper references for converter operation.

One of the main reason for implementing PR controller is their ability to provide a selective and accurate control with offering an infinite gain for the fundamental frequency of the gird. By means of this control an acceptable performance for current controller could be achieved. In this control structure, a PLL will be used just for better tuning and better estimation of the grid frequency. This control will be based on stationary reference frames [3.3].

$$PR = K_p + \frac{K_I s}{s^2 + \omega^2} \tag{3.1}$$

The AC reference for current controllers will be provided by outer loops which are much slower than the inner control loop. Based on the applications for each VSC in the HVDC link, different actions like DC link regulation, controlling of AC voltage or control of active and reactive power can be implemented.

In this averaged model the high-frequency PWM characteristics are neglected and all the scenarios could be based on balanced conditions. As it was explained, the average model consists of a controllable voltage source for the AC part and a controllable current sources for the DC part of the converter station. This parts are presented in Figure 3.2.

Therefore, the set-points for voltage references will be generated by the action of inner loop control and a controlled type current source is also used for presenting and modelling the relationship between the AC part and the dynamic variations of the DC voltage caused in DC link capacitors.

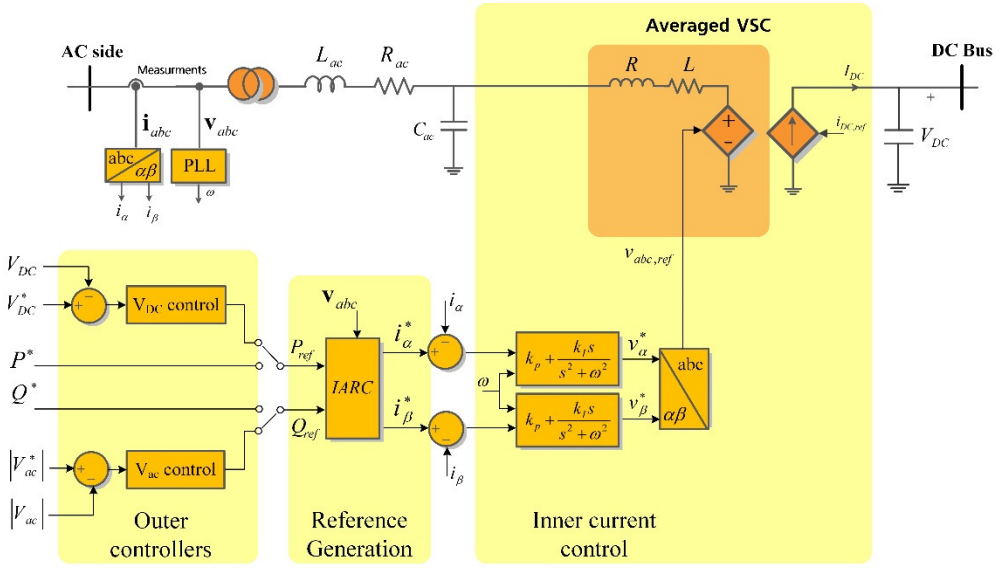

Figure 3.2. Structure of the average model for VSC.

By neglecting the converter losses and considering the balance between ac and dc-side powers, a proper reference for controllable current source in the DC part will be obtained as follows:

$$I_{DC,ref} = \frac{P_{ac}}{V_{DC}} \tag{3.2}$$

$$P_{ac} = v_a i_a + v_b i_b + v_c i_c \tag{3.3}$$

The concept of IARC which is known as Instantaneous Active Reactive Control can be used to determining the set-point values for the current control of the converter. Based on this concept, any current vector which is aligned by voltage vector v will be belonged to active power, while any current vector which is aligned a voltage in quadrature$v_\perp$, can produce the reactive powers, thus the following equations [3.3]:

$$\begin{aligned} i_p^* &= \frac{P}{|v|^2} v \\ i_q^* &= \frac{Q}{|v|^2} v_\perp \\ i^* &= i_p^* + i_q^* \end{aligned} \tag{3.4}$$

where the norm value for the grid side voltage, $|v|^2$, can be obtained in different reference frames [3.3]:

$$|v|^2 = v_a^2 + v_b^2 + v_c^2 = v_\alpha^2 + v_\beta^2 \tag{3.5}$$

The input signals of IARC are active and reactive power references which are generated by outer loop controllers. Generally, for controlling VSC-HVDC systems the following operation modes may be implemented in outer loop control:

- Constant P –V_{AC} control: in this case, the converter station maintains the active power and voltage of the AC grid at fixed levels. In this mode, the reference active power could be generated by higher control layers which are related to frequency droop control in the AC grid.

- V_{DC} –V_{AC} control: in this case, the VSC station will take care of the energy balance in DC-link by controlling the DC link voltage. In case of connecting to a weak AC grid the ac bus voltage could be controlled to have a fixed value.

- P–Q control: in this mode, the VSC will control the active power and the reactive power in a independent manner.

- V_{DC} –Q control: the control mode will be applied in a situation that a stiff network is connected by one of the HVDC terminals and it is necessary to control the DC link voltage and reactive power at the same time.

3.3 Simplified model and control structure of HVDC system

In the case of electromechanical analysis and simulations in multi machine power systems, a simplified model of the converter can be used in two terminal HVDC links. In fact, considering the differences in time constants especially for low frequency analysis and electromechanical application, the action of inner current control loop could be neglected. Because the time scales of current controller and mechanical part of conventional power system regulations are totally different.

This type of simplified modelling will be useful for understanding the dynamic effects of HVDC links on power system stability studies. As explained before, the averaged model of converters consist of a structure based on an inner current loop control and outer loop controls. The dynamic response of the inner current loop is in the range of 20 ms and the electromechanical dynamic response of multi machine power system will be in the range of multi seconds (voltage control) and multi minutes (frequency control). Therefore, it is obvious that the dynamics of the inner current loop is negligible compared to dynamic of multi machine power system. The proposed VSC model with this simplification is presented in Figure 3.3, while inner current control loop is replaced by some second-order time delay function and the rest of the model will be the same.

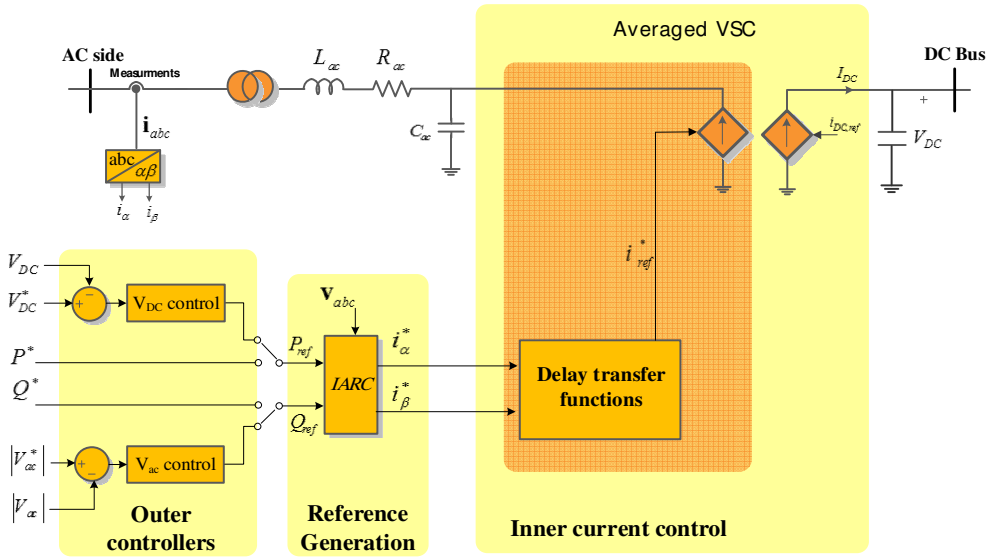

Figure 3.3. Structure of the simplified average modeling for each VSC.

In this model, the DC link control loop will be kept for further analysis and the inner part of the converter will be modeled only as a current source. For achieving the same dynamic as average model with current controller, the sensitivity of the system's response was checked through simulation by adding different steps on P and Q references. Based on the obtained results, higher order properties (dominant second-order dynamics) were observed in the response of the original averaged model. Therefore, as shown in Figure 3.4, four different transfer functions are applied for emulating the dynamics of a complete averaged model with current controller.

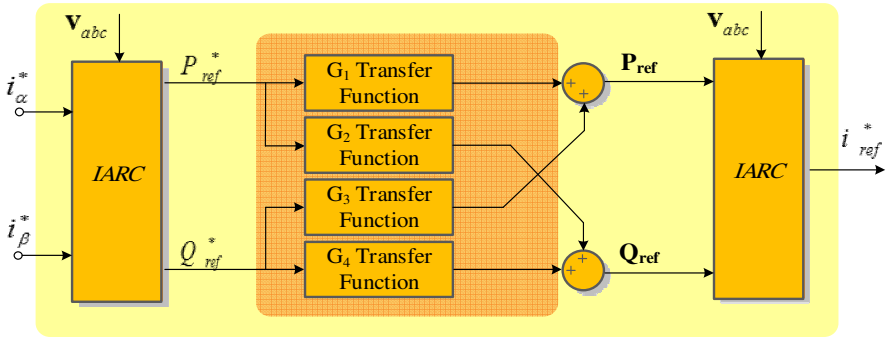

Figure 3.4. Transfer functions that emulate the dynamics of inner loop controller.

For considering the complete effects, the four Transfer functions written as follows are considered:

$$G_1(s) = \frac{\omega_n^2}{2\zeta\omega_n s+\omega_n^2},\quad G_2(s) = \frac{2\zeta\omega_n s}{2\zeta\omega_n s+\omega_n^2},\quad G_3(s) = \frac{0.2(2\zeta\omega_n)s}{2\zeta\omega_n s+\omega_n^2},\quad G_4(s) = \frac{2\zeta\omega_n s+\omega_n^2}{2\zeta\omega_n s+\omega_n^2}$$

For applying this model in discrete mode for different sampling times, all the function should transfer to the z-domain. Assuming that $y_i = \omega_{ni}^2$, and $w_i = 2\zeta_i\omega_{ni}$, and after the z-transformation and the discretization, the following discrete transfer functions can be found:

G1: Tustin method:

$$G_1(z) = \frac{y_1T_sz + y_1T_s}{z(2w_1 + y_1T_s) + (y_1T_s - 2w_1)} \tag{3.6}$$

G2: Forward method:

$$G_2(z) = \frac{w_2 T_s z - w_2 T_s}{z^2 + z(w_2 T_s - 2) + (1 - w_2 T_s + y_2 T_s^2)} \tag{3.7}$$

G3: Forward method:

$$G_3(z) = \frac{0.2(w_3 T_s) z - 0.2(w_3 T_s)}{z^2 + z(w_3 T_s - 2) + (1 - w_3 T_s + y_3 T_s^2)} \tag{3.8}$$

G4: Forward method:

$$G_4(z) = \frac{w_4 T_s z + (y_4 T_s^2 - w_4 T_s)}{z^2 + z(w_4 T_s - 2) + (1 - w_4 T_s + y_4 T_s^2)} \tag{3.9}$$

where T_{sw} is the sampling time, T_s is the stabilization time and f_{sw} is the switching frequency, which can be found as:

$$T_{sw} = \frac{1}{f_{sw}}; \quad f_s = 4 \times f_{sw}; \quad T_s = \frac{1}{f_s}; \quad \zeta \omega_n = \frac{4}{20\, T_{sw}} \tag{3.10}$$

A general comparison between these two different averaged models are presented in Figures 3.2 and 3.3. For checking and evaluating the simplified averaged model of converter, a general case in Matlab platform is simulated.

In this study case it is assumed that a step change for P and Q happens at 0.1 sec. The active and reactive power performance is presented in Figure 3.5. The dynamic response of the averaged model with inner current controller is presented in Figure 3.5.a, and the response of the system with simplified average model without current controller loop is presented in Figure 3.5.b. It is obvious that, considering the added transfer functions in simplified averaged mode, the same dynamics are achieved. In fact, with a proper selection of ζ_i the desired dynamics in simplified model could be achieved.

The main difference lays on the simulation times which is much faster for the simplified average model. This model will be useful during large scale simulations of multi machine power systems. The three-phase current measured at the terminal of each converter is compared and presented in the Figure 3.6.

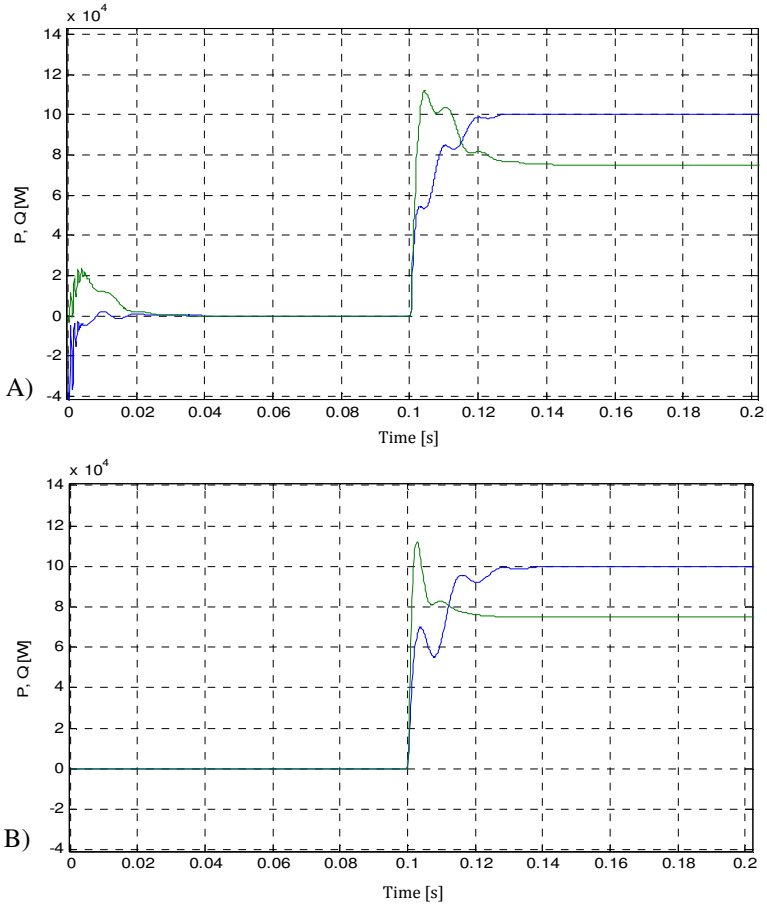

Figure 3.5. Active power and reactive power performance:
a) Average model with current control, b) Simplified model.

The response of averaged model with current controller is depicted in Figure 3.6.a and the response of the simplified averaged model is presented in Figure 3.6.b. It is obvious that the same dynamic is achieved and simplified model could be used for large scale simulations considering the dynamic effects of current controller.

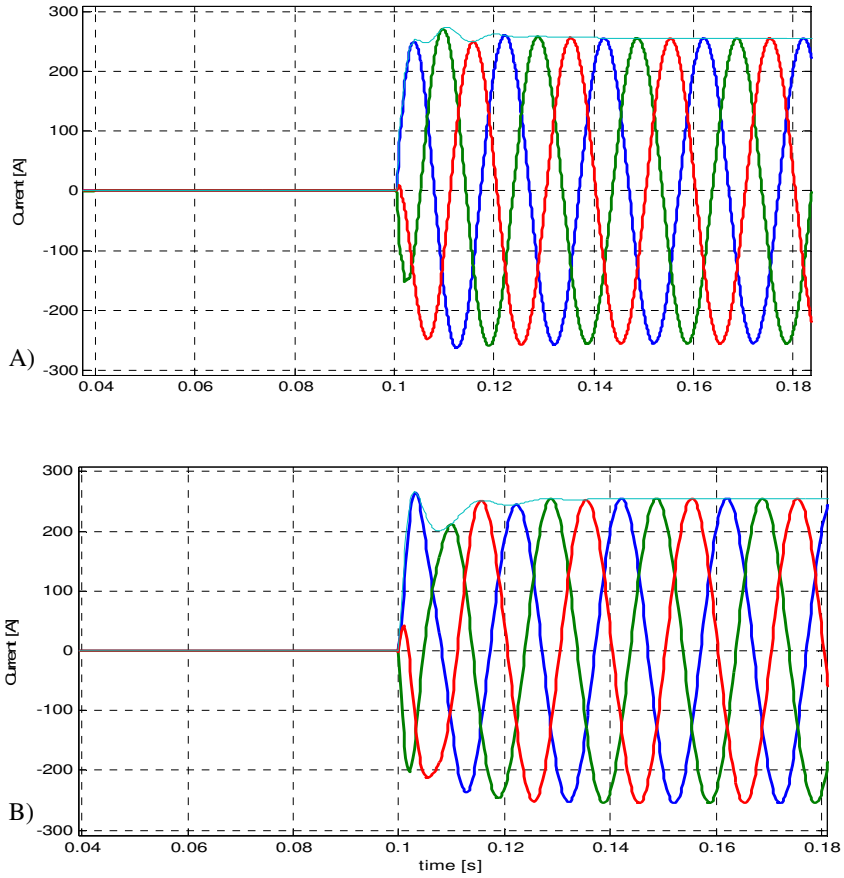

Figure 3.6. Three phase injected currents:
a) Average model with current control, b) Simplified model.

3.4 Small-signal HVDC modeling for higher level control design

In case of small signal modeling for the pre-design process of high level control layers, such as the design of AGC, each converter station could be simplified with a first-order model which a transfer function with a proper time constant. For the HVDC system with two VSC station, the second-order transfer function will be approximated by the equivalent first-order transfer function, emulating the overall time response of HVDC system. Therefore, it can be written as:

$$\frac{1}{1+s\,T_1}\times\frac{1}{1+s\,T_2}=\frac{1}{1+(T_1+T_2)s+(T_1T_2)s^2}\cong\frac{1}{1+s\,T_{DC}} \tag{3.11}$$

where T_1 and T_2 are the time constant of VSC converters and T_{DC} will be the equivalent time constant of overall HVDC control system:

$$T_{DC}=T_1+T_2 \tag{3.12}$$

Therefore, the incremental power flow through the HVDC transmission system could be modeled by using a linear first-order model with a proper time constant (shows in Figure 3.7. Here the linearized first-order model for small signal analysis is presented in [3.4]:

$$T_{DC}\frac{d\Delta P_{DC}}{dt}=\Delta P_{dc,ref}-\Delta P_{DC} \tag{3.13}$$

where $\Delta P_{dc,ref}$ is the desired dc power and ΔP_{DC} will be the real dc power flow through the system.

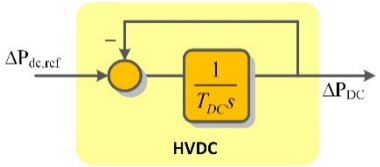

Figure 3.7. Block diagram of the small signal HVDC system.

It is assumed that the DC line has no losses and hence the output power from one converter is transmitted to the other. As shown in Figure 3.8, $\Delta P_{dc,ref}$ is the input signal of HVDC which will be generated by different control signals.

These signals are due to frequency deviations of each interconnected areas and AC power flow deviations (in case of any parallel AC line with HVDC transmission link).

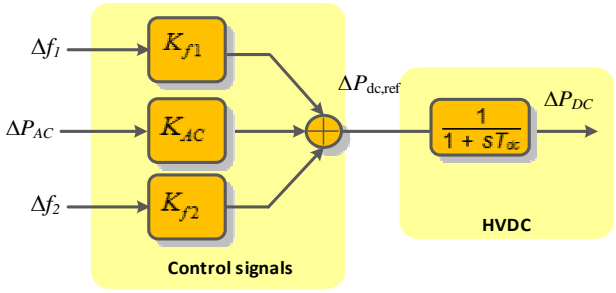

Figure 3.8. Control signals of interconnected area with small signal model of HVDC.

In reality, the time response in HVDC system for transferring multi Megawatt power will be in the range of 300 ms to 500 ms. In most of the power system literature, the typical value is considered to be around 200 ms [3.5]-[3.6]. In reference [3.6], which is based on realistic parameters, the proper time response is 300 ms for T_{dc}.

A general comparison for different values of HVDC time constant is presented in Figure 3.9. This comparison is performed for two-area interconnected power system which is used in details by the next Chapters. The two areas are connected by parallel AC/DC links. As shown in Figure 3.8, is the input reference signal of the HVDC link is generated by different control signals, (deviations of frequency in both areas and tie-line power deviations). These control signals will be provided from supervisory control layer and k_{f1}, k_{f2}, and k_{AC} will be the corresponding control gains.

Based on the presented response of DC link derivation, it is obvious that different time constant for DC link will have some effects for the system behavior. Higher time constant will bring slower response with smaller peak values. This value should be selected based on the realistic values for each application.

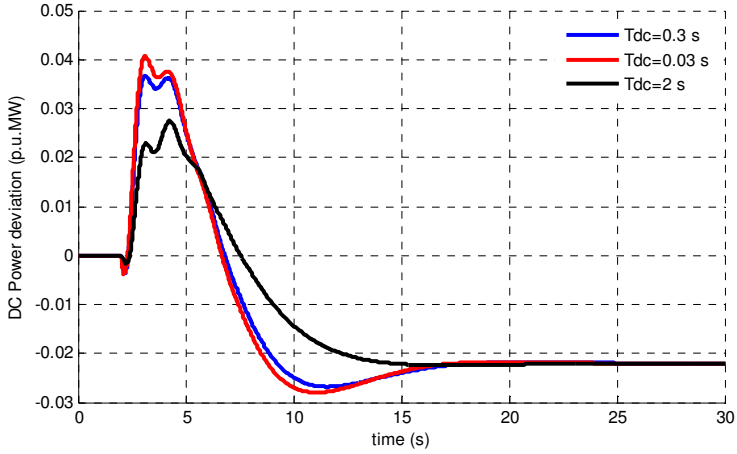

Figure 3.9. Comparisons of DC power deviation for different time constants.

CHAPTER 4.

Automatic Generation Control of Interconnected Power Systems

This Chapter is devoted to carry out a brief presentation and explanation of the active power regulation and control structure in AGC, which is known to be as one of the most important control actions in large-scale multi area interconnected power systems. The AGC concept belongs to a high level control stage at the transmission level. This control layer will generate the set-points for all the local components which are in turn controlled by their local controllers [4.1]-[4.2].

4.1 Introduction

AGC of a large scale multi area interconnected system during load/resource variation is known as a very important mechanism that could facilitates various tasks like: frequency restoration, tie-line power control between authority areas and economic dispatch of generation units [4.3]-[4.5]. Interconnections of several areas could be provided by AC or DC lines considering their specific values for exchanging the power between different areas. This interconnections can also provide sufficient support from each neighboring area in case of abnormal conditions [4.1].

Because of several limitations associated with AC lines especially for long distance connections, HVDC links have received an increasing attention in recent years. HVDC interconnection is one of the main applications of power converters in multi-area interconnected power systems and it provides several advantages such as: Fast and

bidirectional controllability, power oscillation damping and frequency stability support [4.6]-[4.7]. As it was explained in previous Chapters, the HVDC systems can contribute actively in improving the reliability and dynamics of multi area interconnected systems. It could also act as a kind of firewall avoiding different cascaded disturbances, preventing thus the propagation of global blackouts. For these reasons, in some parts of the world, HVDC or hybrid interconnections, consisting of parallel AC and DC interconnections became already the preferred solution [4.8]-[4.9]. It is worth to mention that in addition to emergency control of frequency stability in conventional AGC structure; a proper coordination of AGC with modern HVDC transmission would be also possible [4.10]-[4.11].

Therefore, in this Chapter, a brief explanation about AGC model in AC connections and AC/DC interconnections will be presented. The model proposed model in this Chapter is based on small signal modelling and dynamics of large scale interconnected systems though HVDC and HVAC lines leading to a new control block diagram. This model is very suitable for pre-evaluations of dynamic effects of DC links in large scale power system design. In the future modern power system, DC interconnects and energy storage devices will play a very important roles in system stability and it would be very important to have clear idea about the system dynamics and power ratings for different case studies.

Modern power system with several DC interconnections and renewable resources made the electrical system more and more complex and conducting dynamic analysis based on realistic values of our power system is necessary. By means of using the proposed model, it would be possible to model the power system in several areas considering their nature and their possible inertia. The proposed model should provide a systematic modelling and dynamic control for the interconnected systems and it should be easily extended for any type of complex system with more interconnected areas. This model is related to frequency support (LFC) and POD considering hybrid AC/DC transmission line with HVDC and storage technologies in AGC systems.

4.2 Fundamental of frequency control

Power balance is a very important factor which will affect the frequency of the system. Any type of mismatch between consumption and generation will bring deviation on frequency of the grid [4.4]. Hence, the control of the generated power and the frequency in large scale power systems is usually referred as (LFC) load frequency control.

4.2.1 Primary active power/frequency control

Frequency of the grid is a global factor through the interconnected systems. This is due to the nature of the power grid when any load perturbation or any type of mismatch will be reflected in all the part of the system (Figure 4.1). This issue mainly is related to LFC concept.

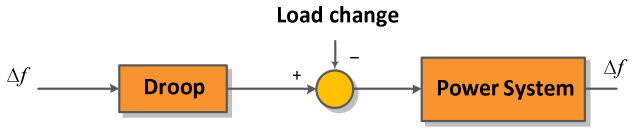

Figure 4.1. Generic representation of the frequency dependency on load changes.

The primary (droop) control is a common concept in large scale power systems studies. As shown in Figure 4.2, the first reaction of speed governors of generation units is due to the primary control or load frequency control. At this stage the system will try to stabilize the load change and the contingencies. As shown in this figure, later, when the secondary frequency control is applied, the steady state error of the frequency will be cancelled out [4.1].

4.2.2 Supplementary higher level control

It should be noted that, the primary control will not return the frequency to its nominal value, it just limits the drop leaving thus a steady state error which should be later cancelled in order to leave the frequency to the desired value (depend on the system it could be 50 Hz or 60). Therefore, an additional control called AGC will be applied to ensure that the area absorbs its own load change and also to maintain net interchanges and frequency at their schedule values.

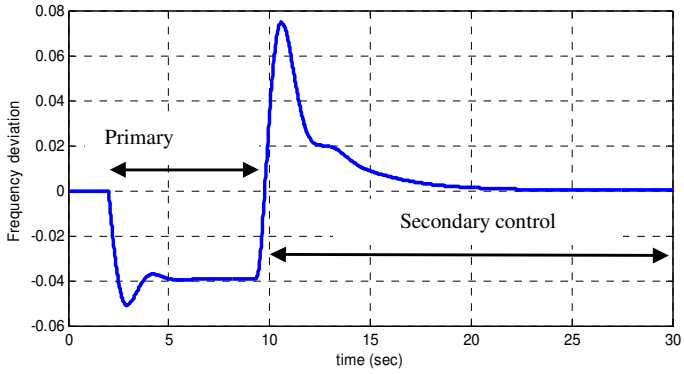

Figure 4.2. Frequency performance in Hz when the primary and secondary controls are applied.

As shown in Figure 4.3, the usual response time window for primary control goes from 10 to 60 seconds (NERC standards) and for secondary responses is in the range of 1 to 10 minutes [4.1].

It should be noted that the time constant of AVR or excitation system in generation unit is much smaller than the time related to the governor/prime mover actions. Therefore, the transient decay of excitation is much faster than governor and it will not affect the dynamics of LFC. Therefore, the coupling between frequency control action and voltage regulation control loops will be trivial and it is a very common practice to analyse the frequency stability issue independently [4.1].

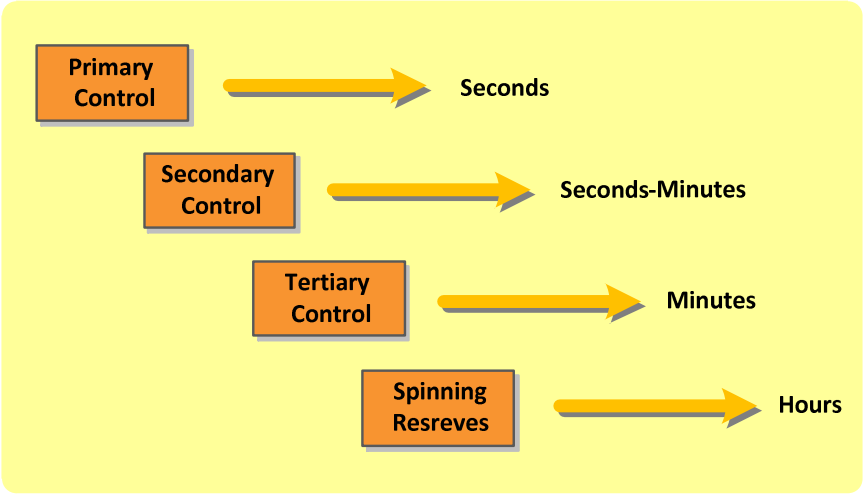

Figure 4.3. Control continuum [18].

4.2.2.1 Area Control Error

The area control error or the ACE signal is an important index for frequency control task. It will represent any type of imbalance between the demands and the generation levels for each area. The ACE signal will be a linear combination of frequency deviation and power mismatches [4.1]–[4.4].

$$ACE_i = \Delta P_{tieAC,ij} + \beta_i \Delta f \tag{4.1}$$

where $\Delta P_{tieAC,ij}$ is known as tie line power deviation between areas and β_i is known as a frequency bias in the area. This bias factor can be calculated like this:

$$\beta_i = \frac{1}{R_i} + D_i \tag{4.2}$$

considering R_i is the droop value for the GENCO units and D_i will be a the load-damping constant.

4.2.2.2 Area Participation Factor

The ara participation factor (apf) is another important signal for performing the AGC through the secondary control. In fact, if there are more than one generation unit in one area or if some generation units cannot participate in AGC, there is a possibility to manage their participation by means of the participation factor. It should be note that, sum of the all participation factors in each area should be is equal to one [4.2].

Therefore, as shown in Figure 4.4, by means of ACE signal and corresponding *apf*s, the new set-point for all the generation units within the areas will be determined.

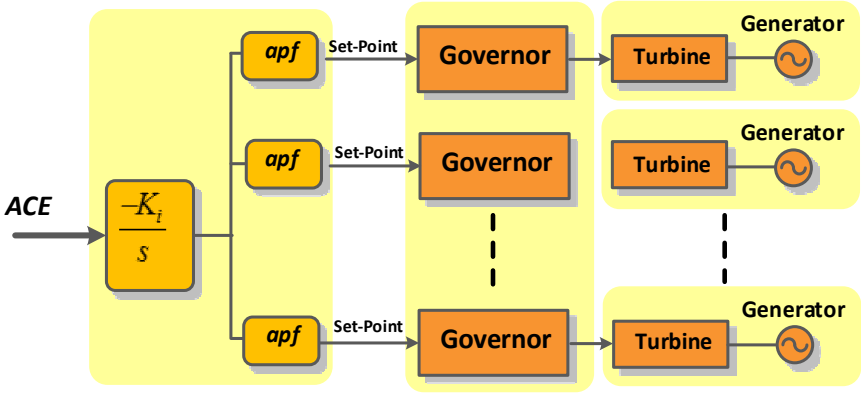

Figure 4.4. General strategy for power sharing in AGC control.

4.3 Mathematic dynamical model

In this Section, the mathematical equations for AGC in the interconnected system are presented. This modeling will be used for further detailed analyses which are based on the study of the eigenvalues and state space representation.

4.3.1 Generator-Load dynamic model

This model is based on the swing equation of synchronous generators. The stored energy in the mechanical part of the generator could be calculated as follows:

$$W_{ke}^{0} = H \times S_b \tag{4.3}$$

where S_b is the rated power in MW and H is known and constant of inertia. It should be noted that, kinetic energy will be proportional to the square value of the frequency/speed (fundamental one) and therefore the associated energy of $(f_0 + \Delta f)$ could be calculated as follows:

$$\begin{aligned} W_{ke} &= W_{ke}^{0}\left(\frac{(f_0 + \Delta f)}{f_0}\right)^2 \\ W_{ke} &\approx HS_b\left(1 + \frac{2\Delta f}{f_0}\right) \\ \frac{d}{dt}(W_{ke}) &= \frac{2HS_b}{f_0}\frac{d}{dt}(\Delta f) \end{aligned} \tag{4.4}$$

Then the power balance equation could be written as:

$$\Delta P_g - \Delta P_L = \frac{2HS_b}{f_0}\frac{d}{dt}(\Delta f)$$

$$\frac{\Delta P_g}{S_b} - \frac{\Delta P_L}{S_b} = 2H\frac{d}{dt}\left(\frac{\Delta f}{f_0}\right)$$

and in per unit, Δf is the same as $\Delta\omega$:

$$\Delta P_g(pu) - \Delta P_L(pu) = 2H\frac{d}{dt}\Delta\omega \tag{4.5}$$

In the dynamic analysis of the frequency stability, the most important part of damping is the one related to the sensitivity of load to the frequency variation which will define like this:

$$\left(\frac{\partial P_L}{\partial f}\right)\Delta f = D_f.\Delta f$$

where D_f (pu/Hz) is the sensitivity of the load change when there is a 1% of frequency change. In per-unit this sensitivity could be calculated as:

$$D(pu) = D_{unit}(pu) = \frac{P_{G,unit}}{S_{base,unit}}\ (pu), \text{ and } D_f(pu) = D_{unit}(p.u).f_0\ (\frac{pu}{Hz}) \tag{4.6}$$

Therefore, the complete swing equation considering the damping in p.u. could be written as:

$$\Delta P_g(pu) - \Delta P_L(pu) = 2H\frac{d}{dt}\Delta\omega(pu) + D(pu).\Delta\omega(pu) \tag{4.7}$$

where in p.u. $\Delta f(pu) = \Delta\omega(pu)$ and finally in the Laplace domain we will have:

$$\Delta f(s) = \left[\Delta P_g(s) - \Delta P_L(s)\right]\frac{K_P}{1 + sT_P} \tag{4.8}$$

where, considering inertia and damping of the system, we can define:

$T_p = \frac{2H}{D}$ (time constant of power system)

$K_p = \frac{1}{D}$ (power system gain)

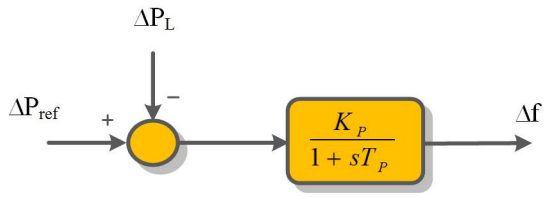

Figure 4.5. Block diagram representation of the generator-load in power system.

4.3.2 Governor-Turbine model

As explained before, the output of the generator is adjusted by means of the droop governor action. Moreover, for modelling the governor action a simple first-order function could be used.

$$\Delta P_g = \Delta P_{ref} - \frac{1}{R}\Delta f \tag{4.9}$$

$$\Delta P_v = \frac{1}{1 + T_g s}\Delta P_g \tag{4.10}$$

where ΔP_{ref} is coming from the area error performed when determining the set-points and ΔP_g is the input signal for governor system.

As shown in Figure 4.6, for modelling the turbine it is also possible to use the reduced order model of compound turbine with reheat system or a non-reheat simple model and the turbine could be presented as a first–order model [4.1].

$$\Delta P_m = \frac{1}{1 + T_t s} \Delta P_v \tag{4.11}$$

where the ΔP_v is the input signal that changes the steam valve position and T_t is the time constant.

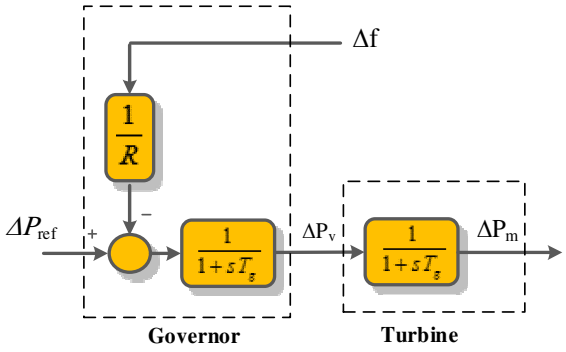

Figure 4.6. Turbine-governor model.

4.4 Multi-area interconnected AGC systems

4.4.1 Area Interface

Since the frequency is a global factor, any deviation will be reflected in the whole system, even in multi area interconnected systems. Therefore, the trend of the frequency measurement as an indicator should not be limited only for one area. The signal related to the tie line power deviations between areas should be properly considered in the LFC action.

Ideally, with using this supplementary control action, perturbation in any area should be corrected by the units of the same area, producing thus minor effects on the other area. While in the reality, (or when using more realistic modelling), we can see that by using AGC based on area control errors, contingencies in each area will have some effects on the neighbour areas which are closer.

The general model of an interconnected AGC systems is presented in Figure 4.7. Based on this model, it is obvious that ACE signals will be modified with new tie-line signals which are related to other interconnected areas.

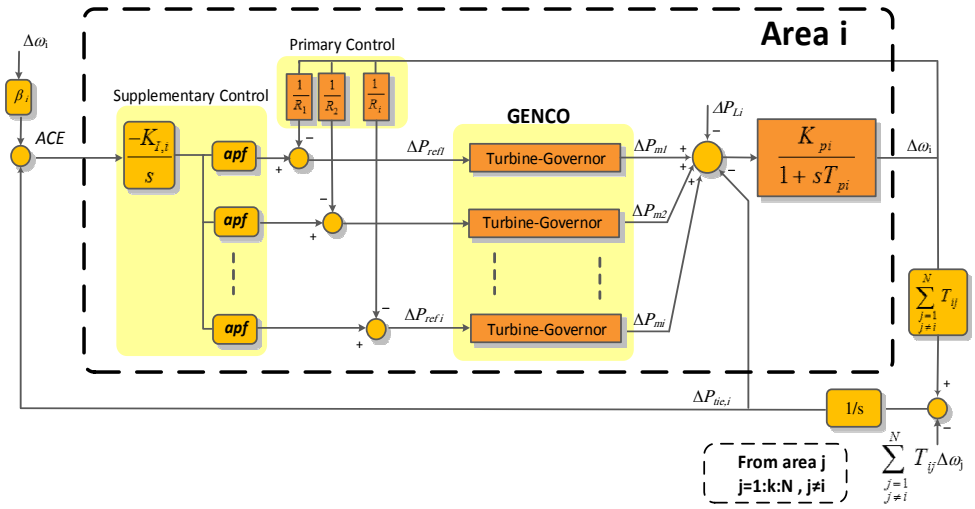

Figure 4.7. Frequency control strategy for dynamic analysis of interconnected systems.

The ACE control signal of multi-area systems, will perform the coordinated supplementary services like restoration of the nominal frequency, maintenance of the scheduled power flow between authority areas:

$$ACE_i = \beta_i \Delta\omega_i + \Delta P_{tieAC,i} \tag{4.12}$$

The power flow between areas is modelled by means of frequency deviations in the control areas. For modelling the interconnections between N areas in multi-area AGC system, tie line power deviation could be used as an additional signal. This deviation between i^{th} area and the rest of the system areas can be calculated like this [4.2]:

$$\Delta P_{tieAC,i} = \sum_{\substack{j=1 \\ j\neq i}}^{N} \Delta P_{tieAC,ij} = \frac{1}{s}\left[\sum_{\substack{j=1 \\ j\neq i}}^{N} T_{ij}\Delta\omega_i - \sum_{\substack{j=1 \\ j\neq i}}^{N} T_{ij}\Delta\omega_j\right] \tag{4.13}$$

$$\Delta P_{tieAC,ji} = \alpha_{ij}\Delta P_{tieAC,ij} \tag{4.14}$$

$$\alpha_{ij} = -\frac{P_{ri}}{P_{rj}} \tag{4.15}$$

where T_{ij} is the synchronizing coefficient between areas and P_{ri} is the rated power of each area.

4.4.2 Dynamic model of two-area AC system

A typical system for presenting a general model of interconnected systems is a modified Kundur model as an interconnected system with two areas [4.3] which is shown in Figure 4.8. It has two GENCOs and one DISCOs in each area. DISCOs can be considered as load demands.

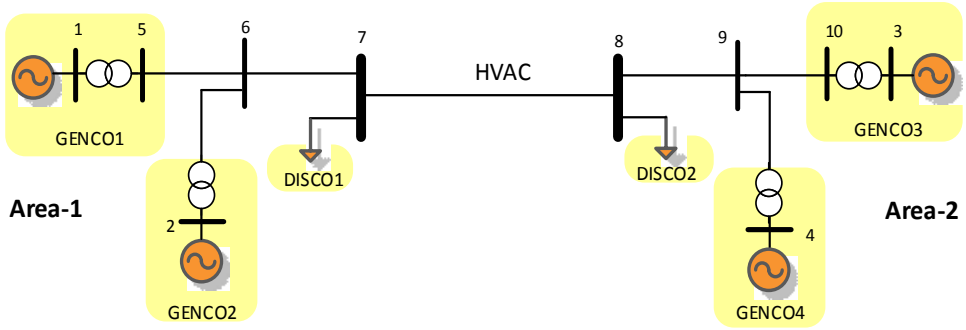

Figure 4.8. A two-area system with AC connection.

Therefore, the ACE signals for this interconnected model can be represented as follows:

$$ACE_1 = \beta_1 \Delta f_1 + \Delta P_{12} \tag{4.16}$$

$$ACE_2 = \beta_2 \Delta f_2 + \Delta P_{21} \tag{4.17}$$

considering *ACE* signal as control error for each area and:

$$\Delta P_{12} = \Delta P_{tieAC,12} \tag{4.18}$$

$$\Delta f = f_{actual} - f_{schedule} \tag{4.19}$$

while P_{12} is the deviation of transmission line, f is known as the grid frequency; β_i will be the bias factor [4.3].

Then, the closed loop system for LFC with two area interconnected system can be presented in the form of a state space as follows:

$$\dot{\mathbf{x}} = \mathbf{A}\mathbf{x} + \mathbf{B}\mathbf{u} \quad , \quad x(t_0) = 0 \tag{4.20}$$

$$\mathbf{y} = \mathbf{C}\mathbf{x} \tag{4.21}$$

This linearization can be used for control design steps and analysis. Considering **x** as the state vector and **u** as input vector of power demands.

$$\mathbf{u} = [\Delta P_{d1} \quad \Delta P_{d2}]^T$$
$$\mathbf{x} = [\Delta f_1 \quad \Delta f_2 \quad \Delta P_{m1} \quad \Delta P_{m2} \quad \Delta P_{m3} \quad \Delta P_{m4} \quad \int ACE_1 \quad \int ACE_2 \quad \Delta P_{DC} \quad \Delta P_{tieAC,12}]^T \tag{4.22}$$

In the *s*-domain, the complete state space presentation of a two-area system could be as follows:

$$\Delta\omega_1(s) = \frac{K_{p1}}{1 + s\,T_{p1}}(\Delta P_{m1} + \Delta P_{m2} - \Delta P_{d1} - \Delta P_{tieAC,12}) \tag{4.23}$$

$$\Delta\omega_2(s) = \frac{K_{p2}}{1 + s\,T_{p2}}(\Delta P_{m3} + \Delta P_{m4} - \Delta P_{d2} + \Delta P_{tieAC,12}) \tag{4.24}$$

where $\Delta P_{Li}(i = 1, 2)$ is local load deviation, K_{pi} is the power system gain, T_{pi} is the power system time constant.

The rest of the variables could be defined as indicated in the following equations:

$$\Delta P_{m1} = \frac{1}{1+sT_{tg1}}\left[\frac{\Delta\omega_1}{R_1 \times 2\pi} - K_{I1}\Delta P_{ref1}\right] \tag{4.25}$$

$$\Delta P_{m2} = \frac{1}{1+sT_{tg2}}\left[\frac{\Delta\omega_1}{R_2 \times 2\pi} - K_{I1}\Delta P_{ref1}\right] \tag{4.26}$$

$$\Delta P_{m3} = \frac{1}{1+sT_{tg3}}\left[\frac{\Delta\omega_2}{R_3 \times 2\pi} - K_{I2}\Delta P_{ref2}\right] \tag{4.27}$$

$$\Delta P_{m4} = \frac{1}{1+sT_{tg4}}\left[\frac{\Delta\omega_2}{R_4 \times 2\pi} - K_{I2}\Delta P_{ref2}\right] \tag{4.28}$$

$$\Delta P_{ref1} = \frac{ACE_1}{s} = \frac{1}{s}\left[\frac{\beta_1}{2\pi}\Delta\omega_1 + \Delta P_{tieAC,12}\right] \tag{4.29}$$

$$\Delta P_{ref2} = \frac{ACE_2}{s} = \frac{1}{s}\left[\frac{\beta_2}{2\pi}\Delta\omega_2 - \Delta P_{tieAC,12}\right] \tag{4.30}$$

$$\Delta P_{tieAC,12} = \frac{T_{12}}{s}[\Delta\omega_1 - \Delta\omega_2] \tag{4.31}$$

where R_k $(k = 1{:}4)$ is considered as a droop for each generation company (GENCO), T_{tg} is the time constant of the GENCOs and T_{ij} is the synchronization power coefficient. For transmitted power between Area *i* and Area *j* we will have:

$$P_{tieAC,ij} = \frac{U_i U_j}{X_T}\sin(\delta_i - \delta_j) \tag{4.32}$$

After the linearization on the operating points for a two-area case, we have:

$$\Delta P_{tieAC,12} = 2\pi T_{12}[\int \Delta f_1 dt - \int \Delta f_2 dt], \tag{4.33}$$

$$T_{12} = \frac{U_1^0 U_2^0}{P_{r1} X_T}\cos(\delta_2^0 - \delta_1^0) \tag{4.34}$$

$$\Delta P_{tieAC,21} = 2\pi T_{21}[\int \Delta f_2 dt - \int \Delta f_1 dt], \tag{4.35}$$

$$T_{21} = \frac{U_2^0 U_1^0}{P_{r2} X_T}\cos(\delta_2^0 - \delta_1^0) \tag{4.36}$$

$$a_{12} = -\frac{P_{r1}}{P_{r2}} \tag{4.37}$$

where P_{r1} and P_{r2} are known as rated powers in each area, which are usually equal and T_{ij} is the synchronization torque coefficient.

4.5 Multi-area interconnected AGC system with HVDC model

4.5.1 Supplementary power modulation controller for HVDC

As it explained before, for high level control design like AGC, the HVDC system could be modelled as control block with a first order system indicating the overall constant time of the HVDC link (Figure 4.9).

$$T_{DC}\frac{d\Delta P_{DC}}{dt} = \Delta P_{dc,ref} - \Delta P_{DC} \tag{4.38}$$

where $\Delta P_{dc,ref}$ is the desired dc power and ΔP_{DC} is real dc power flow through the system.

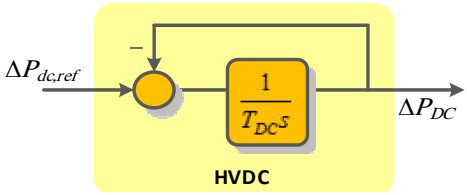

Figure. 4.9. Block diagram of a small signal HVDC system.

It is assumed that the DC line is lossless and the DC power flow goes from one converter to the other. The proposed model for parallel AC/DC interconnection AGC systems is based on the Supplementary Power Modulation Controller (SPMC) shown in Figure 4.10.

This controller modulates both frequency and active power by processing the frequency signal obtained from local measurements. The objective is to damp critical low frequency inter-area modes that can affect the stability during load variations. It should be noted that, the input signals generating the reference for DC link consists of deviation of frequencies in the interconnected areas and the deviation of transmitted power in the parallel AC line.

In this study, the dynamics of fast transient HVDC power electronic parts is neglected because the time constant of electronic parts is much smaller than the mechanical part involved in dynamic analysis of large scale power system. Supplementary Modulation Controller (SMC) is designed as high level damping controller, devoted to improving the overall performance of interconnected system during load step changes.

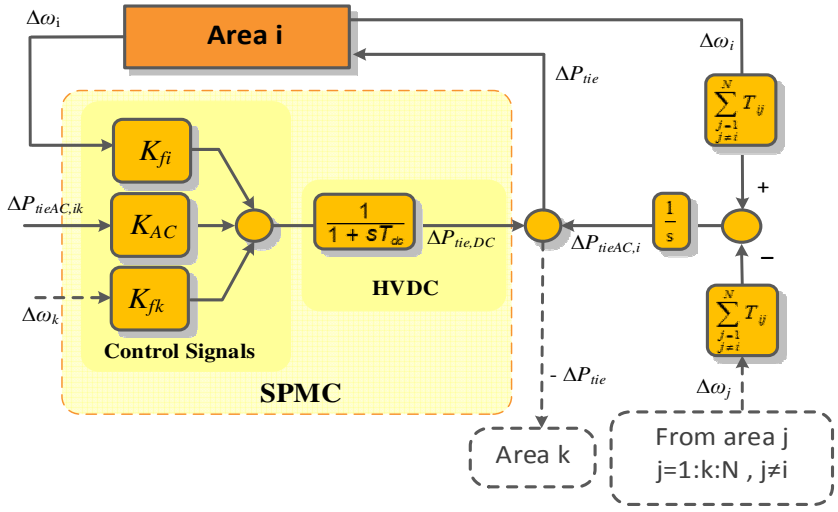

Figure 4.10. Diagram of SPMC to the power system with parallel HVAC and HVDC links.

It should be noted that by using this supplementary controller for the DC link, the capability of steady state transferring power between two AC systems will be increased. A major feature that such SPMC offer is the use of signals obtained from local measurements to synthesize the control signal for damping critical modes.

In this model, the deviation of frequency in each area is used like a control signal generating the proper higher level references for HVDC links. These references will be used by VSC station to control the power by modifying their duty cycles. The studied model is based on a VSC technology and the HVDC system is a bidirectional system with the ability of power flow control in both direction. Therefore, it is necessary to sense the frequency of both interconnected area. The feedback signal from the interconnected system will generated the power references and it consists of three signals: These signals are deviation of frequency in Area1 and Area2 each area and deviations of AC transmission line. Therefore the proposed coordinated control, which can act as a supplementary power modulation, for two-area with parallel AC/DC link can be presented as follows:

$$\Delta x_{DC} = K_{f1}\Delta\omega_1 + K_{AC}\Delta P_{tieAC,12} + K_{f2}\Delta\omega_2 \tag{4.39}$$

where Δx_{DC} will be a control signal for HVDC line and K_{f1}, K_{f2} and K_{DC} will be used as control gains. While the DC link could be presented as follows:

$$\Delta P_{DC} = G_p x_{DC} \tag{4.40}$$

$$G_p(s) = \frac{1}{1 + sT_{DC}} \tag{4.41}$$

where the time constant for the DC link is presented by T_{DC} .

As shown in Figure 4.10 and 4.11, the $\Delta P_{dc,ref}$ is the input signal of HVDC which will be generated by different control signals. These signals are the deviation of frequencies of Area1 and Area2 and the transmitted power from the AC line. (The AC signal will be used if the transmission line be a parallel AC/DC system). The action of this control strategy is like a power modulation controller which is implemented as a proportional control.

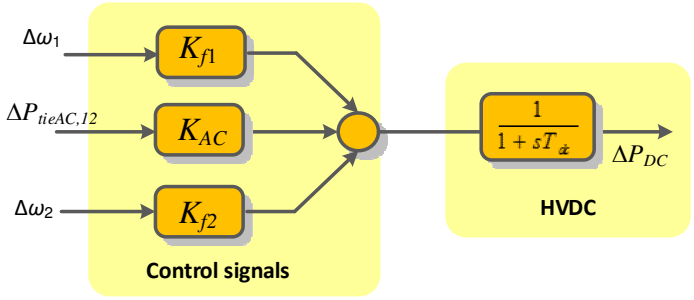

Figure 4.11. Control actions of interconnected area with small signal of HVDC.

In the reality, the time response of HVDC system, for transferring multi megawatt power, will be in the range of 200 *ms* to 500 *ms*. In most of the power system literature focused on this type of high level control design, the typical value is around 200 *ms*. As mentioned in several references [4.10]-[4.11], the proper time response could be between 100 *ms* to 300 *ms*. Therefore, in this study, the time constant will be assumed to be 300 *ms* for T_{DC}. Therefore, the total transmitted power deviation for AC/DCC system will be as follows:

$$\Delta P_{12} = \Delta P_{DC} + \Delta P_{tieAC,12} \tag{4.42}$$

$$\Delta P_{tieAC,12} = \frac{2\pi T_{12}}{s}[\Delta\omega_1 - \Delta\omega_2] \tag{4.43}$$

where $\Delta P_{tieAC,12}$ is the deviation of AC power flow, ΔP_{DC} is the DC power deviation for the DC link and T_{12} is the synchronizing coefficient for transmission line [4.1]. In order

to apply supplementary power modulation, the state space equations in the Laplace domain should be analysed.

4.5.2 Dynamic model of two-area AC/DC system with SPMC

The general structure of test model with two areas and a parallel AC/DC link is presented in Figure 4.12. In this case, it is assumed that in each area two generation companies (GENCOs) are located.

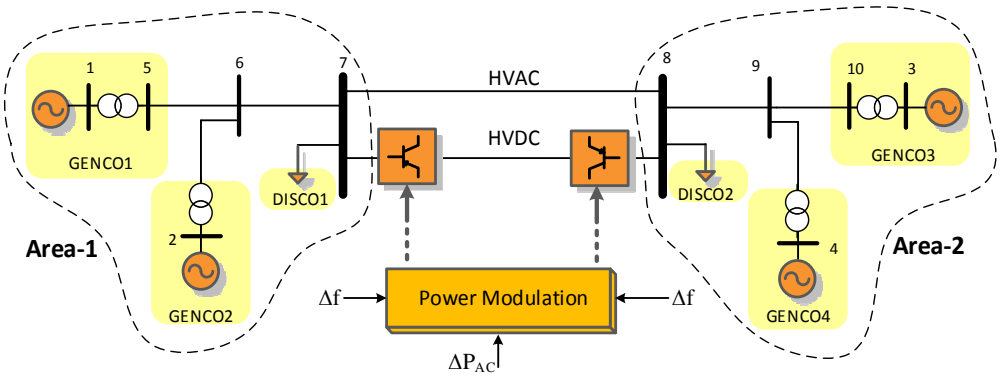

Figure 4.12. A two-area system with a parallel AC/HVDC link.

Since the dynamic response of HVDC link is much faster than mechanical part of conventional power system and after a sudden change/perturbation it will act very fast. Therefore, upon a sudden change in load for example, the HVDC will quickly start its control to suppress the dynamic behaviors of the system. Then subsequently, the AGC will start to act to eliminate the steady state errors in the frequency and tie line power deviations. As explained before, the positive effects from parallel HVDC link can be explained by the modification made in the following equation. This modification is related to new ACE signal.

Considering this new DC signal (ΔP_{DC}) in addition to the states in Eq. (4.20), the ACE signal of each area in AGC operation will be changed as follows:

$$ACE_{i,new} = \beta_i \Delta\omega_i + \Delta P_{DC} + \Delta P_{tieAC,12} \tag{4.44}$$

Also, it would be possible to have a higher tuning level of the HVDC set-points when the inputs of the proposed supplementary power modulation controller are coming from the AGC control center and the outputs of the AGC will generate the new set-points, power references, for VSC stations and generation units. As in the previous case for AC

systems, the complete state space presentation of two-area systems considering the dynamics of HVDC could be found as:

$$\Delta\omega_1 = \frac{K_{p1}}{1+sT_{p1}}[\Delta P_{m1} + \Delta P_{m2} - \Delta P_{L1} - \Delta P_{tieAC,12} - \Delta P_{DC}] \tag{4.45}$$

$$\Delta\omega_2 = \frac{K_{p2}}{1+sT_{p2}}[\Delta P_{m3} + \Delta P_{m4} - \Delta P_{L2} + \Delta P_{tieAC,12} + \Delta P_{DC}] \tag{4.46}$$

where

$$K_{p1} = \frac{1}{D_{sys-i}},\ T_{pi} = \frac{M_{sys-i}}{D_{sys-i}} = \frac{2H_{sys-i}/\omega_0}{D_{sys-i}} \tag{4.47}$$

In this case, M_{sys-i} is the total inertia in i^{th} area of the system and D_{sys-i} is the related damping. It should be noted that the model will be based on pu. values.

$$\Delta P_{m1} = \frac{1}{1+sT_{tg1}}\left[\frac{\Delta\omega_1}{R_1 \times 2\pi} - K_{I1}\Delta P_{ref1}\right] \tag{4.48}$$

$$\Delta P_{m2} = \frac{1}{1+sT_{tg2}}\left[\frac{\Delta\omega_1}{R_2 \times 2\pi} - K_{I1}\Delta P_{ref1}\right] \tag{4.49}$$

$$\Delta P_{m3} = \frac{1}{1+sT_{tg3}}\left[\frac{\Delta\omega_2}{R_3 \times 2\pi} - K_{I2}\Delta P_{ref2}\right] \tag{4.50}$$

$$\Delta P_{m4} = \frac{1}{1+sT_{tg4}}\left[\frac{\Delta\omega_2}{R_4 \times 2\pi} - K_{I2}\Delta P_{ref2}\right] \tag{4.51}$$

$$\Delta P_{ref1} = \frac{ACE_1}{s} = \frac{1}{s}\left[\frac{\beta_1}{2\pi}\Delta\omega_1 + \Delta P_{tieAC,12} + \Delta P_{DC}\right] \tag{4.52}$$

$$\Delta P_{ref2} = \frac{ACE_2}{s} = \frac{1}{s}\left[\frac{\beta_2}{2\pi}\Delta\omega_2 - \Delta P_{tieAC,12} - \Delta P_{DC}\right] \tag{4.53}$$

$$\Delta P_{tie,AC} = \frac{T_{12}}{s}[\Delta\omega_1 - \Delta\omega_2] \tag{4.54}$$

$$s\Delta P_{DC} = \frac{K_{f1}}{2\pi T_{DC}}\Delta\omega_1 + \frac{K_{f2}}{2\pi T_{DC}}\Delta\omega_2 + \frac{K_{AC}}{T_{DC}}\Delta P_{tieAC,12} - \frac{1}{T_{DC}}\Delta P_{DC} \tag{4.55}$$

So, as explained before, the state variables of the system are chosen as follows:

$$x_1 = \Delta\omega_1\ ,\quad x_2 = \Delta\omega_2\ ,\quad x_3 = \Delta P_{m1}\ ,\quad x_4 = \Delta P_{m2}\ ,\quad x_5 = \Delta P_{m3}\ , \tag{4.56}$$

$x_6 = \Delta P_{m4}$, $x_7 = \Delta ACE_1$, $x_8 = \Delta ACE_2$, $x_9 = \Delta P_{tieAC,12}$, $x_{10} = \Delta P_{DC}$

and control inputs are load changes in each area can be written as:

$$u_1 = \Delta P_{L1} \ , \quad u_2 = \Delta P_{L2}$$

The closed loop system for such system can be presented in the form of a state space:

$$\begin{gathered} \dot{\mathbf{x}} = \mathbf{A}\mathbf{x} + \mathbf{B}\mathbf{u} \ , \ x(t_0) = 0 \\ \mathbf{y} = \mathbf{C}\mathbf{x} \end{gathered} \tag{4.57}$$

where **x** will be state vector and **u** will be the input vector related to the power demands:

$$\begin{gathered} \mathbf{u} = [\Delta P_{L1} \quad \Delta P_{L2}]^T \\ \mathbf{x} = \left[\Delta\omega_1 \ \Delta\omega_2 \ \Delta P_{m1} \ \Delta P_{m2} \ \Delta P_{m3} \ \Delta P_{m4} \ \Delta P_{ref1} \ \Delta P_{ref2} \ \Delta P_{tieAC,12} \ \Delta P_{DC}\right]^T \end{gathered} \tag{4.58}$$

where $\Delta\omega_i (i = 1, 2)$ is the frequency deviation in p.u., $\Delta P_{mk} (k = 1{:}4)$ is the output power of each generation unit, ΔP_{refi} is the setpoint for each generator comming from area control error, ΔP_{DC} is the DC power deviation and $\Delta P_{tieAC,12}$ is the deviation in the AC transmitted power.

4.5.3 Simulation of two area power system example

In this Section, the model presented in Figure 4.12, which has a parallel AC/HVDC link is used for simulation. It is considered in this study case that two contingencies are happening. The first contingency will be a load step change in Area1 by increasing to 0.03 p.u. after t=3.5 sec and the second event is a decrement in the load at t=30 sec. Parameters of the system are presented in Tables 4.1 and 4.2. Considering T_t and T_g as the time constants of turbine and governor, respectively. Participation of generators are defined with these *apf*s:

$$apf_1 = 0.50 \quad , \quad apf_2 = 1 - apf_1 = 0.50$$
$$apf_3 = 0.50 \quad , \quad apf_4 = 1 - apf_3 = 0.50$$

Table 4.1. GENCOs parameters.

Parameters	Area1		Area2	
	GENCO1	GENCO2	GENCO3	GENCO4
T_t (sec)	0.32	0.30	0.30	0.32
T_g (sec)	0.06	0.08	0.06	0.07
$R\ (Hz/pu)$	2.4	2.5	2.5	2.7

Table 4.2. Parameters of control area.

Parameters	Area1	Area2
$K_P\ (pu/Hz)$	102	102
$T_P\ (\text{sec})$	20	25
$\beta\ (pu/Hz)$	0.425	0.396
$T_{12}\ (pu/Hz)$	0.245	

The frequency deviations in both areas and also the generated power of the GENCOs are presented in Figures 4.13 and 4.14, respectively.

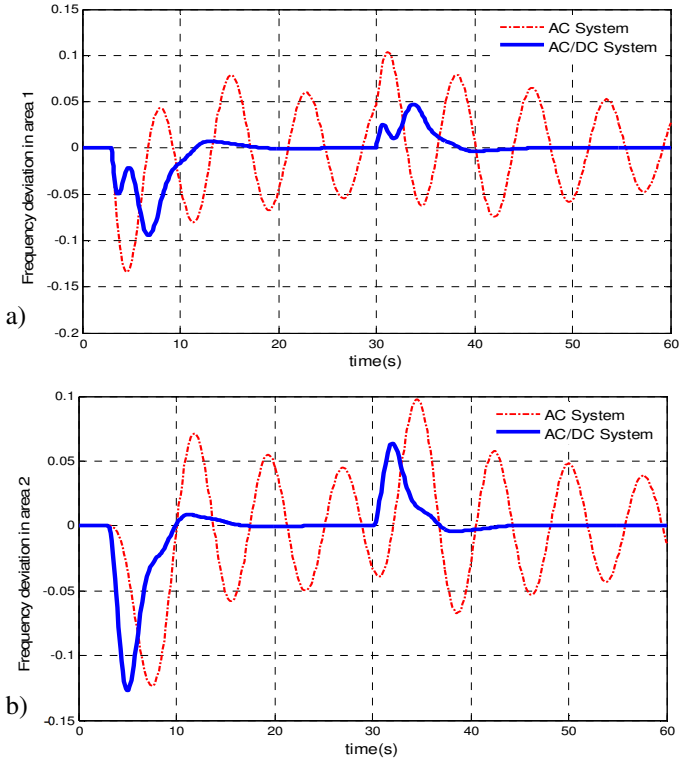

Figure 4.13. Frequency deviations of both areas. a) Area1, b) Area2.

Based on the results, it can be observed that, the original model with the standard AC link will have huge oscillations while, when the proposed AC/DC with SPMC is applied, the dynamic responses of the system is clearly improved. With the HVDC link, the dynamic responses of overall system are improved efficiently, and all the deviations in all areas are suppressed quickly with zero steady state error.

The response of generated power for each generation unit is also presented in Figure 4.14. Based on the presented results, the magnitude of the oscillations in generated power is damped by the HVDC link. This result, clearly confirms the positive damping effects of HVDC link on improving the dynamic stability of the system. It is also clear that, the steady state values of each GENCO is controlled according to their *apf* values.

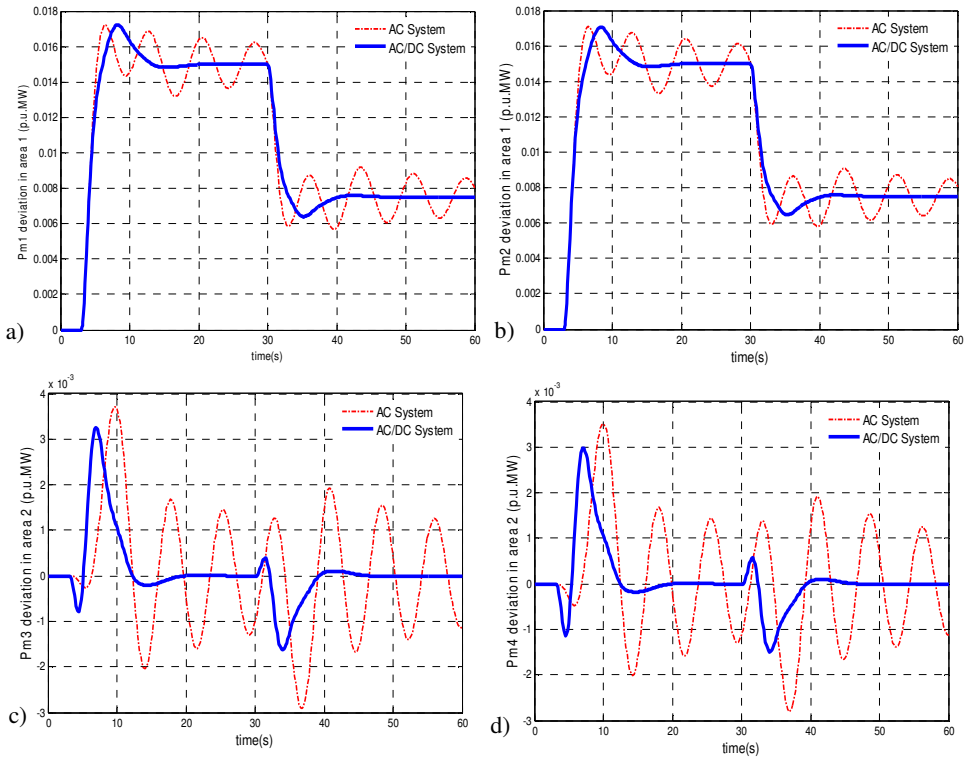

Figure 4.14. Active power generations. a) GENCO1, b) GENCO2, c) GENCO3, and d) GENCO4.

The dynamic response of the DC power and the AC transmitted power are presented in Figures 4.15 and 4.16, respectively. From these figures, it can be observed that adding a parallel DC link with one AC link can improve the dynamic stability of the system while, at the same time, the transmission capability between the areas can increase.

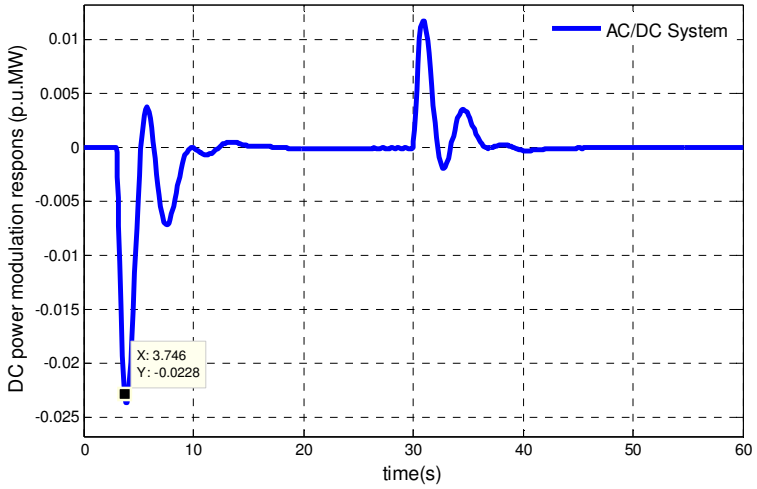

Figure 4.15. DC power deviation.

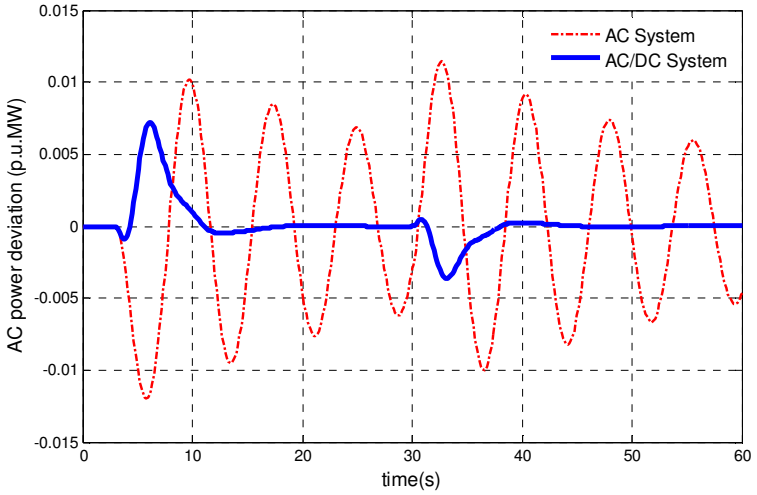

Figure 4.16. Tie-line AC power deviation.

The eigenvalues of two systems, AC system and AC/DC systems, are presented in Tables 4.3 and 4.4. The comparison between the exact locations of the eigenvalues is also plotted in Figure 4.17.

Table 4.3. Eigenvalues comparison.

Modes	AC System	AC/DC System
$\boldsymbol{\lambda_1}$	-0.0275 + 0.8256i	-23.9299
$\boldsymbol{\lambda_2}$	-0.0275 - 0.8256i	-0.4945 + 1.6611i
$\boldsymbol{\lambda_3}$	-0.3423 + 0.3995i	-0.4945 - 1.6611i
$\boldsymbol{\lambda_4}$	-0.3423 - 0.3995i	-0.3437 + 0.4245i
$\boldsymbol{\lambda_5}$	-0.7023	-0.3437 - 0.4245i
$\boldsymbol{\lambda_6}$	-1.8271	-0.8974
$\boldsymbol{\lambda_7}$	-2.1073	-1.9374 + 0.1752i
$\boldsymbol{\lambda_8}$	-2.6872	-1.9374 - 0.1752i
$\boldsymbol{\lambda_9}$	-2.6316	-2.6850
$\boldsymbol{\lambda_{10}}$	--------	-2.6316

As shown in Table 4.4, after adding the DC link, the total damping of the AC-DC model is increased. Improvement of the eigenvalues in Figure 4.17 is also confirming the positive effects of the proposed power modulation damping for the HVDC link. The red circles are the eigenvalues of the AC system and the blue squares are the ones related to the AC/DC system. In the AC system, there will be two critical modes ($\lambda_1$and λ_2). These modes are very close to the imaginary axis and adding DC link will shift these modes to a better place in the s-plane.

Table 4.4. Eigen index comparisons of different systems.

Index	AC System	AC/DC System
Total damping of eigenvalues	6.3678	7.8211

As a summary, considering the obtained results and comparisons between the normal AC and AC/DC systems, it can be state that application of DC link in parallel with AC line can help the system performance especially during contingencies. This help can be reflected by considerable improvements on dynamic responses and huge improvement in damping of oscillations. The presented SPMC is a suitable strategy for coordination of DC link with the rest of AC system. It can be used for analysing the effects of HVDC control system in higher level AGC application. It can model bidirectional behaviours of

the DC link. It became evident that positive effects of DC link could be achieved if a proper coordination is made in term of control. Proper coordination with acceptable tuning of control gains can guaranty the suitable operation of AC/DC system.

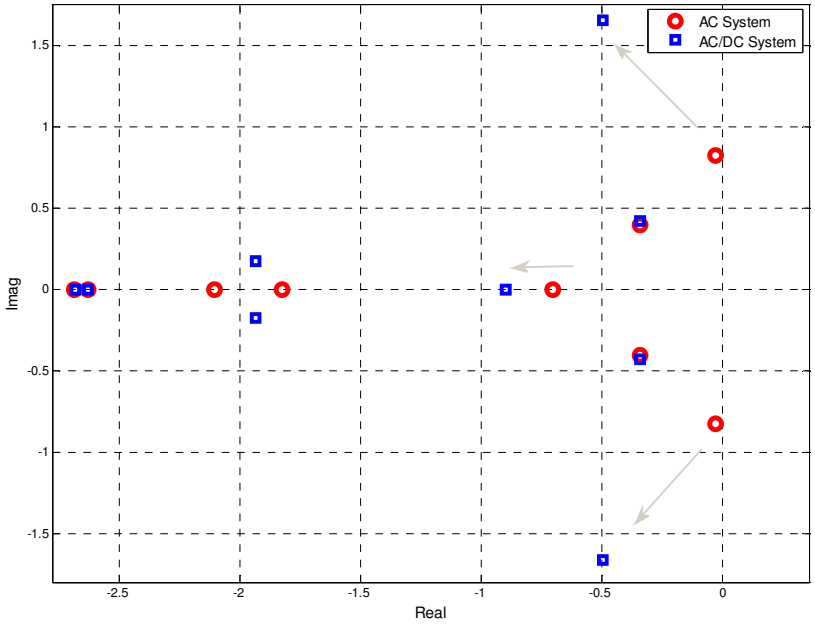

Figure 4.17. Eigenvalues of different systems: AC and AC/DC systems.

CHAPTER 5.

Virtual Inertia for Interconnected Systems using Derivative Control

This Chapter is related to inertia emulation by a derivative term control strategy suitable for power oscillation damping and frequency support applications in large-scale AGC interconnected power systems. The AGC as a higher level control strategy generates the set-points for all the local components which are under control by their local controllers. The studied model in this work consists of parallel AC and HVDC lines and energy storage systems (ESS) with a scheme of a two-area AC/DC power system. This study provides an essential model to be used for modelling and analysing the behaviours of large complex HVDC interconnected systems in the power industry. It shows how and in which level the maximum advantages can be obtained from the power system components. In this work, a model of AC/DC interconnections for the AGC dynamic model with a new approach based on derivative control method for providing inertia is presented. All the results of the proposed method are compared with the conventional model. Power and energy ratings are also added in this Chapter by conducting eigenvalue and sensitivity analyses. The proposed model should provide a systematic modelling and control technique for large scale interconnected power systems, specifically for frequency support and power oscillation damping (POD) applications with parallel AC/DC transmission line and ESS in AGC systems of the power industry. It should be noted that the ESS will be used to provide inertia to the system, especially during transient conditions. In this study, by means of the proposed control strategy, it is possible to have a clear image about the system conditions and required energy or power references.

5.1 Review and SOA in the subject

As mentioned in previous Chapters, the study of the AGC and POD is very important in both power system dynamic analysis [5.1]-[5.2] and changing conventional power system through deregulation [5.3], existing many proposals in these important research areas [5.4]-[5.5]. In parallel to liberalization in the power industry, high penetration of renewable resources and required technology for their integration provide new research challenges [5.6]. In this sense, recent trends of research lie with the adoption of previous concepts and conventional models considering new AC/DC complex scenarios with more application of DC interconnections and renewable energy systems (RES) penetration [5.7]-[5.8]. Since last decade, many researchers tried to propose new models for load frequency control considering the competitive environment, usually extending previous conventional approaches [5.4]-[5.5], by introducing more detailed models of generation based on renewable resources [5.5]-[5.8]. Nowadays, integration of RES is the main challenge of the industry. During the steady state operation, the generation and consumption of energy must be balanced and any imbalance could bring severe deviations on the frequency and on the transmitted power. As it is well-known, the rate of change of frequency depends on the initial power disparity and system inertia, which is a serious issue when dealing with a power system with high penetration of renewables with low inertia. Actually the lack of inertia, due to the high penetration of RES and systems based on power electronics, results in a big challenge for power systems control in future power systems. For example, in PV generation, there is not any mechanical parts with inertia. Likewise, in wind and wave power generation cannot contribute directly to the total inertial of the system because of decoupling the prime mover from electrical generator [5.8]. Therefore, technical solutions for providing additional inertia are very useful.

So far, there are several research works dealing with improving grid integration of generation units. For example, derivative control of frequency is used in [5.7] to modify the references of a wind farm to contribute in supporting the grid frequency. At the transmission level, however, it is difficult to find deeply detailed analyses with a final solution for this issue, especially for the high-level control of multi-area interconnected systems.

At the generation level, applications of ESS is very significant in order to recover the lack of inertia of generation based on power electronics [5.9]-[5.11] and facilitating RES to act as a conventional generator for frequency support issues. New concepts like virtual inertia and virtual synchronous generation (VSG) are among of the main research topics in this field [5.12].

Moreover, there is a huge increase of installations and applications in the HVDC interconnections after 2010, especially at the transmission level. In fact, in parallel to the high penetration of RES, application of HVDC interconnections have increased as well. Positive effects of DC interconnections are clear and various advantages, like frequency regulation, connections of asynchronous areas, high controllability and expandability are reported by many researchers. In the case of AGC for a two-area power system, the effects of applying parallel AC and HVDC lines with superconducting magnetic energy storage (SMES) are explained in [5.13]-[5.14]. In these works, previous models of conventional power systems are modified by adding a DC link model or storage devices. However, these works do not consider inertia emulation and they do not conduct any analysis regarding its rating and its detailed effects on the system performance during contingencies, especially for AGC study.

In [5.11], a generic modelling of the system is proposed. This type of modelling is useful to model each component individually to see the effects on the frequency of the system. However, this approach cannot be directly used for modelling virtual inertia in DC transmission lines for large area power systems. Some other research works are focused on SMES effects on system stability and are aimed to show the positive effects of SMES when added to an HVDC link. However, there is not any information regarding inertia emulation concept and they do not deal with large interconnected systems [5.13]-[5.15]. In [5.16], the frequency control of a system with HVDC connection based on contributions of turbine generator and VSC is presented. In [5.17], a new controller for emulating the inertia, named inertia emulation control (IEC) is proposed, which will give more ability to the DC link for using the energy of DC link in emulating inertia. In this way, it shows a similar behaviour to a synchronous generator. But since the presented results in these references shows significant variations in DC link, it doesn't seem to be a fully realistic method and more research in this field is necessary.

5.2 Higher level control technique for inertia emulation by derivative control

5.2.1 The concept of virtual inertia

Generally, if the derivation signal of the grid frequency is used proportionally for modifying the active power reference of a converter, a virtual inertia can be emulated for the system. This virtual inertia can contribute actively on improving the dynamic performance of the system, especially the inertial response. Therefore, the general control law for this inertia, regarding control of power converters, is as follows [5.10]:

$$P_{emulate} = k_a \omega_0 \frac{d(\Delta\omega)}{dt} \tag{5.1}$$

where $P_{emulate}$ is the power of derivative control, k_a is the inertial proportional conversion gain and ω_0 is the nominal grid frequency. This concept could be used in per unit for different applications, like analysis of AGC model considering a system which is able to provide this virtual inertia to the network [5.10]-[5.11].

5.2.2 Modelling of inertia emulation in AC/DC interconnected AGC systems

In this Section, an inertial emulation technique is presented. In the future modern power industry, based on AC/DC grids with high penetration of renewable resources, there will be a lack of inertia in the whole system and control methods for providing inertia will be very important [5.18]-[5.19]. Therefore, a new high-level control model is proposed to simulate and analyse the behaviour of the AC/DC transmission system with the ability of providing synthetic inertia. Based on the obtained results, it would be possible to indicate the necessary values for power references and required capacities into the system. Some of the advantages of inertia emulation are load levelling and POD, facilitate the frequency support for AC grid and contribute in virtual inertia. In this study, the power system considering inertia is assumed to consist of two interconnected areas with parallel AC/DC links, while two GENCOs exist in each area. The studied model consists of parallel AC and HVDC lines with added ESS. It should be noted that, new technologies, which help to add more flexibility/inertia to the system, are essential for the future power industry. ESS are one of the more promising tools for adding more beneficial advantages from HVDC and converter based systems [5.20].

ESS at the large scale for the grid application have a great potential to play a key role in the future, especially for providing inertia and adding more flexibility to the system

[5.21], which leads to more research investigation on both technical and economic issues surrounding ESS applications. Until now, various types of battery technologies are tested at the grid level [5.21]. These batteries have a great ability for supporting different tasks, like customers and distribution grid services, as well as contributing on frequency regulation. As reported in [5.22]-[5.23], battery and super-capacitor units can be used for high power applications. Application of SMES units, as another bulk ESS, is also reported in references [5.13] and [5.24].

Therefore, in this study, a bulk ESS with a converter station is added to the test grid. The diagram for two area load frequency control (LFC) system is presented in Figure 5.1. In this model, power converters are used as interfaces for controlling the behaviour of the ESS in response to AGC signals for minimizing frequency deviations [5.21]-[5.24]. The converter will be controlled to keep the storage element properly charged during normal operation and then help the system during contingencies. Based on this explanation, the ESS is used to provide additional inertia using a derivative control method.

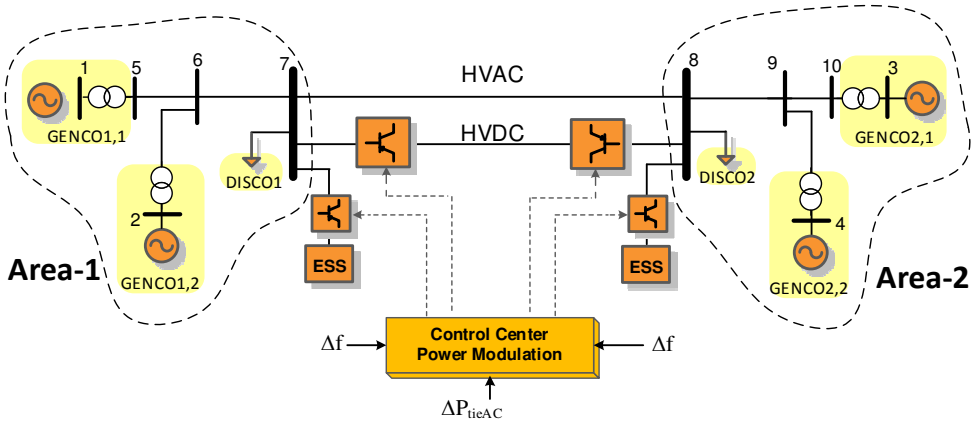

Figure 5.1. Configuration of the test system with storage and parallel AC/DC link.

The proposed control structure for hybrid AC/DC link with the ability of storing energy and inertia emulation by derivative control is presented in Figure 5.2. This model is presented in the Laplace domain with per unit values in the following.

Based on the proposed model for the system of Figure 5.1, frequency variations can be written as follows:

$$\Delta\omega_i(s) = \frac{K_{pi}}{1 + s\,T_{pi}}[(\Delta P_{mi} - \Delta P_{Li} - (\Delta P_{tieAC,ij} + \Delta P_{DC} + \Delta P_{ESSi})] \tag{5.2}$$

where ΔP_{ESS} is the power variation for emulating inertia, ΔP_{mi} is the total generated power by GENCOS in each area, ΔP_{Li} is the load variation, while $\Delta P_{tieAC,ij}$ and ΔP_{DC} are the AC and DC power flow between the two areas, respectively. The power deviation from ESS in each area ($\Delta P_{ESS,i}$) can be defined like this:

$$\Delta P_{ESSi}(s) = \frac{J_i}{1 + s\,T_{ESS,i}}[s\,\Delta\omega_i(s)] \tag{5.3}$$

where T_{ESS} is the time constant of an added filter for imitating the control dynamic characteristic of the storage devices and the new area control error of i^{th} area will be like this:

$$ACE_i = \beta_i \Delta\omega_i + [\Delta P_{tieAC,ij} + \Delta P_{DC}] \tag{5.4}$$

By neglecting the damping (D_i) and dynamics of the filter in the generated power signal, equation (5.2) could be written as:

$$(M_i + J_i)[s\,\Delta\omega_1(s)] = \Delta P_a \tag{5.5}$$

where ΔP_a is the total accelerating power and M_i is the system inertia. Therefore, it is obvious that using derivative control technique, the total inertia ($M_i + J_i$) of the system is increased.

This control concept is proposing a derivative based controller that can calculate the rate of change of frequency (ROCOF) signal and then, with a control gain, can modify the active power reference of the ESS for emulating the inertia. The derivative based control strategy is also sensitive to the noises especially during measurements of frequency signals. Therefore, a low-pass filter can be added to the model for eliminating the effects of noises. This filter could also simulate the dynamics of a storage device, which should be fast.

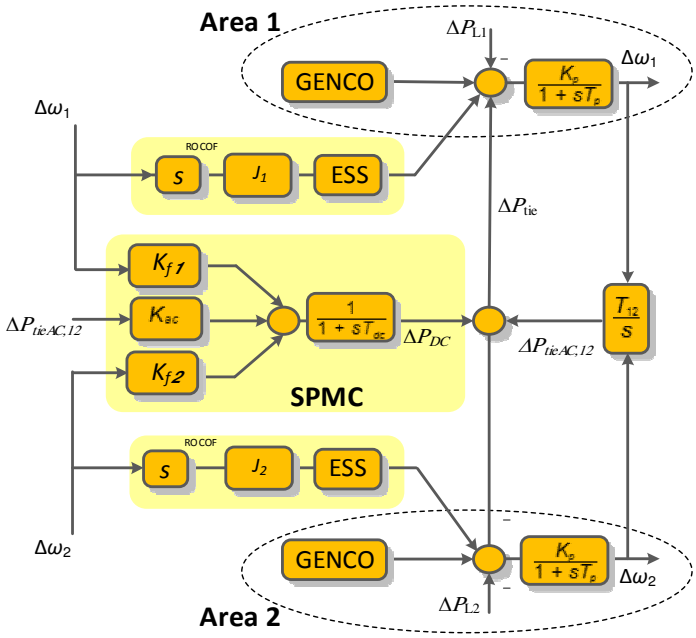

Figure 5.2. Proposed higher level control for HVDC-ESS for interconnected AGC system.

As explained, derivation signal of grid frequency can be used proportionally for modifying the active power reference of converters for emulating the inertia to the large scale multi-area interconnected power systems. For doing that, as shown in Figure 5.3, a control law for active power emulation is considered:

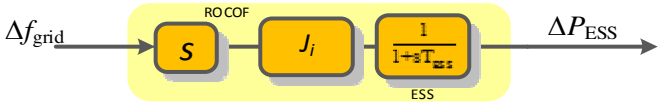

Figure 5.3. Block diagram of the derivative inertia emulation strategy.

As shown in this model, there will be two gains ($J_1$and J_2) related to inertia emulators for both areas. Usually, it would be possible to define a cost function for locating the most optimal values for all of these gains. Therefore, derivative control gain could be defined based on optimization theory by minimizing the following cost function [5.1]-[5.5]:

$$J = \int [ACE_1^2 + ACE_2^2]\, dt \tag{5.6}$$

This objective function is one of the common objective functions, which follows the integral of the squared error (ISE) method [5.5]. It should be noted that the ACE, which is used in this function, is consisted of frequency and power flow deviations (equation 5.4) in each area of the interconnected system. Therefore, the state space equations of two-area systems for frequency deviations, area control error and power of ESS in the Laplace domain will be as follows:

$$\Delta\omega_1(s) = \frac{K_{p1}}{1 + s\,T_{p1}} \left[(\Delta P_{m1} + \Delta P_{m2} - \Delta P_{L1} - \left(\Delta P_{tieAC,12} + \Delta P_{DC} + \Delta P_{ESS1}\right)\right] \tag{5.7}$$

$$\Delta\omega_2(s) = \frac{K_{p2}}{1 + s\,T_{p2}} \left[\left(\Delta P_{m3} + \Delta P_{m4} - \Delta P_{L2} - (\Delta P_{tieAC,21} - \Delta P_{DC} + \Delta P_{ESS2}\right)\right] \tag{5.8}$$

$$ACE_1 = \beta_1 \Delta\omega_1 + [\Delta P_{tieAC,12} + \Delta P_{DC}] \tag{5.9}$$

$$ACE_2 = \beta_2 \Delta\omega_2 + [\Delta P_{tieAC,21} - \Delta P_{DC}] \tag{5.10}$$

$$\Delta P_{ESS1}(s) = \frac{J_1}{1 + s\,T_{ESS,1}} [\frac{-1}{T_{p1}} \Delta\omega_1 + \frac{K_{p1}}{T_{p1}} \Delta P_{m1} + \frac{K_{p1}}{T_{p1}} \Delta P_{m1} - \frac{K_{p1}}{T_{p1}} \Delta P_{L1} - (\frac{K_{p1}}{T_{p1}} \Delta P_{tieAC,12} + \frac{K_{p1}}{T_{p1}} \Delta P_{DC} + \frac{K_{p1}}{T_{p1}} \Delta P_{ess1})] \tag{5.11}$$

$$\Delta P_{ESS2}(s) = \frac{J_2}{1 + s\,T_{ESS,2}} [\frac{-1}{T_{p2}} \Delta\omega_2 + \frac{K_{p2}}{T_{p2}} \Delta P_{m3} + \frac{K_{p2}}{T_{p2}} \Delta P_{m4} - \frac{K_{p2}}{T_{p2}} \Delta P_{L2} - (\frac{K_{p2}}{T_{p2}} \Delta P_{tieAC,21} - \frac{K_{p2}}{T_{p2}} \Delta P_{DC} + \frac{K_{p2}}{T_{p2}} \Delta P_{ess2}] \tag{5.12}$$

It should be mentioned that, the dynamic equations of other AC areas which are connected with AC lines will be the same as the ones presented in the previous section.

Therefore, in a two-area AC/DC interconnected power system, which will have two ESS controllers, four new states variables of synchronous controllers will be added to the system. The overall system will have twelve state variables as it is written as follows:

$$\mathbf{x} = [\Delta\omega_1 \;\; \Delta\omega_2 \;\; \Delta P_{m1} \;\; \Delta P_{m2} \;\; \Delta P_{m3} \;\; \Delta P_{m4} \;\; \Delta ACE_1 \;\; \Delta ACE_2 \;\; \Delta P_{tieAC,12} \;\; \Delta P_{DC} \;\; \Delta P_{ESS,1} \;\; \Delta P_{ESS,2}]^T \tag{5.13}$$

and control inputs are load changes in each area:

$$\mathbf{u} = \begin{bmatrix} \Delta P_{L1} \\ \Delta P_{L2} \end{bmatrix} \tag{5.14}$$

The complete state matrix **A** of the studied power system including the derivative based control is presented here:

$$\mathbf{A} = \begin{bmatrix}
\frac{-1}{T_{p1}} & 0 & \frac{K_{p1}}{T_{p1}} & \frac{K_{p1}}{T_{p1}} & 0 & 0 & 0 & 0 & \frac{-K_{p1}}{T_{p1}} & \frac{-K_{p1}}{T_{p1}} & \frac{-K_{p1}}{T_{p1}} & 0 \\
0 & \frac{-1}{T_{p2}} & 0 & 0 & \frac{K_{p2}}{T_{p2}} & \frac{K_{p2}}{T_{p2}} & 0 & 0 & \frac{K_{p2}}{T_{p2}} & \frac{K_{p2}}{T_{p2}} & 0 & \frac{-K_{p2}}{T_{p2}} \\
\frac{-1}{2\pi R_1 T_{tg1}} & 0 & \frac{-1}{T_{tg1}} & 0 & 0 & 0 & \frac{-K_{I1}}{T_{tg1}} & 0 & 0 & 0 & 0 & 0 \\
\frac{-1}{2\pi R_2 T_{tg2}} & 0 & 0 & \frac{-1}{T_{tg2}} & 0 & 0 & \frac{-K_{I1}}{T_{tg2}} & 0 & 0 & 0 & 0 & 0 \\
0 & \frac{-1}{2\pi R_3 T_{tg3}} & 0 & 0 & \frac{-1}{T_{tg3}} & 0 & 0 & \frac{-K_{I2}}{T_{tg3}} & 0 & 0 & 0 & 0 \\
0 & \frac{-1}{2\pi R_4 T_{tg4}} & 0 & 0 & 0 & \frac{-1}{T_{tg4}} & 0 & \frac{-K_{I2}}{T_{tg4}} & 0 & 0 & 0 & 0 \\
\frac{\beta_1}{2\pi} & 0 & 0 & 0 & 0 & 0 & 0 & 0 & 1 & 1 & 0 & 0 \\
0 & \frac{\beta_2}{2\pi} & 0 & 0 & 0 & 0 & 0 & 0 & -1 & -1 & 0 & 0 \\
\frac{T_{12}}{2\pi} & -\frac{T_{12}}{2\pi} & 0 & 0 & 0 & 0 & 0 & 0 & 0 & 0 & 0 & 0 \\
\frac{K_{f1}}{T_{DC}} & \frac{K_{f2}}{T_{DC}} & 0 & 0 & 0 & 0 & 0 & 0 & \frac{K_{AC}}{T_{DC}} & \frac{-1}{T_{DC}} & 0 & 0 \\
\frac{-J_1}{T_{ess1}T_{p1}} & 0 & \frac{J_1 K_{p1}}{T_{ess1}T_{p1}} & \frac{J_1 K_{p1}}{T_{ess1}T_{p1}} & 0 & 0 & 0 & 0 & \frac{J_1 K_{p1}}{T_{ess1}T_{p1}} & \frac{J_1 K_{p1}}{T_{ess1}T_{p1}} & \frac{-1}{T_{ess1}} - \frac{J_1 K_{p1}}{T_{ess1}T_{p1}} & 0 \\
0 & \frac{-J_2}{T_{ess2}T_{p2}} & 0 & 0 & \frac{J_2 K_{p2}}{T_{ess2}T_{p2}} & \frac{J_2 K_{p2}}{T_{ess2}T_{p2}} & 0 & 0 & \frac{-J_2 K_{p2}}{T_{ess2}T_{p2}} & \frac{-J_2 K_{p2}}{T_{ess2}T_{21}} & 0 & \frac{-1}{T_{ess2}} - \frac{-J_2 K_{p2}}{T_{ess2}T_{p2}}
\end{bmatrix} \tag{5.15}$$

Finally the **B** matrix could be presented as follows where the control vector will consists of load variations in each area:

$$\mathbf{B} = \begin{bmatrix}
\frac{-K_{p1}}{T_{p1}} & 0 \\
0 & \frac{-K_{p2}}{T_{p2}} \\
0 & 0 \\
0 & 0 \\
0 & 0 \\
0 & 0 \\
0 & 0 \\
0 & 0 \\
0 & 0 \\
0 & 0 \\
\frac{-J_1 K_{p1}}{T_{ess,1}\, T_{p1}} & 0 \\
0 & \frac{-J_2 K_{p2}}{T_{ess,2}\, T_{p2}}
\end{bmatrix}_{(12\times 2)} \tag{5.16}$$

5.2.3 Rating the required energy for inertia emulation

Usually, it is difficult to identify the exact amount of required energy to be stored in a power system. This is due to the dynamic nature of rotational machines and the unpredictability of load variations in terms of location and their degree of severity. But some sort of assumptions can be made for estimating the require energy for improving the transient response of the system [5.25].

The simplified swing equation of the system can be presented as:

$$\frac{2H}{\omega_s}\Delta\dot{\omega} = \Delta P_m - \Delta P_e = \Delta P_a \tag{5.17}$$

where H is the system inertia constant, P_e is the electrical power (load demand and power generation changes), P_m is the mechanical power, and P_a is the accelerating power.

After any sudden load change, the machine will accelerate or decelerate. Usually, the control strategies don't need to be fast for the steady state/regular operation. But in terms of transients, for fitting the system dynamics, it is expected to have a very fast control strategy to follow the derivations of the signals which are related to swing dynamics. This ability can be accomplished by using fast power electronic components for absorption or injection of transient power, while the problem of lack of energy reserve for emulating the inertia can be solved by using storage devices. Considering the swing equation, any mismatch between the electrical power and the mechanical power will bring the accelerating power, P_a, variation. For normal operation, the final value of this accelerating power will be zero in steady state. During transients however, it will become a non-zero value. So the objective is to minimize this accelerating power and back to the steady state (balanced) situation as soon as possible. Therefore, the stability margin of the studied system can be increased if a certain amount of power is added/subtracted from the value of accelerating power. This can happen during fast transient after faults.

For doing that, the motion equation introducing the contribution of virtual inertia power can be presented as follows [5.25]:

$$\frac{2H}{\omega_s}\Delta\dot{\omega} = \Delta P_m - \Delta P_e \pm \Delta P_s = \Delta P_a \pm \Delta P_s \tag{5.18}$$

where P_s can be the power supplied/absorbed by the ESS.

The time frame for the dynamic response of storage device for emulating power will be in the range of hundreds of milliseconds until seconds to support the other generation during the contingencies and load changes. Therefore, by assuming a constant value for input mechanical power and neglecting the damping factor, a linearized equation for estimating the required energy can be obtained.

It should be noted that, this amount of storage is related to the amount of load variation in AGC model. In the case of multi-area interconnected AGC systems with some support from a neighbour area (especially for fast DC links), the contributions of tie-line AC/DC power could be also considered. Based on these assumptions, the total amount of power delivered by the ESS is equal to the total power mismatch related to load variations and subtracting the tie-line contributions in multi-area interconnected systems:

$$\Delta P_s = \Delta P_L - (\Delta P_{DC} + \Delta P_{ac}) \tag{5.19}$$

where ΔP_L is load variations, ΔP_{DC} is the deviations of dc power flow and ΔP_{ac} is the deviations of AC tie-line power flow. Usually, in order to assure enough capacity, the size of ESS should be based on the worst case scenario. The usual faulty situation from the dynamic point of view, in the case of LFC analysis, could be a usual disturbance for generation drops or load variation around 4% to 10% of the rated value, which is known as common maximum mismatch power [5.25]. For normal contingencies, like normal load variations, the mismatch value can be determined based on the average statistical exchange between load and generation. Short term and long term demand forecasting based on the history of the statistical exchange power is one of the tools for predicting the possible load variation.

For implementing the virtual inertia control in the system, some parameters should be defined for rating the ESS. Considering Figure 5.4, the following parameters can be defined [5.26]:

- $P_{char}|_{t_{max}}$: maximum charging power.
- $P_{disch}|_{t_{max}}$: maximum discharging power.
- E_{char}: maximum charging capacity (equal to the dashed space C_2 in Fig 5.4).
- E_{char}: maximum discharging capacity (equal to the dashed space C_1 in Fig 5.4).

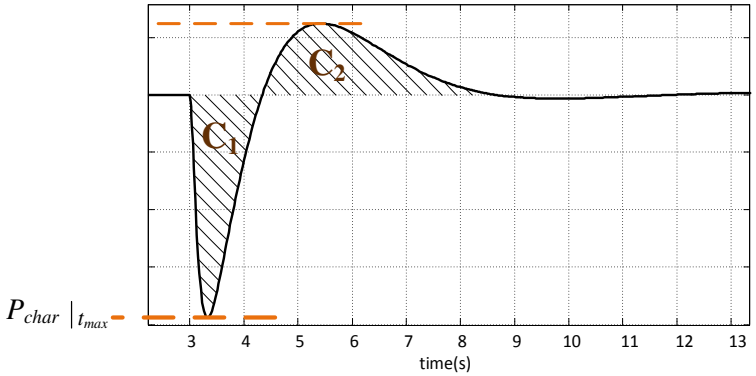

Figure 5.4. A general example of injected power by storage device [5.26].

The energy of ESS component can be calculated according to the following equation:

$$E_{ESS} = \int_0^t P_{ESS}(t)dt + E_{ESS,0} \tag{5.20}$$

where P_{ESS} is the instantaneous power of storage device and $E_{ESS,0}$ is the initial stored energy.

5.2.3.1 Case study analysis for AC/DC system with inertia emulation

Based on presented information in the previous Sections, the performance of proposed model to present the dynamic response of the model is evaluated though a general study case. In this study, two sequential steps are considered, the first one at 3 s and the second one at 30 s. As shown in Figure 5.5, the first contingency is a 0.03 p.u. load step change at 3 s and the second happens at 30 s by decreasing the demand to 0.015 p.u., both in the Area1.

The system parameters are given in Tables 4.1 and 4.2 in the Chapter 4 and the control parameter for this case study is presented in Table 5.1. As mentioned before, these values are obtained using (5.6) and the classical FMINCON function in Matlab software. The generic non-linear optimization routine FMINCON solver has been used as a classical optimization which implements the SQP for optimization of LFC problem.

Table 5.1. Control parameters considering derivative control.

Parameters	Value
K_{f1}	0.3
K_{f2}	0.1
K_{AC}	2.2
J_1	0.85
J_2	0.093

In the following, the dynamic behaviour for several system configurations is presented and compared. The comparisons are mainly related to the normal case, considering only an AC interconnection line between the two areas, the case of considering AC and DC interconnection lines, and the case of considering AC and DC interconnection lines with inertia emulation capability.

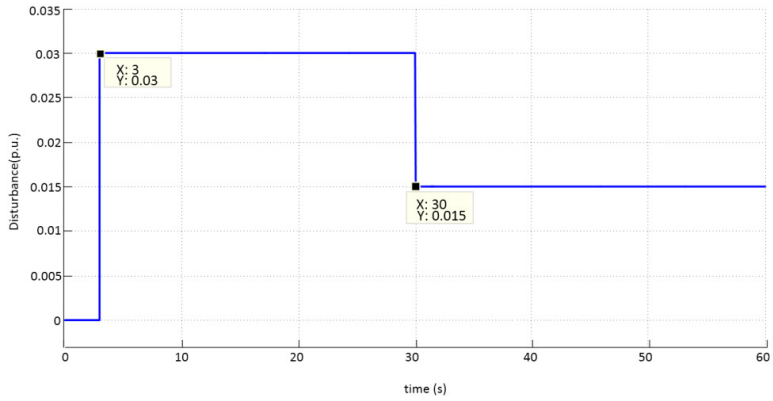

Figure 5.5. Load demand changes to the system as a disturbance at 3 sec and 30 sec.

Frequency deviations in both areas are presented in Figures 5.6 and 5.7, respectively. The output power generated by each unit is also presented in Figures 5.8 to 5.11. It is clear that, by means of inertia emulation, it is possible to change the dynamic performance of the system, being the final response smoother than in the normal case.

As shown in Figure 5.6, a remarkable improvement is achieved in damping of frequency oscillations when inertia is emulated by using derivative control. The blue trace in Figure 5.6 is related to the system with an HVDC link, which shows how the DC link contributes to damp frequency oscillations. After adding the derivative control for inertia emulation, the first overshoot in the system frequency is attenuated even more than the two other cases, as the black trace shows.

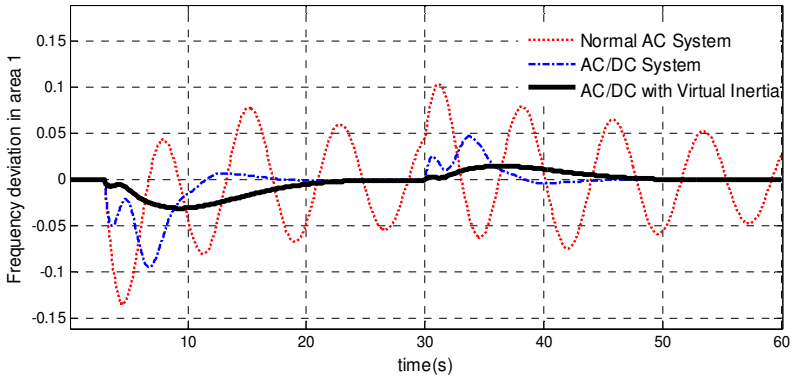

Figure 5.6. Dynamic response of frequency in Area 1.

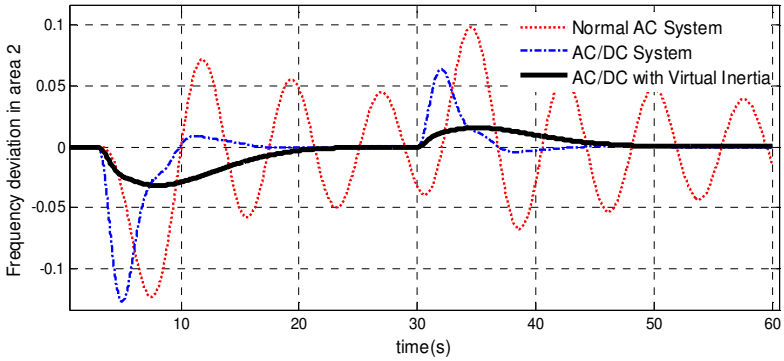

Figure 5.7. Dynamic response frequency in Area 2.

The response of active power delivered by generators and tie line powers is shown in Figures 5.8 to 5.14. Since dynamics of the mechanical parts are slow, it can be observed that at t = 3.5 s, when the power of ESS in the Area 2 (ESS2) is at its maximum level (Figure 5.14), the mechanical parts just start to change their power level and their contribution at 3.5 s is negligible, much less than maximum power resulting from the inertia emulated by the ESS in the Area 1 (ESS1).

Considering the fact that the time constant of ESS and power converters in the DC link are much lower than the time constant of mechanical parts in conventional generators, the ESS1 will start quickly to compensate the contingency in a very short time. As shown in Figure 5.14 the inertial power response reaches its maximum value in less than 0.5 s while the active power from electromechanical generators just starts to

change at that time. Therefore, for estimating the required energy to emulate an inertial power response by the ESS in both areas during its fast initial response, it is possible to assume a constant value for electromechanical power.

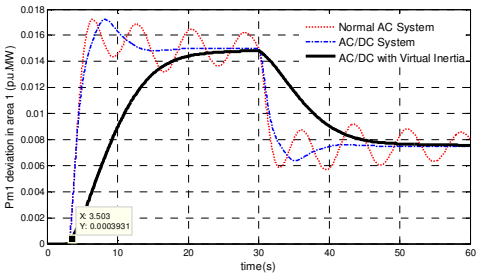

Figure 5.8. Output power of Generator 1

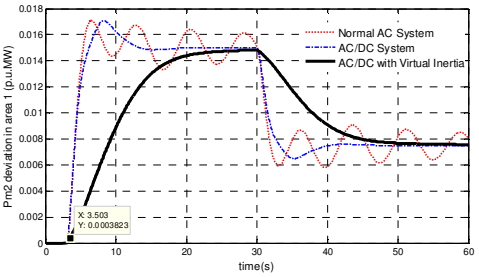

Figure 5.9. Output power of Generator 2.

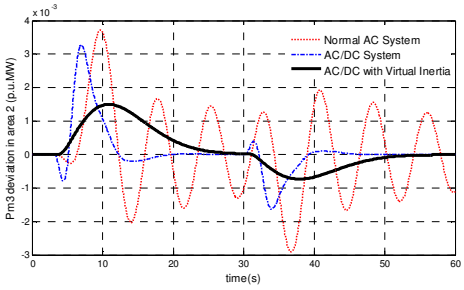

Figure 5.10. Output power of Generator 3

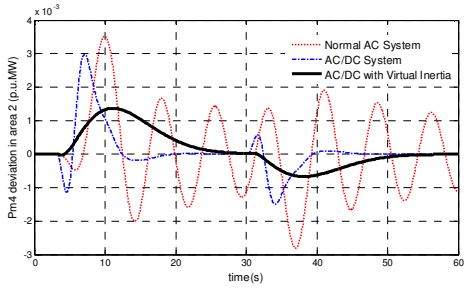

Figure 5.11. Output power of Generator 4.

The AC tie-line power and DC power deviations are also depicted by Figures 5.12 and 5.13, respectively. Their values at 3.5 s, especially for AC tie-line power (0.0001 p.u.), compared to ESS power are also very small.

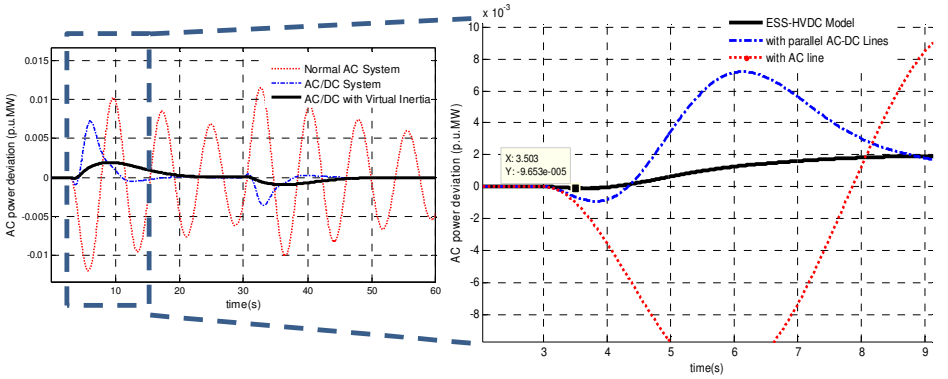

Figure 5.12. Power variations of AC line in pu.

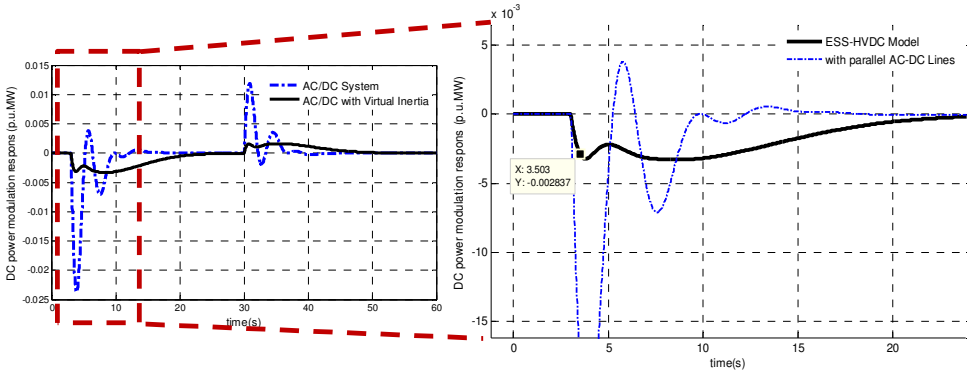

Figure 5.13. Power variation of HVDC link for different systems (AC/DC, AC/DC with inertia).

The power and energy variations of the ESS in both areas are presented in Figures 5.14 and 5.15, respectively. In this study case, based on the obtained results in Figure 5.14, the maximum value of emulated inertial power which is injecting to the grid is 0.0262 at 3.5 s.

$$P_{dischar}|_{t=3.5s} = 0.0262 \text{ p.u.}$$
(Maximum emulated power for injecting to the grid) (5.21)

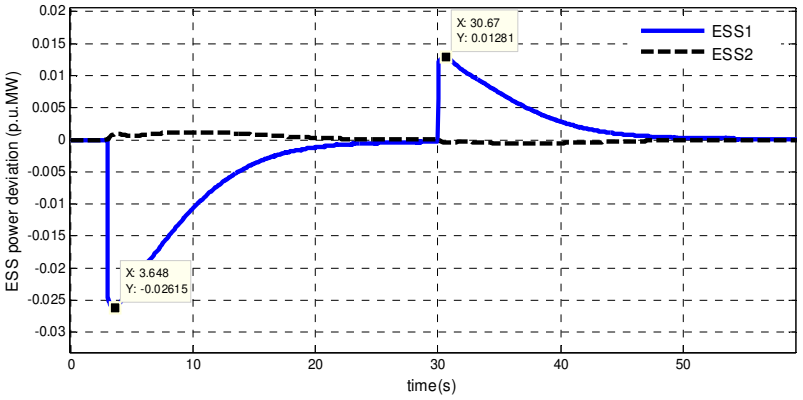

Figure 5.14. Emulated inertial power by using derivative control method.

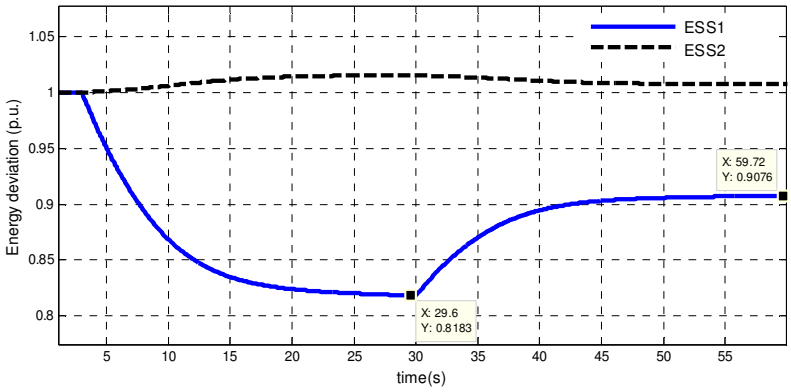

Figure 5.15. Energy variations of ESS during inertia emulation.

Based on these results, the maximum required power for inertia emulation will be around %3 of the rated power in this study case.

$$P_{dischar}|_{t_{max}} = P_d|_{t_{max}} - (P_{m1}|_{t_{max}} + P_{m2}|_{t_{max}} - P_{dc}|_{t_{max}} - P_{ac}|_{t_{max}}) \tag{5.22}$$

$$\begin{aligned} P_{dischar}|_{t_{3.5}} &= 0.03 - (0.0004 + 0.0004 + 0.00284 + 0.0001) \\ &= 0.03 - 0.00374 = 0.0262 \ \text{p.u.} \end{aligned} \tag{5.23}$$

Also, as shown in Figure 5.15, the amount of energy for the ESS1 in the first contingency will reach to 0.818 p.u.

$$E_{dischar} = 0.818 \ \text{p.u.}$$
(Maximum energy of ESS1 in the first contingency) (5.24)

This method provides a high-level estimation for defining operating references for converter stations and capacitors rating, which will be very useful for pre-evaluation and design before installation of the transmission system.

In the second contingency, at t = 30 s, a sudden decrement for load demand will happen at the Area 1. As a consequence of this contingency, the frequency is increased. Therefore, the frequency derivative control, which is located in the Area 1, will start reacting. For this second contingency, after a very short time, the ESS1, which is much faster than the electromechanical power, will reach to its maximum power:

$P_{char} = 0.0128$ p.u. (Maximum charging power) (5.25)

Also, as shown in Figure 5.15, the level of energy for the ESS1 is around 0.907 p.u in second contingency.

$E_{char} = 0.907$ p.u. (Energy of ESS1 for the second contingency) (5.26)

Therefore, as shown the required power for storage device can be estimated based on (5.18), while the maximum power can be predicted by (5.19). A comparison between the actual and the estimated power during the transient of load change is presented in Figure 5.16.

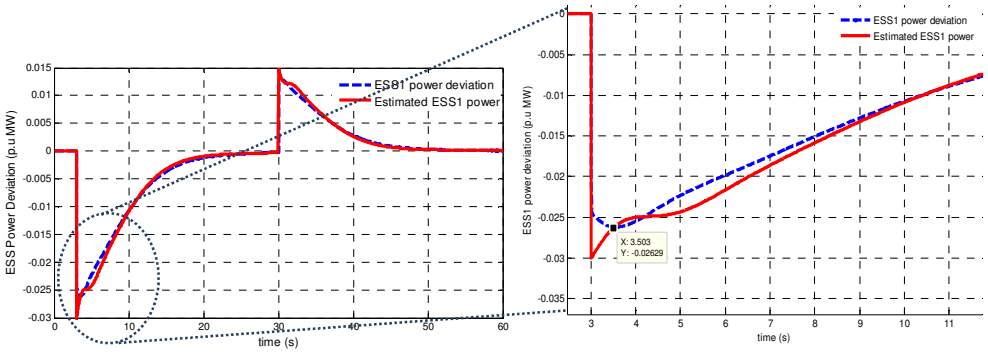

Figure 5.16. Status of power and energy in ESS1 during inertia emulation.

In this Section, the comparisons were presented for two continues contingencies at 3.5 s and 30 s. In the following chapters, more detailed analyses for the case considering only the first contingency (load change at t=3.5 in Area1) are presented to define the proper values for controller parameters and required energy. As explained, the required power for ESS1 is around 0.026 p.u which will be the same as the ones presented by the following sections.

It should be noted that, the main focus was on introducing the concept of the use of the energy storage devices as virtual inertia, including of these devices in the frequency and active power stability analysis.

5.3 System Analyses

In this Section, the dynamic effects of inertia emulation by using the derivative control method are analyzed by performing numerical, parameter sensitivity and eigenvalue (modal) analyses.

5.3.1 Eigenvalue analysis

By using the state space model of the power system under study, it can be analyzed by examining its eigenvalues and eigenvectors. In the Laplace domain, the following equation can be used to obtain the eigenvalues of the system under study from its state matrix **A**:

$$\det(\mathbf{A} - \boldsymbol{\lambda}\mathrm{I}) = 0 \tag{5.27}$$

This formula is also referred as the characteristic equation of the state matrix of the system. It is worth to mention in this point that the matrix **A** matches a type of a Jacobian matrix, in which the elements a_{ij} can be presented as partial derivatives at the equilibrium point [5.1].

Depending on the location of the poles of the terms in **A**, the eigenvalues can be real or complex. In a normal $n \times n$ matrix, the number of eigenvalues is equal to n. While the eigenvalues with a complex conjugates pairs can be defined as follows:

$$\lambda_i = \sigma \pm j\omega \tag{5.28}$$

Eigenvalues and Stability analysis

In principle, a given power system shows a stable response when all of the eigenvalues of the system are placed in the stable area in the complex plane, which means all of them are in the left side of the imaginary axis; if do not so, it will result in an unstable mode. The appearance of some of the eigenvalues in the right side of the imaginary axis is a clear sign of unstable modes, which lead the system to the instability.

The objective in the eigenvalue and system stability analysis is to verify that all the eigenvalues are located in the left-hand side. All of the obtained results from eigenvalue analysis can be checked through their time-dependent characteristic of the oscillatory modes, which corresponds to some specific eigenvalue λ_i.

The non-oscillatory modes are related to real eigenvalues. All the eigenvalues with a negative real part correspond to damped modes with a given decay time, which depends

on the magnitude of their real parts, i.e., the higher module for the real part the shorter time constant for such a mode.

Damping ratio and frequency of oscillations are two important factors in the eigenvalue analysis. The real component of an eigenvalue corresponds to damping ratio while the imaginary part indicates the frequency of oscillation. Both factors are defined as follow:

Frequency of oscillation (Hz):

$$f = \frac{\omega}{2\pi} \tag{5.29}$$

The damping ratio:

$$\zeta = \frac{-\sigma}{\sqrt{\sigma^2 + \omega^2}} \tag{5.30}$$

Therefore, damped oscillations will be represented by eigenvalues with negative real components, while unstable modes, with increasing trend in magnitude, will be represented by eigenvalues with positive real components. The eigenvalue analysis is one of the most popular analysis methods, which makes possible to evaluate the evolution of system eigenvalues as a function of changes in some of the system parameters. The complete state matrix **A** of the studied multi-area system, with the derivative based control, was presented in Section 5.2.2.

In Table 5.2, the values for all the modes of the system with the derivative control are calculated for different values for control gain J_1 (corresponding to Area 1). From the presented information in Table 5.2, it could be observed that the first mode, λ_1 , presents the highest variation degree respect to the value of J_1, which indicates that it is the most sensitive mode to the changes in such parameter in Area 1. This issue is also justified by performing the sensitivity analysis in the next Section. As shown in Table 5.2, λ_6 is another mode with some negative effects on the system stability, since it moves towards the right-hand side of the s-plane as the value for J_1 increases.

As it will be explained in the next Section, this mode is related to the 7th state (ACE_1) of the system. By performing a time domain analysis, it will be shown that the higher value for J_1 will lead to higher settling time for this state. This issue is also depicted in Figure 5.17, shows the higher settling time for higher values of J_1.

Therefore, it should be kept in mind that selection of the values for the control gains of the system will result from a trade-off for achieving the most optimal response at the same time that some system constrains are fitted. These constrains will result from the limitations in the desired system response and from the physical requirements set by the ESS components.

Table 5.2. Eigenvalues for different values of J_1 (with J_2=0.093).

Modes	$J_1 = 0.1$	$J_1 = 0.8$	$J_1 = 1.5$	$J_1 = 2.2$	$J_1 = 2.9$
λ_1	**-58.45**	**-195.6**	**-332.84**	**-470.12**	**-607.41**
λ_2	-52.96	-52.97	-52.96	-52.96	-52.96
λ_3	-23.25	-23.65	-22.57	-22.51	-22.51
λ_4	-0.78+i1.87	-1.17+i1.90	-1.23+i1.90	-1.25+i1.89	-1.27+i1.89
λ_5	-0.78-i1.87	-1.17-i1.90	-1.23-i1.90	-1.25-i1.89	-1.27-i1.89
λ_6	**-0.21+i0.36**	**-0.180**	**-0.101**	**-0.0007**	**-0.0005**
λ_7	-0.21-i0.36	-0.19+i0.24	-0.21+i0.22	-0.22+i0.22	-0.23+i0.22
λ_8	-0.427	-0.19-i0.24	-0.21-i0.22	-0.22-i0.22	-0.23-i0.22
λ_9	-2.154	-2.201	-2.201	-2.201	-2.201
λ_{10}	-2.248	-2.491	-2.550	-2.571	-2.590
λ_{11}	-2.695	-2.701	-2.701	-2.701	-2.701
λ_{12}	-2.631	-2.631	-2.631	-2.631	-2.631

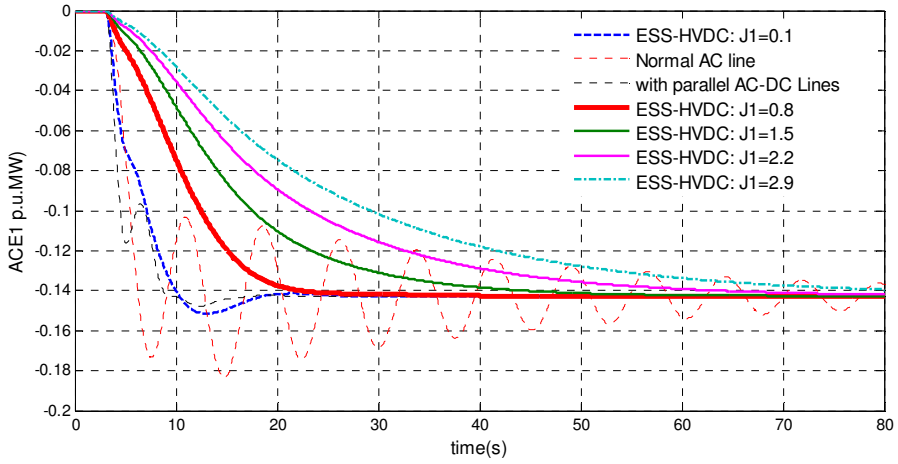

Figure 5.17. ACE1 response for different values of J_1.

The stability of the system under study with the derivative control can be also evaluated by analyzing the eigenvalues trajectory of matrix **A** versus changes on the control gains of the derivative control of the system. Figure 5.18 shows the trajectory of all the modes of the system for different values of the control gain J_1. In this study, as the load changes are occurring in Area 1, the control gain of the first derivative controller in the Area 1 will present the most significant impact. This issue will be observed also in the sensitivity analysis conducted in the following Sections.

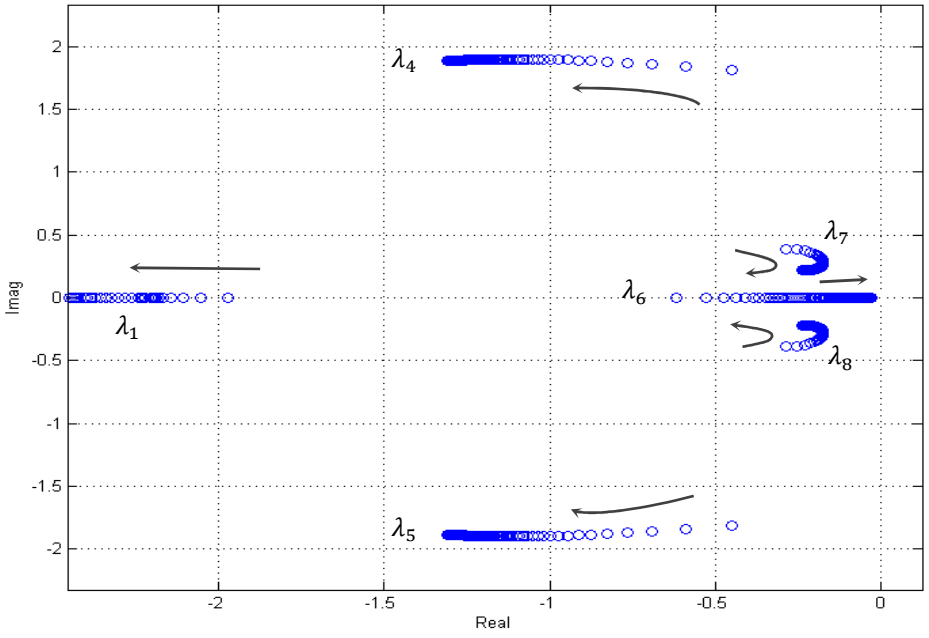

Figure 5.18. Eigenvalue trajectory of dominant poles over J_1 changes.

Based on the eigenvalue trajectory of Figure 5.18, moving the control gain of the first derivative controller (J_1) will affect at least six dominant poles of the system. The movements of these modes are presented in this figure. It is clear that, by increasing this control gain most of the modes (J_1, J_4, J_5, J_7 and J_8) are moved toward the left side of the s-plane, which will improve the stability of the system. As shown in this plot, the first mode (λ_1) is the most sensitive mode to the variations of the control gain (J_1). In addition to shifting the modes to the left side of s-plan, we can observe that the amplitude of imaginary axis for two of important modes, J_7 and J_8, are decreasing which can results in less oscillatory modes to the system. Therefore, it shows that by increasing the control gain of J_1, the dynamics of the system can improved with less oscillatory

behavior. But, on the other hand, there is another mode (λ_6) that trends towards zero as the control gain increases. This is the reason why it is necessary a trade-off for a proper selection of the control gains. The results of this analysis show that the system with the derivative based control can make a considerable improvement in the dynamic behavior of the studied system. In fact, by adding the derivative control for inertia emulation, the stability of system is improved.

The effect of various changes in the other control parameter (J_2), which is located in the Area 2 (the area without contingency) is presented in Table 5.3 and in Figure 5.19. As shown in the Table 5.3, the second mode λ_2 will have the highest variation as the value of J_2 changes, which indicates that this mode of the state matrix will have the highest sensitivity to any change from J_2. By increasing J_2, several modes, like $\lambda_4, \lambda_5, \lambda_6, \lambda_7$ and λ_8, will move to the right, which will deteriorate the dynamic performance of the system.

Table 5.3. Eigenvalues for different values of J_2 (with J_1=0.870).

Modes	$J_2 = 0.01$	$J_2 = 0.05$	$J_2 = 0.09$	$J_2 = 0.15$	$J_2 = 0.5$
λ_1	-209.32	-209.32	-209.32	-209.32	-209.32
λ_2	**-40.10**	**-46.23**	**-52.49**	**-61.90**	**-116.87**
λ_3	-22.42	-22.55	-22.63	-22.70	-22.83
λ_4	-1.29+i1.7	-1.22+i1.82	-1.18+i1.90	-1.15+i1.97	-1.10+i2.01
λ_5	-1.29-i1.7	-1.22-i1.82	-1.18-i1.90	-1.15-i1.97	-1.10-i2.01
λ_6	-0.22+i0.11	-0.201	-0.17	-0.15	-0.08+i0.22
λ_7	-0.22-i0.11	-0.24+i0.20	-0.20+i0.23	-0.16+i0.24	-0.08-i0.22
λ_8	-0.460	-0.24-i0.20	-0.20-i0.23	-0.16-i0.24	-0.101
λ_9	-1.80	-2.07	-2.20	-2.30	-2.65
λ_{10}	-2.50	-2.50	-2.50	-2.50	-2.50
λ_{11}	-2.69	-2.69	-2.70	-2.70	-2.55
λ_{12}	-2.63	-2.63	-2.63	-2.63	-2.63

As shown in Figure 5.19, the control gain effect of the second derivative controller, J_2, located in the Area 2 is analyzed considering the movements of the system's modes for different gain value. From this figure, it can be observed that several modes of the system are approaching to the right. This makes the system less stable, with more oscillation. This is due to approaching five dominant poles, J_4, J_5, J_6, J_7 and J_8, to the imaginary axis. This is more critical in case of J_1, J_4, J_5, J_7 and J_8 modes which challenge the stability of the system. Furthermore, it is clear that, by increasing the control gain J_2, the amplitude of imaginary component of the two other modes, J_4 and J_5, are increased which will bring more oscillatory behavior to the system.

The stability analysis is meaningful to avoid the instability issues induced by improper control parameters in the system. The obtained results from this eigenvalue analyses will help us for better understanding the effects of control gains of derivative controllers, J_1 and J_2 which are located in both areas, on the system modes. This gives an idea about the proper ranges of each control gain and their limits in each study case to guaranty the stability of the system. In the following sections, more detailed analysis supporting this issue are presented and discussed.

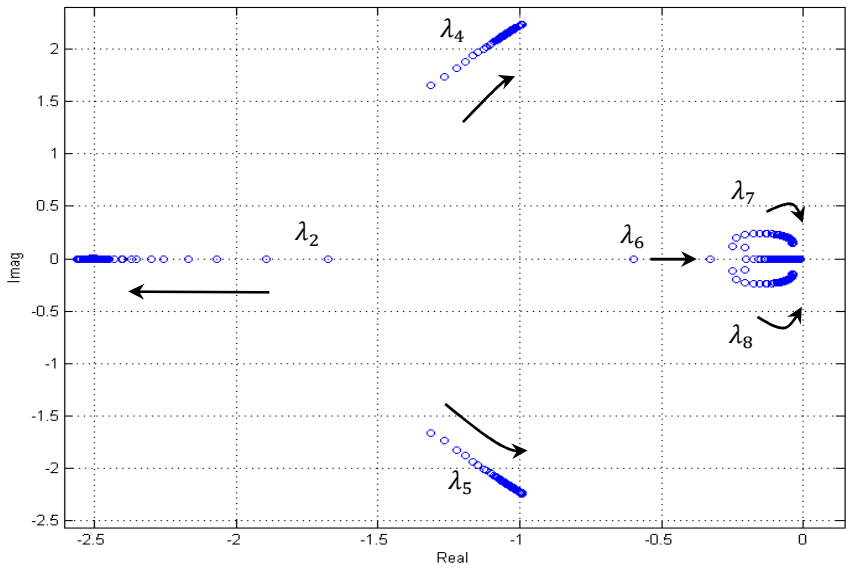

Figure 5.19. Eigenvalue trajectory of dominant poles over J_2 changes.

A general eigenvalues comparison for different area interconnection systems discussed in previous Sections is presented in Table 5.4. It can be observed in this table that the system response is improved when the derivative based control for emulating inertia is enabled, since the eigenvalues are shifted to a better place in the left-hand side of the s-plane. As a consequence, less oscillatory modes with higher damping are achieved with this frequency derivative control strategy.

Table 5.4. Eigenvalues comparison for different interconnection systems.

Modes	AC System	AC/DC System	AC/DC System with Derivative Control
λ_1	-0.027 + 0.825I	-23.9299	-209.32
λ_2	-0.027 - 0.825I	-0.4945 + 1.6611I	-52.96
λ_3	-0.342 + 0.399I	-0.4945 - 1.6611I	-22.63
λ_4	-0.342 - 0.399I	-0.3437 + 0.4245I	-1.1 + 1.9I
λ_5	-0.7023	-0.3437 - 0.4245I	-1.1 - 1.9I
λ_6	-1.8271	-0.8974	-0.201
λ_7	-2.1073	-1.9374 + 0.1752I	-0.1 + 0.2I
λ_8	-2.6872	-1.9374 - 0.1752I	-0.1 - 0.2I
λ_9	-2.6316	-2.6850	-2.30
λ_{10}	--------	-2.6316	-2.50
λ_{11}	--------	--------	-2.70
λ_{12}	--------	--------	-2.63

5.3.2 Sensitivity Analyses

As explained before, the most important parameter in derivative control is the control gain (J_i), which determines how much active power should be released from the storage elements in response to a load step-change. This active power will change the dynamic behaviors of other state variables, like frequency of the studied system.

For analyzing the dynamic effects of control gains on the system behavior, numerical simulations are conducted for different values of the control gain J_1. These analyses are performed for a two-area system under a typical load step-change around 0.03 p.u at 3 s. The dynamic response of system frequency are presented and compared in Figures 5.20

and 5.21, where it can be observed that the peaks in frequency of both areas is reduced as the value of J_1 is increased from 0.1 to 2.9.

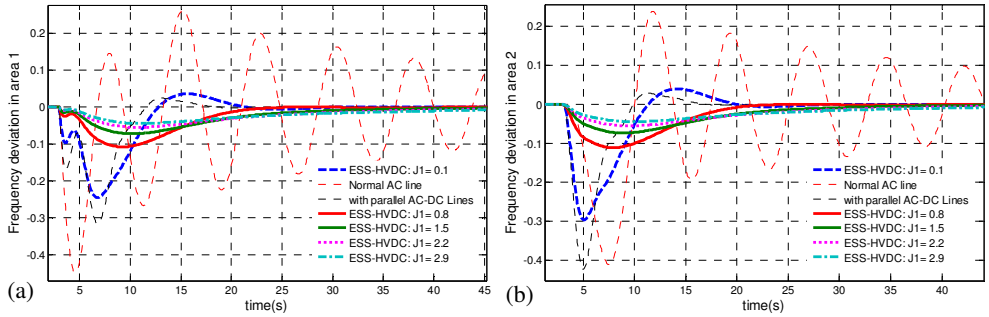

Figure 5.20. Frequency response in Area 1 and 2 for different values of the control gain J_1.

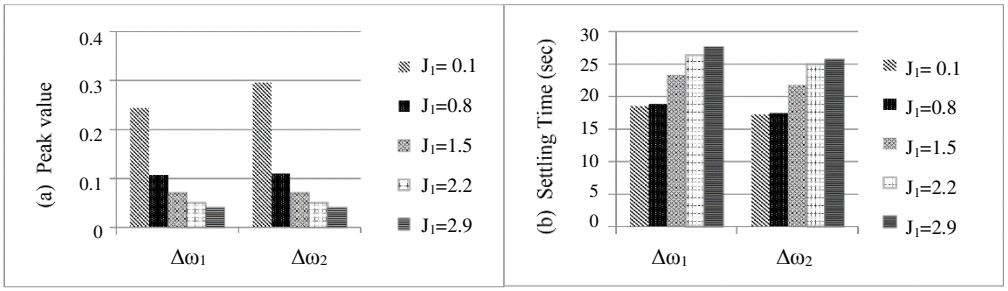

Figure 5.21. Frequency characteristics: (a) Peak overshoot, and (b) Settling time.

The effects of the control gain J_1 over the damping and the frequency of oscillations in the oscillatory modes are also presented in Table. 5.5 and 5.6. These tables evidence that better damping with less oscillation is obtained by increasing the control gain J_1.

Table 5.5. The damping value of oscillatory modes for different control gain.

Damping of oscillatory modes	$J_1 = 0.8$	$J_1 = 1.5$	$J_1 = 2.2$	$J_1 = 2.9$
$\zeta_{\lambda_{4,5}}$	0.5252	0.5446	0.5524	0.5666
$\zeta_{\lambda_{7,8}}$	0.6273	0.6933	0.7114	0.7290

Table 5.6. The Frequency of oscillatory modes for different control gain.

Frequency of oscillatory modes	$J_1 = 0.8$	$J_1 = 1.5$	$J_1 = 2.2$	$J_1 = 2.9$
$f_{\lambda_{4,5}}$	0.3024	0.3017	0.3013	0.3010
$f_{\lambda_{7,8}}$	0.0377	0.0354	0.0350	0.0349

Analyzing dynamics, it is worth to remark that the overshoot of frequency in both areas decreases and the settling time increases as the control gain J_1 is increased. This is evidenced in Figure 5.22. Therefore, as previously mentioned, there will be a trade-off between amplitude and dynamic constrains for selecting the proper value for control gain of the derivative control method. As shown in Figure 5.22, a proper settling time could be achieved for values of J_1 around 0.8. However, for higher values, the settling times will radically increase from 40 s to 80 s, which is not desirable.

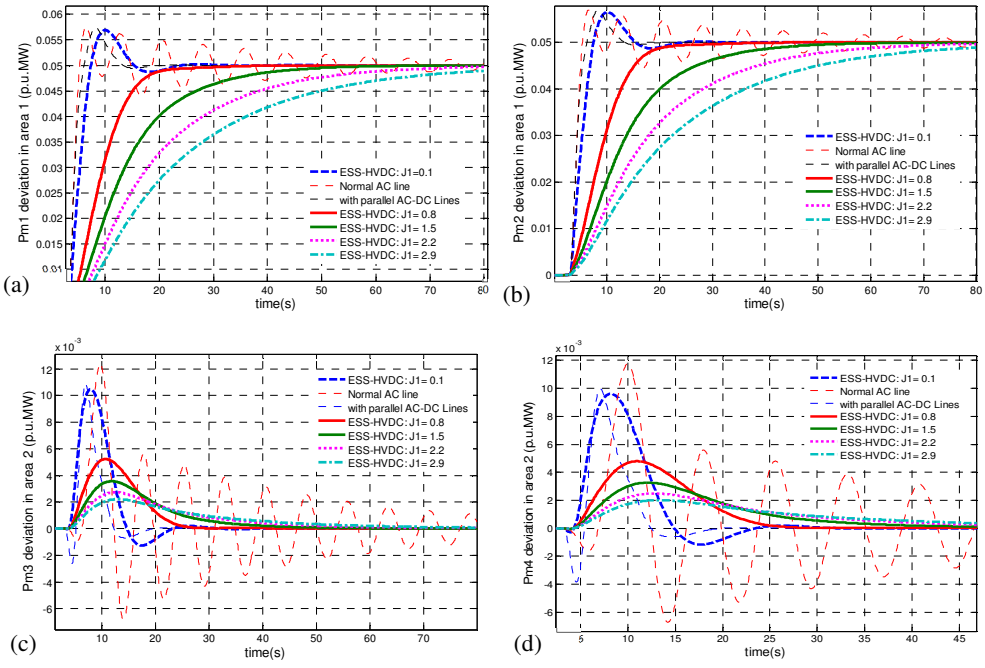

Figure 5.22. Output power of each generation unit: (a) GENCO1, (b) GENCO2, (c) GENCO3 and (d) GENCO4.

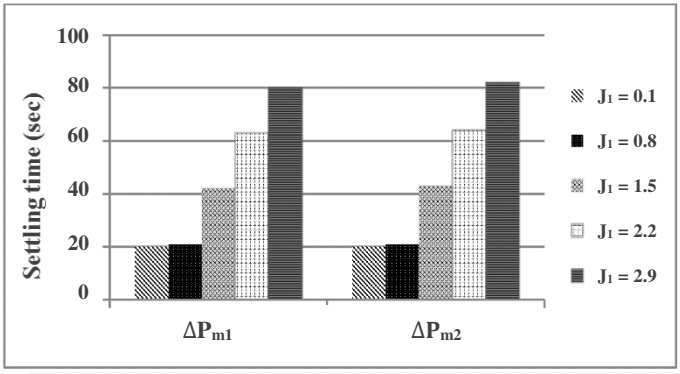

Figure 5.23. Settling times of active power response for GENCO1 and GENCO2.

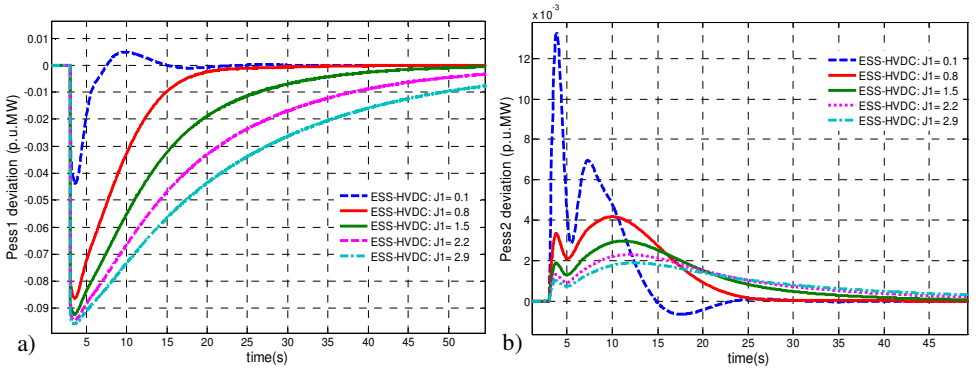

Figure 5.24. Powers generated by the derivative control method: (a) ESS1, (b) ESS2.

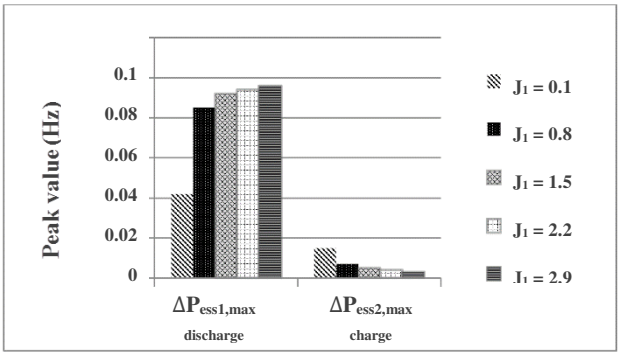

Figure 5.25. Comparisons of peak power during virtual inertia emulation for different gains.

The relationship between the reference powers generated by both derivative controllers, for different value of J_1, is depicted by Figures 5.24 and 5.25. Since the load step-change (disturbance) occurs in Area 1, most of the contribution comes from J_1 (in the same area of disturbance). This contribution is achieved by increasing the control gain value J_1 to a reasonable value.

5.3.2.1 Eigenvalue sensitivity

Normally, the state matrix **A** is a non-diagonal matrix and therefore, the evolution of one state variable will be coupled to the evolution of several state variables. Any square matrix can be diagonalized, or at least brought to Jordan canonical form, by solving left or right eigenvalue problem. This fact is related to the eigen-decomposition of square state matrix **A** in the system [1].

Considering a given eigenvalue λ_i, the related column vector of Φ_i which can fulfill the following equation can be considered as the right eigenvector of the state matrix.

$$\boldsymbol{A\Phi_i = \lambda_i \Phi_i} \tag{5.31}$$

And similarly, a related row vector Ψ_i, which can fulfill the following formula can be considered as the left eigenvector of the state matrix in the system.

$$\boldsymbol{\Psi_i A = \lambda_i \Psi_i} \tag{5.32}$$

Obviously, eigenvectors obtained from these equations are not unique, as they can be rescaled by multiplying or dividing the elements by a nonzero number. Eigenvectors describe the mutual relation between modal and original variables. Analysis of the right eigenvector will give us the mode shape. The mode shape is the relative activity for any state when a specific mode is excited.

Due to the natural scaling of physical-related state space, which usually is not globally normalized, it is not possible to compare how much different variables participate in an oscillation. Therefore, a very useful modal index is the Participation Factor (*PF*).

The *PF* is an indicator of the related participation of any state in any mode and also any mode in any state. Thus, it shows which machine and particular state greatly affects a given eigenvalue of interest. The *PF* is a non-dimensional indicator that mixes the right eigenvectors with left eigenvectors, like this:

$$PF_i = \begin{bmatrix} P_{1i} \\ P_{2i} \\ \vdots \\ P_{ni} \end{bmatrix} = \begin{bmatrix} \phi_{1i}\Psi_{i1} \\ \phi_{2i}\Psi_{i2} \\ \vdots \\ \phi_{ni}\Psi_{in} \end{bmatrix} \tag{5.33}$$

where

ϕ_{ki} = k[th] element of the right eigenvector ϕ_i

Ψ_{ik}= k[th] element of the left eigenvector Ψ_i

Therefore, P_{ki} is a measure of the related participation of the k^{th} state of the system in the i[th] modes of the system.

The participation matrix for multi-area model under study in this work is calculated in the following.

Participation factor Matrix:

0.00	0.00	0.157	**0.814**	**0.814**	03975	0.453	0.453	0.632	0.089	0.00	0.00	$\Delta\omega_1$
0.00	0.001	0.036	**0.401**	**0.401**	0.220	0.544	0.544	0.050	0.003	0.004	0.00	$\Delta\omega_2$
0.00	0.00	0.00	0.008	0.008	0.032	0.013	0.013	0.017	0.518	0.00	0.485	ΔP_{m1}
0.00	0.00	0.00	0.008	0.008	0.032	0.014	0.014	0.015	0.485	0.00	0.517	ΔP_{m2}
0.00	0.00	0.00	0.007	0.007	0.022	0.048	0.048	0.369	0.003	0.750	0.00	ΔP_{m3}
0.00	0.00	0.00	0.010	0.010	0.023	0.050	0.050	0.849	0.027	0.258	0.00	ΔP_{m4}
0.00	0.00	0.00	0.031	0.031	1.257	0.318	0.318	0.014	0.032	0.00	0.00	ΔACE_1
0.00	0.00	0.00	0.087	0.087	0.177	0.570	0.570	0.187	0.011	0.004	0.00	ΔACE_2
0.00	0.00	0.00	0.366	0.366	0.150	0.121	0.121	0.0346	0.011	0.00	0.00	ΔP_{tieAC}
0.00	0.003	1.105	0.056	0.056	0.00	0.00	0.00	0.005	0.001	0.00	0.00	ΔP_{DC}
0.99	0.00	0.008	0.002	0.002	0.003	0.00	0.00	0.00	0.002	0.00	0.00	$\Delta \boldsymbol{P_{ESS1}}$
0.00	**1.01**	0.008	0.004	0.004	0.001	0.00	0.00	0.005	0.00	0.00	0.00	$\Delta \boldsymbol{P_{ESS2}}$
$\boldsymbol{\lambda_1}$	$\boldsymbol{\lambda_2}$	λ_3	λ_4	λ_5	λ_6	λ_7	λ_8	λ_9	λ_{10}	λ_{11}	λ_{12}	

Based on the resulting terms in the participation matrix, it can be clearly observed which states have more participation in sensitive or critical modes. For example, two of the oscillatory modes are related to the eigenvalues λ_4 and λ_5, and by checking the participation factor matrix, it becomes clear that $\Delta\omega_1$ and $\Delta\omega_2$ have the most participation in those modes.

Another objective of performing the analysis for eigenvalue sensitivity will be the identification of related sensitivity for specific eigenvalues to each element of the state matrix **A** in the system under study.

For this purpose, a differentiation can be made from (5.31) with respect to each kjth element of the matrix **A**:

$$\frac{\partial A}{\partial a_{kj}}\Phi_i + A\frac{\partial \Phi_i}{\partial a_{kj}} = \frac{\partial \lambda_i}{\partial a_{kj}}\Phi_i + \lambda_i\frac{\partial \Phi_i}{\partial a_{kj}} \tag{5.34}$$

After multiplication of both sides of this equation by left eigenvector with considering that $\phi_i\Psi_i = 1$ and $\Psi_i(A - \lambda_i\, I) = 0$, then we have:

$$\Psi_i\frac{\partial A}{\partial a_{kj}}\Phi_i = \frac{\partial \lambda_i}{\partial a_{kj}} \tag{5.35}$$

All the elements of $\frac{\partial A}{\partial a_{kj}}$ are zero except for the element in kth row and jth column which is equal to one. Thus, the sensitivity matrix (P_{sens}) is like this:

$$\Psi_{ik}\Phi_{ji} = \frac{\partial \lambda_i}{\partial a_{kj}} \tag{5.36}$$

Therefore, it becomes clear that the sensitivity of each specific eigenvalue λ_i to any element a_{kj} of the state matrix of the studied system will be equal to the production of the left and right eigenvector elements. This indicates that the best way to change the i^{th} mode is to apply a control to the state variable such that the above sensitivity has the largest participating factor.

In order to apply such analysis for the two-area power system under study in this work, the state matrix **A** is partitioned as follows:

$$\mathbf{A} = \begin{bmatrix}\mathbf{A}_{11}\\ \mathbf{A}_{21}\end{bmatrix}_{(12\times 12)} \tag{5.37}$$

Therefore, each sub-matrix will be as follows:

$$\mathbf{A}_{11}=\begin{bmatrix}
\frac{-1}{T_{p1}} & 0 & \frac{K_{p1}}{T_{p1}} & \frac{K_{p1}}{T_{p1}} & 0 & 0 & 0 & 0 & \frac{-K_{p1}}{T_{p1}} & \frac{-K_{p1}}{T_{p1}} & \frac{-K_{p1}}{T_{p1}} & 0\\
0 & \frac{-1}{T_{p2}} & 0 & 0 & \frac{K_{p2}}{T_{p2}} & \frac{K_{p2}}{T_{p2}} & 0 & 0 & \frac{K_{p2}}{T_{p2}} & \frac{K_{p2}}{T_{p2}} & 0 & \frac{-K_{p2}}{T_{p2}}\\
\frac{-1}{2\pi R_1 T_{tg1}} & 0 & \frac{-1}{T_{tg1}} & 0 & 0 & 0 & \frac{-K_{I1}}{T_{tg1}} & 0 & 0 & 0 & 0 & 0\\
\frac{-1}{2\pi R_2 T_{tg2}} & 0 & 0 & \frac{-1}{T_{tg2}} & 0 & 0 & \frac{-K_{I1}}{T_{tg2}} & 0 & 0 & 0 & 0 & 0\\
0 & \frac{-1}{2\pi R_3 T_{tg3}} & 0 & 0 & \frac{-1}{T_{tg3}} & 0 & 0 & \frac{-K_{I2}}{T_{tg3}} & 0 & 0 & 0 & 0\\
0 & \frac{-1}{2\pi R_4 T_{tg4}} & 0 & 0 & 0 & \frac{-1}{T_{tg4}} & 0 & \frac{-K_{I2}}{T_{tg4}} & 0 & 0 & 0 & 0\\
\frac{\beta_1}{2\pi} & 0 & 0 & 0 & 0 & 0 & 0 & 0 & 1 & 1 & 0 & 0\\
0 & \frac{\beta_2}{2\pi} & 0 & 0 & 0 & 0 & 0 & 0 & -1 & -1 & 0 & 0\\
\frac{T_{12}}{2\pi} & -\frac{T_{12}}{2\pi} & 0 & 0 & 0 & 0 & 0 & 0 & 0 & 0 & 0 & 0\\
\frac{K_{f1}}{T_{DC}} & \frac{K_{f2}}{T_{DC}} & 0 & 0 & 0 & 0 & 0 & 0 & \frac{K_{AC}}{T_{DC}} & \frac{-1}{T_{DC}} & 0 & 0
\end{bmatrix} \tag{5.38}$$

and

$$\mathbf{A}_{21}=\begin{bmatrix}
a_{11,1} & 0 & a_{11,3} & a_{11,4} & 0 & 0 & 0 & 0 & a_{11,9} & a_{11,10} & a_{11,11} & 0\\
0 & a_{12,2} & 0 & 0 & a_{12,5} & a_{12,6} & 0 & 0 & a_{12,9} & a_{12,10} & 0 & a_{12,12}
\end{bmatrix} \tag{5.39}$$

As identified in state space presentation of the global system, the terms associated to the derivative control appear in the sub-matrices $\mathbf{A}_{21}$, which are related to the derivative control's state variables. In fact, these parameters are presented in 11th and 12th rows of the global matrix $\mathbf{A}$ and could be used for analyzing the system performance.

Therefore, the elements of interest in matrix $\mathbf{A}$ are the elements which contain the control gains of the derivative control (J_1 and J_2) in sub-matrix $\mathbf{A}_{21}$. The elements in the 11th row, which are associated to J_1, are:

$$\begin{gathered}
a_{11,1}=\frac{-J_1}{T_{ess1}T_{p1}},\ a_{11,3}=\frac{J_1 K_{p1}}{T_{ess1}T_{p1}}, a_{11,4}=\frac{J_1 K_{p1}}{T_{ess1}T_{p1}}, a_{11,9}=\frac{J_1 K_{p1}}{T_{ess1}T_{p1}},\\
a_{11,10}=\frac{J_1 K_{p1}}{T_{ess1}T_{p1}},\ a_{11,11}=\frac{-J_1 K_{p1}}{T_{ess1}T_{p1}}+\frac{-1}{T_{ess1}}
\end{gathered} \tag{5.40}$$

The results regarding sensitivities to this relevant elements in state matrix $\mathbf{A}_{(12\times12)}$ are presented in Tables 5.7 and 5.8. In these tables, the absolute value for the sensitivity of each mode to the elements of sub-matrix $\mathbf{A}_{21}$, which are of our interest, is presented.

Table 5.7. Absolute value of sensitivity of each mode for elements in the 11th row of **A** matrix.

Absolute Sensitivity of λ_i	$a_{11,1}$	$a_{11,3}$	$a_{11,4}$	$a_{11,9}$	$a_{11,10}$	$\boldsymbol{a_{11,11}}$
$\boldsymbol{\lambda_1}$	0.0243	0.000	0.000	0.000	0.000	**0.9982**
λ_2	0.000	0.000	0.000	0.000	0.000	0.000
λ_3	0.0041	0.000	0.000	0.000	0.096	0.0088
λ_4	0.020	0.000	0.000	0.000	0.0044	0.0029
λ_5	0.020	0.000	0.000	0.000	0.0044	0.0029
λ_6	0.0097	0.0021	0.0021	0.000	0.0011	0.0038
λ_7	0.0111	0.000	0.000	0.000	0.000	0.0014
λ_8	0.0111	0.000	0.000	0.000	0.000	0.0014
λ_9	0.0016	0.000	0.000	0.000	0.000	0.000
λ_{10}	0.0022	0.0019	0.0017	0.000	0.000	0.0028
λ_{11}	0.000	0.000	0.000	0.000	0.000	0.000
λ_{12}	0.000	0.000	0.000	0.000	0.000	0.000

From the presented information in Table 5.7, it can be concluded that the sensitivity for $a_{11,11}$ is higher than other elements. For this element of matrix **A**, the first mode (λ_1) has the highest sensitivity, which matches previous results obtained from the eigenvalue analysis. From the participation factor matrix, it could be realized that this mode is related to 11th state (ΔP_{ess1}).

Similarly, the elements from the 12th row of matrix $\mathbf{A_{21}}$, which are associated to J_2, are:

$$a_{12,2} = \frac{-J_2}{T_{ess2}\,T_{p2}},\ a_{12,5} = \frac{J_2\,K_{p2}}{T_{ess2}T_{p2}},\ a_{12,6} = \frac{J_2\,K_{p2}}{T_{ess2}T_{p2}},\ a_{12,9} = \frac{J_2\,K_{p2}}{T_{ess2}T_{p2}},$$
$$a_{12,10} = \frac{J_2\,K_{p2}}{T_{ess2}T_{p2}},\ a_{12,12} = \frac{-J_2\,K_{p2}}{T_{ess2}T_{p2}} + \frac{-1}{T_{ess2}}. \tag{5.41}$$

The sensitivity of the system modes to these elements is presented in Table 5.8. From this table, it can be observed that, the most of the elements have very low sensitivities except for the $a_{12,12}$ element, since the second mode of the system (λ_2) has

the highest sensitivity for this element. Therefore, from the participation factor matrix, it can be indicated that the 12th state (ΔP_{ess2}) has the main participation for this mode.

Table 5.8. Absolute value of sensitivity of each mode for elements in the 12th row of **A** matrix.

Absolute Sensitivity of λ_i	$a_{12,2}$	$a_{12,5}$	$a_{12,6}$	$a_{12,9}$	$a_{12,10}$	$\boldsymbol{a_{12,12}}$
λ_1	0.000	0.000	0.000	0.000	0.000	0.000
$\boldsymbol{\lambda_2}$	0.0780	0.000	0.000	0.000	0.0069	**1.0051**
λ_3	0.0049	0.000	0.000	0.000	0.0183	0.0087
λ_4	0.0317	0.000	0.000	0.0022	0.0131	0.0041
λ_5	0.0317	0.000	0.000	0.0022	0.0131	0.0041
λ_6	0.0170	0.0015	0.0015	0.0012	0.0024	0.0012
λ_7	0.0421	0.0033	0.0031	0.0033	0.0045	0.0022
λ_8	0.0421	0.0033	0.0031	0.0033	0.0045	0.0022
λ_9	0.0040	0.0059	0.0085	0.000	0.0069	0.0059
λ_{10}	0.000	0.000	0.000	0.000	0.000	0.000
λ_{11}	0.000	0.0017	0.000	0.000	0.000	0.000
λ_{12}	0.000	0.000	0.000	0.000	0.000	0.000

A summary of eigenvalue sensitivity analyses is presented in Table 5.9. As shown by the sensitivity matrices, modes λ_1 and λ_2 present the main sensitivities. Considering the results of participation matrix, it can be stated that the 11th and 12th states are the most important states in the design of the control for these modes.

Table 5.9. Summary of eigen sensitivity analyses.

Elements of A matrix	**Sensitive modes**	**Participant states**
$a_{11,11}$	λ_1	ΔP_{ess1}
$a_{12,12}$	λ_2	ΔP_{ess2}

As explained before, these two states ($\Delta P_{ess1}$and ΔP_{ess2}) are affected by their control gains J_1 and J_2, respectively. Therefore, with proper selection of these two gains, the desired dynamic response could be obtained.

To finalize the sensitivity analysis, it is required to investigate the proper range of control gain parameters. Therefore, a complete test of system characteristics (damping and frequency of oscillatory modes) over a wide range of variation for J_1 and J_2 is performed in the following.

As shown in Figure 5.26, the 3-D plot shows the values of frequency for oscillatory modes regarding the variation of derivative control parameters in p.u. This figure shows that the oscillatory index of the system could be minimized for different values of two control gains. For example, the minimum values for the oscillatory index of the studied system can be obtained for the region defined by $J_1 > 1$ and $J_2 < 0.5$.

From Figure 5.27, it could be also observed that the proper range of J_1 and J_2 for achieving the maximum damping will lead to the same result by Figure 5.26. These ranges could be also verified through eigenvalue trajectories during parameter changes which were presented before.

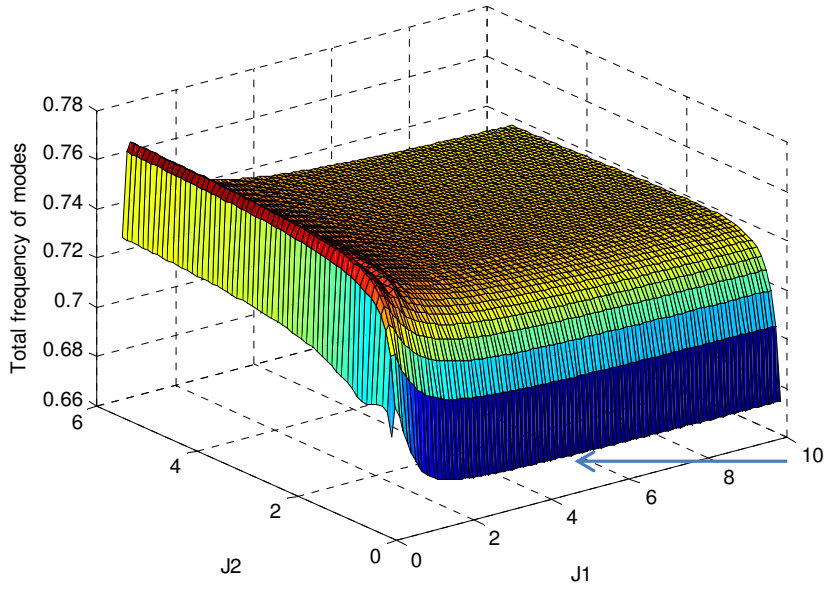

Figure 5.26. Three-dimensional presentation for sum of the frequencies of oscillatory modes (Hz) for different values of both control gains (J_1 and J_2).

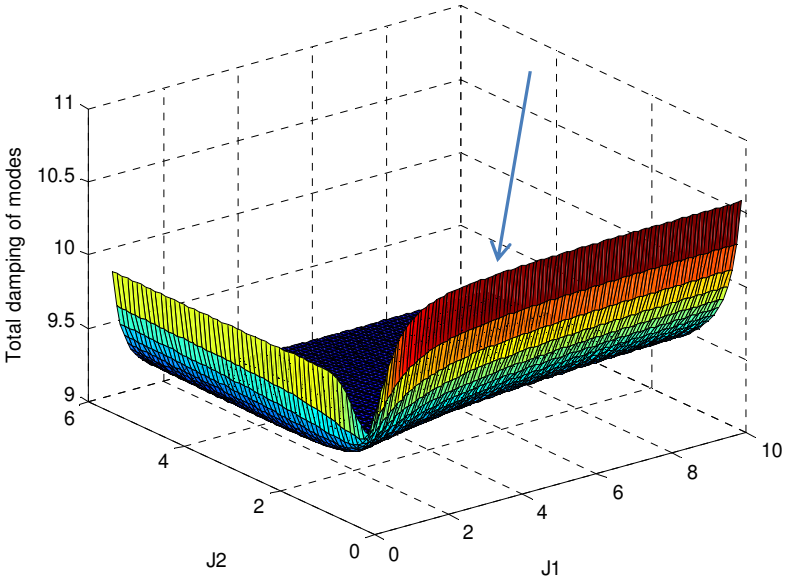

Figure 5.27. Three-dimensional presentation for total damping of oscillatory modes for change in both control gains (J_1 and J_2).

To summarize, these results show that a relatively acceptable performance can be obtained for low values for J_2, while the system performance will be sharply degraded for the high values for J_2 and very low values for J_1. In the system under study, it have been considered that appropriate results could be obtained for $J_1 > 0.6$ and $J_2 < 0.1$.

5.4 Dynamic effects of measurements

5.4.1 Dynamic model of PLL

A phase-locked loop (PLL) is one of the methods commonly used for grid synchronization of grid-connected converters [5.27]. The PLL is one of the synchronization components of power converters and the delays introduced by some elements can be compensated by just advancing the phase-angle detected by the PLL [5.27].

A general control structure of grid-connected converter with DC link and PLL is shown in Figure 5.28.

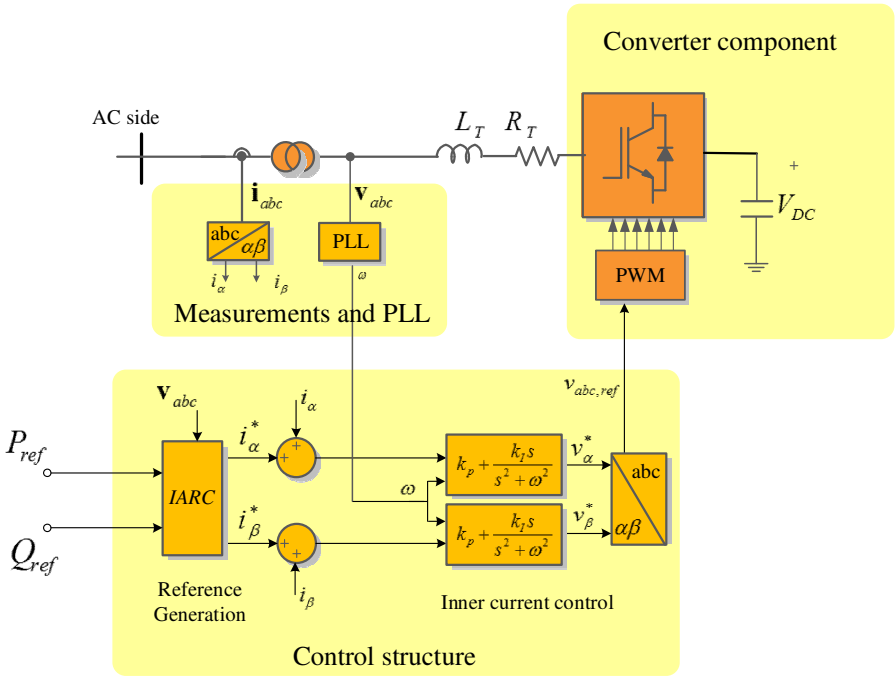

Figure 5.28. A typical control structure of grid-connected converters.

As shown in Figure 5.28, the reference values for active and reactive powers are coming for the higher level control actions, like droop control or the derivative control for emulating the inertia in the two-area interconnected power system. Related current references could be obtained based on the concept of Instantaneous Active-Reactive Control (IARC). The inner current loop controller is used for providing the reference

voltage for converter control. The angle of the grid voltage is estimated and provided by a PLL. This estimation is very important for proper action of the inner current controller.

As explained before, the dynamics of the power converter and the HVDC bus could be modeled by a first-order transfer function with a proper time constant, imitating the control time of this component. In this Section, in order to evaluate the dynamic effects of PLL and delayed measurements, a more detailed model of the power converter control is considered by adding an additional transfer function, which models the dynamics of PLL measurements. The general block diagram of the derivative control with the PLL is presented in Figure 5.29.

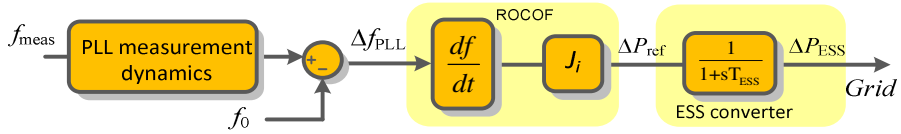

Figure 5.29. Block diagram of derivative inertia emulation strategy.

For defining a proper model imitating the dynamics of a PLL in higher level control analysis, a brief review is presented over the normal components of PLL. The general configuration of PLL is presented in Figure 5.30. It contains a Phase Detector (FD), a Loop filter (LF) and a Voltage-Controlled Oscillator (VCO).

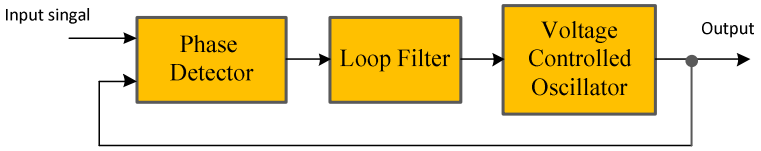

Figure 5.30. The basic structure of a PLL.

The phase detector is responsible for checking the phase differences between input and output signals of the VCO. In the output of VCO block, an AC signal will be generated, being its frequency shifted from a given central frequency according to the output of the LF block. Usually, this filter could be in a form of a PI controller, which will determine the dynamics of the PLL. The linearized model of a common PLL is presented in Figure 5.31.

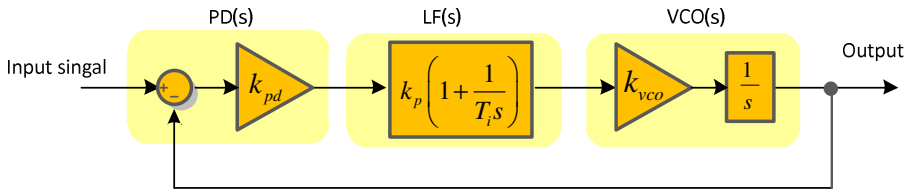

Figure 5.31. Small signal model of a basic PLL.

Considering unitary values for PD and VCO gains of this closed-loop system ($k_{pd} = k_{vco} = 1$), the following characteristic transfer functions can be obtained:

Open-loop phase transfer function:

$$F_{OL}(s) = PD(s).LF(s).VCO(s) = \frac{k_p(1+\frac{1}{T_i s})}{s} = \frac{k_p s + \frac{k_p}{T_i}}{s^2} \tag{5.42}$$

Therefore, the close-loop transfer function:

$$H(s) = \frac{F_{OL}(s)}{1+F_{OL}(s)} = \frac{k_p s + \frac{k_p}{T_i}}{s^2 + k_p s + \frac{k_p}{T_i}} \tag{5.43}$$

This second-order transfer function can be presented in a normalized form, like this:

$$\boldsymbol{H_{PLL}}(s) = \frac{2\zeta\omega_n \boldsymbol{s} + \omega_n^2}{\boldsymbol{s}^2 + 2\zeta\omega_n \boldsymbol{s} + \omega_n^2} \tag{5.44}$$

where

$$\omega_n = \sqrt{\frac{k_p}{T_i}} \quad \text{and} \quad \zeta = \frac{\sqrt{k_p T_i}}{2}$$

As the dynamic response of second-order is studied in many references, the following assumption can be used as an initial estimation of the settling time (t_s) for reaching 1% of the steady-state response [5.27]:

$$t_s = 4.6\,\tau \quad \text{with} \quad \tau = \frac{1}{\zeta\omega_n} \tag{5.45}$$

This simplification based on the second-order model is completely sufficient to determine the power system requirements of the dynamic analysis in the AGC systems.

Therefore, a second-order block with a zero will be considered for imitating the dynamic of remote PLL, its measurements and communication delay during inertia emulation of the power converter in the two-area AGC power system.

5.4.2 Model of two-area system with derivative control and PLL dynamics

In a real practice of derivative control implementation, measurement of frequency is very important. For estimating or measuring the frequency, different components like the PLL can be used. These components will introduce some delay with specific dynamics to the system. In control systems, it is well known that time delays and dynamics from measuring components can degrade the system's performance and even causes system instability [5.28]. So it would be important to take into account these effects for obtaining more accurate analysis in term of the derivative control implementation on the frequency regulation of the transmission system. As explained before, a second-order function could be considered for dynamic behaviors of PLL in the derivative control method. The modified model of two-area power system with the derivative control method adding the PLL is depicted by Figure 5.32.

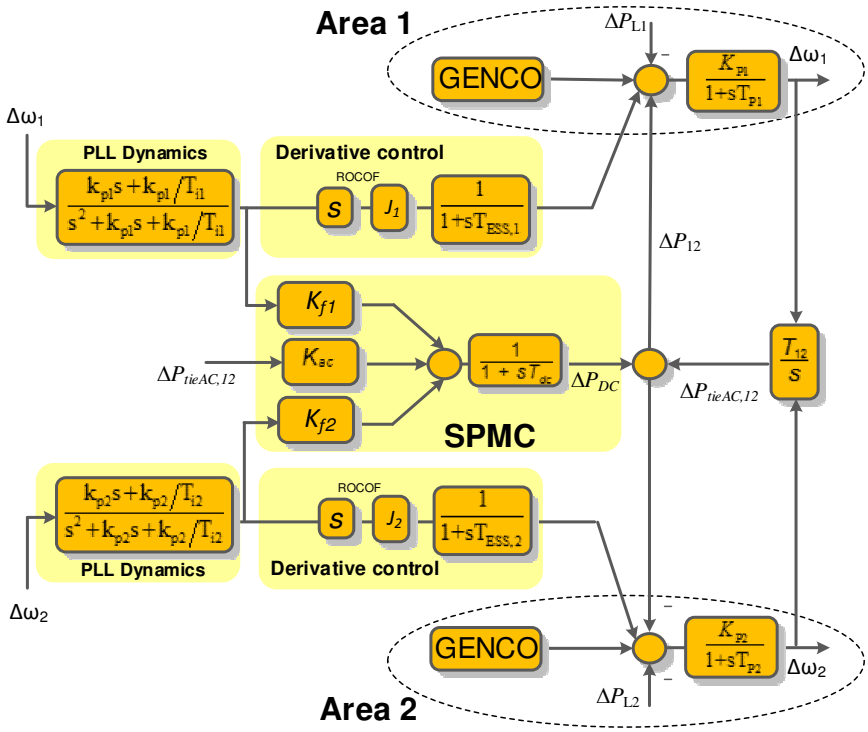

Figure 5.32. Higher level model of AC/DC system with derivative control and PLL dynamics.

It should be mentioned that, this dynamic block is added just to imitate the dynamics of remote PLL with communication delays during inertia emulation. Since the behavior of the PLL measurements is like a second-order function, the dynamic transfer function for measurement should be a second-order block as well.

As shown in Figure 5.32, for each area one specific derivative controller is assigned. Therefore, two second-order dynamic models are added into the two-area system. As explained before, in the second-order transfer function, there is one zero in the numerator. This zero will exhibit some overshoots in the system response.

The relationship between input and output signals in this second-order system with one zero in the numerator could be identified as follows:

$$\ddot{y} + 2\zeta\omega_n\dot{y} + \omega_n^2\, y = 2\zeta\omega_n\dot{u} + \omega_n^2\, u \tag{5.46}$$

The input signal, $u(t)$, is the grid frequency $\Delta\omega_i$ which is related to the other states of the global multi-area system and the output signal will consist of two states variables.

$$\Delta Y_P = \Delta P_{ESS,P} = \begin{bmatrix} \Delta x_{1,P} \\ \Delta x_{2,P} \end{bmatrix} \tag{5.47}$$

Based on classic control concepts, this second-order system could be represented by a set of two linear state equations.

$$\begin{bmatrix} \Delta\dot{x}_{1,P} \\ \Delta\dot{x}_{2,P} \end{bmatrix} = \begin{bmatrix} 0 & 1 \\ -\omega_n^2 & -2\zeta\omega_n \end{bmatrix} \begin{bmatrix} \Delta x_{1,P} \\ \Delta x_{2,P} \end{bmatrix} + \begin{bmatrix} 0 & 0 \\ 2\zeta\omega_n & \omega_n^2 \end{bmatrix} \begin{bmatrix} \Delta\dot{u} \\ \Delta u \end{bmatrix} \tag{5.48}$$

Therefore, considering the input signals ($\Delta\omega_i$) for the i^{th} area ($i = 1{:}\,2$) of the two-area interconnected system, the complete state equations of these new states could be written as follows:

$$\Delta\dot{x}_{1,Pi} = \Delta x_{1,Pi} \tag{5.49}$$

$$\begin{aligned} \Delta\dot{x}_{2,Pi} = {} & \beta_{1,i}\,\Delta\omega_i + \beta_{2,i}\,\Delta P_{mi} + \beta_{3,i}\,\Delta P_{tieAC,ij} \\ & + \beta_{4,i}\,\Delta P_{DC} + \beta_{5,i}\,\Delta P_{ESS,i} \\ & + \beta_{6,i}\,\Delta x_{1,Pi} + \beta_{7,i}\,\Delta x_{2,Pi} \\ & + \beta_{8,i}\,\Delta P_{Li} \end{aligned} \tag{5.50}$$

where

$$\beta_{1,i} = \frac{-2\zeta_i\omega_{ni}}{T_{pi}} + {\omega_{ni}}^2 \ , \beta_{2,i} = \frac{2\zeta_i\omega_{ni}\,K_{pi}}{T_{pi}}$$
$$\beta_{3,i} = \frac{-2\zeta_i\omega_{ni}\,K_{pi}}{T_{pi}} \ , \beta_{4,i} = \frac{-2\zeta_i\omega_{ni}\,K_{pi}}{T_{pi}}$$
$$\beta_{5,i} = \frac{-2\zeta_i\omega_{ni}\,K_{pi}}{T_{pi}} \ , \beta_{6,i} = -\omega_{ni}^2 \tag{5.51}$$
$$\beta_{7,i} = -2\zeta_i\omega_{ni} \ , \beta_{8,i} = \frac{-2\zeta_i\omega_{ni}\,K_{pi}}{T_{pi}}$$

Since, one of the input signals of DC link system and storage devices is the frequency detected by the PLL second-order function, the equation of DC power (ΔP_{DC}) and the emulated inertial power of ESS ($\Delta P_{ESS,i}$) used in previous sections should be modified.

Therefore, based on the presented information about adding new second-order blocks, the complete linearized mathematical presentation of the studied two-area system could be updated as follows:

$$\Delta\dot{\mathbf{x}} = \mathbf{A_p}\Delta\mathbf{x} + \mathbf{B_p}\Delta\mathbf{u} \tag{5.52}$$

where the state variables are chosen as follows:

$$\mathbf{x} = [\Delta\omega_1 \ \Delta\omega_2 \ \Delta P_{m1} \ \Delta P_{m2} \ \Delta P_{m3} \ \Delta P_{m4} \ \Delta ACE_1 \ \Delta ACE_2 \ \Delta P_{tieAC,12} \ \Delta P_{DC} \ \Delta P_{ESS1} \ \Delta P_{ESS2} \ \Delta x_{1,P1} \ \Delta x_{2,P1} \ \Delta x_{1,P2} \ \Delta x_{2,P2}]^T \tag{5.53}$$

and control inputs are load changes in each area:

$$\mathbf{u} = \begin{bmatrix}\Delta P_{L1}\\ \Delta P_{L2}\end{bmatrix} \tag{5.54}$$

The $\mathbf{A}_\mathrm{p}$ state matrix is the new state matrix considering the dynamics of PLL and measurements in the whole system with the derivative controllers.

$$\mathbf{A_p} = \begin{bmatrix}\mathbf{A_{p,11}} & \mathbf{A_{p,12}}\\ \mathbf{A_{p,21}} & \mathbf{A_{p,22}}\end{bmatrix}_{(16\times16)}. \tag{5.55}$$

Therefore all the sub-matrices are as follow:

$$\mathbf{A_{p,12}} = \begin{bmatrix} \frac{-K_{p1}}{T_{p1}} & \frac{-K_{p1}}{T_{p1}} & 0 & 0 & \dots & 0 \\ \frac{K_{p2}}{T_{p2}} & 0 & \frac{-K_{p2}}{T_{p2}} & 0 & \dots & 0 \\ 0 & 0 & 0 & 0 & \dots & 0 \\ \vdots & \vdots & \vdots & \vdots & & \vdots \\ 1 & 0 & 0 & 0 & \dots & 0 \\ -1 & 0 & 0 & 0 & \dots & 0 \\ 0 & 0 & 0 & 0 & \dots & 0 \end{bmatrix}_{(9\times 7)}$$

$$\mathbf{A_{p,11}} = \begin{bmatrix} \frac{-1}{T_{p1}} & 0 & \frac{K_{p1}}{T_{p1}} & \frac{K_{p1}}{T_{p1}} & 0 & 0 & 0 & 0 & \frac{-K_{p1}}{T_{p1}} \\ 0 & \frac{-1}{T_{p2}} & 0 & 0 & \frac{K_{p2}}{T_{p2}} & \frac{K_{p2}}{T_{p2}} & 0 & 0 & \frac{K_{p2}}{T_{p2}} \\ \frac{-1}{2\pi R_1 T_{tg1}} & 0 & \frac{-1}{T_{tg1}} & 0 & 0 & 0 & \frac{-K_{I1}}{T_{tg1}} & 0 & 0 \\ \frac{-1}{2\pi R_2 T_{tg2}} & 0 & 0 & \frac{-1}{T_{tg2}} & 0 & 0 & \frac{-K_{I1}}{T_{tg2}} & 0 & 0 \\ 0 & \frac{-1}{2\pi R_3 T_{tg3}} & 0 & 0 & \frac{-1}{T_{tg3}} & 0 & 0 & \frac{-K_{I2}}{T_{tg3}} & 0 \\ 0 & \frac{-1}{2\pi R_4 T_{tg4}} & 0 & 0 & 0 & \frac{-1}{T_{tg4}} & 0 & \frac{-K_{I2}}{T_{tg4}} & 0 \\ \frac{\beta_1}{2\pi} & 0 & 0 & 0 & 0 & 0 & 0 & 0 & 1 \\ 0 & \frac{\beta_2}{2\pi} & 0 & 0 & 0 & 0 & 0 & 0 & -1 \\ \frac{T_{12}}{2\pi} & -\frac{T_{12}}{2\pi} & 0 & 0 & 0 & 0 & 0 & 0 & 0 \end{bmatrix}_{(9\times 9)} \tag{5.56}$$

$$\mathbf{A_{p,21}} = \begin{bmatrix} 0 & 0 & 0 & 0 & 0 & 0 & 0 & 0 & \frac{K_{ac}}{T_{dc}} \\ \frac{J_1\beta_{1,1}}{T_{ess.1}} & 0 & \frac{J_1\beta_{2,1}}{T_{ess,1}} & \frac{J_1\beta_{2,1}}{T_{ess,1}} & 0 & 0 & 0 & 0 & \frac{-J_1\beta_{3,1}}{T_{ess,1}} \\ 0 & \frac{J_2\beta_{1,2}}{T_{ess.2}} & 0 & 0 & \frac{J_2\beta_{2,2}}{T_{ess,2}} & \frac{J_2\beta_{2,2}}{T_{ess,2}} & 0 & 0 & \frac{J_2\beta_{3,2}}{T_{ess,2}} \\ 0 & 0 & 0 & 0 & 0 & 0 & 0 & 0 & 0 \\ \beta_{1,1} & 0 & \beta_{2,1} & \beta_{2,1} & 0 & 0 & 0 & 0 & \beta_{3,1} \\ 0 & 0 & 0 & 0 & 0 & 0 & 0 & 0 & 0 \\ 0 & \beta_{1,2} & 0 & 0 & \beta_{2,2} & \beta_{2,2} & 0 & 0 & \beta_{3,2} \end{bmatrix}_{(7\times 9)}$$

$$\mathbf{A_{p,22}} = \begin{bmatrix} \frac{-1}{T_{dc}} & 0 & 0 & \frac{K_{f1}}{T_{dc}} & \frac{K_{f1}}{T_{dc}} & \frac{K_{f2}}{T_{dc}} & \frac{K_{f2}}{T_{dc}} \\ \frac{-J_1\beta_{4,1}}{T_{ess.1}} & \frac{J_1\beta_{5,1}-1}{T_{ess.1}} & 0 & \frac{J_1\beta_{6,1}}{T_{ess,1}} & \frac{J_1\,(\beta_{7,1}+1)}{T_{ess.1}} & 0 & 0 \\ \frac{J_2\beta_{4,2}}{T_{ess.2}} & 0 & \frac{J_2\beta_{5,2}-1}{T_{ess.2}} & 0 & 0 & \frac{J_2\beta_{6,2}}{T_{ess,2}} & \frac{J_2\,(\beta_{7,2}+1)}{T_{ess.2}} \\ 0 & 0 & 0 & 0 & 1 & 0 & 0 \\ \beta_{4,1} & \beta_{5,1} & 0 & \beta_{6,1} & \beta_{7,1} & 0 & 0 \\ 0 & 0 & 0 & 0 & 0 & 0 & 1 \\ -\beta_{4,2} & 0 & \beta_{5,2} & 0 & 0 & \beta_{6,2} & \beta_{7,2} \end{bmatrix}_{(7\times7)}$$

Finally the sub-matrices of $\mathbf{B}_p$ matrix could be presented as follows, where the control vector consists of the load variations in each area:

$$\mathbf{B_p} = \begin{bmatrix} \frac{-K_{p1}}{T_{p1}} & 0 \\ 0 & \frac{-K_{p2}}{T_{p2}} \\ 0 & 0 \\ 0 & 0 \\ 0 & 0 \\ 0 & 0 \\ 0 & 0 \\ 0 & 0 \\ 0 & 0 \\ 0 & 0 \\ \frac{J_1\beta_{8,1}}{T_{ess,1}} & 0 \\ 0 & \frac{J_2\beta_{8,2}}{T_{ess,2}} \\ 0 & 0 \\ \beta_{8,1} & 0 \\ 0 & 0 \\ 0 & \beta_{8,2} \end{bmatrix}_{(16\times2)} \tag{5.57}$$

5.4.3 Analyses the dynamic effects of second-order PLL on AGC response

In this Section, the dynamic effects of the frequency measurement, mainly related to a second-order remote PLL, is analyzed. A general comparison between the system of inertia emulation by the derivative controller with and without PLL is presented. To have a fair comparison for high-level application, a range between 100 ms to 700 ms delay could be assumed for the time response of the second-order system, which is assigned for the measurement delay and remote PLL effects together [5.29]-[5.32]. As shown in Figure 5.33, the frequency response of the system in Area1 is plotted for the original AC system (the red trace), the system with an AC/DC interconnection line (the blue trace), the system with an AC/DC interconnection line and without PLL (the green trace), and the system with an AC/DC interconnection line and with PLL (the black trace).

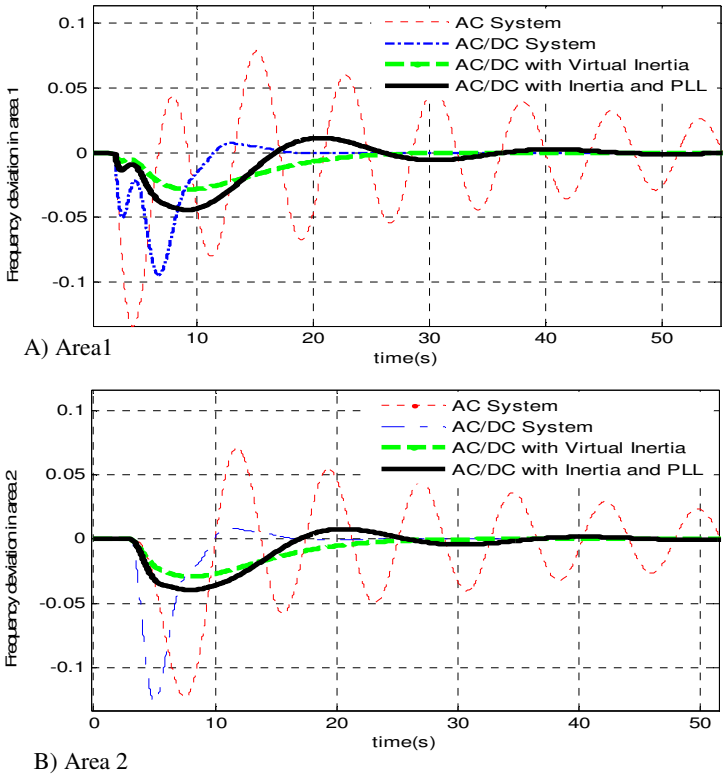

Figure 5.33. System frequency deviations with and without PLL effects. A) Area 1, B) Area 2.

From these responses shown in Figure 5.33, it could be concluded that adding a PLL, with a time constant of around 0.4 s, affects the dynamic performance of the system. Note that, because of the zero in the numerator of a second-order PLL model, the system exhibits more overshoots in dynamic responses. In Figures 5.34 and 5.35, the variation of the power delivered by ESS and DC power deviations are presented, respectively.

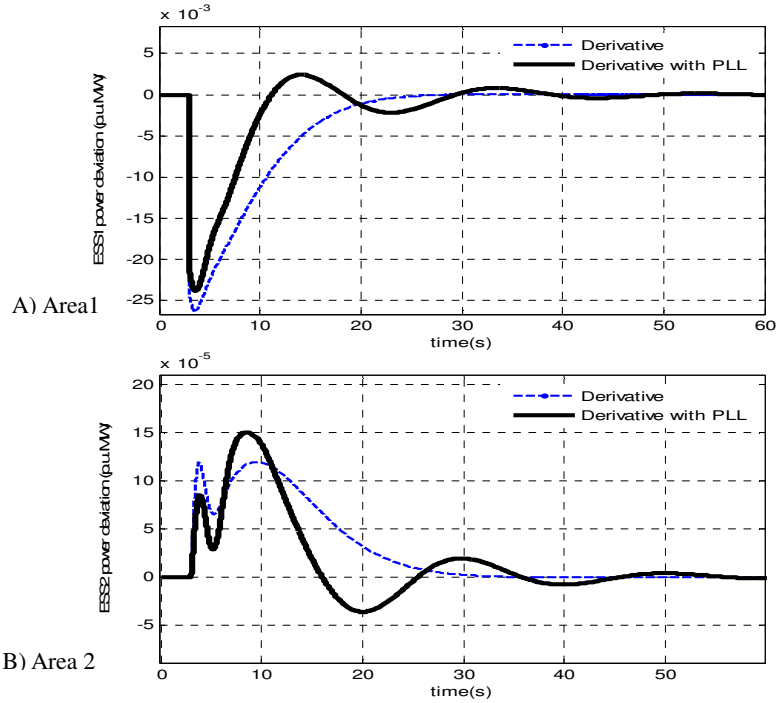

Figure 5.34. Dynamic response of ESS power reference with and without PLL effects.

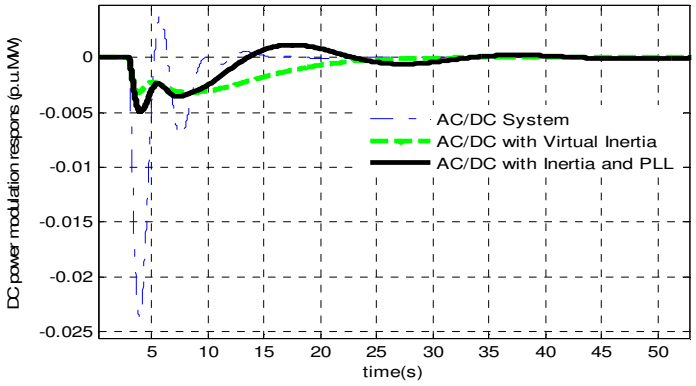

Figure 5.35. Dynamic response of DC power for different systems.

The results are compared for the system with and without PLL. As observed in these plots, the ESS device will exhibit more oscillations on the DC link when the effect of the PLL is added to the model.

Another comparison regarding the eigenvalue of the system with and without considering the PLL effects are presented in Table 5.10. It is clear in this table that by adding the PLL dynamics, the number of oscillatory modes is increased from 4 to 8, which can deteriorate the dynamic performance of the overall system by increasing the oscillations and settling time of the system. Some of these oscillatory modes are also close to zero.

Table 5.10. Eigenvalues comparison for different systems.

Modes	AC/DC System with Derivative Control	AC/DC with Derivative Control and PLL Effects
λ_1	-209.32	-134.07
λ_2	-52.96	-39.375
λ_3	-22.63	-23.740
λ_4	-1.1 + 1.9I	-0.791 + 1.961I
λ_5	-1.1 - 1.9I	-0.791 - 1.961I
λ_6	-0.201	-0.450 + 0.520I
λ_7	-0.1 + 0.2I	-0.450 - 0.520I
λ_8	-0.1 - 0.2I	-0.341 + 0.501I
λ_9	-2.30	-0.341 - 0.501I
λ_{10}	-2.50	-0.0781 + 0.503I
λ_{11}	-2.70	-0.0781 - 0.503I
λ_{12}	-2.63	-0.2102
λ_{13}	------	-2.041
λ_{14}	------	-2.423
λ_{15}	------	-2.631
λ_{16}	------	-2.690

In order to analyze the dynamic effects of the PLL in the system, further numerical analysis is presented in the following. These analyses are performed to check the response of the system for various changes in the parameters of the PLL second-order function. In this comparisons, it is assumed that both PLLs (each one located in one

area) are using the same values for their parameters ($\zeta_1 = \zeta_2 = \zeta$ and $\omega_{n1} = \omega_{n2} = \omega_n$). The frequency responses in Area 1 and 2 are presented in Figure 5.36. In this figure, it is assumed that the value for ζ is equal to 1.2 and the other parameter, ω_n, takes several values to imitate different time constant of the PLL and measurement dynamics. It is worth to mention in this regard that the time response of PLL is inversely proportional to ω_n [5.27].

In fact, with lower values of ω_n the system performance will be deteriorated and more oscillatory modes will appear. High values of ω_n result in a fast reacting system and in such situation, the actual positive effects of the virtual inertia control could be visible. However, very high values of ω_n would result in a very noisy system.

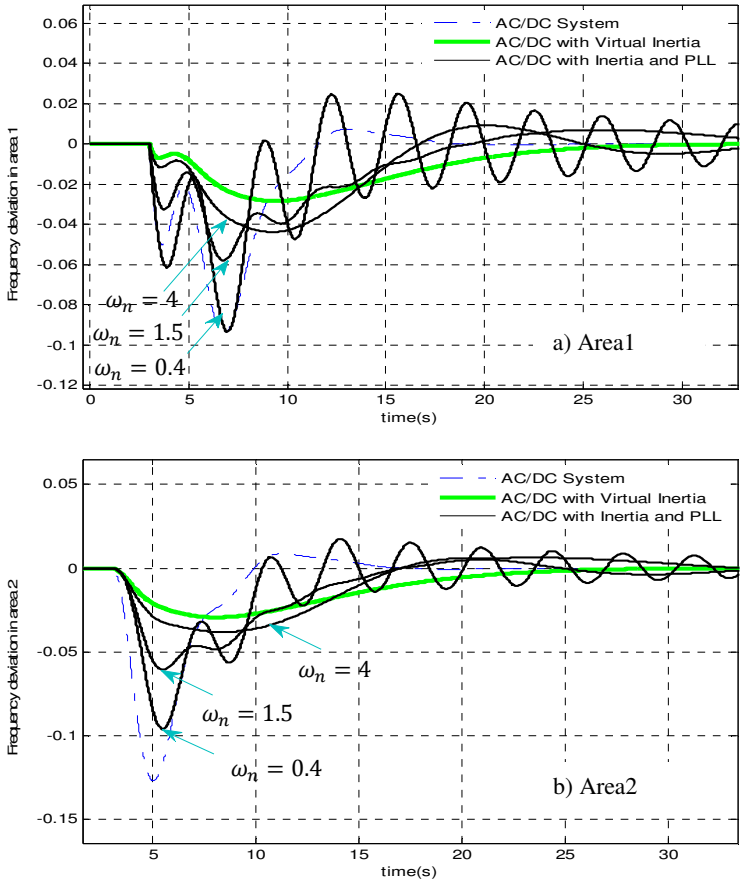

Figure 5.36. Response of frequency deviations.

The dynamic responses for the power deviations generated by the derivative control in both areas and DC link response are also presented by Figures 5.37 and 5.38. Based on the presented results, the effects of the PLL can be explained based on its time response. When the time constant is too high, (which means very low values for ω_n according to (5.45)), it can be observed that the real effects of the derivative control can be canceled out. Therefore, there is no possibility to take any advantage from the derivative control if the time constant of the PLL is too high, and more oscillation and even un-stability could occur.

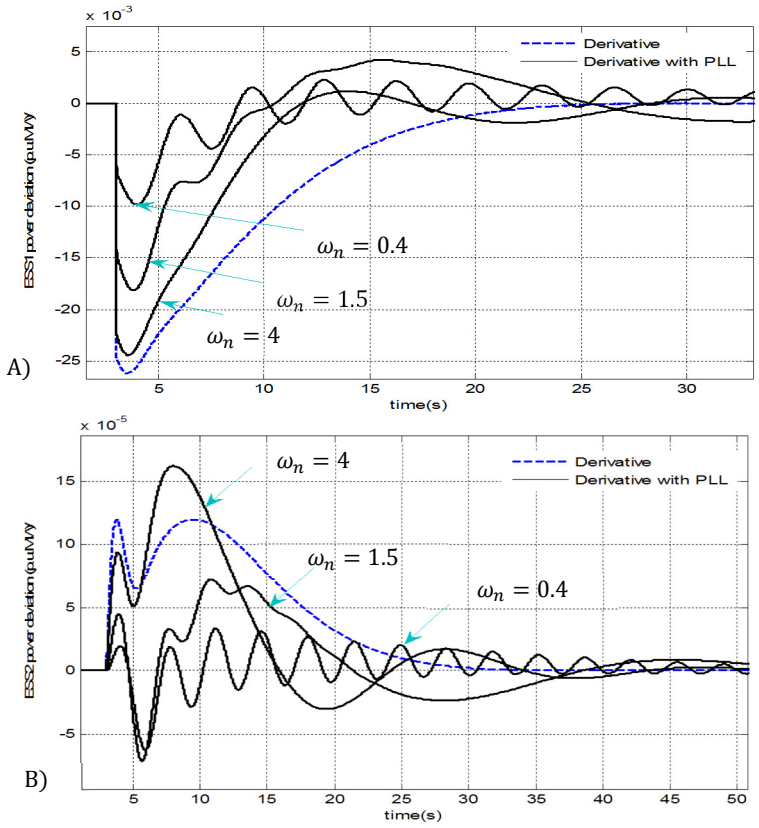

Figure 5.37. Power deviations generated by derivative control, A) ESS1, B) ESS2.

The responses of the DC link for different systems is also presented in Figure 5.38. In this figure, the response of the normal AC/DC system is depicted by a blue trace, the dynamics response of the system with the derivative control is depicted by a green trace and the ones related to the system with PLL effects are also presented by black traces.

The comparisons show how the high time constant for PLL (low values for ω_n) make the system response unacceptable and oscillatory.

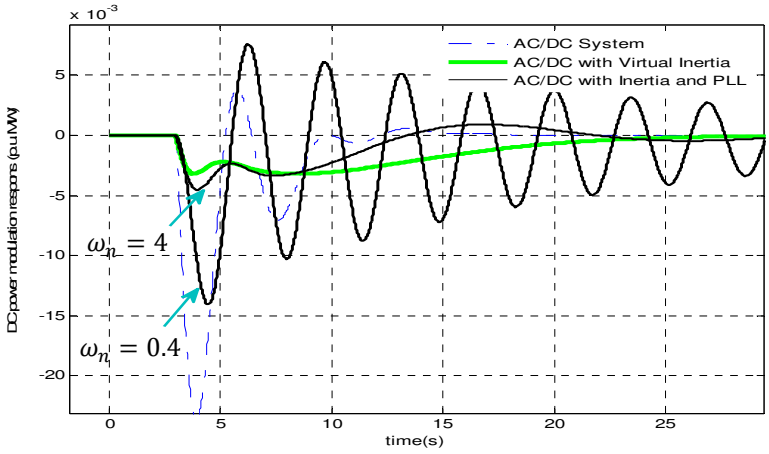

Figure 5.38. Dynamic performance of DC link power, considering PLL effects (black curves).

As a conclusion, the PLL has important effects on the dynamic performance of the derivative control technique for emulating the inertia in the system. If the PLL measurements are affected by long delays, the effects of derivative control will be decreased. The PLL malfunction can also deteriorate the dynamic of the overall system during the inertia emulation task.

CHAPTER

6.

Virtual Inertia Emulation for Interconnected Systems using VSP

This Chapter is devoted to the implementation of the VSP control concept into the high control layer of AGC, needed in modern interconnected power systems. This control technique is suitable for power oscillation damping and frequency support applications in large-scale AGC interconnected power system. The studied model consists of parallel AC and HVDC lines and it is assumed that the HVDC transmission counts on a high controllability degree due to the use of advanced high power converters, with the capability of storing energy for performing inertia emulation functionalities. This study provides an essential model to be used for modelling and analyzing the behaviour of large complex HVDC interconnected systems in power industry. It shows how, and in which level, the maximum advantages can be taken from the system components through interconnected power systems. A model of AC/DC interconnections in dynamic AGC model with a new approach based on VSP for providing inertia is presented. The proposed model should provide a systematic modelling and control technique for large scale interconnected power system, with parallel AC/DC transmission lines and VSP technologies under AGC operation in an electrical network. In this Chapter, a new application of VSP technique for high level applications in AGC power system oriented to provide inertia for performing frequency support and POD tasks will be presented. By means of the proposed technique based on VSP control, a better dynamic performance compared to other methods of inertia emulation, like derivative control, is obtained. The proposed control of VSP is based on providing synchronous generation functionalities taking advantage of the high controllability of electronic power converters based systems, which would permit them to be naturally synchronized with the electrical grid by balancing the exchange of power with AC grid, as well as to provide inherent support the network. By means of this approach it is not required to use any external synchronization system, such as a PLL, to work, hence all the limitations and dependencies linked to the use of PLLs and frequency measurements will be avoided.

6.1 Review and SOA in the subject

The growth and rapid extension of AC systems into multi-area interconnected scenario, considering the increasing level of high power converter applications in modern power systems, is giving rise to a very complex and challenging issue, which will affect the overall power system and particularly the frequency control in AC/DC systems [6.1]. AGC of a multi-area power system during load and resource variation is a very important mechanism that can facilitates various tasks like: frequency restoration, tie-line power flow control between authority areas and economic dispatch of generation units [6.2]-[6.3]. Multi-area interconnections can be provided by AC or DC tie-lines enabling the scheduled power exchange between different control areas and also to provide sufficient support in case of abnormal conditions [6.2]. Because of several limitations associated with AC lines, especially for long distance connections, HVDC links have received an increasing attention over the last years. HVDC interconnection is one of the main applications of power converters in multi-area interconnected power systems, which could bring beneficial advantages like: fast and bidirectional controllability, POD and frequency stability support [6.4]-[6.6]. HVDC systems can essentially improve the reliability of complex interconnected systems and could act as a kind of firewall against cascading disturbances to prevent global blackouts. For these reasons, in some parts of the world, HVDC or hybrid interconnections, consisting of parallel AC and DC interconnections became already the preferred solution [6.7]-[6.9].

Usually, conventional generators with droop capability can provide inertia and governor responses against frequency deviations. Until now, several classical and advanced control techniques have been implemented to solve load frequency control problem [6.10]-[6.14]. But in case of renewable generations, the lack of sufficient inertia will be the main limitation of grid connected renewable electrical energy systems, which will give rise to negative impacts on the power system operation [6.15]-[6.16]. A widespread installation of distributed renewable energy generators over a given power system, with stochastic behaviour and high variability, makes difficult to guarantee power balancing in the system under specific operating conditions. In such complex AC/DC modern power system with the low inertia, controlling the power exchange through tie-lines of multi-area interconnected systems makes frequency regulation more complex with several stability problems [6.16]-[6.17]. It is obvious that the matter of modelling and controlling considering the methods for providing virtual inertia to the system is critical, and the role of advanced technologies such as the use of modern power processing systems, energy storage, and advanced converters in HVDC links will be essential. Power electronic based components, which are used through the AC grid

should be provided with specific functionalities to make them compatible with the operational principles of synchronous power systems and thereby effectively achieving their large-scale integration.

Recently, for improving the dynamic performance of AC/DC systems, several efforts have been carried out to make grid-connected converters behave like synchronous generators, by providing more inertia to the system [6.18]-[6.21]. This virtual inertia is emulated by using advanced control of power converters considering their short term energy storage, [6.20] which gives rise to the possibility of having a higher amount of distributed generation systems, connected to the grid through power converters, without hindering the system stability. However, the application of this kind of converters are not restricted to low power applications or generation parts. For instance, it can be an advantageous solution for HVDC power converters. Therefore, thanks to these improvements in control concepts like Virtual Synchronous Generator and new converter technologies, the ability of simultaneous damping and inertia emulation could be another advantage of HVDC systems in addition to the previous mentioned ones.

In this work, a new application of VSP concept through the converter stations of HVDC link is applied in multi-machine AGC system. The used VSP is based on the concept of synchronous controller, which was patented in 2012. This control strategy is proposing a new method in power converter control behaving as a synchronous generator with the ability of emulating synchronous inertia without the drawbacks of conventional generators [6.21]-[6.22].

The main objective of this work is to propose a new approach of frequency stability analysis in multi-area AGC system adding the VSP concept in HVDC links of interconnected systems. In the last decades, traditional LFC models have been modified and revised to add different functionalities in reformulation of conventional power systems. Most of those modifications are related to AGC in a deregulated market scenario [6.23], different types of power plants like renewable generation [6.24] and recently the demand side dynamic models [6.25]. There are also some works considering the DC link effect which are limited without considering the new abilities of inertia emulation by power converter stations in HVDC link for AGC modelling [6.26]. Therefore, the general model of multi-area AGC system will be modified by introducing VSP control strategy in HVDC links (VSP based HVDC) of AGC model for high level frequency control studies.

6.2 Higher level control technique for inertia emulation by VSP

6.2.1 Virtual synchronous power strategy

In this section the concept of Virtual Synchronous Power (VSP) which is based on the control of voltage source converter though an active power synchronization loop and a virtual admittance is presented.

The general structure of synchronous power control for each converter of VSC-HVDC line is presented in Figure 6.1. This control structure stems from programming the electrical performance of a Synchronous Generator (SG) in a digital framework which is responsible for controlling the VSC-converter. However, it is worth to point that the this synchronous controller does not aim to faithfully mimic the response of the synchronous generator, but it overcomes the drawbacks of the inherent oscillatory response of the conventional synchronous generator in case of perturbation and fluctuations by introducing a second-order over-damped response [6.21]-[6.22].

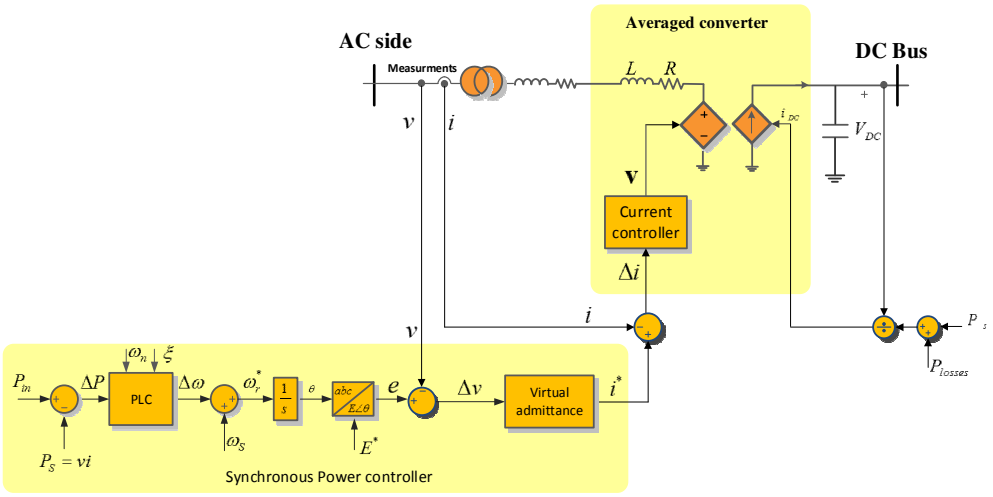

Figure 6.1. The configuration of simplified synchronous power controller.

It should be note that, in this scheme the protection controllers are not included. The DC energy storage element represented by capacitor in Figure 6.1, is in charge of absorption of any transient unbalance between the two power converters connected to the DC link. This energy storage element can be inserted in the converter topology or implemented by any additional power converter storage.

By modifying the swing equation of conventional synchronous generator, the general electromechanical control loop for VSP application in transient contingencies can be presented based on the diagram of Figure 6.2.

This diagram represents a PLL, in which any variation between the delivered power by the converter (P_{out}) and the input power, (P_{in}) is processed by a Power Loop Controller (PLC) to set a relative frequency that should be added to the synchronous frequency of the grid, for generating the rotating frequency of a virtual rotor. The integral of such frequency gives the angular position of the virtual rotor leading to the power delivered by the power converter.

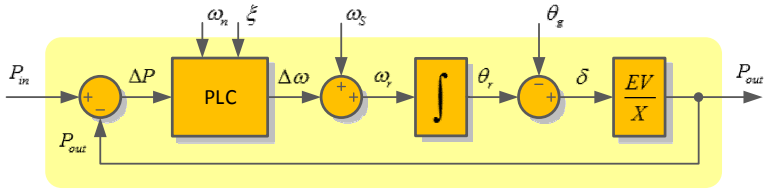

Figure 6.2. Electromechanical representation of synchronous power controller.

The transfer function of a simple controller for PLC which will represent the mechanical behaviour of synchronous generator might be written as:

$$PLC(s) = \frac{N(s)}{D(s)} = \frac{\omega_n^2/P_{max}}{s + 2\zeta\omega_n} \tag{6.1}$$

where ζ is damping factor, ω_n is the natural frequency and P_{max} is the maximum value of the active power that can be delivered:

$$P_{max} = \frac{E\,V}{X} \tag{6.2}$$

where E, V and X are internal *emf* voltage, grid voltage and overall impedance, respectively. Usually, the values for E and V are close to the rated ones and the value for the load angle (δ), uses to be very small. Under such conditions, the value of $sin(\delta)$ can be simply approximated by δ, and thereby the delivered electrical power can be approximated to ($P_{out} = \frac{E\,V}{X}\delta$). The transmitted power could be easily adjusted by shifting the output voltage phase of the converter forward or backward. A straightforward analysis of such electromechanical model leads to the flowing transfer function describes the dynamic relationship between the input and output powers [6.21]:

$$\frac{P_{out}}{P_{in}} = \frac{\omega_n^2}{s^2 + 2\zeta\omega_n\, s + \omega_n^2} = \frac{\frac{P_{max}}{J.\,\omega_s}}{s^2 + \frac{k}{J.\,\omega_s} s + \frac{P_{max}}{J.\,\omega_s}} \tag{6.3}$$

where P_{in}, P_{out}, J, k and ω_s are input power, delivered active power, the moment of inertia, damping constant and synchronous frequency respectively. From this transfer function, the relationships of natural frequency, ω_n, and the damping factor, ζ, of the virtual electromechanical system to the rest of parameters would be given by:

$$\omega_n = \sqrt{\frac{P_{max}}{J.\,\omega_s}} \tag{6.4}$$

$$\zeta = \frac{k}{2\sqrt{P_{max}\, J.\,\omega_s}} \tag{6.5}$$

Therefore, the virtual inertia (J) and desired damping of the system could be emulated by a proper selections of these control parameters of VSP strategy.

6.2.2 Modelling of VSP based inertia emulation in AC/DC interconnected AGC system

In this section the concept of VSP will be implemented in multi-area interconnected AGC system which contains HVDC links.

As explained in the previous section, the dynamic relationships between input and output power of each converter station could be a second-order transfer function. The relationship between input and output signals in this second-order system could be identified using its characteristic equation of the VSP dynamic model:

$$\ddot{y} + 2\zeta\omega_n\dot{y} + \omega_n^2\, y = \omega_n^2\, u \tag{6.6}$$

The input signal, u, is the reference DC power which is related to other state of the global multi-area system and the output signal will consist on two states variables.

$$\Delta\mathbf{Y_{VSP}} = \Delta\mathbf{P_{DC,VSP}} = \begin{bmatrix}\Delta x_{p,VSP}\\ \Delta x_{f,VSP}\end{bmatrix} \tag{6.7}$$

where $\Delta X_{p,VSP}$ represents the injected power ($\Delta P_{DC,VSP}$) and ($\Delta X_{f,VSP}$) is the derivative term of this power for each VSP, respectively. Based on classic control concepts, this second-order system could be represented by a set of two linear state equations.

$$\begin{bmatrix}\Delta\dot{x}_{p,VSP}\\ \Delta\dot{x}_{f,VSP}\end{bmatrix} = \begin{bmatrix}0 & 1\\ -\omega_n^2 & -2\zeta\omega_n\end{bmatrix}\begin{bmatrix}\Delta x_{p,VSP}\\ \Delta x_{f,VSP}\end{bmatrix} + \begin{bmatrix}0\\ \omega_n^2\end{bmatrix}\Delta u \tag{6.8}$$

where u is the reference signal coming from a higher level control which is define as:

$$\Delta u = \Delta P_{DC,ref} = K_{fi,VSP}\Delta\omega_i + K_{fk,VSP}\Delta\omega_k + K_{AC}\Delta P_{tieAC,ik} \tag{6.9}$$

As the HVDC line is located between Area i and Area k, the frequency deviation of those areas is the most suitable control signals. This selection of control signals are also analysed through the sensitivities analysis presented in Section 4.3. In case of parallel AC/DC lines, the AC tie-line power deviation could be used as another control signal in order to achieve suitable coordination between two lines. This state space presentation will be part of the global system and it could be added to the rest of state space model of a multi-area AGC system.

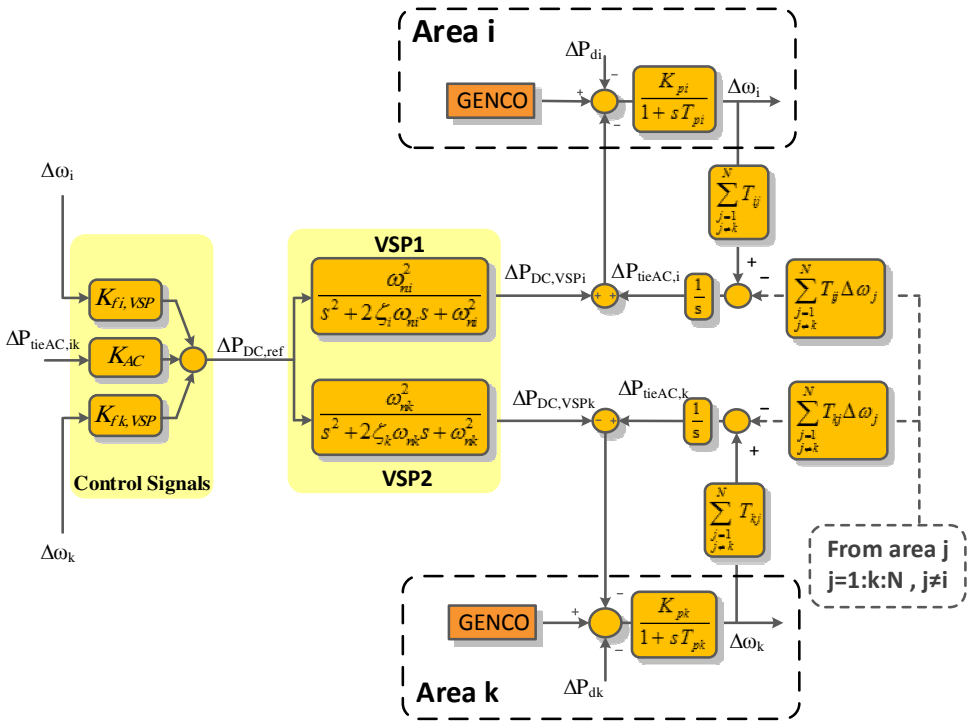

Figure 6.3. Basic frame of AGC in multi-area systems with a VSP based AC/DC transmission.

As shown in Figure 6.3, it is assumed that there is a parallel AC/HVDC link between Area *i* and Area *k*, where both converter stations of the HVDC link are facilitated by VSP functionalities. The dynamic equations of these two AC/DC interconnected areas considering the dynamic of VSP based HVDC link in the Laplace domain will be as follows:

$$\Delta\omega_i = \frac{K_{pi}}{1+sT_{pi}}[\Delta P_{mi} - \Delta P_{L1} - (\Delta P_{tieAC,i} + \Delta x_{p,VSPi})] \tag{6.10}$$

$$\Delta\omega_k = \frac{K_{pk}}{1+sT_{pk}}[\Delta P_{mk} - \Delta P_{Lk} - (\Delta P_{tieAC,k} + \Delta x_{p,VSPk})] \tag{6.11}$$

$$ACE_i = \beta_i\Delta\omega_i + [\Delta P_{tieAC,i} + \Delta x_{p,VSPi}] \tag{6.12}$$

$$ACE_k = \beta_k\Delta\omega_k + [\Delta P_{tieAC,k} - \Delta x_{p,VSPk}] \tag{6.13}$$

$$s\,\Delta x_{p,VSPi} = \Delta x_{f,VSPi} \tag{6.14}$$

$$s\Delta x_{f,VSPi} = \left[\frac{K_{fi,VSP}\omega_{ni}^2}{2\pi}\right]\Delta\omega_i + \left[\frac{K_{fk,VSP}\omega_{ni}^2}{2\pi}\right]\Delta\omega_k + \left[K_{AC,VSP}\omega_{ni}^2\right]\Delta P_{tieAC,ik} - \omega_{ni}^2\Delta x_{p,VSPi} - 2\zeta_i\omega_{ni}\Delta x_{f,VSPi} \tag{6.15}$$

$$s\,\Delta x_{p,VSPk} = \Delta x_{f,VSPk} \tag{6.16}$$

$$s\Delta x_{f,VSPk} = \left[\frac{K_{fi,VSP}\omega_{nk}^2}{2\pi}\right]\Delta\omega_i + \left[\frac{K_{fk,VSP}\omega_{nk}^2}{2\pi}\right]\Delta\omega_k + \left[K_{AC,VSP}\omega_{nk}^2\right]\Delta P_{tieAC,ik} - \omega_{nk}^2\Delta x_{p,VSPk} - 2\zeta_k\omega_{nk}\Delta x_{f,VSPk} \tag{6.17}$$

It should be mentioned that, the dynamic equations of other AC areas which are connected with AC lines will be the same as the ones presented in the previous section.

Therefore, in a two-area AC/DC interconnected power system, which will have two synchronous controllers, four new states variables of synchronous controllers will be added to the system. The overall system will have thirteen state variables as it is written as follows:

$$\mathbf{x} = [\Delta\omega_1 \;\; \Delta\omega_2 \;\; \Delta P_{m1} \;\; \Delta P_{m2} \;\; \Delta P_{m3} \;\; \Delta P_{m4} \;\; \Delta ACE_1 \;\; \Delta ACE_2 \;\; \Delta P_{tieAC,12} \;\; \Delta x_{p,VSP1} \;\; \Delta x_{f,VSP1} \;\; \Delta x_{p,VSP2} \;\; \Delta x_{f,VSP2}\,]^T \tag{6.18}$$

and control inputs are load changes in each area:

$$\mathbf{u} = [\Delta P_{L1} \;\; \Delta P_{L2}\,]^T \tag{6.19}$$

The complete state matrix **A** of the two-area power system including the synchronous power control technique is presented in the following:

$$\mathbf{A}=\begin{bmatrix}
\frac{-1}{T_{p1}} & 0 & \frac{K_{p1}}{T_{p1}}\frac{K_{p1}}{T_{p1}} & 0 & 0 & 0 & 0 & \frac{-K_{p1}}{T_{p1}} & \frac{-K_{p1}}{T_{p1}} & 0 & 0 & 0\\
0 & \frac{-1}{T_{p2}} & 0 & 0 & \frac{K_{p2}}{T_{p2}}\frac{K_{p2}}{T_{p2}} & 0 & 0 & \frac{K_{p2}}{T_{p2}} & 0 & 0 & \frac{K_{p2}}{T_{p2}} & 0\\
\frac{-1}{2\pi R_1 T_{tg1}} & 0 & \frac{-1}{T_{tg1}} & 0 & 0 & 0 & \frac{-K_{I1}}{T_{tg1}} & 0 & 0 & 0 & 0 & 0 & 0\\
\frac{-1}{2\pi R_2 T_{tg2}} & 0 & 0 & \frac{-1}{T_{tg2}} & 0 & 0 & \frac{-K_{I1}}{T_{tg2}} & 0 & 0 & 0 & 0 & 0 & 0\\
0 & \frac{-1}{2\pi R_3 T_{tg3}} & 0 & 0 & \frac{-1}{T_{tg3}} & 0 & 0 & \frac{-K_{I2}}{T_{tg3}} & 0 & 0 & 0 & 0 & 0\\
0 & \frac{-1}{2\pi R_4 T_{tg4}} & 0 & 0 & 0 & \frac{-1}{T_{tg4}} & 0 & \frac{-K_{I2}}{T_{tg4}} & 0 & 0 & 0 & 0 & 0\\
\frac{\beta_1}{2\pi} & 0 & 0 & 0 & 0 & 0 & 0 & 0 & 1 & 1 & 0 & 0 & 0\\
0 & \frac{\beta_2}{2\pi} & 0 & 0 & 0 & 0 & 0 & 0 & -1 & 0 & 0 & -1 & 0\\
\frac{T_{12}}{2\pi} & -\frac{T_{12}}{2\pi} & 0 & 0 & 0 & 0 & 0 & 0 & 0 & 0 & 0 & 0 & 0\\
0 & 0 & 0 & 0 & 0 & 0 & 0 & 0 & 0 & 0 & 1 & 0 & 0\\
\frac{K_{f1,VSP}\omega_{n1}^2}{2\pi} & \frac{K_{f2,VSP}\omega_{n1}^2}{2\pi} & 0 & 0 & 0 & 0 & 0 & 0 & K_{AC,VSP}\omega_{n1}^2 & -\omega_{n1}^2 & -2\zeta_1\omega_{n1} & 0 & 0\\
0 & 0 & 0 & 0 & 0 & 0 & 0 & 0 & 0 & 0 & 0 & 0 & 1\\
\frac{K_{f1,VSP}\omega_{n2}^2}{2\pi} & \frac{K_{f2,VSP}\omega_{n2}^2}{2\pi} & 0 & 0 & 0 & 0 & 0 & 0 & K_{AC,VSP}\omega_{n2}^2 & 0 & 0 & -\omega_{n2}^2 & -2\zeta_2\omega_{n2}
\end{bmatrix}$$

As shown in this model, we will have more control gains (ζ_i and ω_{ni}) related to VSP controller in each station of the HVDC link. Usually, it would be possible to define a cost function in a two-are AGC system for obtaining the optimum values for all of these gains. These gains could be defined based on the optimization theory by minimizing the following common cost function [6.1]-[6.5]:

$$J=\int[ACE_1^2+ACE_2^2]\,dt \tag{6.20}$$

This cost function is the regular function which is based on the ISE (Integral Square Error) method [6.5]. It should be noted that the ACE is the area error which consisted of the frequency and tie-line power deviations in each area. These control gains (ζ_i and ω_{ni}) could be obtained using the optimization toolboxes from MATLAB. The FMINCON solver can be used as a classical optimization algorithm, which implements the SQP and the interior-point method for optimization of LFC problem. The gradients of the objective and constraint functions can be provided as the user-defined functions.

6.2.3 Generalized AGC with multiple VSP based HVDC links

The previous formulation, can be generalized for a multi-area system with multiple VSP based HVDC links shown in Figures 6.4 and 6.5. As depicted in Figure 6.4, *N* areas can be connected with different AC, DC or parallel AC/DC lines.

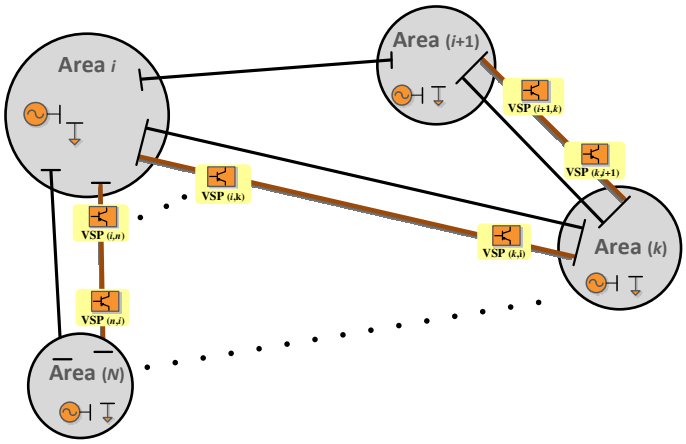

Figure 6.4. The basic frame of multi area system with multiple VSP based AC/DC transmission.

Therefore, considering Figure 6.5, the generalized formulation for the frequency deviation in Area i (i=1:N) with several DC interconnection (L=1:M) adding the modified HVDC with VSP concept can be expressed in the Laplace domain by the following equations:

$$\Delta\omega_i = \frac{K_{pi}}{1+sT_{pi}}[\Delta P_{mi} - \Delta P_{Li} - \Delta P_{tie,i} - \Delta P_{DC-VSP,i}] \tag{6.21}$$

where the $\Delta P_{DC-VSP,i}$ is the total VSP based DC transmitted by the Area i. Also, the modified ACE signal ($ACE_{v,i}$) considering this new VSP signals will be modified as follows:

$$ACE_{v,i} = \beta_i \Delta\omega_i + [\Delta P_{tie,i} + \Delta P_{DC-VSP,i}] \tag{6.22}$$

and the set-points can be defined as follows:

$$\Delta P_{refv,i} = \frac{ACE_{v,i}}{s} \tag{6.23}$$

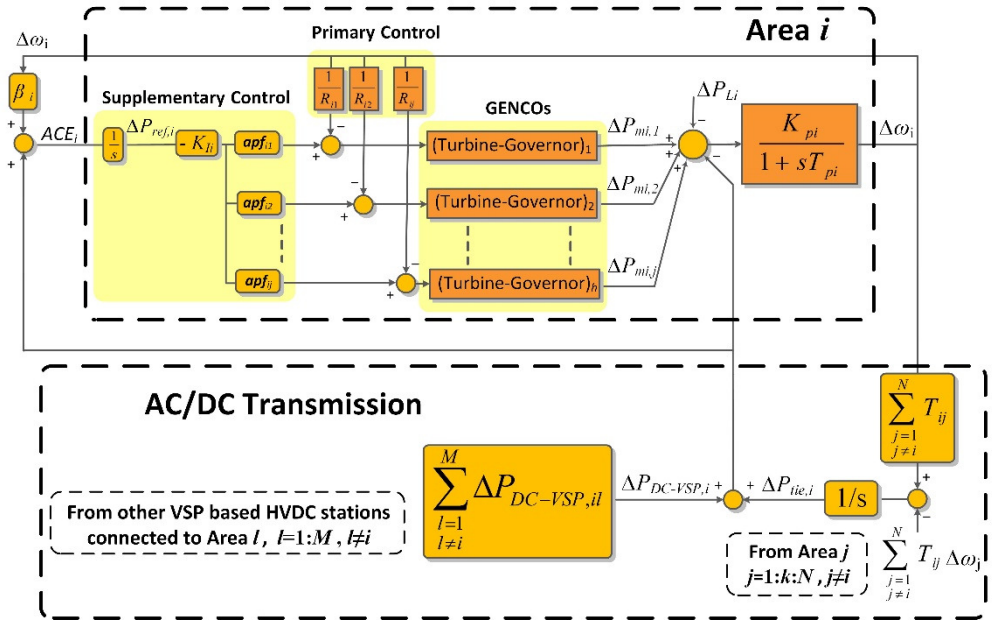

Figure 6.5. Control frame of the i^{th} area in AGC implementation connected to multiple VSP based AC/DC lines

In the case of multiple VSP based HVDC links, the total output of VSP based DC transmitted power ($\Delta P_{DC-VSP,i}$) by the i^{th} area, can be:

$$\Delta P_{DC-VSP,i} = \sum_{\substack{l=1 \\ l\neq i}}^{M} \Delta P_{DC-VSP,il} \tag{6.24}$$

where, $\Delta P_{DC-VSP,il}$ is the output power state ($\Delta X_{p-VSP,il}$) for each second-order VSP controller between Areas i and l. Therefore, the generalized equations of this state is as follows:

$$\Delta X_{p-VSP,i} = \sum_{\substack{l=1 \\ l\neq i}}^{M} \Delta X_{p-VSP,il} \tag{6.25}$$

where the complete state space form of the generalized system in the Laplace domain will be as follows:

$$s\Delta X_{p-VSP,il} = \Delta X_{f-VSP,il} \tag{6.26}$$

$$\begin{aligned} s\Delta X_{f-VSP,il} = &\left[\frac{K_{f-VSP,il}\omega_{n,il}^2}{2\pi}\right]\Delta\omega_i + \left[\frac{K_{f-VSP,li}\omega_{n,il}^2}{2\pi}\right]\Delta\omega_l \\ &+ \left[K_{AC-VSP,i}\ \omega_{n,il}^2\right]\Delta P_{tie,il} - \omega_{n,il}^2\Delta X_{p-VSP,il} \\ &- 2\zeta_{il}\omega_{n,il}\ \Delta X_{f-VSP,il} \end{aligned} \tag{6.27}$$

where $l = 1{:}M$ and is related to the other areas which are connected by a VSP based HVDC link to the Area i. The rest of the dynamic equations from the AC interconnected system will be the same as before.

6.3 System analysis

In this section, the dynamic effects of inertia emulation using virtual synchronous power concept in a two-area AGC interconnected model, is analysed by performing the numerical analysis, parameter sensitivity and eigenvalue (modal) analysis. As explained before, the studied two-area power system contains on two generation units and one load demand center in each area (Figure 4.12).

The parameters of the studied two-area power system are given in Tables 4.1 and 4.2, shown in previous chapters, and the control parameters for this study case are presented in Table 6.1. These values are obtained using the equation (6.20) and the classical FMINCON (find minimum of constrained function) of Matlab. The generic non-linear optimization routine FMINCON solver has been used as a classical optimization which implements the SQP (Sequential Quadratic Programming) and the interior-point method for taking care of the optimization of the LFC problem. For doing the optimization process depend on the system requirement, available stored energy and control limitation design, various constraints can be added during minimization of the objection function.

Table 6.1. Control parameters for studied two-area AC/DC model with VSP.

Parameters	Value
$K_{f1,VSP}$	3.5
$K_{f2,VSP}$	-1.61
$K_{AC,VSP}$	3.1
ω_{n1}	6.9
ω_{n2}	0.022
ζ_1	1.30
ζ_2	1.01

6.3.1 Eigenvalue analysis

Likewise, based on the obtained linearized model of two-area power system in a state space form, the system can be analyzed through the use of eigenvalues and eigenvectors. As it was explained in section 5.2.4.1, the stability of power system can be guaranteed if all the eigenvalues are located on the left-hand side of the imaginary axis of the complex plane; otherwise it will be unstable. The analysis of eigenvalues is one of the most popular methods that permits to analyze the effects of system parameter changes.

Considering the system parameters given in Table 4.1 and 4.2, the eigenvalue of such system for different parameters of VSP control gains can be obtained. In this section the effects of each of the control parameters of two VSP controllers over the system behavior are evaluated by means of the eigenvalue analyses.

6.3.1.1 Eigenvalues under VSP1 parameters changes

As explained before, the main parameters of VSP1 are ω_{n1} and ζ_1. In the Table 6.2, the values of all the modes for the system with synchronous power control are compared for different values of control gain ω_{n1} (VSP1 is located in area one). It should be mentioned that all the parameters for both VSPs are the same as the ones presented in Table 6.1 and each time one specific parameter is changing and the effects are analyzed.

From the information presented in this table it could be observed that the fourth and fifth modes, λ_4 and λ_5, have the highest variation indicating their sensitivity to the parameter changes in the Area 1. As shown in this table, the real part of these modes are positive (unstable) for very small values of ω_{n1}. If the value of ω_{n1} increases they will move these two modes to the stable region of the s-plane.

Table 6.2. Eigenvalues of two-area system for different values of $\boldsymbol{\omega_{n1}}$.

Modes	$\boldsymbol{\omega_{n1} = 0.2}$	$\boldsymbol{\omega_{n1} = 0.9}$	$\boldsymbol{\omega_{n1} = 2.9}$	$\boldsymbol{\omega_{n1} = 6.9}$
$\boldsymbol{\lambda_1}$	-1.8204	-0.214 + 1.259i	-7.2356	-15.1962
$\boldsymbol{\lambda_2}$	-2.1075	-0.214 - 1.259i	-1.203 + 1.065i	-10.2239
$\boldsymbol{\lambda_3}$	-2.6872	-0.222 + 0.504i	-1.203 - 1.065i	-1.4311
$\boldsymbol{\lambda_4}$	**0.010 + 0.987i**	-0.222 - 0.504i	-0.201 + 0.549i	-0.958 + 0.491i
$\boldsymbol{\lambda_5}$	**0.010 - 0.987i**	-0.7598	-0.201 - 0.549i	-0.958 - 0.491i
$\boldsymbol{\lambda_6}$	-0.716 + 0.098i	-0.4759	-0.9246	-0.191 + 0.561i
$\boldsymbol{\lambda_7}$	-0.716 - 0.098i	-0.0469	-0.5775	-0.191 - 0.561i
$\boldsymbol{\lambda_8}$	-0.258 + 0.498i	-0.0088	-0.0472	-0.6072
$\boldsymbol{\lambda_9}$	-0.258 - 0.498i	-2.070 + 0.041i	-0.0088	-0.0473
$\boldsymbol{\lambda_{10}}$	-0.2898	-2.070 - 0.041i	-2.1199	-0.0088
$\boldsymbol{\lambda_{11}}$	-0.0419	-2.5810	-2.8428	-2.1129
$\boldsymbol{\lambda_{12}}$	-0.0097	-2.6877	-2.6886	-2.6873
$\boldsymbol{\lambda_{13}}$	-2.6316	-2.6316	-2.6316	-2.6316

This issue is also investigated by plotting the eigenvalue trajectory over the change of ω_{n1}. This trajectory is presented in Figure 6.6. As shown in this figure, for the values of ω_{n1}, which are between 0.14 and 0.36 ($0.14 < \omega_{n1} < 0.36$), two modes of the system (λ_4 and λ_5) will be in the unstable region of the s-plane. Therefore, for the design process, it is better to keep higher values for ω_{n1}. This issue is also justified by the sensitivity analysis presented in the next sections considering that for the studied system the bigger values for ω_{n1} are preferable.

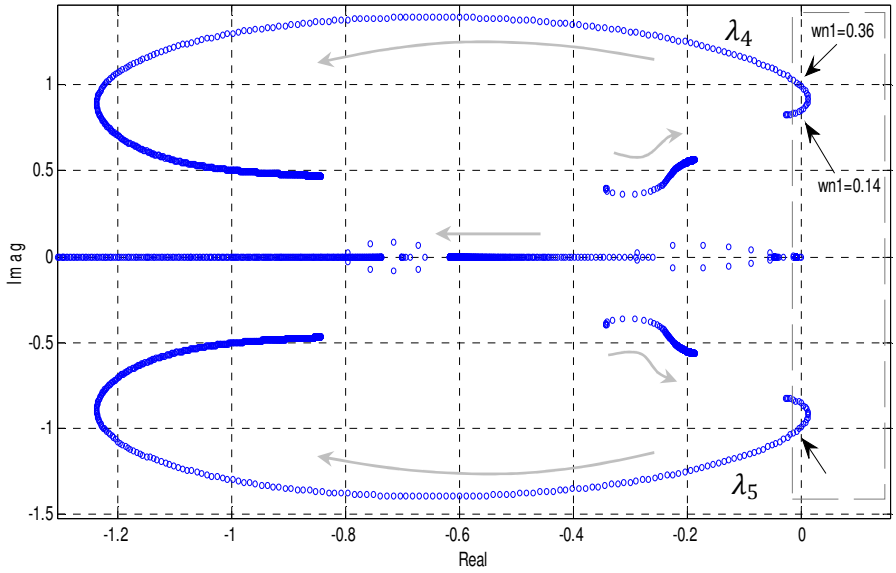

Figure 6.6. Eigenvalue trajectory of dominant modes for ω_{n1} variations.

Eigen index properties like total damping and total frequency of oscillatory modes are compared in Table. 6.3. As shown in this table, for larger values of ω_{n1}, a higher damping with less oscillation is achieved.

Table 6.3. Eigen index for different values of ω_{n1}.

Index	$\omega_{n1} = 0.2$	$\omega_{n1} = 0.9$	$\omega_{n1} = 2.9$	$\omega_{n1} = 6.9$
Damping of critical eigenvalues	9.8791	10.1416	11.1857	**11.4254**
Frequency of oscillatory modes	0.5144	0.5749	0.5140	**0.3352**

The effects of the damping parameters in VSP1 over the system behavior is also investigated by means of the eigenvalue analysis of the system. The eigen-trajectory of the system modes for the damping parameter of VSP1(ζ_1) variations are plotted in Figure 6.7. In turn, the comparative analysis is presented in Table 6.4. This analysis are useful for finding the proper range for damping. Based on the presented results, it is obvious that always a minimum damping is required to keep the system in the stable situation. As shown in the figure, the system for values lower than 0.075 will have positive modes (λ_1 and λ_2) in the s-plane.

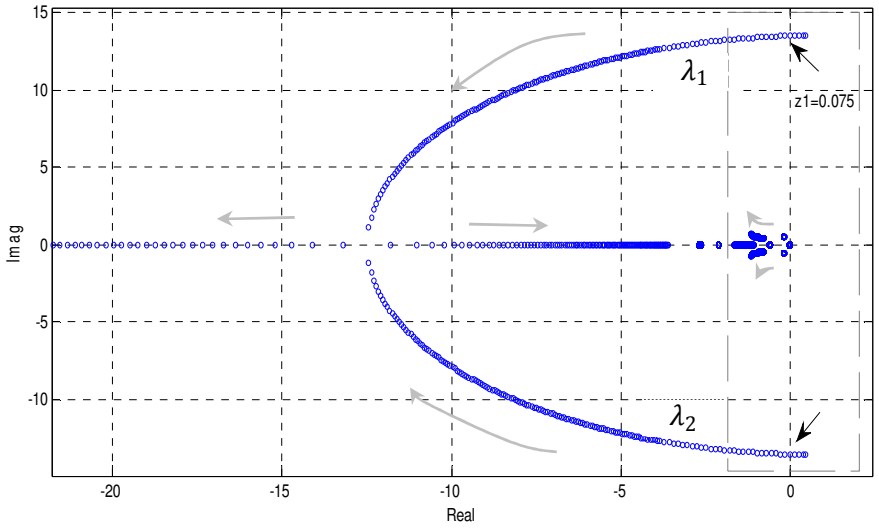

Figure 6.7. Eigenvalue trajectory of system modes for ζ_1 variations.

Table 6.4. Eigenvalues of two-area system for different values of ζ_1.

Modes	$\zeta_1 = 0.05$	$\zeta_1 = 0.1$	$\zeta_1 = 2$	$\zeta_1 = 6$
λ_1	**0.121 + 13.532i**	-0.220+13.5i	-38.0970	-108.73
λ_2	**0.1211 - 13.532i**	-0.220-13.5i	-3.5577	-0.610 + 1.220i
λ_3	-2.1110	-2.110	-2.1157	-0.610 - 1.220i
λ_4	-1.6430	-1.643	-1.162 + 0.693i	-1.970
λ_5	-0.183 + 0.570i	-0.180+0.560i	-1.162 - 0.693i	-2.101
λ_6	-0.183 - 0.570i	-0.180-0.560i	-0.196 + 0.556i	-2.691
λ_7	-0.781 + 0.457i	-0.780+0.45i	-0.196 - 0.556i	-0.210 + 0.530i
λ_8	-0.781 - 0.457i	-0.780-0.45i	-1.0735	-0.210 - 0.530i
λ_9	-0.6255	-0.6250	-0.5935	-0.8010
λ_{10}	-0.0440	-0.04730	-0.0472	-0.5301
λ_{11}	-0.0094	-0.0089	-0.0088	-0.0510
λ_{12}	-2.6872	-2.6801	-2.6874	-0.0101
λ_{13}	-2.6316	-2.6316	-2.6316	-2.6316

Based on the presented information in Table 6.4, the results of the eigen trajectory is also confirmed by checking the exact location of each mode for different values of damping for VSP1. It is clear that the first and second modes have the highest sensitivity. These modes are in the right side of the s-plane for very small values of damping.

The total damping of eigenvalues and the frequency of oscillatory modes are also compared in Table 6.5. Based on the obtained results the most suitable value for damping VSP1 is around 1.3. In this value the system reached a higher damping and a lower frequency of oscillation. This range is also justified by the sensitivity analyses of the studied system in the next section.

Table 6.5. Eigen index for different values of ζ_1.

Index	$\zeta_1 = 0.05$	$\zeta_1 = 0.1$	$\zeta_1 = 1.3$	$\zeta_1 = 6$
Damping of critical eigenvalues	9.3199	9.380	**11.3850**	10.4622
Frequency of oscillatory modes	4.6343	4.6210	**0.3970**	0.5582

6.3.1.2 Eigenvalues under VSP2 parameters changes

Regarding the parameters of the second synchronous power control, VSP2, another set of eigenvalue analyses is performed to identify the effects of ω_{n2} and damping ζ_2 over the system modes and its stability. These results are presented in Tables 6.6 and 6.7.

In Table 6.6, the eigenvalues of the system for different values of ω_{n2} in VSP2, is presented. In order to evaluate the results, the total damping and also the frequency of oscillatory modes in Table 6.6 are calculated and presented in Table 6.7. Based on the results presented in Table 6.7, it is obvious that the lowest value for ω_{n2} will provide the best results. When the value of ω_{n2} is low, the number of oscillatory modes are lower. When the value of ω_{n2} is high, a huge increase on the oscillatory modes occurs. The lower frequency values for the oscillatory modes in Table 6.7, are achieved with a low value of ω_{n2}. These results are also confirmed by the sensitivity analyses performed in the next section.

Table 6.6. Eigenvalues of a two-area system for different values of $\boldsymbol{\omega_{n2}}$.

Modes	$\boldsymbol{\omega_{n2} = 0.1}$	$\boldsymbol{\omega_{n2} = 0.3}$	$\boldsymbol{\omega_{n2} = 4.9}$	$\boldsymbol{\omega_{n2} = 8.9}$
$\boldsymbol{\lambda_1}$	-15.1973	-15.2064	-17.9106	-21.6555
$\boldsymbol{\lambda_2}$	-10.2217	-10.2021	-8.726 + 6.659i	-11.477 +10.674i
$\boldsymbol{\lambda_3}$	-0.188 + 0.566i	-0.197 + 0.601i	-8.726 - 6.659i	-11.477 -10.674i
$\boldsymbol{\lambda_4}$	-0.188 - 0.566i	-0.197 - 0.601i	-0.313 + 0.417i	-0.291 + 0.413i
$\boldsymbol{\lambda_5}$	-0.958 + 0.491i	-0.1012	-0.313 - 0.417i	-0.291 - 0.413i
$\boldsymbol{\lambda_6}$	-0.9586 - 0.4912i	-0.957 + 0.489i	-0.983 + 0.478i	-0.975 + 0.478i
$\boldsymbol{\lambda_7}$	-0.0378	-0.957 - 0.489i	-0.983 - 0.478i	-0.975 - 0.478i
$\boldsymbol{\lambda_8}$	-0.2245	-0.633 + 0.085i	-0.5092	-0.5274
$\boldsymbol{\lambda_9}$	-0.6051	-0.633 - 0.085i	-1.4199	-1.4247
$\boldsymbol{\lambda_{10}}$	-1.4311	-1.4307	-2.168 + 0.074i	-3.0777
$\boldsymbol{\lambda_{11}}$	-2.1129	-2.1130	-2.168 - 0.074i	-2.1231
$\boldsymbol{\lambda_{12}}$	-2.6873	-2.6873	-2.6844	-2.6913
$\boldsymbol{\lambda_{13}}$	-2.6316	-2.6316	-2.6316	-2.6316

Table 6.7. Eigen index for different values of ω_{n2} .

Index	$\omega_{n2} = 0.1$	$\omega_{n2} = 0.3$	$\omega_{n2} = 4.9$	$\omega_{n2} = 8.9$
Damping of critical eigenvalues	11.4112	11.3857	11.5867	11.4109
Frequency of oscillatory modes	**0.3366**	**0.3744**	**2.4289**	**3.6819**

The effect of various changes in the damping parameter of VSP2 (ζ_2), which is located in the second area are presented in Table 6.8 and 6.9. As in the previous case, the minimum damping is required, while the higher values for this damping parameter will lead to higher damping for the system modes. Based on the results presented in Table 6.9, higher values for the total damping are achieved when the value of damping is higher than 1. The same conclusions are obtained performing the sensitivity analyses in the next section.

Table 6.8. Eigenvalues of two-area system for different values of ζ_2.

Modes	$\zeta_2 = 0.01$	$\zeta_2 = 1.1$	$\zeta_2 = 5$	$\zeta_2 = 8$
λ_1	-15.1973	-15.2064	-17.9106	-21.6555
λ_2	-10.2217	-10.2021	-8.726 + 6.659i	-11.477 +10.674i
λ_3	-0.188 + 0.566i	-0.197 + 0.601i	-8.726 - 6.659i	-11.477 -10.674i
λ_4	-0.188 - 0.566i	-0.197 - 0.601i	-0.313 + 0.417i	-0.291 + 0.413i
λ_5	-0.958 + 0.491i	-0.1012	-0.313 - 0.417i	-0.291 - 0.413i
λ_6	-0.9586 - 0.4912i	-0.957 + 0.489i	-0.983 + 0.478i	-0.975 + 0.478i
λ_7	-0.0378	-0.957 - 0.489i	-0.983 - 0.478i	-0.975 - 0.478i
λ_8	-0.2245	-0.633 + 0.085i	-0.5092	-0.5274
λ_9	-0.6051	-0.633 - 0.085i	-1.4199	-1.4247
λ_{10}	-1.4311	-1.4307	-2.168 + 0.074i	-3.0777
λ_{11}	-2.1129	-2.1130	-2.168 - 0.074i	-2.1231
λ_{12}	-2.6873	-2.6873	-2.6844	-2.6913
λ_{13}	-2.6316	-2.6316	-2.6316	-2.6316

Table 6.9. Eigen index for different values of ζ_2.

Index	$\zeta_2 = 0.01$	$\zeta_2 = 1.1$	$\zeta_2 = 5$	$\zeta_2 = 8$
Damping of critical eigenvalues	**9.4757**	**10.7736**	**11.4254**	**11.4254**
Frequency of oscillatory modes	0.3417	0.3401	0.3353	0.3353

A general comparison of eigenvalues for different inertia emulation methods, derivative and VSP based control, is presented in Table 6.10. As shown in this Table, the damping and oscillations of the overall system modes improves significantly after using the VSP based control method. Moreover, a higher damping with less oscillations is achieved using the synchronous power controller.

Table 6.10. Eigen index comparison for different methods of emulating the inertia.

Methods	Damping of critical eigenvalues	Frequency of oscillatory modes
Derivative Control	10.3349	0.6790
VSP Control	11.4254	0.3352

6.3.2 Sensitivity analyses

In order to analyze the effects of synchronous power control gains, (ω_{n1}, ζ_1, ω_{n2}, and ζ_2), on the system behavior, numerical simulations are performed with different values of control gains in the VSP controllers. These analyses are performed for two-area system under a large load step-change, around 0.03 p.u, at t = 3.5 sec. The effects of each VSP controller in the system behavior is presented.

6.3.2.1 Effects of variations in VSP1 parameters

As explained before, the VSP1 has two important parameters, ζ_1 and ω_{n1}. The effects of ω_{n1} on the system`s behavior are presented in Figure 6.8-6.11, considering an increase of ω_{n1} from 0.3 to 6.5. As it is shown in the Figure 6.8, the dynamic performance can be improved by increasing the ω_{n1} of the VSP1. This is evidenced when comparing the results depicted in Figure 6.9, where it can be seen that after increasing ω_{n1} the transient peak value decreases and, at the same time, a lower settling time is achieved.

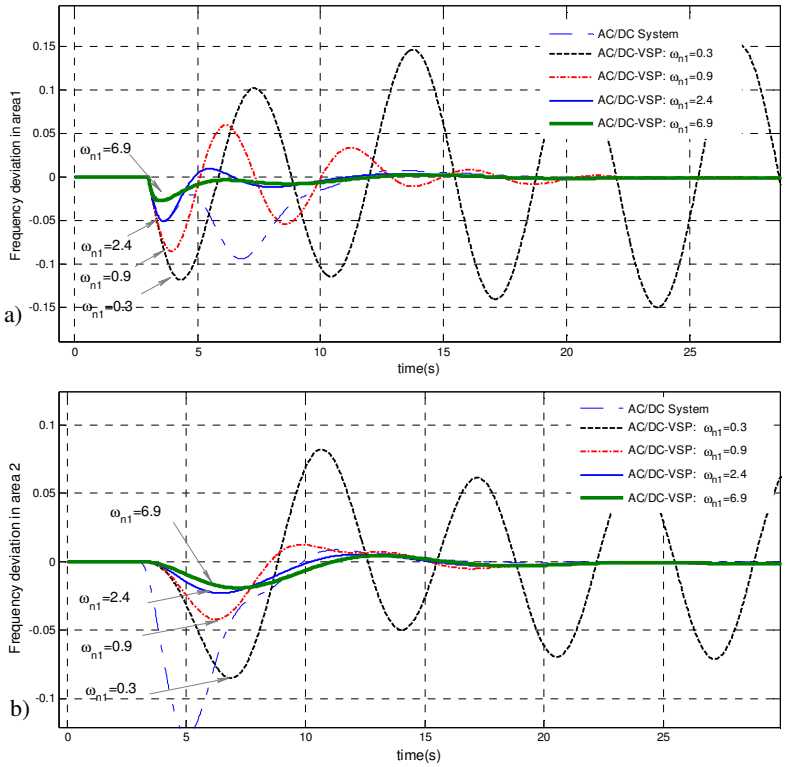

Figure 6.8. Frequency deviations in Area 1 and 2 for difference control gain values.

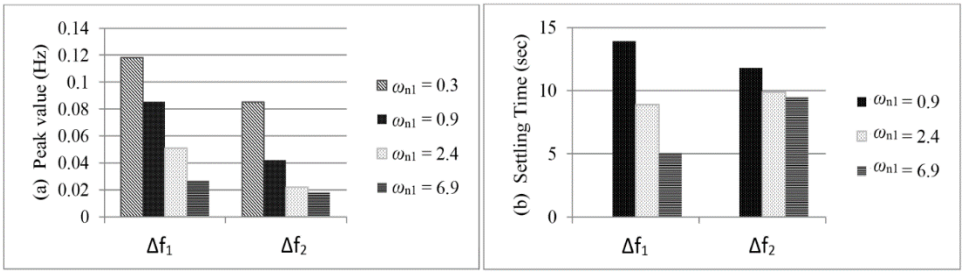

Figure 6.9. Frequency characteristics: (a) Peak overshoot, and (b) Settling time.

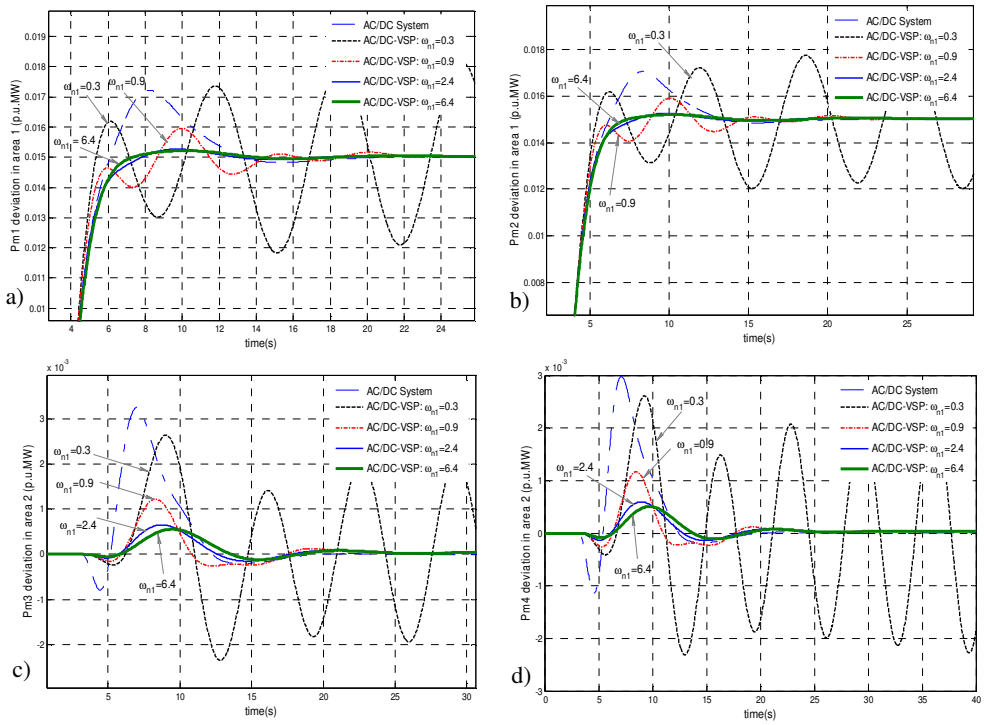

Figure 6.10. Active power generations. a) GENCO1, b) GENCO2, c) GENCO3, d) GENCO4.

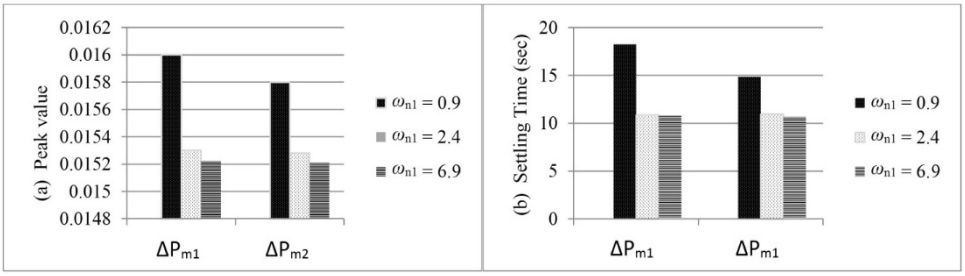

Figure 6.11. Settling times of active power response for GENCO1 and GENCO2.

The effects of the damping parameter (ζ_1) in VSP1 is presented in Figures 6.12-6.15. In this study case the damping factor has changed from 0.08 to 2.6 and the system response for each situation is presented and compared. As shown in Figure 6.12, lower values of damping will be translated into various oscillation in frequency in Area1.

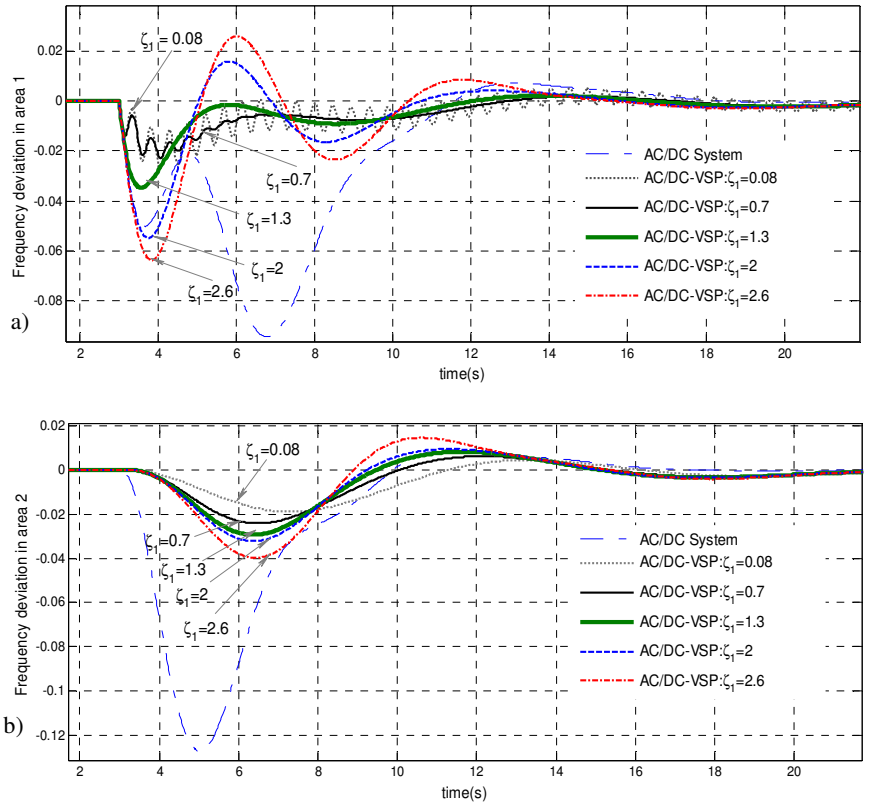

Figure 6.12. Frequency deviations for different damping factors in VSP1, a) Area1, b) Area2.

Therefore, for having a suitable dynamic response, a proper damping is necessary. By means of comparing the results in Figure 6.13, it can be concluded that the best value for damping is around 1.3, which will provide the best dynamic performance with less oscillation and minimum settling time.

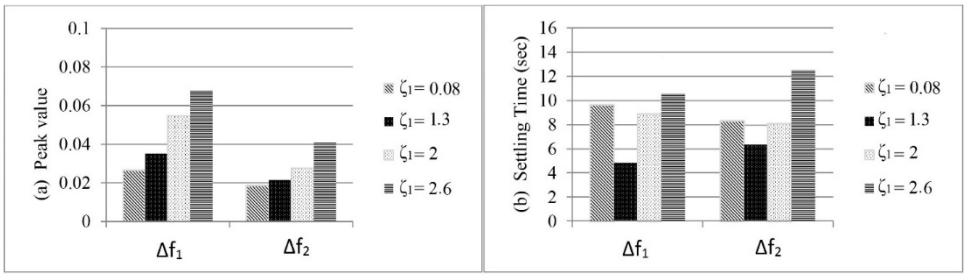

Figure 6.13. Frequency characteristics: (a) Peak overshoot, (b) Settling time.

The dynamic response of the injected power by the VSP1 ($\Delta x_{p,VSP1}$) is also presented in Figure 6.14. It is obvious that a lower damping will give rise to high oscillations, which is totally unacceptable. On the other hand, by increasing the damping of the VSP1 a better dynamic response can be achieved.

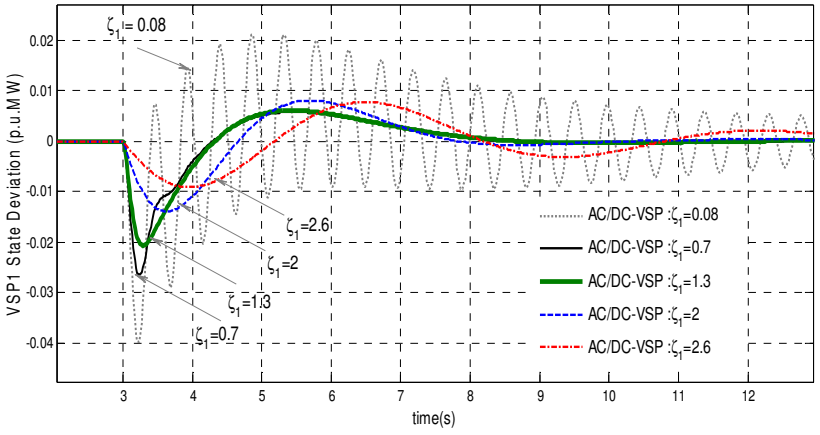

Figure 6.14. Power variations of the VSP1.

6.3.2.2 *Effects of variations in VSP2 parameters*

The effect of the second synchronous power controller, which is located in the second area, is presented. In this case the control parameters are ω_{n2} and ζ_2. The frequency deviations for different values of ω_{n2} are presented in Figures 6.15 and 6.16.

By means of increasing the ω_{n2} value the participation of VSP2 can be higher compared to the one of VSP1, but since in the studied system the load contingency is in Area 1, this increase will not have a positive effect in the overall system behavior. Therefore, a lower value of ω_{n2} in VSP2 is desirable.

As shown in the next figures, the value of ω_{n2} is increasing from 0.02 to 8. It is observed that lower values for ω_{n2} are preferable, as high values of ω_{n2} give rise to a high overshoot during the transients.

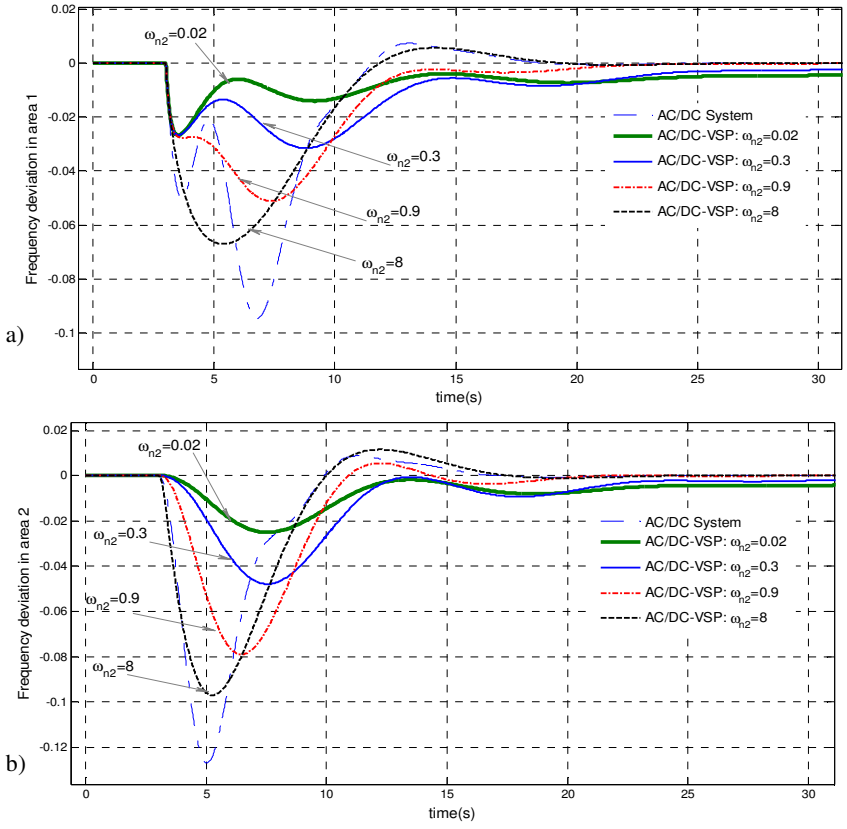

Figure 6.15. Frequency deviations in Area 1 and 2 for difference control gain values.

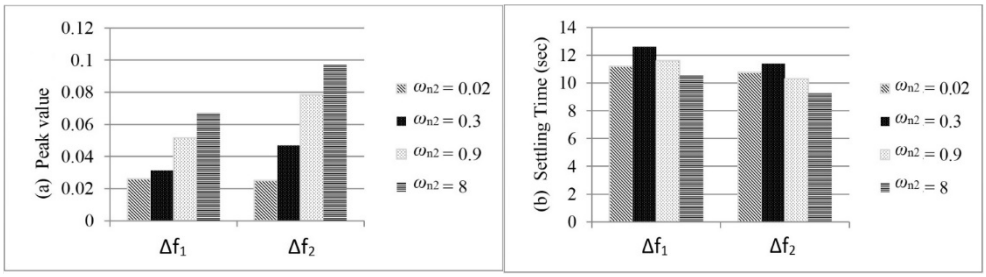

Figure 6.16. Frequency characteristics: (a) Peak overshoot, and (b) Settling time.

The effect of the damping parameter (ζ_2) of VSP2 is also presented in Figures 6.17-6.18. The damping factor has changed from 0.3 to 5 and the system response for each situation is presented and compared.

As it was expected, damping is necessary to reach a better and a more stable dynamic performance. As shown in Figure 5.17, lower value of damping in VSP2 is leading to steady state error with unacceptable performance.

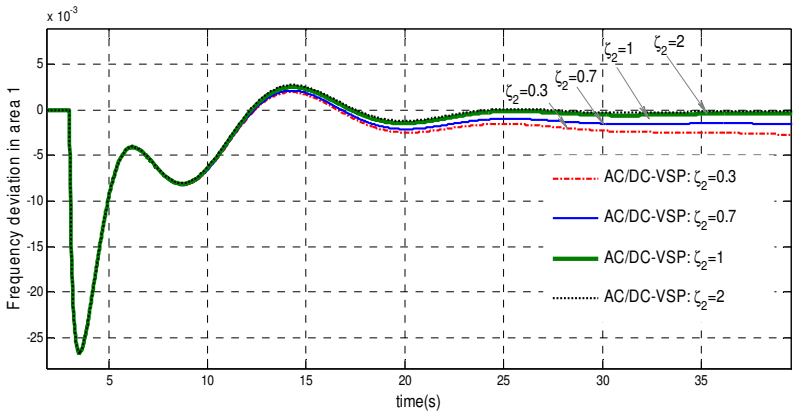

Figure 6.17. Frequency deviations in area 1 for different damping in VSP2.

Figure 6.18, is also presenting the response of the power state emulated by VSP2 ($\Delta x_{p,VSP2}$) for different values of damping. As shown in this figure, higher values for damping in VSP2 will bring a better response with less time response.

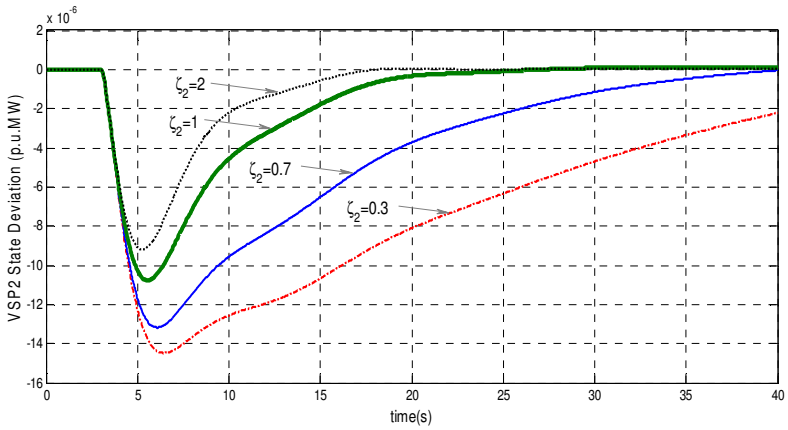

Figure 6.18. Power variations of VSP2 for different damping values.

6.3.2.3 Eigenvalue sensitivities

Based on the explanation given in section 5.2.4.3, in order to perform eigen sensitivity analyses, the matrix of participation factors should be calculated. The participation matrix for the two-area power system studied in this case is calculated in this section. Based on the obtained result, it can be concluded which states have a higher participation in sensitive or critical modes.

For this study case the participation factor is shown in the following:

1.75	**2.55**	0.49	0.76	0.79	0.05	0.05	0.11	0.00	0.00	0.00	0.00	0.00	$\Delta\boldsymbol{\omega_1}$
0.00	0.00	0.00	0.00	0.00	0.57	0.57	0.37	0.00	0.00	0.31	0.00	0.00	$\Delta\omega_2$
0.00	0.00	1.13	0.41	0.41	0.00	0.00	0.02	0.00	0.00	0.00	0.00	0.50	ΔP_{m1}
0.00	0.00	1.12	0.41	0.41	0.00	0.00	0.02	0.00	0.00	0.00	0.00	0.49	ΔP_{m2}
0.00	0.00	0.00	0.00	0.00	0.03	0.03	0.10	0.00	0.00	0.45	0.69	0.00	ΔP_{m3}
0.00	0.00	0.00	0.00	0.00	0.04	0.04	0.11	0.00	0.00	0.82	0.31	0.00	ΔP_{m4}
0.01	0.06	1.39	1.40	1.40	0.04	0.04	0.02	0.00	0.00	0.00	0.00	0.00	ΔACE_1
0.00	0.00	0.01	0.01	0.01	0.49	0.49	0.33	0.00	0.00	0.04	0.00	0.00	ΔACE_2
0.039	0.08	0.02	0.11	0.11	0.27	0.27	0.49	0.00	0.00	0.00	0.00	0.00	$\Delta P_{tie,AC}$
0.55	**0.76**	0.62	0.49	0.49	0.01	0.01	0.07	0.00	0.00	0.00	0.00	0.00	$\Delta\boldsymbol{x_{p,VSP1}}$
3.28	**2.29**	0.01	0.01	0.01	0.00	0.00	0.00	0.00	0.00	0.00	0.00	0.00	$\Delta\boldsymbol{x_{f,VSP1}}$
0.00	0.00	0.00	0.00	0.00	0.00	0.00	0.00	**0.20**	**1.21**	0.00	0.00	0.00	$\Delta\boldsymbol{x_{p,VSP2}}$
0.00	0.00	0.00	0.00	0.00	0.00	0.00	0.00	**1.22**	**0.22**	0.00	0.00	0.00	$\Delta\boldsymbol{x_{f,VSP2}}$
$\boldsymbol{\lambda_1}$	$\boldsymbol{\lambda_2}$	λ_3	λ_4	λ_5	λ_6	λ_7	λ_8	$\boldsymbol{\lambda_9}$	$\boldsymbol{\lambda_{10}}$	λ_{11}	λ_{12}	λ_{13}	

Another objective in eigenvalue sensitivity analysis is to identify the sensitivity of eigenvalues to each element of state space matrix **A** of the system. As it was explained before, the sensitivity matrix of the elements in matrix **A** can be written as follows:

$$P_{sens} = \Psi_{ik}\Phi_{ji} = \frac{\partial \lambda_i}{\partial a_{kj}} \tag{6.28}$$

where, the sensitivity of the eigenvalue λ_i to the element a_{kj} of the state matrix **A** will be equal to the product of the left eigenvector element $\Psi_{ik}$and the right eigenvector element Φ_{ji}. This tells us that the best way to change the i^{th} mode is to apply a control to the state variable such that the above sensitivity has the largest participating factor.

In order to apply such analysis for the studied two-area power system, the state space matrix **A** of the studied two-area system with VSP is partitioned as shown in the following:

$$\mathbf{A} = \begin{bmatrix} \mathbf{A_{11}} \\ \mathbf{A_{21}} \end{bmatrix}_{(13\times 13)} \tag{6.29}$$

Each sub-matrix are written as follows:

$$\mathbf{A_{11}} = \begin{bmatrix}
\frac{-1}{T_{p1}} & 0 & \frac{K_{p1}}{T_{p1}} & \frac{K_{p1}}{T_{p1}} & 0 & 0 & 0 & 0 & \frac{-K_{p1}}{T_{p1}} & \frac{-K_{p1}}{T_{p1}} & 0 & 0 & 0 \\
0 & \frac{-1}{T_{p2}} & 0 & 0 & \frac{K_{p2}}{T_{p2}} & \frac{K_{p2}}{T_{p2}} & 0 & 0 & \frac{K_{p2}}{T_{p2}} & 0 & 0 & \frac{K_{p2}}{T_{p2}} & 0 \\
\frac{-1}{2\pi R_1 T_{tg1}} & 0 & \frac{-1}{T_{tg1}} & 0 & 0 & 0 & \frac{-K_{I1}}{T_{tg1}} & 0 & 0 & 0 & 0 & 0 & 0 \\
\frac{-1}{2\pi R_2 T_{tg2}} & 0 & 0 & \frac{-1}{T_{tg2}} & 0 & 0 & \frac{-K_{I1}}{T_{tg2}} & 0 & 0 & 0 & 0 & 0 & 0 \\
0 & \frac{-1}{2\pi R_3 T_{tg3}} & 0 & 0 & \frac{-1}{T_{tg3}} & 0 & 0 & \frac{-K_{I2}}{T_{tg3}} & 0 & 0 & 0 & 0 & 0 \\
0 & \frac{-1}{2\pi R_4 T_{tg4}} & 0 & 0 & 0 & \frac{-1}{T_{tg4}} & 0 & \frac{-K_{I2}}{T_{tg4}} & 0 & 0 & 0 & 0 & 0 \\
\frac{\beta_1}{2\pi} & 0 & 0 & 0 & 0 & 0 & 0 & 0 & 1 & 1 & 0 & 0 & 0 \\
0 & \frac{\beta_2}{2\pi} & 0 & 0 & 0 & 0 & 0 & 0 & -1 & 0 & 0 & -1 & 0 \\
\frac{T_{12}}{2\pi} & -\frac{T_{12}}{2\pi} & 0 & 0 & 0 & 0 & 0 & 0 & 0 & 0 & 0 & 0 & 0
\end{bmatrix} \tag{6.30}$$

$$\mathbf{A_{21}} = \begin{bmatrix}
0 & 0 & 0 & 0 & 0 & 0 & 0 & 0 & 0 & 0 & 1 & 0 & 0 \\
a_{11,1} & a_{11,2} & 0 & 0 & 0 & 0 & 0 & 0 & a_{11,9} & a_{11,10} & a_{11,11} & 0 & 0 \\
0 & 0 & 0 & 0 & 0 & 0 & 0 & 0 & 0 & 0 & 0 & 0 & 1 \\
a_{13,1} & a_{13,2} & 0 & 0 & 0 & 0 & 0 & 0 & a_{13,9} & 0 & 0 & a_{13,12} & a_{13,13}
\end{bmatrix}$$

As identified in the state space presentation of the global system, the parameters of the synchronous power control appeared in the sub-matrix $\mathbf{A_{21}}$, which are related to the VSP control state variables. In fact, these parameters are presented in the 11th and 13th rows of the global system matrix **A**, and could be used for analyzing the system's performance. Therefore, the elements of interest in matrix **A** are the elements which contain the control gains of the VSP control components (ω_{n1}, ω_{n2}, ζ_1 and ζ_2) in the sub-matrix $\mathbf{A_{21}}$. These elements are written as follows:

$$a_{11,1} = \frac{K_{f1,VSP}\omega_{n1}^2}{2\pi}, a_{11,2} = \frac{K_{f2,VSP}\omega_{n2}^2}{2\pi}, \; a_{11,9} = K_{AC,VSP}\omega_{n1}^2 \;, \\ a_{11,10} = -\omega_{n1}^2 \;, a_{11,11} = -2\zeta_1\omega_{n1} \tag{6.31}$$

The results of sensitivities to the state matrix $\mathbf{A_{(12\times12)}}$ parameters are presented in Tables 6.11 and 6.12. In these tables the absolute sensitivity value of each mode to the elements of the sub-matrix $\mathbf{A_{21}}$, are presented.

Table 6.11. Normalized sensitivity of each mode for important elements of the **A** matrix.

Absolute Sensitivity of λ_i	$a_{11,1}$	$a_{11,2}$	$a_{11,9}$	$a_{11,10}$	$a_{11,11}$
λ_1	0.3120	0.0003	0.0003	0.065	1.001
λ_2	0.3138	0.0007	0.0005	0.0679	0.697
λ_3	0.0020	0.000	0.000	0.0036	0.0036
λ_4	0.0044	0.0003	0.000	0.0035	0.0036
λ_5	0.0044	0.0003	0.000	0.0035	0.0036
λ_6	0.0020	0.0029	0.000	0.000	0.000
λ_7	0.0020	0.0029	0.000	0.000	0.000
λ_8	0.0011	0.0016	0.000	0.0004	0.000
λ_9	0.0004	0.0004	0.000	0.000	0.000
λ_{10}	0.0004	0.0004	0.000	0.000	0.000
λ_{11}	0.000	0.000	0.000	0.000	0.000
λ_{12}	0.000	0.000	0.000	0.000	0.000
λ_{13}	0.3120	0.0003	0.0003	0.065	1.001

From the presented information in Table 6.11, it is obvious that the sensitivity for $a_{11,1}$ and $a_{11,11}$ are higher than for other elements. For these elements of matrix **A**, the first and the second modes (λ_1 and λ_2) have the highest sensitivities. From the participation factor matrix it can be observed that these modes are related to the first,

10th and 11th states of the system ($\Delta\omega_1$,$\Delta x_{p,VSP1}$ and $\Delta x_{f,VSP1}$). Likewise, the sensitivities to the rest of elements are presented in Table 6.12. These elements are the ones from matrix $\mathbf{A_{21}}$ which contain VSP2 parameters:

$$a_{13,1} = \frac{K_{f1,VSP}\omega_{n2}^2}{2\pi}, a_{13,2} = \frac{K_{f2,VSP}\omega_{n2}^2}{2\pi}, \; a_{13,9} = K_{AC,VSP}\omega_{n2}^2 \;, \\ a_{13,12} = -\omega_{n2}^2 \;, a_{13,13} = -2\zeta_2\omega_{n2} \tag{6.32}$$

From the presented information in Table 6.12, it can be observed that most of the elements have a considerable sensitivities to 9th and 10th modes (λ_9 and λ_{10}). From the participation factor matrix it can be indicated that the 12th and 13th states ($\Delta x_{p,VSP2}$ and $\Delta x_{f,VSP2}$) have the main participation for these two modes.

Table 6.12. Normalized sensitivity of each mode for important elements of **A** matrix.

Absolute Sensitivity of λ_i	$a_{13,1}$	$a_{13,2}$	$a_{13,9}$	$a_{13,12}$	$a_{13,13}$
λ_1	0.0012	0.000	0.000	0.000	0.000
λ_2	0.0025	0.000	0.000	0.000	0.000
λ_3	0.000	0.000	0.000	0.000	0.000
λ_4	0.0002	0.000	0.000	0.000	0.000
λ_5	0.0002	0.0026	0.000	0.000	0.000
λ_6	0.0301	0.0435	0.0025	0.000	0.000
λ_7	0.0301	0.0435	0.0025	0.000	0.000
λ_8	0.0035	0.0053	0.0007	0.000	0.000
$\boldsymbol{\lambda_9}$	**0.9920**	**0.9001**	**0.0941**	**0.1529**	0.0076
$\boldsymbol{\lambda_{10}}$	**1.001**	**0.9810**	**0.0941**	**0.1529**	0.00135
λ_{11}	0.0004	0.00122	0.000	0.000	0.000
λ_{12}	0.000	0.000	0.000	0.000	0.000
λ_{13}	0.000	0.000	0.000	0.000	0.000

The summary of eigenvalue sensitivity analysis is presented in Table 6.13. As shown by the sensitivity matrices in Tables 6.11 and 6.12, λ_1, λ_2, λ_9 and λ_{10} have the main sensitivity. Considering the results of the participation matrix, it can be concluded that controlling the 10th, 11th, 12th, and 13th states (the states of both VSP controllers) is most important target.

Table 6.13. Summary of eigen sensitivity analysis.

Sensitive modes to A matrix elements	Participant states
λ_1	$\Delta x_{p,VSP1}$, $\Delta x_{f,VSP1}$, $\Delta\omega_1$
λ_2	$\Delta x_{p,VSP1}$, $\Delta x_{f,VSP1}$, $\Delta\omega_1$
λ_9	$\Delta x_{p,VSP2}$, $\Delta x_{f,VSP2}$
λ_{10}	$\Delta x_{p,VSP2}$, $\Delta x_{f,VSP2}$

As explained before, the VSP states ($\Delta x_{p,VSP1}$, $\Delta x_{f,VSP1}$, $\Delta x_{p,VSP2}$ and $\Delta x_{f,VSP2}$) are affected by their control gains. So with a proper selection of the control gains, the desired dynamic response can be obtained.

In the last part of the analyses, in order to analyze the effects of VSP based HVDC parameters on the system performance and to identify their proper ranges, another analyses for modal characteristics (like damping and frequency of oscillatory modes) of the studied system, considering parameter variations of VSP stations, are performed in the following. The relationship between the ω_n gains (ω_{n1} and ω_{n2}) of the synchronous controllers and the total damping of modes is presented in Figure 6.19.

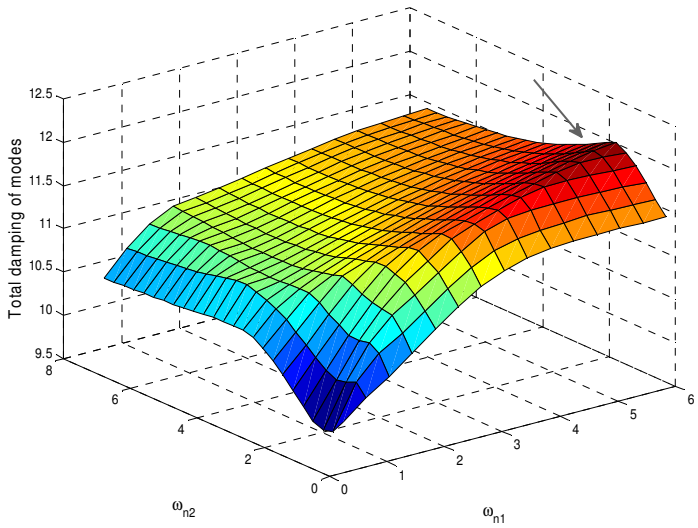

Figure 6.19. 3-D presentation for damping of the system for different values of ω_{n1} and ω_{n2}.

The 3-D presentation shown in figure 6.19, indicates the area with highest damping. As shown in this figure, the highest damping will be achieved for high values of ω_{n1} and low values for ω_{n2}. Therefore, for the studied two-area case, the values of ω_{n1} should be higher than 5 and the values for ω_{n2} should be lower than 1. This result is exactly the same than the one obtained from the eigenvalue analyses presented before.

For investigating the proper range of damping in VSP1, another plot is presented in Figure 6.20. In this figure, the relationships between the control parameters of VSP1 (ω_{n1} and ζ_1) and the system's damping is also presented. As shown in this figure, the highest damping is achieved for the area with damping values higher than 1 and lower than 3. For the other parameters of VSP1,ω_{n1}, the range are the same as the ones presented in Figure 6.19.

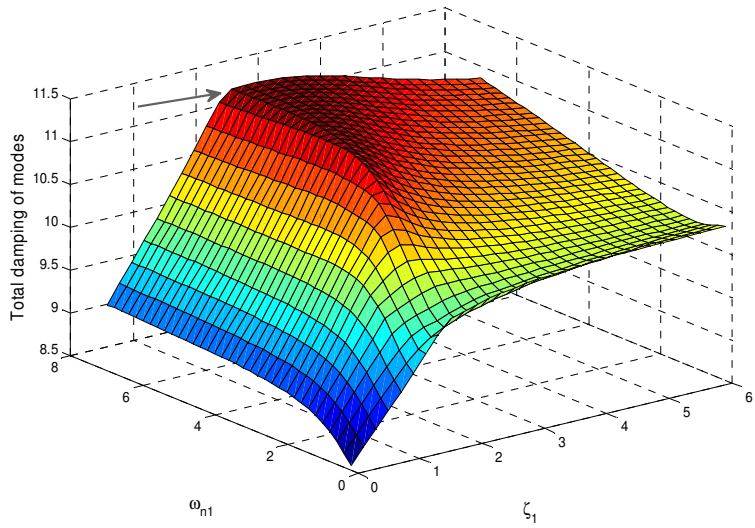

Figure 6.20. 3-D presentation for damping of the system for different values of ω_{n1} and ζ_1.

For investigating the proper range of damping in the second VSP controller, another plot is presented in Figure 6.21. In this figure, the relationships between the damping ratio parameters of both VSP controllers (ζ_1 and ζ_2) and system damping is presented.

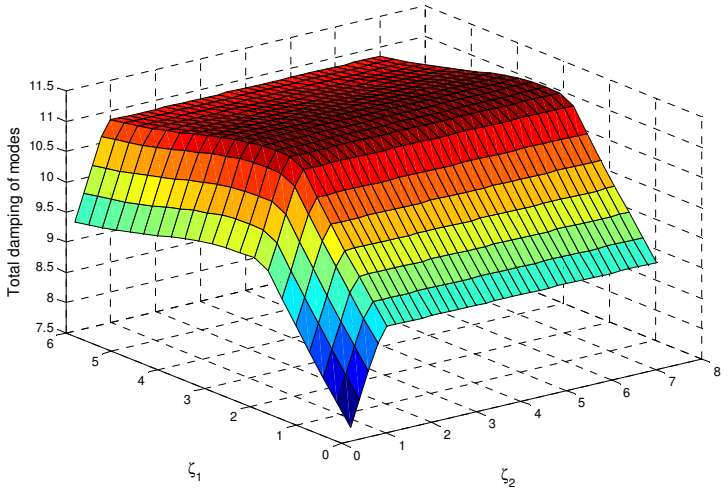

Figure 6.21. 3-D presentation for damping of the system for different values of ζ_1 and ζ_2.

As shown in Figure 6.21, the highest damping in the system's modes is achieved for the area with values higher than 0.5 for ζ_2. The proper range for the other damping ratio, ζ_1, is the same as the one from Figure 6.20.

Therefore, based on the presented analysis, the acceptable range of VSP parameter variations, which will guaranty a stable and acceptable dynamic response in the studied case, can be summarized as follows:

$$\omega_{n1} > 5$$
$$\omega_{n2} < 1$$
$$1 < \zeta_1 < 3$$
$$\zeta_2 > 0.5$$

6.4 Comparison and simulation results

6.4.1 Two-area system with comparisons

In order to validate and evaluate the positive effects of the proposed VSP-based AC/DC system on the AGC dynamics and to show how the proposed approach can contribute positively to the system dynamics during contingencies, a common scenario for the two-area test system which was explained in the previous sections is considered. In this case it is assumed that the contingency is a sudden load variation in Area 1 around 0.03 pu at 3 sec.

Several comparisons are performed during this simulation. These comparisons are related to the normal AC system, the normal AC/DC system, the AC/DC system with derivative control based virtual inertia and the proposed model for AC/DC system with VSP based inertia emulation. Considering these simulations, the positive effects of the VSP method will be identified. It should be note that in the model of AC/DC system with derivative control, the PLL effects is also considered. Considering the disturbance that was previously mentioned, the frequency deviations in both areas are presented in Figure 6.22.

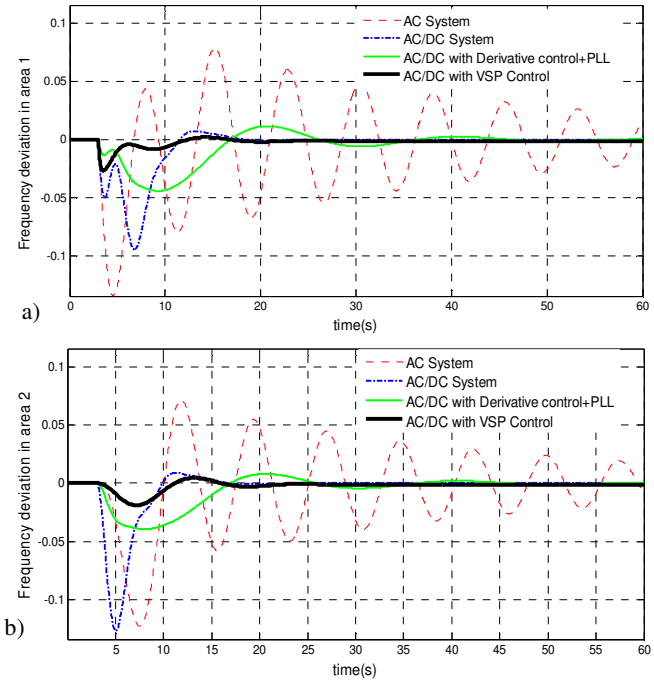

Figure 6.22. Dynamic response of frequency deviations; a) Area1, b) Area2.

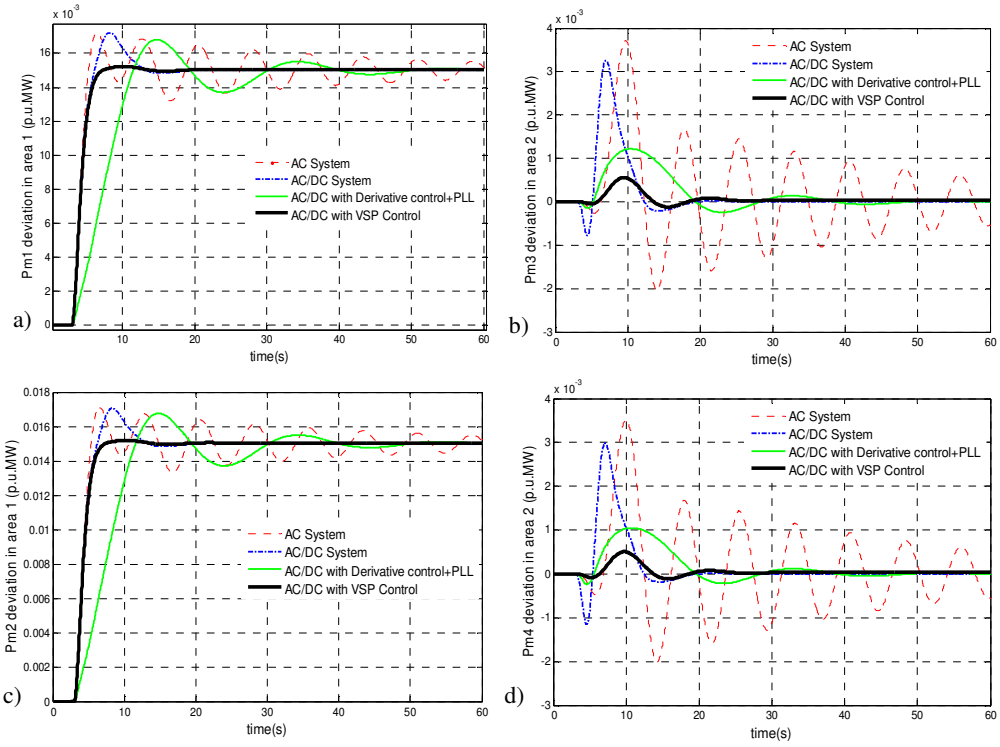

Figure 6.23. Output power generation; a) GENCO1, b) GENCO2, c) GENCO3, and d) GENCO4.

The output power generated by each unit is also presented in Figure 6.23. It is clear that by means of using the inertia emulation it would be possible to change the dynamic response of the system and the final response will be smoother than in a normal system without storage capabilities. This is especially relevant when comparing the results with the AC/DC system with a derivative control method, as it is clear that the synchronous power control technique offers a better performance.

As it was discussed before, in the synchronous power control technique there is no need of using a PLL or frequency estimation, and considering the fact that simultaneous damping and inertia can be emulated, a powerful method for improving the system dynamics during the contingencies is proposed.

The dynamic behaviour of different methods for performing inertia emulation are also presented in Figure 6.24. The comparison is made between the derivative method with PLL effects and the proposed method based on synchronous power control. Based on the obtained results for the studied two-area system, it is obvious that a better

performance could be achieved using the synchronous power control method. Since the load change occurs in Area 1, it can be foreseen that the controller in Area1 will have a higher and a faster contribution compared to the second controller in Area2. As shown in Figure 6.24.a, in both methods the maximum injected power is less than 2% of the rated power. With a close comparison, it could be observed that this maximum peak using synchronous power controller is less than the one obtained from the derivative control method for inertia emulation. This improvement is clearer in Figure 6.24.b, that corresponds to the performance in the second area. It is also obvious that using the synchronous power controller the dynamics of the injected power has a lower oscillation, which is very important during the operation of the system.

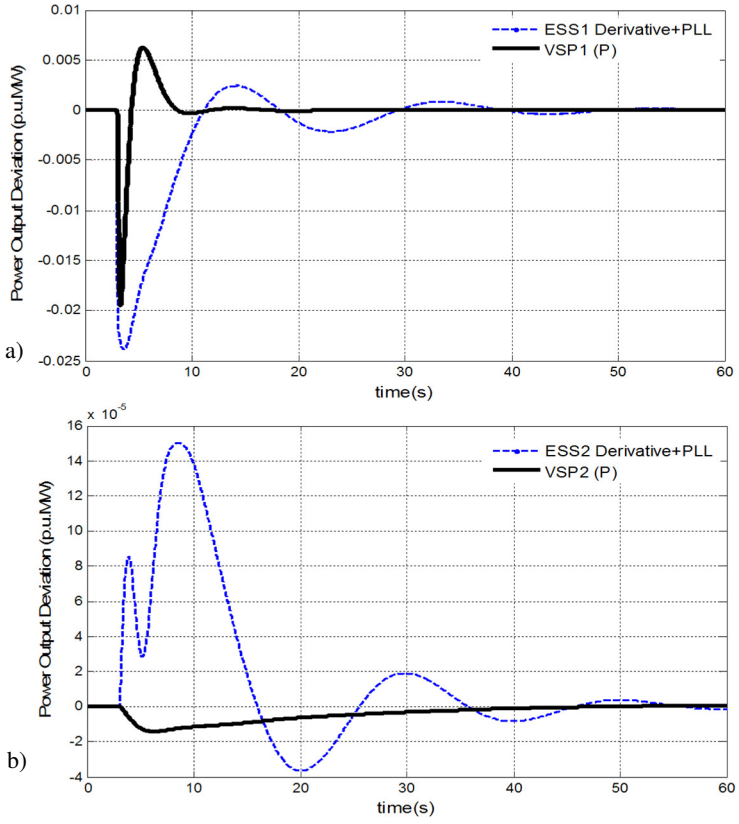

Figure 6.24. Power deviations with the derivative method and the VSP control method); a) Controller in Area1, b) Controller in Area2.

Another comparison regarding the eigenvalues of the system, considering different methods of inertia emulation, is presented in Table 6.14. It is clear that the method based on synchronous power strategy has a better performance with less oscillatory modes and a higher damping. In general, the advantage of the VSP method over the other methods like derivative based methods is obvious.

Moreover, the proposed control of VSP is naturally synchronized with the electrical grid by balancing the exchange of power with such grid. Therefore, it does not require any external synchronization system, such as a PLL, to work. Therefore, in addition to the dynamic improvements, all the limitations and dependencies derived from the use of PLLs and frequency measurements will be avoided.

Table 6.14. Eigenvalue comparisons for different two-area systems.

Modes	AC/DC with Derivative	AC/DC with Derivative and PLL	AC/DC with VSP method
λ_1	-209.32	-134.07	-15.1962
λ_2	-52.96	-39.375	-10.2239
λ_3	-22.63	-23.740	-1.4311
λ_4	-1.1 + 1.9I	-0.791 + 1.961I	-0.9586 + 0.4913I
λ_5	-1.1 - 1.9I	-0.791 - 1.961I	-0.9586 - 0.4913I
λ_6	-0.201	-0.450 + 0.520I	-0.1916 + 0.5618I
λ_7	-0.1 + 0.2I	-0.450 - 0.520I	-0.1916 - 0.5618I
λ_8	-0.1 - 0.2I	-0.341 + 0.501I	-0.6072
λ_9	-2.30	-0.341 - 0.501I	-0.0473
λ_{10}	-2.50	-0.0781 + 0.503I	-0.0088
λ_{11}	-2.70	-0.0781 - 0.503I	-2.1129
λ_{12}	-2.63	-0.2102	-2.6873
λ_{13}	------	-2.041	-2.6316
λ_{14}	------	-2.423	------
λ_{15}	------	-2.631	------
λ_{16}	------	-2.690	------

6.4.2 Case study of three-area system

In this part of study, a more complex system, a network with more areas as the well-known 3 area 39-bus system is considered. This system is widely used as a standard system for testing of new power system analysis and control synthesis methodologies. Figure 6.25 shows a single-line diagram of the test system.

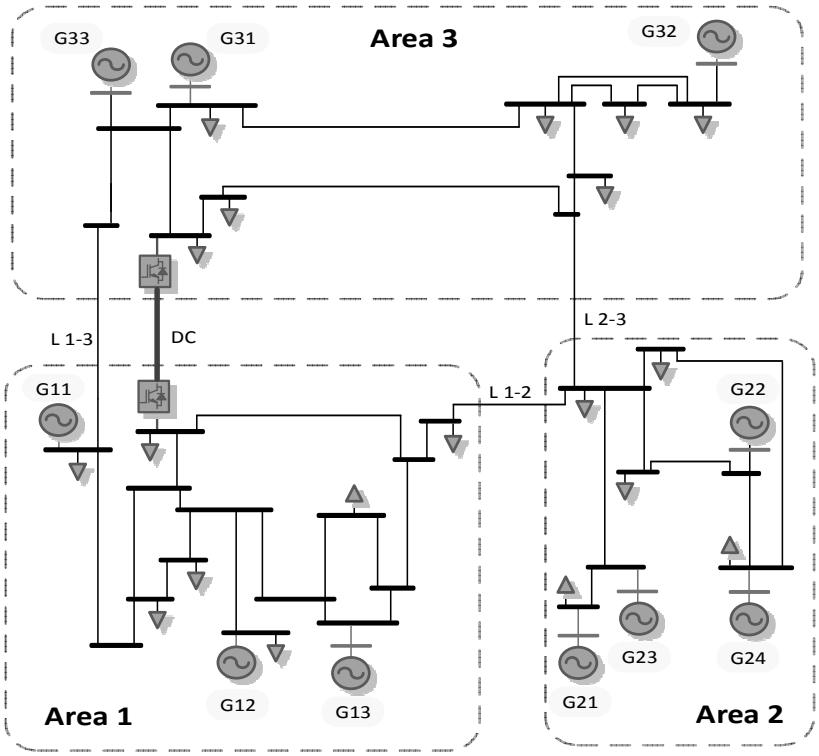

Figure 6.25. The configuration of the three-area power system with HVDC link.

This system consists of 3 areas, 10 generators and the system parameters are shown in Table 6.15 [1.5].The total load in this system is assumed to be 5.483 GW for the base system of 100 MVA and 60 Hz. More details about this system data can be found in [1.5] and [5.28]. As mentioned, the main objective of this paper is to propose an effective LFC scheme with a desirable performance in the presence of the VSP based HVDC system. Therefore, the case study is updated by adding a VSP based HVDC line between Area1 and 3. As shown in Figure 6.25, the tie-line flows are used for control studies. In this simulation, the important inherent requirement such as governor dead band and generation rate constraint imposed by physical system dynamics are considered.

In this scenario, it is assumed that the main contingency happened as a load change in Area3 by increasing to 0.1 p.u. at t = 3 s. All generators participate in LFC with equal participation factors. In the simulation, the parameters of the VSP based HVDC system are obtained using optimization theory as explained in previous sections. These values are presented in Table 6.16.

Table 6.15. Parameters of the three-area test system. (Base power of 100 MVA).

Area	GENCO	H	X_d	X_q	T'_{do}	X_l
1	G11	70.0	0.02	0.019	7.0	0.003
	G12	30.3	0.295	0.282	1.5	0.035
	G13	35.8	0.249	0.237	1.5	0.030
2	G21	28.6	0.262	0.258	1.5	0.029
	G22	26.0	0.67	0.620	0.44	0.054
	G23	34.8	0.254	0.241	0.4	0.022
	G24	26.4	0.259	0.292	1.5	0.032
3	G31	24.3	0.290	0.280	0.41	0.028
	G32	34.5	0.261	0.205	1.96	0.029
	G33	20.0	0.10	0.069	0.0	0.012

Table 6.16. Control parameters for studied 3-area AC/DC model with VSP.

Parameters	Value
$K_{f1,VSP}$ (puMW/rad)	1.8
$K_{f3,VSP}$ (puMW/rad)	-4.5
$K_{AC,VSP}$ (puMW)	0.015
ω_{n1}(rad/sec)	1.3
ω_{n3} (rad/sec)	4.1
ζ_1 (pu)	0.8
ζ_3 (pu)	2.6

It is worth to mention that, it is not necessary to equip all the converters with the VSP control during AGC task. In fact, the number of converters which are facilitated by VSP control will be depended on grid topology and specific conditions and requirements of each area in terms of ancillary services. In our work, we assumed that both converters of HVDC line are equipped with VSP control to improve local and global stability of the system.

The simulation results of the three-area test system including VSP based HVDC line are also compared with the system including a normal DC and normal AC lines. In

Figure 6.26, the frequency deviation of all areas following the applied load disturbances in Area 3 is presented. These figures show the superior performance of the proposed VSP based method to the classical model in deriving the frequency deviation close to zero with a better dynamic.

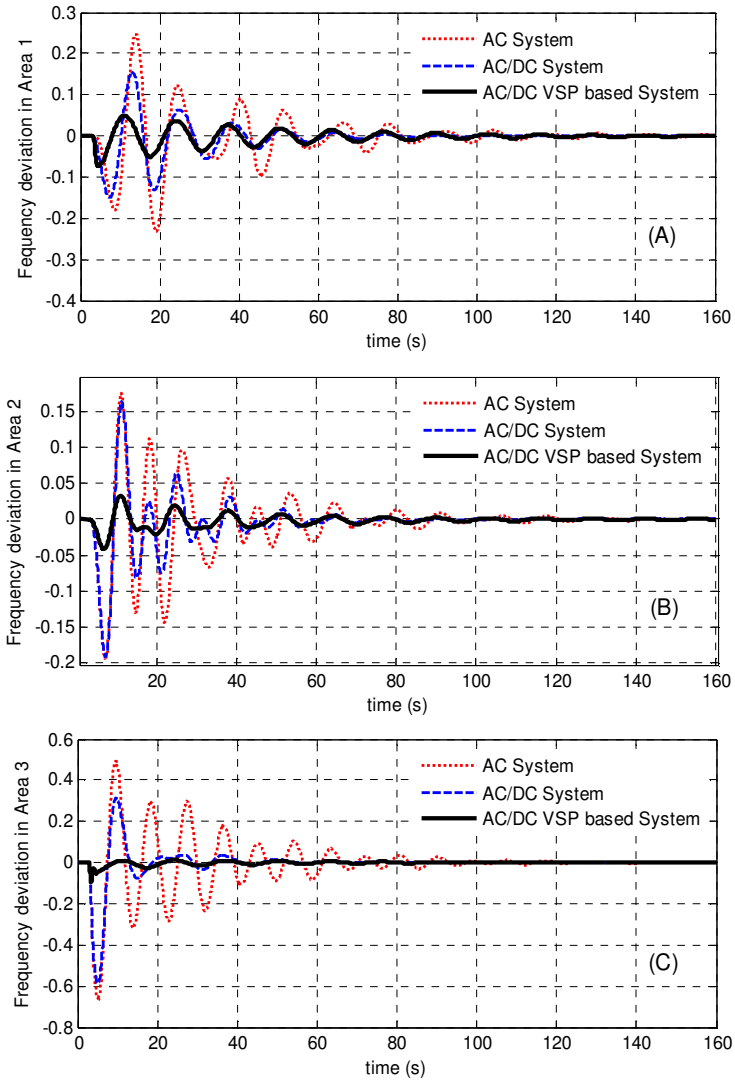

Figure 6.26. Dynamic response of frequency deviations for three-area system (rad/sec); A) Area1, B) Area2 and C) Area3.

The dynamic responses of generated power for all the generation units in different areas are depicted in Figures 2.27-6.29. It is clear that the units in Area3, the area with 0.1 pu load change, are responding equally to regulate their area control error.

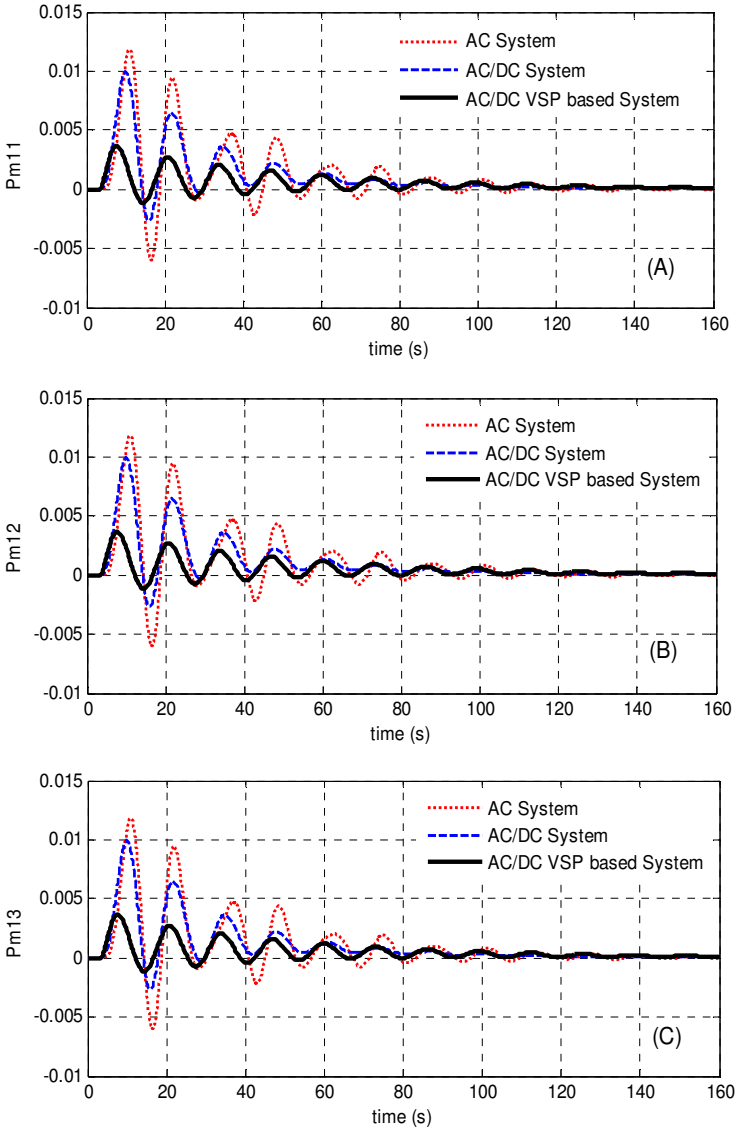

Figure 6.27. Power generations in Area1; A) GENCO11, B) GENCO12, and C) GENCO13.

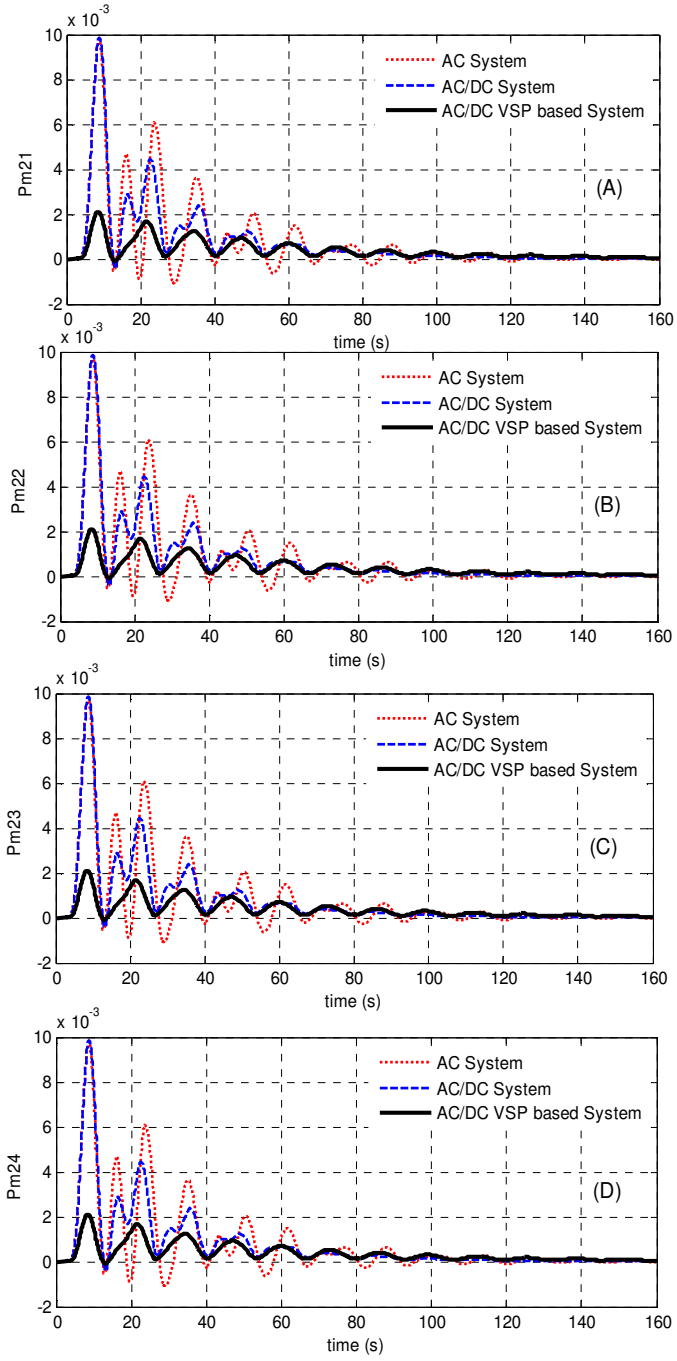

Figure 2.28. Power generations in Area2; A) GENCO21, B) GENCO22, C) GENCO23, and GENCO24.

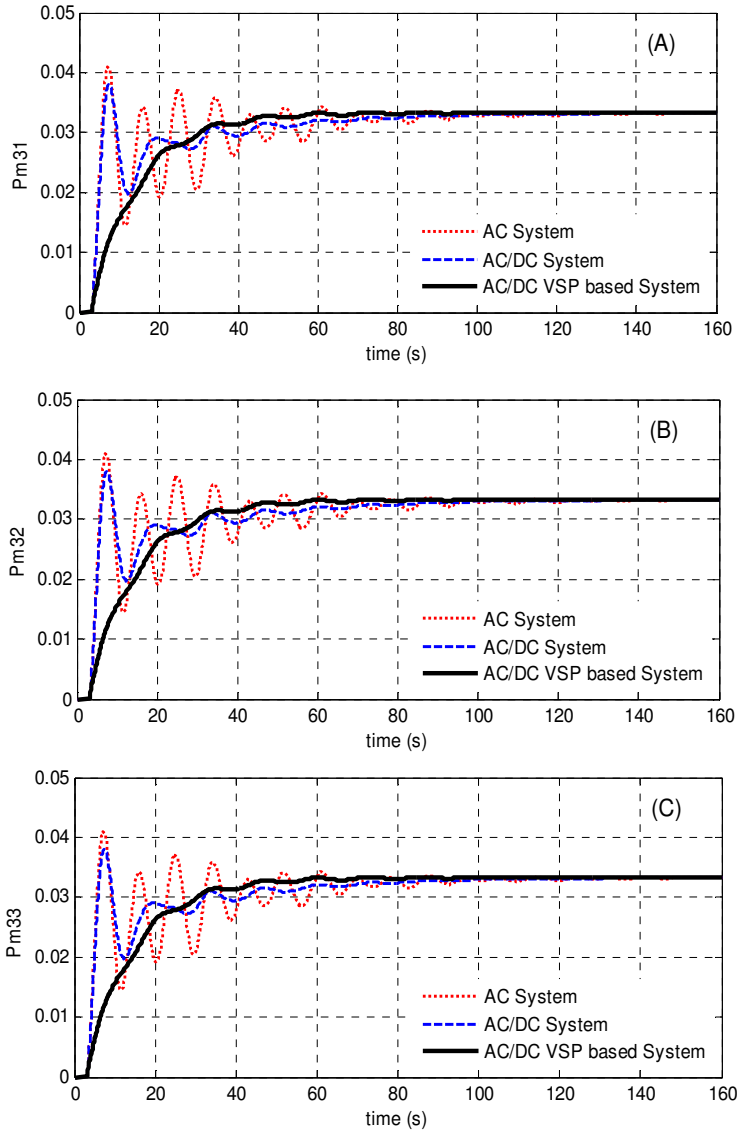

Figure 6.29. Power generations in Area3; A) GENCO31, B) GENCO32, and C) GENCO33.

The tie-line power of all areas are shown in Figure 6.30. It can be seen that the tie-line power flows in the normal systems without VSP, show more oscillations and poor performance in keeping the tie-line power interchanges in the scheduled values.

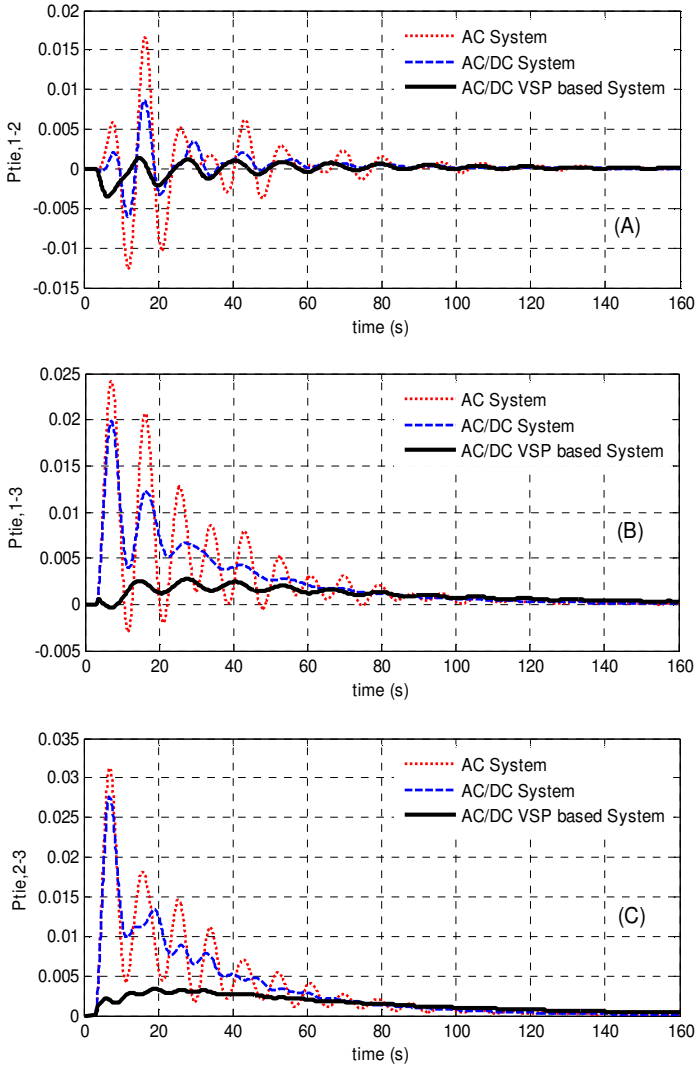

Figure 6.30. Tie-line AC power exchanges; A) Line 1-2, A) Line 1-3, and A) Line 2-3.

The power variations of each VSP station is also presented in Figure 6.31. Based on the obtained result for this case, the main part of the generated power is related to VSP3 located in Area3, the area with contingency. Based on the obtained results, the reference

power for VSP system is clarified in Figure 6.31. Based on each study case and considering the worst case scenario, the proper ratings of power converters with the required amount of energy can be obtained which will be helpful for pre-design stages. In practice, the required energy for emulating sufficient virtual inertia in period of t can be directly calculated according to the following equation for period of t:

$$E_{VSP,i} = \int_0^t P_{VSP,i}(t)dt + E_{VSP0,i} \tag{6.33}$$

where $P_{VSP,i}$ was the instantaneous power of VSP components ($\Delta X_{p,VSP,i}$) and $E_{VSP0,i}$ is the initial energy. For this study, the energy trace is depicted by Figure 6.32. The required energy for VSP1 is 0.1 p.u. and the energy for VSP3 is equal to 0.22 p.u. Thus, knowing the base values for each application, the real values of energy with the required DC capacitance can be calculated.

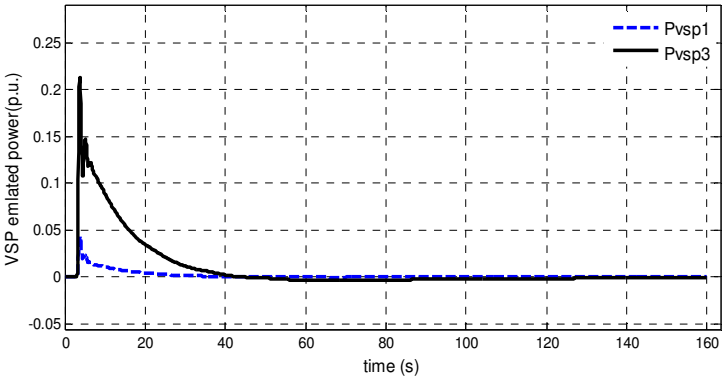

Figure 6.31. Power deviation from VSP based HVDC system; VSP1 in Area1 and VSP3 in Area3.

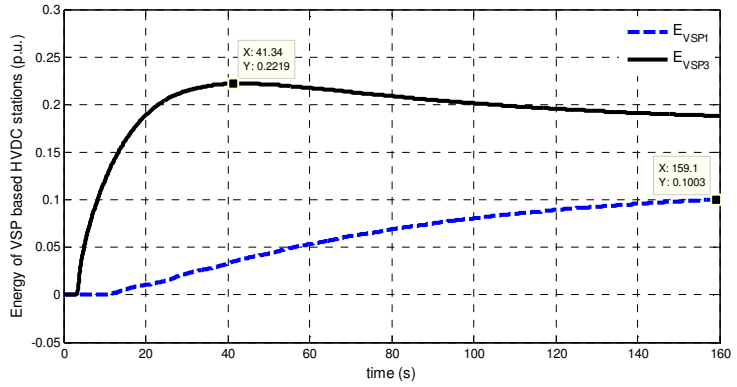

Figure 6.32. Required energy by VSP based HVDC stations (p.u.).

6.4.3 Case study of four-area system

As shown in the Figure 6.33, a generic four-area power system based on 12-bus multi machine benchmark which consists of four Gencos (Generation Companies) and four Discos (Distribution Companies) is implemented. The basic parameters of this system, for the base power grid of 100 MVA and the frequency of 60 Hz, are shown in Table 6.17 [6.17]. The 12-bus model is coming from North America, representing the Manitoba Chicago network, is adaptable with the power system of other countries like US, UK and Germany as simplified power system model [6.27]. The studied HVDC link is located in parallel with AC line between Area 1 and 3, with 600 kV of rated DC side voltage. In this scenario, it is assumed that there is a load change around 0.1 p.u. in Area 3 and the effects of this change on dynamic response considering normal AC system, AC/DC system and VSP based AC/DC system are discussed and compared.

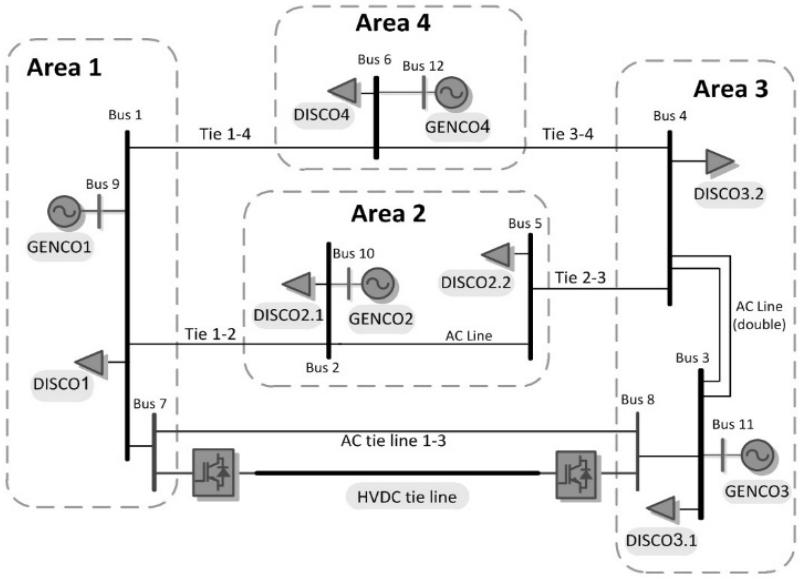

Figure 6.33. Single-line diagram of the studied four-area interconnected system.

Mathematical equations for this case study is written based on the generalized formulation presented Section 6.2.3 (the AC/DC line is between Area 1 and 3, where i=1, l=3). The linearized state space representation of a four-area AGC model with the VSP based DC connection could be as follows:

$$\Delta\dot{\mathbf{x}} = \mathbf{A}\,\Delta\mathbf{x} + \mathbf{B}\,\Delta\mathbf{u} \tag{6.34}$$

$$\Delta \mathbf{y} = \mathbf{C}\,\Delta \mathbf{x}$$

where **x** is the state vector matrix, u is the input vector, **A** is the system matrix, **B** is the input matrix, **C** is the output matrix and y is the system output.

Table 6.17. Parameters of the studied four-area interconnected system.

Parameters	Area 1	Area 2	Area 3	Area 4
K_{pi} (rad/pu MW)	76	141.7	139.6	114.2
T_{pi} (sec)	14.4	19.1	9.39	9.12
R_i (Hz/pu)	3	3	3	3
β_i (pu./Hz)	0.416	0.377	0.378	0.388
K_{Ii}	0.131	0.131	0.131	0.131
$T_{tg,i}$ (s)	0.38	0.38	0.38	0.38
T_{ij} (pu/rad)	T_{12}=0.029 T_{13}=0.0143 T_{14}=0.0099	T_{21}=0.029 T_{23}=0.0205	T_{31}=0.0143 T_{32}=0.0205 T_{34}=0.0089	T_{41}=0.0099 T_{43}=0.0089

State variables consist of frequency deviations of four areas ($\Delta\boldsymbol{\omega}_{1:4}$), generated power deviations of Gencos ($\Delta\mathbf{P}_{\mathbf{m1:4}}$), power set-points coming from ACE ($\Delta\mathbf{P}_{\mathbf{refv1:4}}$), group of states related to tie-line power deviations ($\Delta\mathbf{x}_{\mathbf{tie}}$), and states related to VSP based DC connections ($\Delta\mathbf{x}_{\mathbf{VSP}}$) are as follows:

$$\mathbf{x} = [\Delta\omega_{1:4} |\, \Delta P_{m1:4} |\, \Delta P_{refv1:4} | \Delta x_{tie} |\, \Delta x_{VSP}\,]^T \tag{6.35}$$

where:

$$\Delta\mathbf{x}_{\mathbf{tie}} = \begin{bmatrix}\Delta P_{tie,12} & \Delta P_{tie,13} & \Delta P_{tie,14} & \Delta P_{tie,23} & \Delta P_{tie,34}\end{bmatrix}^T$$

$$\Delta\mathbf{x}_{\mathbf{VSP}} = \begin{bmatrix}\Delta X_{p-VSP,13} & \Delta X_{f-VSP,13} & \Delta X_{p-VSP,31} & \Delta X_{f-VSP,31}\end{bmatrix}^T$$

Based on different types of these state variables, the system matrix is partitioned as follows:

$$\mathbf{A} = \begin{bmatrix} \mathbf{A_{11}} & \mathbf{A_{12}} & \mathbf{0} & \mathbf{A_{14}} \\ \mathbf{A_{21}} & \mathbf{A_{22}} & \mathbf{A_{23}} & \mathbf{0} \\ \mathbf{A_{31}} & \mathbf{0} & \mathbf{0} & \mathbf{A_{34}} \\ \mathbf{A_{41}} & \mathbf{0} & \mathbf{0} & \mathbf{0} \\ \mathbf{A_{51}} & \mathbf{0} & \mathbf{0} & \mathbf{A_{54}} \end{bmatrix}_{(\mathbf{21\times 21})} \tag{6.36}$$

Therefore, each sub-matrix will be as follows:

$$\mathbf{A_{11}} = \text{diag}\left(\frac{-1}{T_{p1}},\ \frac{-1}{T_{p2}},\ \frac{-1}{T_{p3}},\ \frac{-1}{T_{p4}}\right),$$

$$\mathbf{A_{12}} = \text{diag}\left(\frac{K_{p1}}{T_{p1}},\ \frac{K_{p2}}{T_{p2}},\ \frac{K_{p3}}{T_{p3}},\ \frac{K_{p4}}{T_{p4}}\right),$$

$$\mathbf{A_{21}} = \text{diag}\left(\frac{-1}{2\pi R_1 T_{tg,1}},\ \frac{-1}{2\pi R_2 T_{tg,2}},\ \frac{-1}{2\pi R_3 T_{tg,3}},\ \frac{-1}{2\pi R_4 T_{tg,4}}\right),$$

$$\mathbf{A}_{22} = \text{diag}\left(\frac{-1}{T_{tg,1}},\ \frac{-1}{T_{tg,2}},\ \frac{-1}{T_{tg,3}},\ \frac{-1}{T_{tg,4}}\right),$$

$$\mathbf{A_{23}} = \text{diag}\left(\frac{-K_{I1}\, apf_1}{T_{tg,1}},\ \frac{-K_{I2}\, apf_2}{T_{tg,2}},\ \frac{-K_{I3}\, apf_3}{T_{tg,3}},\ \frac{-K_{I4}\, apf_4}{T_{tg,4}}\right),$$

$$\mathbf{A_{31}} = \text{diag}\left(\frac{\beta_1}{2\pi},\ \frac{\beta_2}{2\pi},\ \frac{\beta_3}{2\pi},\ \frac{\beta_4}{2\pi}\right),$$

$$\mathbf{A_{34}} = \begin{bmatrix} 1 & 1 & 1 & 0 & 0 & 1 & 0 & 0 & 0 \\ -1 & 0 & 0 & 1 & 0 & 0 & 0 & 0 & 0 \\ 0 & -1 & 0 & -1 & 1 & 0 & 0 & -1 & 0 \\ 0 & 0 & -1 & 0 & -1 & 0 & 0 & 0 & 0 \end{bmatrix},$$

$$\mathbf{A_{14}} = \begin{bmatrix} \frac{-K_{p1}}{T_{p1}} & \frac{-K_{p1}}{T_{p1}} & \frac{-K_{p1}}{T_{p1}} & 0 & 0 & \frac{-K_{p1}}{T_{p1}} & 0 & 0 & 0 \\ \frac{K_{p2}}{T_{p2}} & 0 & 0 & \frac{-K_{p2}}{T_{p2}} & 0 & 0 & 0 & 0 & 0 \\ 0 & \frac{K_{p1}}{T_{p1}} & 0 & \frac{K_{p3}}{T_{p3}} & \frac{-K_{p3}}{T_{p3}} & 0 & 0 & \frac{K_{p3}}{T_{p3}} & 0 \\ 0 & 0 & \frac{K_{p1}}{T_{p1}} & 0 & \frac{K_{p1}}{T_{p1}} & 0 & 0 & 0 & 0 \end{bmatrix}, \tag{6.37}$$

$$\mathbf{A_{41}} = \begin{bmatrix} T_{12} & -T_{12} & 0 & 0 \\ T_{13} & 0 & -T_{13} & 0 \\ T_{14} & 0 & 0 & -T_{14} \\ 0 & T_{23} & -T_{23} & 0 \\ 0 & 0 & T_{34} & -T_{34} \end{bmatrix}, \mathbf{A_{51}} = \begin{bmatrix} 0 & 0 & 0 & 0 \\ a_{19,1} & 0 & a_{19,3} & 0 \\ 0 & 0 & 0 & 0 \\ a_{21,1} & 0 & a_{21,3} & 0 \end{bmatrix},$$

$$\mathbf{A_{54}} = \begin{bmatrix} 0 & 0 & 0 & 0 & 0 & 0 & 1 & 0 & 0 \\ 0 & a_{19,14} & 0 & 0 & 0 & a_{19,18} & a_{19,19} & 0 & 0 \\ 0 & 0 & 0 & 0 & 0 & 0 & 0 & 0 & 1 \\ 0 & a_{21,14} & 0 & 0 & 0 & 0 & 0 & a_{21,20} & a_{21,21} \end{bmatrix}$$

As identified in the state space presentation of the system, the parameters of the VSP are appeared in sub-matrices $\mathbf{A_{51}}$ and $\mathbf{A_{54}}$ which are related to VSP state variables.

$$\begin{gathered} a_{19,1} = \frac{K_{f-VSP,13}\omega_{n,13}^2}{2\pi},\ a_{19,3} = \frac{K_{f-VSP,31}\omega_{n,13}^2}{2\pi},\quad a_{19,14} = K_{AC-VSP,13}\omega_{n,13}^2, \\ a_{19,18} = -\omega_{n,13}^2,\quad a_{19,19} = -2\zeta_{13}\omega_{n,13}, \\ a_{21,1} = \frac{K_{f-VSP,13}\omega_{n,31}^2}{2\pi}, a_{21,3} = \frac{K_{f-VSP,31}\omega_{n,31}^2}{2\pi}\quad a_{21,14} = K_{AC-VSP,13}\omega_{n,31}^2 \\ a_{21,20} = -\omega_{n,31}^2,\quad a_{21,21} = -2\zeta_{31}\omega_{n,31} \end{gathered} \tag{6.38}$$

Finally the **B** matrix and the input vector **u** could be presented as follows:

$$\mathbf{B} = \left[\frac{\mathbf{B_{11}}}{\mathbf{0}}\right]_{(\mathbf{21\times 4})}, \qquad \mathbf{B_{11}} = \text{diag}\left(\frac{-K_{p1}}{T_{p1}}, \quad \frac{-K_{p2}}{T_{p2}}, \quad \frac{-K_{p3}}{T_{p3}}, \quad \frac{-K_{p4}}{T_{p4}}\right), \tag{6.39}$$

$$\boldsymbol{u} = [\Delta P_{L1} \quad \Delta P_{L2} \quad \Delta P_{L3} \quad \Delta P_{L4}]^T \tag{6.40}$$

For the high-level controller design of the AGC, which its main concern relates to inter-area modes, the first task is to validate the selection of suitable control signal inputs in the supplementary controller of the HVDC link. For doing this, the eigenvalues of the studied four-area system are presented in Table 6.18.

Table 6.18. Eigenvalues of the studied four-area system.

$\boldsymbol{\lambda}$	**Eigenvalues**	**Damping**	$\boldsymbol{f}$ **(Hz)**
$\boldsymbol{\lambda_1}$	-18.8045	1.000	0.000
$\boldsymbol{\lambda_2}$	-2.612+1.622i	0.849	0.258
$\boldsymbol{\lambda_3}$	-2.612-1.622i	0.849	-0.258
$\boldsymbol{\lambda_4}$	-2.522	1.000	0.000
$\boldsymbol{\lambda_5}$	-2.460	1.000	0.000
$\boldsymbol{\lambda_6}$	-2.303	1.000	0.000
$\boldsymbol{\lambda_7}$	-1.826	1.000	0.000
$\boldsymbol{\lambda_8}$	-0.170+1.153i	0.146	0.183
$\boldsymbol{\lambda_9}$	-0.170-1.153i	0.146	-0.183
$\boldsymbol{\lambda_{10}}$	-0.091+0.905i	0.109	0.144
$\boldsymbol{\lambda_{11}}$	-0.091-0.905i	0.109	-0.144
$\boldsymbol{\lambda_{12}}$	-0.095+0.809i	0.117	0.128
$\boldsymbol{\lambda_{13}}$	-0.095-0.809i	0.117	-0.128
$\boldsymbol{\lambda_{14}}$	-0.799	1.000	0.000
$\boldsymbol{\lambda_{15}}$	-0.338	1.000	0.000
$\boldsymbol{\lambda_{16}}$	-0.200	1.000	0.000
$\boldsymbol{\lambda_{17}}$	-0.105	1.000	0.000
$\boldsymbol{\lambda_{18}}$	-0.069	1.000	0.000
$\boldsymbol{\lambda_{19}}$	-0.030	1.000	0.000
$\boldsymbol{\lambda_{20}}$	-0.0001	1.000	0.000
$\boldsymbol{\lambda_{21}}$	-0.0001	1.000	0.000

These eigenvalues will be used for Eigen-sensitivity analysis of the system. The residue sensitivity analysis is applied to check the suitable control signals that can be used for introducing the supplementary damping control strategy.

From sensitivity analysis presented in Figure 6.34, it was observed that $\lambda_{1,2}$ and $\lambda_{14,15}$ have the maximum sensitivities regarding the VSP based HVDC link parameters in 19th and 21th rows of the state matrix **A**.

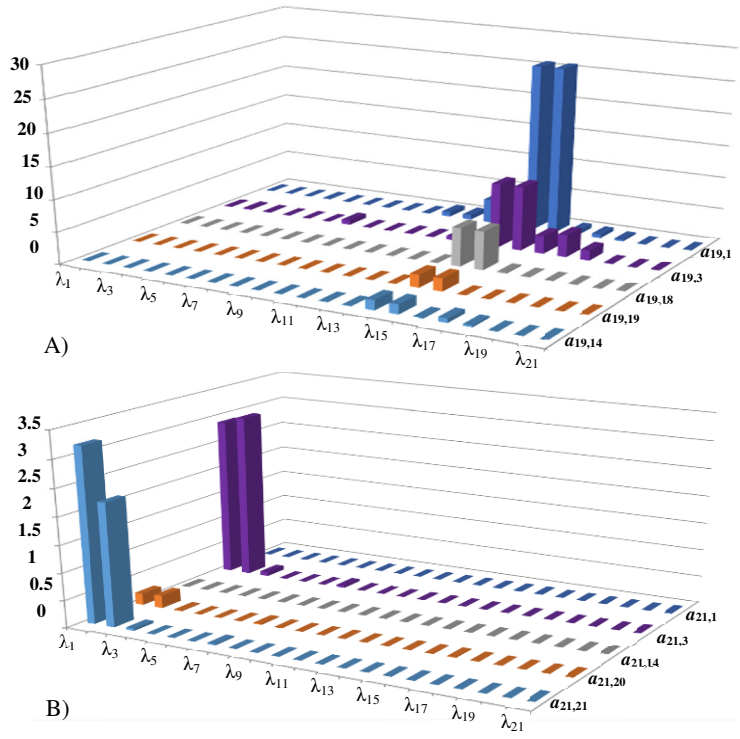

Figure 6.34. Sensitivities of important elements to the system modes. (A) VSP elements in 19th row of **A** matrix, (B) VSP elements in 21th row of **A** matrix.

Then from the mode shapes presented in Figures 6.53(a) and 6.35(b), it will be obvious that the states involved in Area 3 and 1 (Genco3 and Genco1) are the main participants on those modes ($\lambda_{1,2}$ and $\lambda_{14,15}$). Thus, the effective higher level control signals for DC power reference, should be selected from Area 3 and Area 1 which are the ones connected to the HVDC link.

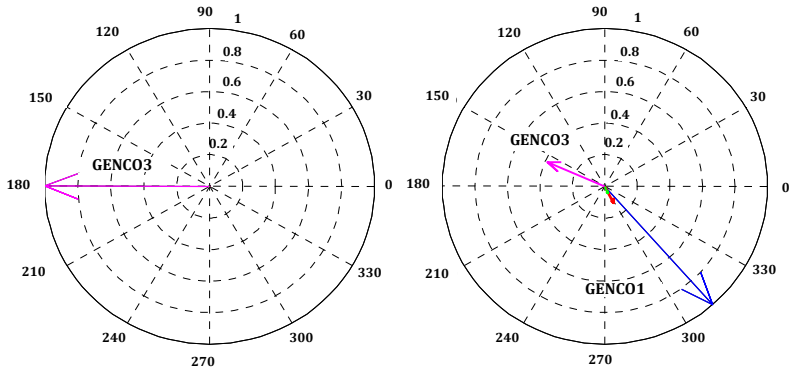

Figure 6.35. Mode shape. (a) $\lambda_{1,2}$ (b) $\lambda_{14,15}$.

In order to show the effectiveness of the proposed approach in LFC problem, a comparative study is presented between the obtained results from the proposed VSP-based AC/DC system, the normal AC/DC system without VSP and the classic AC interconnected systems. Based on the analysis presented in the previous parts, the appropriate values of the VSP based DC link parameters can be similar to the ones presented in Table 6.19.

Table 6.19. VSP based HVDC control parameters in studied 4-area system.

Parameters	Area 1	Area 3
$\omega_{n,13}$	0.27	------
$\omega_{n,31}$	------	5.92
ζ_{13}	1.83	------
ζ_{31}	------	1.70
$K_{f\text{-}VSP,13}$	-0.255	------
$K_{f\text{-}VSP,31}$	------	-1.018
$K_{AC\text{-}VSP}$	1.91	1.91

As explained, it is assumed the base power of the system is 100 MVA, the rated pole to pole voltage of DC link is 600 kV and the frequency is 60 Hz. The base power of each unit in Area1, 2, 3 and 4 are 750 MW, 640 MW, 388 MW and 474 MW, respectively. One step load change around 10% occurs at t = 5 s in Area 3.

The frequency deviations, the generated power of all units, AC tie-line variations and VSP output variations are depicted in Figure 6.36-6.38, respectively. As shown in Figure

6.36, the frequency oscillations are quickly damped out to reach zero steady state error. It should be noted that the normal DC link is contributing just in damping of oscillations without especial improvements in first overshoot. But after implementing the VSP concept, a simultaneous inertia emulation could be possible and huge improvements in the first overshoot with a damping are accessible.

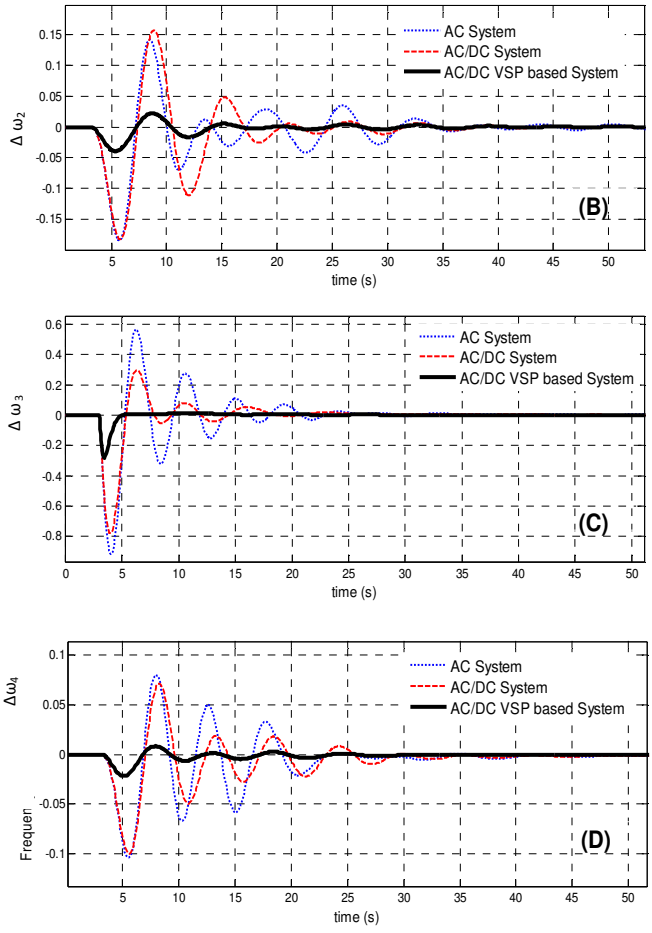

Figure. 6.36. Frequency deviations of different areas (radian/sec). (A) Area1, (B) Area2, (C) Area3, (D) Area4.

The damping factor and virtual inertia are very important terms for tuning the VSP based HVDC system. From the presented figures, it can be observed that the peak values of oscillation in Area3 are higher than other areas. This is due to the fact that, load change is happening in Area3. The dynamic response of the generated power for different GENCOs are also depicted in Figure 6.37. Based on the presented results in Figure 6.37, it is clear that the steady state output of the GENCO3 will be equal to the load variation in the same area (0.1 p.u.).

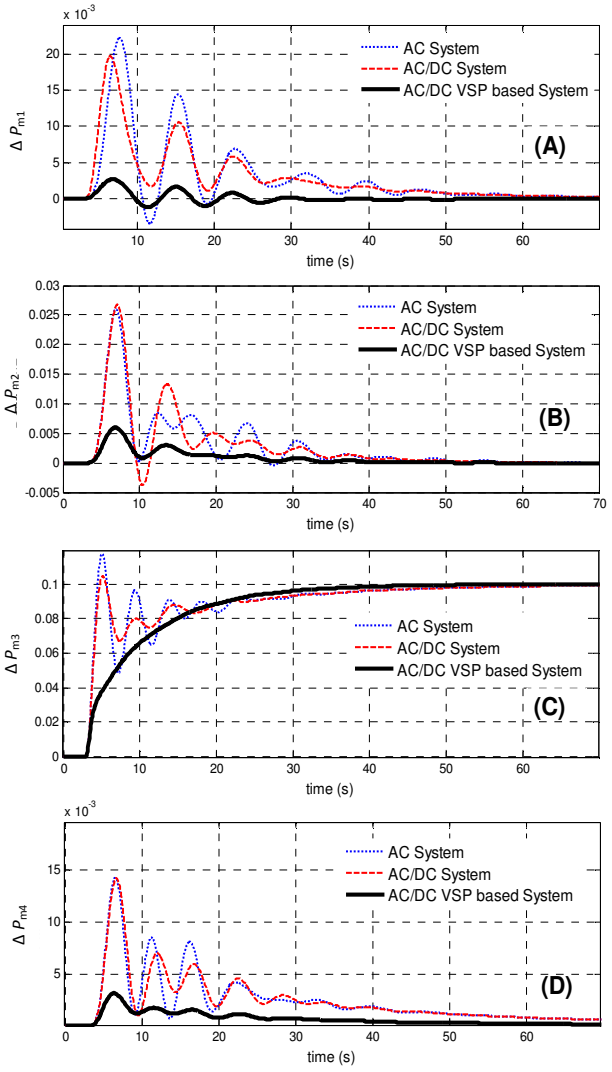

Figure 6.37. Generated power deviation of all generation units (p.u); (A) GENCO1, (B) GENCO2, (C) GENCO3 and (D) GENCO4.

The AC tie-line power flow response is depicted in Figure 6.38. These figures show the superior performance of the proposed LFC scheme with a VSP based HVDC system compared to the conventional AC/DC model.

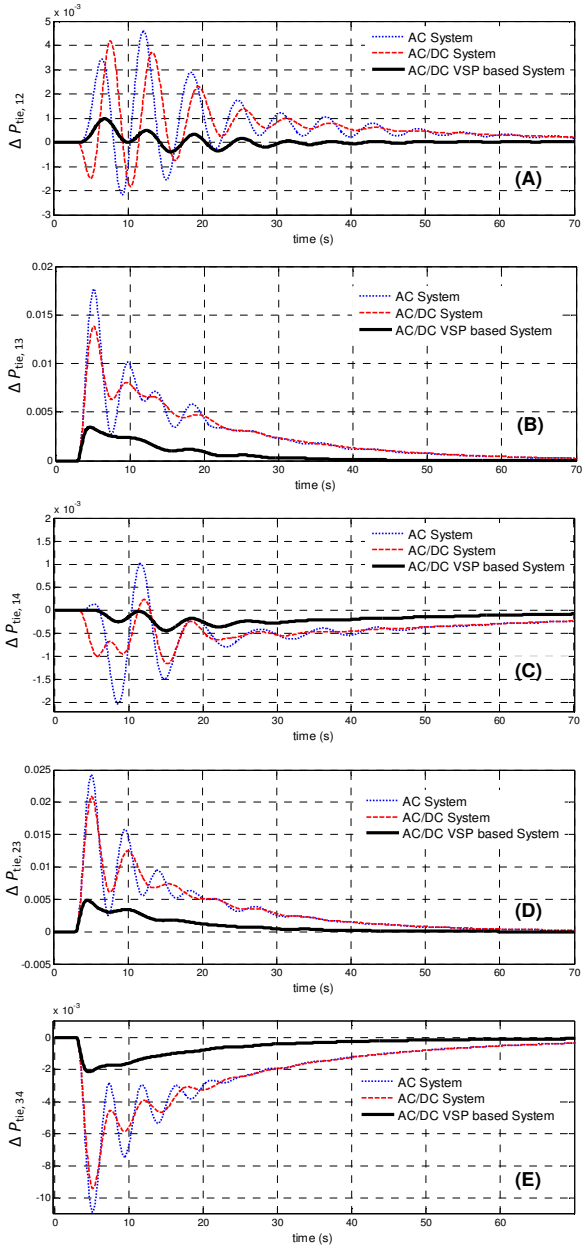

Figure 6.38. Deviation of AC tie-line power for different lines (p.u).

From these figures, it is obvious that significant dynamic improvements are achieved during step load variation. The oscillation of tie-line power is also quickly damped because of the contribution of DC link. The fast controllable HVDC links helped to transfer sufficient emergency power to the disturbed Area 3 with a satisfactory dynamic performance. As a result, better dynamics with more reliability on AC line power transfer capability can be achieved.

The dynamic behaviors of generated power by VSP based HVDC stations ($X_{p-VSP,13}$ and $X_{p-VSP,31}$) are also depicted in Figure 6.39. Based the obtained result, for this case study, the maximum peak of variation is related to the VSP31 close to Area 3 (the area with the step load) which is less 6% of the rated power. These values can identify the ratings of converter stations in DC link. The energy trace is also depicted by Figure 6.40 in p.u. The required energy for VSP13 is 0.026 p.u. and the energy for VSP31 is equal to 0.57 p.u.

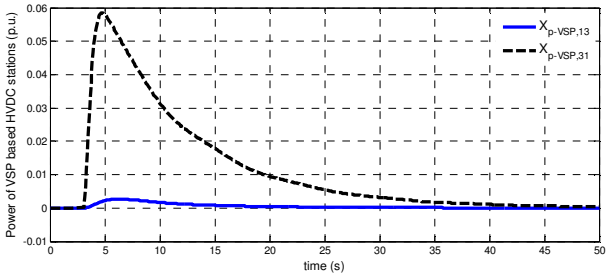

Figure 6.39. Power variations of VSP stations (p.u).

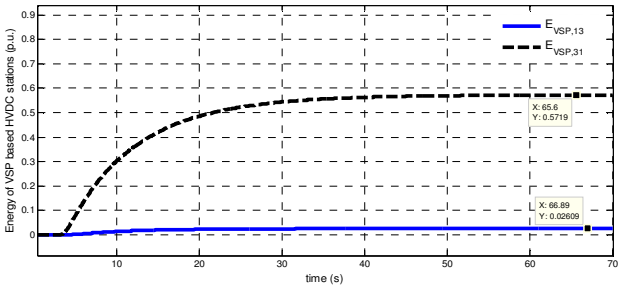

Figure 6.40. Required energy by VSP based HVDC stations (p.u).

CHAPTER 7.

Conclusions

The concept of virtual inertia and the associated methods for emulating it are extremely important for modern power systems. As it has been shown throughout this dissertation, the electrical power system is facing a great challenge due to the high penetration of generation systems based on renewable energy sources with low inertia. Therefore, it is necessary to devote more research effort at different levels, in order to make this compatible with the evolution of the future electrical network. In this framework, the research conducted in this Ph.D. work has intended to contribute on improving the control of HVDC interconnected networks in terms of AGC and frequency control.

Since the role of AGC is very important in the future modern power systems, it is necessary to perform proper adaptions and modifications to take into account new scenarios like a liberalized market, the high penetration of renewable generation or the inertia emulation by means of using power converter devices. In this thesis, different approaches for implementing the virtual inertia in multi-area AC/DC interconnected AGC system have been proposed and analyzed. The main conclusions and possible future work are explained in this Chapter.

7.1 Introduction

As it was explained, due to increasing level of power converter based component and high penetration of renewable resources, the structure of conventional power system is changing. The lack of sufficient inertia is the main limitation of the grid connected

renewable electrical energy systems, which can give rise to negative effects on power system operation. In such complex scenario, with the lack of inertia, controlling the power exchange through tie-lines of multi-area interconnected systems makes the frequency regulation more complex, with several stability problems. It is obvious that there is a research gap in the transition from conventional to modern structure of power systems and more detailed analysis considering these new terms, like virtual inertia emulation, is necessary. Based on these concerns, this research work tried to take into account some of the important concerns and main questions in term of multi-area AC/DC interconnected AGC systems.

- *Modelling of complex interconnected systems and frequency control*

AGC of interconnected systems are experiencing different challenges and it is obvious that the matter of modelling and control, considering the methods of providing virtual inertia to the system, is a critical issue and the role of advanced technologies such as the use of modern power processing systems, energy storage, and advanced converters in HVDC links will be essential. Considering these new challenges, one of the main concerns is related to modeling and control of such complex interconnected system in terms of frequency and active power control stability. Therefore, the main question would be: “What would happen to the frequency regulation and the AGC requirements if a significant amount of power electronics based DC parts is joined to the current generation portfolio?” It is very important to explore a model which is very useful for pre-evaluation and analysis for dynamic effects of converter stations in high level control design in power systems applications. In a modern power system, it would be valuable to have a clear idea about the required energy through the transmission line, with proper dynamic analysis, considering worst case studies.

- *HVDC links and coordination*

The need for transmitting power over long distances with low losses and high stability has been always the main challenge for transmission technologies. Because of several limitations associated with AC lines, especially for long distance connections, and in parallel recent developments of renewable energy integration and super-grid interconnections, a lot of attention has been attracted to HVDC (High Voltage Direct Current) transmission. HVDC links are recognized as a proven tool for dealing with new challenges of the future power system. The HVDC interconnection is one of the main applications of power converters in multi-area interconnected power systems, which could bring beneficial advantages, like fast and bidirectional controllability, Power Oscillation Damping (POD) and frequency stability support. In modern power systems

however, the main focus is not just having long distance HVDC links for interconnecting the system. The main challenge and concern is related to coordination of this DC part to the rest of AC system, especially when a new DC line is installed in parallel with other previous AC lines. In this sense, the design of proper high-level control methods to achieve the maximum benefit from these equipment is vital.

- *Different techniques for providing virtual inertia*

Usually, conventional generators can provide inertia and governor responses against frequency deviations. As it was explained in previous Chapters, several classical and advanced control techniques have been implemented to solve Load Frequency Control (LFC) problem. But in order to cope with the matter of inertia, research for exploring different ways/techniques of providing virtual inertia by power converters is crucial to improve the response of the overall system. Therefore, one important concern will be related to the method of implementing such inertia into multi-area interconnected system. This virtual inertia is emulated by advanced control techniques for power converters equipped with some short-term energy storage system, which make possible to have a huge amount of power converter based stations without comprising the system stability. Therefore, in order to emulate virtual inertia, an energy source is required. Such energy can be supported from neighboring areas of the interconnected system or from an installed storage capacity.

7.2 Main conclusions and thesis achievements

The work presented in this Ph.D. dissertation addresses the control and analysis of HVDC interconnected systems in terms of frequency and active power control with capabilities for emulating inertia.

The starting point of this Ph.D. dissertation was to analyze and to control a multi-area interconnected system with parallel AC/DC lines with a proper high-level AGC operation and coordination of the overall system. Since the amount of power generation systems whose connection is based on power electronics has increased exponentially in large-scale interconnected power systems, it is necessary to develop proper models of their power converters to perform appropriate analyses and design controllers. Therefore, as it was explained in Chapter 3, different models of voltage source converters for grid applications have been developed. As demonstrated in this work, each of these models could be used for different applications. The simplified model is useful for a large-scale multi buses simulation to reduce the simulation time. The small signal model is useful for AGC analyses and frequency stability studies.

As it was mentioned, the objective of this Ph.D. work was not just to add a DC link for long distant power transfer into the system. The main objective was the coordination and proper high-level control of the AC/DC interconnections to obtain the maximum benefits from such element, which means that the HVDC link had be controlled in a proper and coordinated manner. Therefore, the concept of AGC is used and implemented at high-level control of the AC/DC coordinated system. In this way, a complete explanation about fundamental of frequency control and AGC for an interconnected system was presented in Chapter 4. For achieving a generalized model and coordinated approach, a complete mathematical model of multi-area AGC system, with the AC and DC interconnections, was obtained and presented. The concept of SPMC was introduced and implemented at the DC links of interconnected AGC systems. This enabled the investigation of the dynamic effects of HVDC links in the system considering active power and frequency control issues. After implementing this AC/DC model for the AGC, it was easy to understand and observe the real effects of the HVDC link on shifting the eigenvalues of the system for better damping of oscillatory modes. From this knowledge, it was possible to go in further details considering different approaches of inertia emulation for improving dynamics. This allowed to improve the response of the system by damping of oscillations, but without considerable improvement in first overshoot of the system. This issue is very important, especially considering a situation with high uncertainty, which might bring a critical situation that would compromise the system stability. For overcome such a critical situation, it is very important to provide inertia to the system, especially during the primary frequency control and first overshoot responses.

Therefore, from the first control approach, a new model for AGC interconnected systems with the capability of virtual inertia emulation was proposed. This approach is based on derivative control, where the derivation of the grid frequency is used to provide virtual inertia to the system. In addition to incorporating the coordinated model of DC link in AGC model, this method was one of the first contributions of this Ph.D. work. Detailed explanations of the proposed idea for inertia emulation in AGC interconnected systems were presented in Chapter 5. For better understanding and deep insight into different effects of control gains of virtual inertia controller considering the required energy, a complete eigenvalue and sensitivity analysis were performed.

Once the derivative control model was developed and analyzed, the effects of the PLL and frequency measurements were taking into account in the implementation of the derivative control method. Since inertia emulation based on the derivative control method relies heavily on frequency measurements, it was considered necessary to get in

depth in the analysis of the effects of dynamic response of the PLL on the system performance. This study gave rise to another contribution by proposing a complete model of the interconnected AGC system considering PLL and virtual inertia emulation effects.

Based on the studies conducted in this Ph.D. work, it can be concluded that the use of derivative control for emulating inertia in AC/DC interconnections can help the system during severe contingencies. In this sense, it was proven through analyses and simulations that proposed approach improves significantly the stability of the system. At the same time, it was possible to show that PLL brings several limitations on the system performance that can deteriorate its response until reaching unacceptable levels. This made necessary to find a proper solution to cope with this limitation.

A novel solution based on virtual synchronous power strategy was proposed to overcome limitations of frequency measurement in the previous approach. In Chapter 6, a general approach for implementing the virtual synchronous power strategy in HVDC links (VSP based HVDC system) of multi-area interconnected AGC systems is proposed. The concept of VSP stemmed from the synchronous power control (SPC) method, which proposes a new way for controlling power converters to behave as a synchronous generator, with the ability of emulating synchronous inertia, but without the drawbacks of conventional generators. In this method, the electromechanical control loop for virtual synchronous power concept is presented as a second-order function that describes the relationship between input and output power of the power converter. The characteristic equation of the VSP is added to the AGC interconnected model, which leaded to a generalized AC/DC interconnected model of an AGC system with the capability of emulating virtual inertia. This new approach for AGC operation in interconnected power systems was presented in detail in this Ph.D. dissertation. Likewise, a detailed analysis in terms of parameter sensitivities and eigenvalues shows the dynamic effects of the different parameters of the VSP-based controller on the system performance. Based on these analyses, it was possible to define the proper ranges of control parameters for maximizing the system response improvement.

From the results obtained in simulation, it can be concluded that the VSP-based control approach significantly improves the stability of the system. The importance of proposed approach for inertia emulation is more relevant on the presence of severe load variations, especially when the variation of frequency or tie line power become higher than allowable values. This situation would be even worse in a system with high penetration of renewable generation, which suffers from the lack of inertia. During such disturbances, if the system does not have enough inertia, the multi-area interconnected

power grid would definitely go to instability. In such situation, the VSP-based AC/DC system can help the system during sever contingencies.

The study conducted in this Ph.D. dissertation demonstrated that the virtual inertia provided by the VSP-based control method adds an additional degree of freedom to the system dynamics, since it permits to reduce the overshoot in the transients in addition to damping characteristics of the HVDC links. By comparing the results of the derivative control method and the VSP-based method regarding inertia emulation, it was possible to prove that the VSP technique provides a better performance for emulating the inertia, which is due in great extent to the fact that the VSP technique doesn't need PLL for frequency estimation.

The implementation of virtual inertia emulation in a power converter indeed implies the need of having some power reserve capacity, which can be based on stored energy or fast control of some primary reserves in the neighboring areas. The way in which such inertia is implemented, permits the VSP-based HVDC transmission to participate naturally in the grid frequency regulation.

This Ph.D. dissertation has introduced some relevant aspects regarding the inertia emulation concept in AGC structure of multi area interconnected systems. However, a lot of research and development is still required in this field to reach a widespread solution considering different aspects of power systems. Some of the ideas not discussed in this Ph.D. dissertation but deserved to be explored in future works are described in the next Section.

7.3 Future works

The topic of AGC and frequency control in large-scale power systems is a very interesting and challenging area, especially considering new concepts and ideas coming from the exploitation of power electronics. At this time, the control and operation of the power grid in all of its aspects, including the AGC and frequency regulation are experiencing essential changes. These changes are mainly due to deregulation, expansion of new functionalities, high penetration of renewable sources and the developments of new kinds of technologies for power generation and consumption. Therefore, the infrastructure of the future modern grid should efficiently provide the possibilities of supporting different types of ancillary services, like AGC system and frequency control from different sources of energy.

Based on the work presented in this Ph.D. dissertation, some relevant fields for further research could be identified as follows:

- *Extension of the current control approaches to more complex interconnected models*

The control approaches presented in this Ph.D. dissertation are prone to be extended to perform dynamic frequency response analysis from different point of views in the system. In this sense, it would be interesting to define the system model bigger and more complex, considering several DC links, with modified AGC models, and high penetration of different renewable energy sources. Detailed dynamic analyses for AGC studies, with a combination of power electronics based components, would be one of the key topic to give a much better understanding about the dynamic effects of the virtual inertia in the large-scale power systems. In this way, it would be also interesting to analyze the model with virtual inertia in more complex benchmarks with more areas.

- *Applying advanced controller/regulators*

Designing an advanced regulator/controller in a scheme of hierarchical control for the presented approaches of inertia emulation in this Ph.D. dissertation is another field of research for obtaining a better performance considering overall system states. In this way, better coordination between different components could be achieved, especially with mixing centralized and decentralized approaches in the system.

This type of control is also advantageous in terms of better coordination. Coordination with advanced regulators would be very important. Since the time response of the power electronics based component is very fast, any contingencies will be responded by power electronics before mechanical parts of conventional generation units. But, maybe in real practice, the fast power exchange of power electronics could be slow down to some extent, for reaching more optimum states in the overall system. This issue could be possible with better coordination between distributed generations and conventional units in the AGC system.

- *Application of intelligent based techniques*

Another interesting aspect that could be taken into account is the application of intelligent based technologies for online training and tuning of the proposed controller in multi-area interconnected systems. In response to the previously mentioned challenges, intelligent control certainly plays a significant role. It will not be possible to integrate large amounts of renewable resources or distributed generation based virtual inertia into the conventional power systems without intelligent control and advanced regulation systems.

- *Investigate different methods for virtual inertia emulation*

Considering rapid advancement in power electronics based technologies, much more technologies with different power processors for emulating inertia are predictable. Therefore, it is also interesting to extend investigation in this field.

It should be noted that, a better understanding of reliability considerations through effective integration techniques is also vital to identify a variety of ways that bulk power systems can accommodate the large-scale integration of power electronics based components. Additional flexibility will be required from various dispatchable generators, storage, and demand resources, so the system operator can continue to balance supply and demand on the modern bulk power system.

- *Improvement of computing techniques and measurement technologies*

Another field for further research is related to intelligent meters, devices, and communication standards. These technologies should be properly designed and implemented to enable flexible matching of generation and load. Furthermore, an appropriate framework must be developed to ensure that future flexible supply/demand and ancillary services have equal access and are free to the market.

The AGC system of tomorrow must be able to handle complex interactions between control areas, grid interconnections and distributed generating equipment. These efforts are directed at developing computing techniques, intelligent control, and monitoring/measurement technologies to achieve optimal performance. Advanced computational methods are opening up new ways of controlling the power system via supervisory control and data acquisition (SCADA)/AGC centers. Therefore, extensive research could be done in these fields to reach a suitable platform for implementing adaptive/intelligent strategies in the modern power system.

REFERENCES

[1.1] S. Koohi-Kamali, V.V. Tyagi, N.A. Rahim, N.L. Panwar, H. Mokhlis, "Emergence of energy storage technologies as the solution for reliable operation of smart power systems: A review," *Renewable and Sustainable Energy Reviews*, vol. 25, pp. 135-165, Sept. 2013.

[1.2] H. Bevrani, *Robust Power System Frequency Control*, 2th ed., Springer, 2014.

[1.3] Shashi Kant Pandey, Soumya R. Mohanty, Nand Kishor, "A literature survey on load–frequency control for conventional and distribution generation power systems," *Renewable and Sustainable Energy Reviews*, vol. 25, pp. 318–334, 2013.

[1.4] V. Donde, A. Pai, I.A. Hiskens, "Simulation and optimization in an AGC system after deregulation," *IEEE Trans Power Syst*. vol. 16, no. 3, pp. 481–9, 2001.

[1.5] M. H.Variani, and K. Tomsovic, "Distributed Automatic Generation Control Using Flatness-Based Approach for High Penetration of Wind Generation," *IEEE Trans. on Power Systems*, vol. 28, no. 3, 2013.

[1.6] Bevrani, H., Daneshmand, P.R., Babahajyani, P., Mitani, Y., Hiyama, T., Intelligent LFC concerning high penetration of wind power: Synthesis and real-time application, *IEEE Transactions on Sustainable Energy*, 5 (2), 6687253, pp. 655-662, 2014.

[1.7] Bevrani, H.; Ghosh, A.; Ledwich, G.,Renewable energy sources and frequency regulation: survey and new perspectives, IET Renewable Power Generation, Vol. 4, Issue: 5, pp. 438 - 457, 2010.

[1.8] Wang, Y., Delille, G., Bayem, H., Guillaud, X., Francois, B., "High wind power penetration in isolated power systems-assessment of wind inertial and primary

frequency responses", *IEEE Transactions on Power Systems*, 28 (3), 6449333, pp. 2412-2420, 2013..

[1.9] Balamurugan, S., Lekshmi, R.R., "Control strategy development for multi-source multi area restructured system based on GENCO and TRANSCO reserve", International Journal of Electrical Power and Energy Systems, 75, pp. 320-327, 2016.

[1.10] Chandra Sekhar, G.T., Sahu, R.K., Baliarsingh, A.K., Panda, S., Load frequency control of power system under deregulated environment using optimal firefly algorithm, *International Journal of Electrical Power and Energy Systems*, 2016.

[1.11] Arya, Y., Kumar, N., AGC of a multi-area multi-source hydrothermal power system interconnected via AC/DC parallel links under deregulated environment, *International Journal of Electrical Power and Energy Systems*, 75, pp. 127-138, 2016.

[1.12] Khederzadeh, M., Maleki, H., Asgharian, V., Frequency control improvement of two adjacent microgrids in autonomous mode using back to back Voltage-Sourced Converters, *International Journal of Electrical Power and Energy Systems*, 2016.

[1.13] Mc Namara, P., Negenborn, R.R., De Schutter, B., Lightbody, G., McLoone, S., Distributed MPC for frequency regulation in multi-terminal HVDC grids, *Control Engineering Practice*, 46, pp. 176-187, 2016.

[1.14] Hu, J., Cao, J., Guerrero, J. M., Yong, T., Yu, J.,Improving Frequency Stability Based on Distributed Control of Multiple Load Aggregators*, IEEE Transactions on Smart Grid*, 2015.

[1.15] Donde, V., Feng, X., Segerqvist, I., Callavik, M., "Distributed State Estimation of Hybrid AC/HVDC Grids by Network Decomposition", *IEEE Transactions on Smart Grid*, 2015.

[1.16] Ramesh Kumar, S., Ganapathy, S., "Artificial cooperative search algorithm based load frequency control of interconnected power systems with AC-DC tie-lines", *International Journal of Engineering and Technology*, 2014.

[1.17] Donde, V., Feng, X., Segerqvist, I., Callavik, M., "Distributed state estimation of hybrid AC/HVDC grids by network decomposition", IEEE Power and Energy Society General Meeting, 2014.

[2.1] K.H. Solangib, M.R. Islamb, R. Saidura,b, N.A. Rahimb, H. Fayazb, "A review on global solar energy policy," *Renewable and Sustainable Energy Reviews*, vol. 15, pp. 2149–2163, 2011.

[2.2] M. Thirugnanasambandam, S. Iniyan, and R. Goic, "A review of solar thermal technologies," *Renewable and Sustainable Energy Reviews*, vol. 14, pp. 312–322, 2010.

[2.3] Loi lei lai, *Power system restructuring and deregulation, trading, performance* and information technology, John Wiley & Sons, Ltd, UK, 2002.

[2.4] Sadeh, J.; Rakhshani, E., Multi-area load frequency control in a deregulated power system using optimal output feedback method, *International Conference on European Electricity Market, EEM*, 2008.

[2.5] E. Rakhshani and J. Sadeh, "Reduced-Order Observer Control for Two-Area LFC System after Deregulation," Control and Intelligence Systems, vol. 38, no. 4, 2010.

[2.6] E. A. Abdelaziz, R. Saidur, and S. Mekhilef, "A review on energy saving strategies in industrial sector," *Renewable and Sustainable Energy Reviews*, vol. 15, no. 1, pp. 150-168, 2011.

[2.7] W. Hoffmann, "PV solar electricity industry: market growth and perspective," *Solar Energy Materials*, vol. 90, no. 18–19, 23 November. 2006.

[2.8] M. Wittmann, H. Breitkreuz, M. Schroedter-Homscheidt, M. Eck, "Case studies on the use of solar irradiance forecast for optimized operation strategies of solar thermal power plants," *IEEE Journal of Selected Topics in Applied Earth Observations and Remote Sensing*, vol. 1, no. 1, pp. 1939-1404, 2008.

[2.9] IPEA reports, *Global market outlook for photovoltaics until 2015*, European photovoltaic industry association.

[2.10] P. Kundur, *Power System Stability and Control*. McGraw-Hill, 1994.

[2.11] L. Freris and D. Infield, *Renewable Energy in Power Systems*, Wiley, 2008.

[2.12] A.S. Chuang, C. Schwaegerl, "Ancillary services for renewable integration," CIGRE/IEEE PES Joint Symposium on *Integration of Wide-Scale Renewable Resources Into the Power Delivery System*, 2009.

[2.13] UCTE, *UCTE Operation Handbook*, v 2.5E, July 2004.

[2.14] Yann Rebours, Daniel Kischen, *What is spinning reserve?,* University of Manchester publications, 2005.

[2.15] Y. G. Rebours, D. S. Kirschen, M. Trotignon, and S. Rossignol, "Survey of Frequency and Voltage Control Ancillary Services—Part I: Technical Features," IEEE Transaction on Power System, vol. 22, no. 1, 2007.

[2.16] Machowski, J., Bialek, J.W., Bumby, J.R., Power Systems Dynamics Stability and Control., John Wiley & Sons, Ltd., 2008..

[2.17] S. Corsi, P. Marannino, N. Losignore, G. Moreschini, and G. Piccini, "Coordination between the reactive power scheduling function and the hierarchical voltage control of the EHV ENEL system," *IEEE Trans. Power Syst*., vol. 10, no. 2, pp. 686–694, 1995.

[2.18] H. Vu, P. Pruvot, C. Launay, and Y. Harmand, "An improved voltage control on large-scale power system," *IEEE Trans. Power Syst*., vol. 11, no. 3, pp. 1295–1303, 1996.

[2.19] G. N. Taranto, N. Martins, D. M. Falcao, A. C. B. Martins, and M. G. dos Santos, "Benefits of applying secondary voltage control schemes to the Brazilian system," *Power Engineering Society Summer Meeting*, vol. 2, pp. 937 - 942, 2000.

[2.20] S. Corsi P. Marannino N. Losignore G. Moreschini and G. Piccini, "Coordination between the reactive power scheduling functioned the hierarchical voltage control of the EHV ENEL system," *IEEE Transactions on Power Systems*, vol. 10, no. 2, 1995.

[2.21] D. Povh, "Use of HVDC and FACTS," *Proceedings of the IEEE*, vol. 88, no. 2, pp. 235-245, 2000.

[2.22] Y. hulpin, and D. Ernst, Ancillary services and operation of multi-terminal HVDC grids, *International Workshop on Transmission Networks for Offshore Wind Power Plants*, pp. 1-6, Aarhus, Denmark, Oct 2011,

[2.23] R. Da Silva, R. Teodorescu, P. Rodriguez, "Power delivery in multi-terminal VSC-HVDC transmission system for offshore wind power applications," *IEEE PES Innovative Smart Grid Technologies Conference* (ISGT Europe), pp. 1-8, 2010.

[2.24] S. V. Papaefthymiou, E.G. Karamanou, S.A. Papathanassiou, M.P. Papadopoulos, "A Wind-Hydro-Pumped Storage Station Leading to High RES

Penetration in the Autonomous Island System of Ikaria," *IEEE Transactions on Sustainable Energy*, vol. 1 , Issue 3, pp. 163-172, 2010.

[2.25] J. Taylor, and A. Halnes, "Analysis Of compressed air energy storage," *PCIC Europe*, pp. 1 – 5, 2010.

[2.26] R. Bhatt, B. Chowdhury, "Grid frequency and voltage support using PV systems with energy storage," *North American Power Symposium* (NAPS), pp. 1 – 6, 2011.

[2.27] Y. Mitani, K. Tsuji, Y. Murakami, "Application of superconducting magnet energy storage to improve power system dynamic performance," *IEEE Transactions on Power Systems*, vol. 3 , no. 4, pp. 1418 - 1425, 1988.

[2.28] M.P.N.Van Wesenbeeck, S.W.H. de Haan, P. Varela, and K. Visscher, "Grid tied converter with virtual kinetic storage," *IEEE Bucharest PowerTech Conference*, pp. 1 - 7, 2009.

[2.29] K. Visscher, and S.W.H. De Haan, "Virtual synchronous machines (VSG's) for frequency stabilization in future grids with a significant share of decentralized generation," *CIRED Seminar on Smart Grids for Distribution*, IET-CIRED, pp. 1-4, 2008.

[2.30] K. Sakimoto, Y. Miura, T. Ise, "Stabilization of a power system with a distributed generator by a Virtual Synchronous Generator function," International Conference on Power Electronics and ECCE Asia (ICPE & ECCE), pp. 1498 - 1505, 2011.

[2.31] Lobato Miguélez, E., Egido Cortés, I., Rouco Rodríguez, L., López Camino, G., An overview of ancillary services in Spain, Electric Power Systems Research, 78 (3), pp. 515-523, 2008.

.[2.32] Daqiang Bi, Sigeng Wang, Baoming Ge, Xinyu Yang, "Control strategy of grid-connected photovoltaic system with energy storage," International Conference on Electrical *Machines and Systems* (ICEMS), pp. 1-4, 2011.

[2.33] G. Delille, B. Francois, G. Malarange, "Dynamic frequency control support: A virtual inertia provided by distributed energy storage to isolated power systems," *IEEE PES Innovative Smart Grid Technologies Conference Europe* (ISGT Europe), pp. 1-8, 2010.

[2.34] Du Yan; Su Jianhui, and Shi Yong, "A unified power controller for photovoltaic generators in microgrid," *International Conference on Electric Utility Deregulation and Restructuring and Power Technologies* (DRPT), pp. 1121-1125, 2011.

[2.35] J.A. Pec¸as Lopes, N. Hatziargyriou, J. Mutale , P. Djapic, N. Jenkins, "Integrating distributed generation into electric power systems: A review of drivers, challenges and opportunities," *Electric Power Systems Research*, vol.77, pp. 1189-1203, 2007.

[2.36] An agreement report of Brookings and Hoover Institutions: Assessing the Role of Distributed Power Systems in the *U.S. Power Sector*, Oct. 2011, available online:http://www.recycledenergy.com/images/uploads/Brookings_Hoover_DPS_study.pdf

[2.37] Pukar Mahat, Zhe Chen, and Birgitte Bak-Jensen, "Review on Islanding Operation of Distribution System with Distributed Generation," *IEEE, Power and Energy Society General Meeting*, 2011.

[2.38] Changhee Cho, Jin-Hong Jeon, Jong-Yul Kim, Soonman Kwon, Kyongyop Park, and Sungshin Kim, "Active Synchronizing Control of a Microgrid," *IEEE Transaction on Power Electroni*cs, vol. 26, no. 12, 2011.

[2.39] Wei Li, Joos, G., Belanger, J., "Real-Time Simulation of a Wind Turbine Generator Coupled With a Battery Super-capacitor Energy Storage System," *IEEE Transactions on Industrial Electronics*, vol. 57, no. 4, pp. 1137-1145, 2010.

[2.40] Du, W., Wang, H.F., Cao, J., Xiao, L.Y., "Robustness of an energy storage system-based stabilizer to suppress inter-area oscillations in a multi-machine power system," *IET Generation, Transmission & Distribution,* vol. 6, no. 4, pp. 339-351, 2012.

[2.41] Dabbagh, S. R., Sheikh-El-Eslami, M. K., Risk Assessment of Virtual Power Plants Offering in Energy and Reserve Markets, *IEEE Transactions on Power Systems*, 2015.

[2.42] A. Arabali, M. Ghofrani, M. Etezadi-Amoli, M.S. Fadali, and Y. Baghzouz, "Genetic-Algorithm-Based Optimization Approach for Energy Management," *IEEE Transactions on Power Delivery*, vol. 28, no. 1, pp. 162-170, 2013.

[2.43] E. Rakhshani, A. Luna, J. Sadeh, P. Rodriguez, "PSO based optimal output feedback controller for two-area LFC system," *20th Mediterranean Conference on Control & Automation* (MED), pp. 1284-1289, 2012.

[2.44] E. Rakhshani and J. Sadeh, "Intelligent Linear-Quadratic Optimal Output Feedback Regulator for a Deregulated Automatic Generation Control System," *Electric Power Components and Systems*, vol. 40, pp. 513-533, 2012.

[2.45] Haihua Zhou, Tanmoy Bhattacharya, Duong Tran, Tuck Sing Terence, and Ashwin M. Khambadkone, "Composite Energy Storage System Involving

Battery and Ultracapacitor With Dynamic Energy Management in Microgrid Applications," *IEEE Transaction on Power Electronics*, vol. 26, no. 3, 2011.

[2.46] Changsong Chen, Shanxu Duan, Tao Cai, Bangyin Liu, and Guozhen Hu, "Optimal Allocation and Economic Analysis of Energy Storage System in Microgrids," *IEEE Transaction on Power Electronics*, vol. 26, no. 10, 2011.

[2.47] Kai Zou, Ashish Prakash Agalgaonkar, Kashem M. Muttaqi, and Sarath Perera, "Distribution System Planning With Incorporating DG Reactive Capability and System Uncertainties," *IEEE Transaction on Sustainable Energy*, vol. 3, no. 1, Jan. 2012.

[2.48] Robert F. Arritt, and Roger C. Dugan, "Distribution System Analysis and the Future Smart Grid," *IEEE Transaction on industry Applications*, vol. 47, no. 6, 2011.

[2.49] S. Conti, R. Nicolosi, and S. A. Rizzo, "Generalized Systematic Approach to Assess Distribution System Reliability With Renewable Distributed Generators and Microgrids," *IEEE Transaction on Power Delivery*, vol. 27, no. 1, Jan. 2012.

[2.50] Juan A. Martinez, Jean Mahseredjian, "Load Flow Calculations in Distribution Systems with Distributed Resources. A Review," *IEEE Power and Energy Society General Meeting,* 2011.

[2.51] EU-DEEP project, glossaries, online: http://www.eudeep.com/index.php?id=653

[2.52] M. Crappe, L. Gertmar, A. Haböck, W. Leonard and D. Povh, "Power Electronics and Control by Microelectronics in Future Energy Systems," *EPE Journal*, vol. 10, no. 1, pp. 6-10, 40-46, Apr. 2000.

[2.53] C.D. Xu, K.W.E. Cheng, "A survey of distributed power system — AC versus DC distributed power system," 4th *International Conference on Power Electronics Systems and Applications* (PESA), 2011.

[2.54] Marie-Cécile Alvarez-Hérault, Damien Picault, Raphael Caire, Bertrand Raison, Nouredine HadjSaid, and Wojciech Bienia, "A Novel Hybrid Network Architecture to Increase DG Insertion in Electrical Distribution Systems," *IEEE Transaction on Power system*, vol. 26, no. 2, May 2011.

[2.55] K. Purchala, R. Belmans, L. Exarchakos, A.D. Hawkes, "Distributed generation and the grid integration issues, Eususte1 Publication and results," online: http://www.eususte1.be/public/documents_publ/WP/WP3/WP%203.4.1%20Distributed%20generation%20and%20grid%20integration%20issues.pdf

[2.56] Flourentzou, N.; Agelidis, V.G.; Demetriades, G.D., "VSC-Based HVDC Power Transmission Systems: An Overview," *IEEE Transactions on Power Electronics*, vol. 24, no. 3, pp. 592-602, 2009.

[2.57] Nguyen-Mau, C.; Rudion, K.; Styczynski, Z.A., "HVDC application for enhancing power system stability," *International Conference on Science and Technology*, pp. 1-6, 2011.

[2.58] Risheng Li; Bozhko, S.; Asher, G., "Frequency Control Design for Offshore Wind Farm Grid With LCC-HVDC Link Connection," *IEEE Transactions on Power Electronics*, vol. 23, no. 3, pp. 1085-1092, 2008.

[2.59] Hagiwara, M.; Fujita, H.;and Akagi, H., "Performance of a self-commutated BTB HVDC link system under a single-line-to-ground fault condition," IEEE Transactions on Power Electronics, vol. 18, no. 1, Part: 1, pp. 278-285, 2003.

[2.60] Hagiwara, M.; Fujita, H.; Akagi, H., Performance of a self-commutated BTB HVDC link system under a single-line-to-ground fault condition, IEEE Transactions on Power Electronics, Vol. 18, Issue: 1, pp. 278-285, 2003, 2003.

[2.61] M. P. Bahrman, "HVDC transmission overview," IEEE Transmission and Distribution *Conference and Exposition*, 2008. T&D. IEEE/PES, pp. 1-7, 2008.

[2.62] K. R. Padiyar, *HVDC Power Transmission Systems.* John Wiley & Sons, 1990.

[2.63] A. Lesnicar, R. Marquardt, "An innovative modular multilevel converter topology suitable for a wide power range," *IEEE Power Tech Conference*, Bologna, Italy, 2003.

[2.64] J. Rodriguez, J.-S. Lai, F. Z. Peng, "Multilevel inverters: A survey of topologies, controls, and applications," *IEEE Trans. Ind. Electron*., vol. 49, no. 4, pp. 724–738, Aug. 2002.

[2.65] Lennart Harnefors, Antonios Antonopoulos, Staffan Norrga, Lennart Angquist, and Hans-Peter Nee, "Dynamic Analysis of Modular Multilevel Converters," *IEEE Transactions on Industrial Electronics*, 2012.

[2.66] Hui Peng; Hagiwara, M.; Akagi, H., "Modeling and Analysis of Switching-Ripple Voltage on the DC Link Between a Diode Rectifier and a Modular Multilevel Cascade Inverter (MMCI)," *IEEE Transactions on Power* Electronics, vol. 28, no. 1, pp. 75-84, 2013.

[2.67] Teodorescu, Beres, R.; Wang, X.; Blaabjerg, F.; Liserre, M.; Bak, C., A Review of Passive Power Filters for Three-Phase Grid Connected Voltage-Source Converters, *IEEE Journal of Emerging and Selected Topics in Power Electronics*, 2015.

[2.68] A. Yazdani, R. Iravani, "*Voltage-sourced Converters in Power Systems: Modeling Control, and Applications,"* John Wiley & Sons, Inc. Hoboken (New Jersey), 2010.

[2.69] J. Xu, C. Zhao, W. Liu, C. Guo, "Accelerated Model of Modular Multilevel Converters in PSCAD/EMTDC," *IEEE Transactions on Power Delivery*, vol. 28, no. 1, pp. 129 - 136, 2013.

[2.70] E. Solas, G. Abad, J. Barrena, S. Aurtenechea, A. Carcar, L. Zajac, "Modular Multilevel Converter with different Submodule Concepts – Part I: Capacitor Voltage Balancing Method," *IEEE Transactions on Industrial Electronics*, 2012.

[2.71] Lanhua Zhang; Guangzhu Wang, "Voltage balancing control of a novel modular multilevel converter," *International Conference on Electric Utility Deregulation and Restructuring and Power Technologies* (DRPT), pp. 109-114, 2011.

[2.72] G. Bergna, E. Berne, P. Egrot, P. Lefranc, A. Amir, J. Vannier, M. Molinas, "An Energy-based Controller for HVDC Modular Multilevel Converter in Decoupled Double Synchronous Reference Frame for Voltage Oscillations Reduction," *IEEE Transactions on Industrial Electronics*, 2012.

[2.73] Jiangchao Qin, M. Saeedifard, "Predictive control of a three-phase DC-AC Modular Multilevel Converter," *IEEE Energy Conversion Congress and Exposition* (ECCE), pp. 3500-3505, 2012.

[2.74] P. Munch, S. Liu, M. Dommaschk, "Modeling and current control of modular multilevel converters considering actuator and sensor delays," *Conference of IEEE Industrial Electronics,* IECON '09, pp. 1633-1638, 2009.

[2.75] B. Kedjar, K. Al-Haddad, "DSP-Based Implementation of an LQR With Integral Action for a Three-Phase Three-Wire Shunt Active Power Filter," *IEEE Transactions on Industrial Electronics*, vol. 56 , no. 8, pp. 2821-2828, 2009.

[2.76] R. Salim, H.Y. Kanaan, K. Al-Haddad, B. Khedjar, "LQR with integral action controller applied to a three-phase three-switch three-level AC/DC converter," *36th Annual Conference on IEEE Industrial Electronics Society* (IECON), pp. 550 - 555, 2010.

[2.77] I. Ngamroo, "A stabilization of frequency oscillations using a power modulation control of HVDC link in a parallel AC-DC interconnected system," *Proceedings of the Power Conversion Conference*, vol. 3, pp. 1405-1410, 2002.

[2.78] R. Preece, A.M. Almutairi, O. Marjanovic, J.V. Milanovic, "Damping of electromechanical oscillations by VSC-HVDC active power modulation with

supplementary wams based modal LQG controller," *IEEE Power and Energy Society General Meeting*, pp. 1-7, 2011.

[2.79] R. Preece, J.V. Milanovic, A.M. Almutairi, and O. Marjanovic, "Probabilistic Evaluation of Damping Controller in Networks with Multiple VSC-HVDC Lines," *IEEE Transactions on Power System*, 2012.

[2.80] R. Preece, J.V. Milanovic, A.M. Almutairi, and O. Marjanovic, "Damping of Inter-Area Oscillations in Mixed AC/DC Networks Using WAMS Based Supplementary Controller," *IEEE Transactions on Power System*, 2012.

[2.81] A.E Hammad, "Stability and control of HVDC and AC transmissions in parallel," IEEE Transactions on Power Delivery, vol. 14, no. 4, pp. 1545-1554, 1999.

[2.82] Shen, L.; Barnes, M.; Preece, R.; Milanovic, J.; Bell, K.; Belivanis, M., The Effect of VSC HVDC Control and Operating Condition on Dynamic Behavior of Integrated AC/DC System, IEEE Transactions on Power Delivery, 2015.

[2.83] R. Eriksson, L. and Söder, "Wide-Area Measurement System-Based Subspace Identification for Obtaining Linear Models to Centrally Coordinate Controllable Devices," *IEEE Trans. on Power Delivery*, vol. 6, no. 2, pp. 988-997, 2011.

[2.84] Ling Xu, Lingling Fan, "System identification based VSC-HVDC DC voltage controller design," *North American Power Symposium* (NAPS), pp. 1-6, 2012.

[2.85] Mai Huong Nguyen, Saha, T.K., Eghbal, M., "Investigation on the impact of hybrid multi-terminal HVDC system combining LCC and VSC technologies using system identification," *Australasian Universities Power Engineering Conference* (AUPEC), pp. 1-6, 2012.

[2.86] Dehghani, M., Nikravesh, S., "State-Space Model Parameter Identification in Large-Scale Power Systems," *IEEE Transactions on Power Systems*, vol. 23, no. 3, pp. 1449-1457, 2008.

[2.87] Therattil, J.P., Panda, P.C., "Dynamic stability enhancement of a multi-area multi-terminal DC-AC system with self-tuning Static Var Compensator," *Power Electronics, Drives and Energy Systems* (PEDES), pp. 1-6, 2010.

[2.88] Yong Li, Rehtanz, C., Ruberg, S., Longfu Luo; Yijia Cao, "Wide-Area Robust Coordination Approach of HVDC and FACTS Controllers for Damping Multiple Interarea Oscillations," *IEEE Transactions on Power Delivery*, Vol. 27, no. 3, pp. 1096-1105, 2012.

[2.89] Zhuang, Y.; Menzies, R.W.; Nayak, O.B.; Turanli, H.M., Dynamic performance of a STATCON at an HVDC inverter feeding a very weak AC system, IEEE Transactions on Power Delivery, Vol. 11, Issue: 2, pp. 958-964, 1996.

[2.90] Taheri, Nasser, and Banaei, Mohamad Reza, "A supplementary neural controller for novel modeling of VSC HVDC to enhance dynamic stability in a power system," *Power Electronic & Drive Systems & Technologies Conference* (PEDSTC), pp. 7-12, 2010.

[2.91] Dash, P.K., Rout, P.K., Moharana, A.K., "Non-linear control of parallel AC voltage source converter high-voltage DC system using a hybrid input-output linearization evolutionary fuzzy controller," *Electric Power Components and Systems*, vol. 38, no. 8, pp. 881-899, 2010.

[2.92] Liu, C., Bose, A., Hou, Y., "Discussion of the solvability of HVDC systems power flow with a sequential method," *Electric Power Systems Research*, vol. 92, pp. 155-161, 2012.

[2.93] Robert Eriksson, Valerijs Knazkins, and Lennart Söder, "Coordinated control of multiple HVDC links using input–output exact linearization," *Electric Power Systems Research*, vol. 80, no. 12, pp. 1406-1412, 2010.

[2.94] Robert Eriksson, Lennart Söder, "On the coordinated control of multiple HVDC links using input–output exact linearization in large power systems," *International Journal of Electrical Power & Energy Systems*, vol. 43, no. 1, pp. 118-125, 2012.

[2.95] Alain Sarlette, Jing Dai, Yannick Phulpin, Damien Ernst, "Cooperative frequency control with a multi-terminal high-voltage DC network," *Automatica*, vol. 48, no. 12, pp. 3128-3134, 2012.

[2.96] C. Bajracharya, *Control of VSC-HVDC for Wind Power*, (2008) PhD thesis, Department of Electrical Power Engineering, Norwegian University of Science and Technology (NTNU), Trondheim, Norway.

[2.97] J. Beerten, R. Belmans, "Modeling and Control of Multi-Terminal VSC HVDC Systems Review Article," *Energy Procedia*, Vol. 24, pp. 123-130, 2012.

[2.98] Vijay K. Sood, *Power Electronics Handbook* (Second Edition), Chapter 30 - HVDC transmission, pp. 769-795, 2007.

[2.99] Jef Beerten, and Ronnie Belmans, "Modeling and Control of Multi-Terminal VSC HVDC Systems," *Energy Procedia*, Vol. 24, pp. 123-130, 2012.

[3.1] K. R. Padiyar, *Facts controller in power transmission and distribution*, New Age International Ltd., India, 2009.

[3.2] Blasko, V.; Kaura, V., A new mathematical model and control of a three-phase AC-DC voltage source converter, IEEE Transactions on Power Electronics, Vol. 12, Issue: 1, pp. 116-123, 1997..

[3.3] Rodríguez, P.; Luna, A.; Muñoz-Aguilar, R.S.; Otadui, I.E; Teodorescu, R.; Blaabjerg, F., A Stationary Reference Frame Grid Synchronization System for Three-Phase Grid-Connected Power Converters Under Adverse Grid Conditions, IEEE Transactions on Power Electronics, Vol. 27, Issue: 1, pp. 99 - 11, 2012.

[3.4] E. Rakhshani, A. Luna, K. Rouzbehi, P. Rodriguez, I. Etxeberia-Otadui, "Effects of VSC-HVDC on Load Frequency Control in Multi-Area Power System," *IEEE Energy Conversion Congress and Exposition*, ECCE, pp. 4432-4436, 2012.

[3.5] Hua Weng, Zheng Xu, "WAMS based robust HVDC control considering model imprecision for AC/DC power systems using sliding mode control," *Electric Power Systems Research*, vol. 95, pp. 38-46, 2013.

[3.6] Z. Du, Y. Zhang, Z. Chen, P. Li, Y. Ni, L. Shi, "Integrated emergency frequency control method for interconnected AC/DC power systems using center of inertia signals," *IET Generation, Transmission & Distribution*, vol.6, pp. 584-592, 2012.

[4.1] P. Kundur, *Power System Stability and Control*, New York: McGraw-Hill, 1994.

[4.2] H. Bevrani, T. Hiyama, *Intelligent Automatic Generation Control*, CRC Press, 2011.

[4.3] E. Rakhshani, and P. Rodriguez, "Active Power and Frequency Control Considering Large Scale RES," in Large Scale Renewable Power Generation, Springer-Verlag: Berlin Heidelberg, 2014, pp. 233-271.

[4.4] Stanković, A.M.; Tadmor, G.; Sakharuk, T.A., On robust control analysis and design for load frequency regulation, IEEE Transactions on Power Systems, Vol. 13, Issue: 2, pp. 449 - 455, 1998.

[4.5] Rakhshani, E.; Sadeh, J., Load Frequency Control of Multi-Area Restructured International Conference on Power System, IEEE Power India Conference, 2008. POWERCON 2008.

[4.6] Taylor, C.W.; Lefebvre, S., HVDC controls for system dynamic performance, IEEE Transactions on Power Systems, Vol. 6, Issue: 2, pp. 743-752, 1991.

[4.7] Eriksson, R., A New Control Structure for Multi-Terminal dc Grids to Damp Inter-Area Oscillations, IEEE Transactions on Power Delivery, 2014.

[4.8] Z. Jiebei, B.D. Campbell, A.P. Grain, R.J. Andrew, "Inertia Emulation Control of VSC-HVDC Transmission System," *IEEE conf. on Advanced Power System Automation and Protection* (APAP), 2011.

[4.9] S. S. Selvakumaran, S. Parthasarathy, R. Karthigaivel, V. Rajasekaran, Optimal Decentralized Load Frequency Control in a Parallel AC-DC Interconnected Power System Through HVDC Link Using PSO Algorithm, *Energy Procedia*, Vol. 14, pp. 1849-1854, 2012..

[4.10] HuaWeng, ZhengXu, "WAMS based robust HVDC control considering model imprecision for AC/DC power systems using sliding mode control," *Electric Power Systems Research*, vol. 95, pp. 38-46, 2013.

[4.11] E. Rakhshani, A. Luna, K. Rouzbehi, P. Rodriguez, I. Etxeberia-Otadui, "Effects of VSC-HVDC on Load Frequency Control in Multi-Area Power System," *IEEE Energy Conversion Congress and Exposition*, 2012.

[5.1] P. Kundur, *Power System Stability and Control*, New York: McGraw-Hill, 1994.

[5.2] A. Mansingh, and M. York, Automatic Generation Control of a Power Distribution System, *U.S. Patent Documents*, no. US7689323, 2010.

[5.3] V. Donde, A. Pai, I. A. and Hiskens, Simulation and optimization in a AGC system after deregulation, *IEEE Trans. Power Syst.*, Vol. 16, No. 3, pp. 481–489, August 2001.

[5.4] E. Rakhshani, and J. Sadeh, Practical viewpoints on load frequency control problem in a deregulated power system, *Energy Conversion Manag.*, Vol. 51, No. 6, pp. 1148–1156, 2010.

[5.5] N. W. Miller, K. Clark, Automatic Generation Control Augmentation for Wind Plant Integration, *U.S. Patent Documents*, no. US7941246B2, May 2011.

[5.6] A. Keyhani, A. Chatterjee, Automatic Generation Control Structure for Smart Power Grids, *IEEE Transactions on Smart Grid*, Vol. 3, no. 3, pp. 1310-1316, 2012.

[5.7] Z. Miao, L. Fan, D. Osborn, and S. Yuvarajan, "Wind Farms With HVdc Delivery in Inertial Response and Primary Frequency Control," *IEEE Transactions on Energy conversion*, Vol. 25, No. 4, December 2010.

[5.8] G. Delille, B. Francois, G. Malarange, Dynamic Frequency Control Support by Energy Storage to Reduce the Impact of Wind and Solar Generation on Isolated Power System's Inertia, *IEEE Transactions on Sustainable Energy*, Vol. 3 , no. 4, pp. 931-939, 2012.

[5.9] M. Datta, T. Senjyu, A. Yona, T. Funabashi, Chul-Hwan Kim, A Frequency-Control Approach by Photovoltaic Generator in a PV–Diesel Hybrid Power System, *IEEE Transactions on Energy Conversion*, Vol. 26 , no. 2, pp. 559 - 571 , 2011.

[5.10] M. Datta, H. Ishikawa, H. Naitoh, T. Senjyu, "LFC by coordinated virtual inertia mimicking and PEVs in power utility with MW-class distributed PV generation,"IEEE 13th *Workshop on Control and Modeling for Power Electronics* (COMPEL), pp. 1-8, 2012.

[5.11] Prakash K. Ray, Soumya R. Mohanty, Nand Kishor, Proportional–integral controller based small-signal analysis of hybrid distributed generation systems, *Energy Conversion and Management*, vol. 52, pp. 1943–1954, 2011.

[5.12] J. Driesen, and K. Visscher, Virtual synchronous generators, *IEEE Proceeding on Power and Energy Society* - General Meeting, pp. 1-3, 2008.

[5.13] S. Nomura, H. Tsutsui, S. Tsuji-Iio, R. Shimada, Flexible Power Interconnection With SMES, *IEEE Transactions on Applied Superconductivity*, Vol. 16 , no. 2, pp. 616-619, 2006.

[5.14] A. Abu-Siada, and Syed Islam, Application of SMES Unit in Improving the Performance of an AC/DC Power System, *IEEE Transactions on Sustainable Energy*, Vol. 2, no. 2, 2011.

[5.15] T. Nam, J. Shim, K. Hur, Design and Operation of Double SMES Coils for Variable Power System through VSC-HVDC Connections, *IEEE Transactions on Applied Superconductivity*, 2013.

[5.16] Du Cuiqing, E. Agneholm, G. Olsson, Use of VSC-HVDC for Industrial Systems Having Onsite Generation With Frequency Control, *IEEE Transactions on Power Delivery*, Vol. 23, no. 4, pp. 2233-2240, 2008.

[5.17] Zhu Jiebei, Campbell, B.D., Grain, A.P., Andrew, R.J, Inertia Emulation Control of VSC-HVDC Transmission System, *IEEE conference on Advanced Power System Automation and Protection* (APAP 2011), 2011.

[5.18] Hua Weng, Zheng Xu, "WAMS based robust HVDC control considering model imprecision for AC/DC power systems using sliding mode control", *Electric Power Systems Research*, vol. 95, pp. 38-46, 2013.

[5.19] Z. Du, Y. Zhang, Z. Chen, P. Li, Y. Ni, L. Shi, "Integrated emergency frequency control method for interconnected AC/DC power systems using center of inertia signals", *IET Generation, Transmission & Distribution*, vol.6, pp. 584-592, 2012.

[5.20] M.J. Carrizosa , F.D. Navas, G. Dammc, F.L. Lagarrigue, "Optimal power flow in multi-terminal HVDC grids with offshore wind farms and storage devices," *Electrical Power and Energy Systems*, vol. 65, pp. 291–298, 2015.

[5.21] A. Castillo, and D.F. Gayme, "Grid-scale energy storage applications in renewable energy integration: A survey," *Energy Conversion and Management*, vol. 87, pp. 885–894, 2014.

[5.22] S.K. Aditya, D. Das, "Battery energy storage for load frequency control of an interconnected power system", *Electric Power Systems Research*, vo. 58, pp. 179–185, 2001.

[5.23] M. Mufti, S.A., S.J. Iqbal, M. Ahmad, M. Ismail, "Super-capacitor based energy storage system for improved load frequency control", *Electric Power Systems Research*, vol. 79, pp. 226–233, 2009.

[5.24] K.R. Sudha, R. Vijaya Santhi, "Load Frequency Control of an Interconnected Reheat Thermal system using Type-2 fuzzy system including SMES units", *Electrical Power and Energy Systems*, vol. 43, pp.1383–1392, 2012.

[5.25] M. Benidris, J. Mitra, "Enhancing Stability Performance of Renewable Energy Generators by Utilizing Virtual Inertia", *IEEE Power and Energy Society General Meeting*, 2012.

[5.26] Miguel Torres and Luiz A.C. Lopes, "Virtual Synchronous Generator Control in Autonomous Wind-Diesel Power Systems", *IEEE Electrical Power & Energy Conference* (EPEC), 2009.

[5.27] R. Teodorescu, M. Liserre, and P. Rodriguez, *Grid Converters for Photovoltaic and Wind Power Systems*, Hoboken, NJ, USA: Wiley-IEEE Press, Jan 2011.

[5.28] H. Bevrani, Robusr Power System Frequency Control, Springer New York, 2009.

[5.29] Wu. Hongxia, K. S Tsakalis, and G. T. Heydt. “Evaluation of time delay effects to wide-area power system stabilizer design”, *IEEE Trans. on Power Systems*, vol. 19, no. 4, pp. 1935-1941, November 2004.

[5.30] B. Chaudhuri, R. Majumder, B.C. Pal, Wide-area measurement based stabilizing control of power system considering signal transmission delay. *IEEE Trans. Power Syst.* Vol. 19 no. 4, pp. 1971–1979, 2004.

[5.31] H. Wu, K.S. Tsakalis, G.T. Heydt, Evaluation of time delay effects to wide-area power system stabilizer design. *IEEE Trans. Power Syst*. vol. 19, no. 4, pp. 1971–1979, 2004.

[5.32] Peng, C., Zhang, J., Delay-Distribution-Dependent Load Frequency Control of Power Systems with Probabilistic Interval Delays, IEEE Transactions on Power Systems, 2015.

[6.1] S. Tielens, P., Van Hertem, D., The relevance of inertia in power systems Renewable and Sustainable Energy Reviews, Volume 55, 1, pp. 999-1009, march 2016.

[6.2] P. Kunder, *Power System Stability and Control*, USA: McGraw-Hill; 1994.

[6.3] H. Saadat, *Power system Analysis*, McGraw-Hill, 1999.

[6.4] Z. E. Al-Haiki, and A. N. Shaikh-Nasser, "Power Transmission to Distant Offshore Facilities," *IEEE Transactions on Industry Applications*, vol. 47, no. 3, 2011.

[6.5] O.A. Giddani, A. Y.M. Abbas, G. P. Adam, O. Anaya-Lara, K.L. Lo, "Multi-task control for VSC–HVDC power and frequency control," *Electrical Power and Energy Systems*, vol. 53, pp. 684-690, 2013.

[6.6] Lingling Fan, Zhixin Miao, and Dale Osborn, "Wind farms with HVDC delivery in Load Frequency Control," *IEEE Transactions on Power Systems*, vol. 24, no. 4, 2009.

[6.7] Du Cuiqing, E. Agneholm, G. Olsson, "Use of VSC-HVDC for industrial systems having onsite generation with frequency control," *IEEE Trans. on Power Delivery*, vol. 23, no. 4, pp. 2233–2240, 2008.

[6.8] Z.B. Du, Y. Zhang, L. Liu, X.H. Guan, Y.X. Ni, F.F Wu, "Structure-preserved power-frequency slow dynamics simulation of interconnected ac/dc power systems with AGC consideration," *IET Generation, Transmission & Distribution*, vol. 1, pp. 920-927, 2007.

[6.9] Y. Li, Z.Zhanga, Y. Yang, Y. Li, H.Chenc, Z. Xua, "Coordinated control of wind farm and VSC–HVDC system using capacitor energy and kinetic energy to improve inertia level of power systems," *Electrical Power and Energy Systems*, vol. 59, pp. 79-92, 2014.

[6.10] N. Jaleeli et al., "Understanding automatic generation control," *IEEE Trans. on Power Systems*, vol. 7, no. 3, pp. 1106–1112, Aug. 1992.

[6.11] H. Shayeghi, H. A. Shayanfar and O. P. Malik, "Robust decentralized neural networks based LFC in a deregulated power system," *Electric Power Systems Research*, vol. 77, pp. 241–251, April. 2007.

[6.12] E. Rakhshani, and J. Sadeh, "Practical viewpoints on load frequency control problem in a deregulated power system," *Energy Conversion and Management*, vol. 51, no. 6, pp. 1148–1156, 2010.

[6.13] A. Ibraheem, A. Nizamuddin, T.S. Bhatti, "AGC of two area power system interconnected by AC/DC links with diverse sources in each area," *Electrical Power and Energy Systems*, vol. 55, pp. 297–304, 2014.

[6.14] Ibraheem, P. Kumar, and D. P. Kothari, "Recent philosophies of automatic generation control strategies in power systems," *IEEE Trans. on Power Systems*, vol. 20, no. 1, pp. 346–357, Feb. 2005.

[6.15] H. Bevrani, T. Hiyama, *Intelligent Automatic Generation Control*, CRC Press, 2011.

[6.16] Marimuthu, P., Govindaraju, C., Load frequency control of hydrothermal system under open market considering capacitive energy storage, International Review on Modelling and Simulations, 5 (5), pp. 2307-2313, 2012..

[6.17] E. Rakhshani, P. Rodriguez, "*Active Power and Frequency Control Considering Large Scale RES*", in Large Scale Renewable Power Generation: Advances in Technologies for Generation, Transmission and Storage, Springer-Verlag: Berlin Heidelberg, November 2013.

[6.18] L. Zhang, L. Harnefors and H.-P. Nee, "Power-synchronization control of grid-connected voltage-source converters," *IEEE Transactions on Power Systems*, vol. 25, pp. 809-820, May 2010.

[6.19] Q.-C. Zhong, P.-L. Nguyen, Z. Ma and W. Sheng, "Self-syncrhonised synchronverters: inverters without a dedicated synchronization unit," *IEEE Transactions on Power Electronics*, vol. 29, pp. 617-630, 2014.

[6.20] P. Rodriguez, I. Candela, C. Citro, J. Rocabert and A. Luna, "Control of grid-connected power converters based on a virtual admittance control loop," in Proc. 15th *European Conference on Power Electronics and Applications* (EPE), 2013.

[6.21] P. Rodriguez, J. Ignacio Candela and A. Luna, "Control of PV Generation Systems using a Synchronous Power Controller", *IEEE Energy Conversion Congress and Exposition*, ECCE, USA, 2013.

[6.22] P. Rodriguez, "Synchronous power controller of a generation system based on static power converters", *International patent application* WO 2012/117131, September 7th 2012.

[6.23] Parmar, K.P.S., Majhi, S., Kothari, D.P., LFC of an interconnected power system with multi-source power generation in deregulated power environment,

International Journal of Electrical Power and Energy Systems, 57, pp. 277-286, 2014.

[6.24] M. Datta, T.Senjyu, A. Yona, T. Funabashi, K. Chul-Hwan, "A Frequency-Control Approach by Photovoltaic Generator in a PV–Diesel Hybrid Power System," *IEEE Transactions on Energy Conversion*, vol. 26, pp. 559-571, 2011.

[6.25] S. Ali Pourmousavi, and M. HashemNehrir, "Introducing Dynamic Demand Response in the LFC Model," *IEEE Transactions on Power Systems*, 2014.

[6.26] S. Ganapathy, S. Velusami, "MOEA based design of decentralized controllers for LFC of interconnected power systems with nonlinearities, AC–DC parallel tie-lines and SMES units," *Energy Conversion and Management*, vol. 51, pp. 873–880, 2010.

[6.27] Shan Jiang, U. D. Annakkage, and A. M. Gole, "A platform for validation of FACTS models," *IEEE Trans. on Power Delivery*, vol. 21, no. 1, pp. 484-491, Jan 2006.